ERDC/CERL TR-11-2

Construction Engineering
Research Laboratory

US Army Corps
of Engineers®
Engineer Research and
Development Center

Progress in the Production of JP-8 Based Hydrogen and Advanced Tactical Fuels for Military Applications

Christopher J. Zygarlicke, Ted R. Aulich, Chad A. Wocken,
Debra F. Pflughoeft-Hassett, Tera D. Buckley, John P. Hurley,
Junhua Jiang, Benjamin G. Oster, Nikhil M. Patel,
Anthony C. Snyder, Chang W. Sohn, and William T. Brown III

February 2011

ERDC/CERL TR-11-2
February 2011

Progress in the Production of JP-8 Based Hydrogen and Advanced Tactical Fuels for Military Applications

Chang W. Sohn and William T. Brown III

Construction Engineering Research Laboratory (CERL)
U.S. Army Engineer Research and Development Center
2902 Newmark Dr.
Champaign, IL 61822-1076

Christopher J. Zygarlicke, Ted R. Aulich, Chad A. Wocken, Debra F. Pflughoeft-Hassett, Tera D. Buckley, John P. Hurley, Junhua Jiang, Benjamin G. Oster, Nikhil M. Patel, and Anthony C. Snyder

University of North Dakota
Energy & Environmental Research Center
15 North 23rd Street, Stop 9018
Grand Forks, ND 58202-9018

Final Report

Prepared for Headquarters, U.S. Army Corps of Engineers
Washington, DC 20314-1000

Under Project Requisition No. 137573

Abstract: Today's Army is heavily dependent on oil and its byproducts as the primary fuel for the force. Current predictions indicate that the decline of oil reserves will coincide with the timeline for implementing Army After Next (AAN) technologies, which are planned to make fossil fuel powered vehicles up to 75 percent more efficient. This work was undertaken to help achieve that objective by: (1) developing and optimizing the high-pressure water reforming (HPWR) concept for on-demand production of high-pressure Proton Exchange Membrane (PEM) fuel cell-quality hydrogen from JP-8 and other feedstocks; (2) developing advanced tactical fuels with JP-8 drop-in compatibility and superior hydrogen-reforming properties from domestic fossil or renewable feedstocks, and (3) advancing the development of fuel cell electric hybrid (FCEH) vehicles, and demonstrating those vehicles and hydrogen dispensing and refueling systems at military installations. This report provides the research analyses, findings, and results, and describes technology demonstrations.

Executive Summary

Today's Army is heavily dependent on oil and its byproducts as the primary fuel for the force. Yet oil reserves are limited. Current predictions indicate that the decline of oil reserves will coincide with the timeline for implementing Army After Next (AAN) technologies. AAN plans for the year 2025 and beyond call for a more fuel-efficient Army—in particular, making fossil fuel powered vehicles up to 75 percent more efficient.

This work was undertaken to help achieve that objective as part of a multiyear program to develop, optimize, and demonstrate the military viability of a technology for on-demand production of high-pressure hydrogen for fuel cell electric hybrid (FCEH) vehicles. A broad goal of the program was to develop a military logistics fuel-based hydrogen supply scenario that enables battlefield use of hydrogen in highly efficient FCEH vehicles. A second goal of this program was to develop advanced tactical fuels with superior hydrogen-reforming properties, and that may substitute for JP-8 (jet propulsion fuel), from domestic or indigenous fossil feedstocks such as coal, natural gas, and petroleum coke, and renewable feedstocks such as crop oils and biomass.

This report describes technical work conducted under Task 1, hydrogen production, purification, and vehicle development and demonstration, and Task 2, the development of alternative (nonpetroleum) feedstock-based technologies for production of advanced tactical fuels with JP-8 drop-in compatibility and improved properties for use as hydrogen feedstocks. Task 3 includes overall project management and select strategic studies.

Subtask 1.1 — Hydrogen production process optimization

Optimization experiments were conducted in a high-pressure hydrogen production unit. The process converts liquid, organic feedstock, and water into a high-pressure, hydrogen-rich gas stream. A modified reactor was developed and demonstrated. This reactor provided improved heat transfer to the catalyst bed. To decrease the load on downstream purification equipment, the removal of nonhydrogen gases at high pressure was also investigated via high-pressure condensation and physical adsorption techniques.

High-pressure condensation was not effective at removing nonhydrogen gases. Physical adsorption, however, was effective at capturing nonhydrogen gases, specifically carbon dioxide. Installing the physical adsorption vessel resulted in a high-pressure gas stream (6000 psi) that contained 96 mol hydrogen.

Subtask 1.2.1 — ESA process development

This activity evaluated the use of the Oak Ridge National Laboratory (ORNL)-developed electrical swing adsorption (ESA) process for purification of high-pressure hydrogen produced from the high-pressure water reforming (HPWR) process. If successful, the ESA process has the potential to significantly increase the production efficiency and lower the power costs of purification relative to the standard method used at low pressures (i.e., pressure swing adsorption).

The first task was to develop an electrically conductive high-surface-density monolithic adsorber for use in the system. Three routes were pursued, all involving the creation or use of activated carbon as the base adsorber material. In two routes, it was first attempted to make very high density carbon monoliths using carbon fibers and/or phenolic resins and then activate the monolith. This technique was not successful because the level of activation of the carbon; i.e., the increase in adsorptivity due to partial oxidation was always much lower than can be found in commercial activated carbons. The effort then focused on making monoliths from commercially available powdered activated carbon. This effort was successful in making monoliths with approximately twice the surface area density of the powdered material, an electrical resistivity of 1.2 inch-ohms, and a compressive strength of 3500 psi. Adsorptivity of the monoliths was tested by passing a mixture of H_2, CH_4, CO, and CO_2 gases through cylinders of the material at up to 800 psig. These tests demonstrated that the cylinders were very good at providing high-purity hydrogen from a gas mixture. However, significant heating occurred when an electric current was passed through the saturated monoliths during attempted regeneration. Therefore, a method of treating the activated carbon was developed to reduce its electrical resistivity by a factor of 10. The new material will be tested at higher pressures in the pilot-scale test system described below.

Work in this activity also continued with design and construction of the 12,000-psi ESA test system. Before the design of the system was finalized, two project engineers were trained in high-pressure hydrogen technology

and safety. A quantifiable risk assessment of the system was performed to ensure safe remote operation in an open pilot plant setting. Risk needed to be equivalent to or better than that experienced by workers at a commercial hydrogen-fueling station. One engineer also obtained certification as a hydrogen safety engineer. The system was designed for remote operation, and all electrical components met the National Electrical Code Class 1 Division 2 rating for operation in environments that may contain explosive gases.

The 12,000-psi ESA test system creates simulated reformate gases by blending pure gases from cylinders, which are then compressed to up to 12,000 psi and passed through the adsorber monoliths. Changes in gas composition at the outlet can be continuously measured with a laser gas analyzer, and temperature changes in the monoliths can be monitored by six embedded thermocouples. Electric currents can be passed through the monoliths to determine how well the adsorbed gases are driven off and how temperature changes during that process. The system will be used in future work in this activity to refine operating procedures, to determine gas adsorptivity and breakthrough behavior at high pressure, and to develop monolith regeneration procedures. As of the end of this phase of work, the 12,000 psi ESA test system was constructed and ready for shakedown and testing.

Subtask 1.2.2 — Electrochemical hydrogen purification process development

The development of efficient, cost-effective, and scalable hydrogen separation and purification technologies are key requirements for the advancement of a hydrogen economy since ultrapure hydrogen (99.9 percent H_2) is the ideal fuel for polymer electrolyte membrane fuel cells. Electrochemical hydrogen separation and purification using proton exchange membranes was based on reversible hydrogen oxidation and reduction reactions. It is expected that minimal power should be required to operate the electrochemical process, and that the hydrogen purity produced at the cathode would be very high. Hydrogen normally produced from hydrocarbons contains a level of CO up to 2 percent. This high CO level requires the development of an electrochemical hydrogen purification technology based on high-temperature proton-conducting membranes since platinum (PT) catalysts can tolerate such high CO levels without significant activity degradation at increased temperature.

The electrochemical hydrogen purification process was investigated using high temperature polymer electrolyte membranes at ambient and increased pressure. All electrochemical experiments were performed using a 50-cm^2 active area electrochemical cell comprising two metal end plates, two parallel multichannel serpentine flow field graphite plates, and a high-temperature membrane-electrode assembly (MEA). During each run, a simulated gas stream consisting of 76 percent H_2, 2 percent CO, 2 percent CH_4, and 20 percent CO_2 was supplied to the anode side, and high-purity nitrogen was fed to the cathode side to carry hydrogen purified for gas analysis.

The feasibility of the electrochemical hydrogen purification process was demonstrated, and the electrochemical process was optimized at ambient pressure. At three operating temperatures of 140, 160, and 180 °C, only hydrogen was produced at the cathode. Moreover, the current efficiency for the hydrogen purification process was higher than 90 percent at the three temperatures above and at a constant current of 200 mA cm^{-2}. The cell voltage measured at this constant current density was dependent on the operating temperature. At 140 °C, a value of around 0.14 V was obtained. This value was decreased to around 0.06 V when the temperature was increased to 180 °C. Moreover, it was found that the cell voltage almost remained constant at controlled constant current polarizations. The purification process was further investigated as a function of process start-up and shutdown. Exclusive hydrogen gas at the cathode, high current efficiency, and stable low cell voltage were reproduced.

Work was initialized on tailoring the process for use at elevated pressure. The next phase of work will focus on the feasibility demonstration and optimization of the high-pressure hydrogen purification processes.

Subtask 2.1 — Advanced gasifier development for clean syngas generation

An advanced distributed-scale gasifier was developed that can convert widely available complex waste resources into energy, liquid fuels, or hydrogen. The gasifier accommodates fuel composition variations that attain self-sustained, steady-state gasification in the simplest configuration while maintaining near-zero effluent discharge. The new gasification design was tested for improved performance using a wide range of biomass fuel.

The fuels selected for self-sustained gasification experiments were high-moisture biomass waste (moisture ranging from 35 to 60 percent), high-moisture Powder River Basin (PRB) coal (26–30 percent), and creosote treated railroad ties–a hybrid fuel having characteristics of woody biomass (base material is oak wood), but with an included creosote (complex mixture of coal tar).

Woody biomass containing moisture greater than 50 percent was tested during a 24-hour gasification test. Desired variations in syngas composition for application in the liquid synthesis process (high H_2/CO ratio) and electricity production (high CO/H_2) ratio were achieved by varying the gasifier operating condition. The worst-case tar produced in case of wet biomass gasification was 3830 mg/m^3 and 290 mg/m^3 in hot and cold syngas, respectively. The particulate matter concentration determined was 175 and 54 mg/m^3 in hot and cold syngas, respectively.

Tests using high moisture coal as feedstock also showed high H_2/CO and CO/CO_2 ratios in the syngas, which would be excellent syngas quality for hydrogen and liquid fuels production. During 13-hour steady state gasification of 35 percent moisture wood waste, hydrogen rich syngas composition was produced with an achieved average and highest H_2/CO ratio of 1.51 and 2.26, respectively. Such steady state gasification could be obtained on high moisture biomass for commercial liquid production system.

Tests on the creosote treated railroad ties were primarily concerned with lowering tar generation in the gasification process and removing tars with post-gasification scrubbing. The level of tar during steady-state gasification of railroad tie in the unscrubbed hot syngas and scrubbed syngas was determined to be 822 and 200 mg/m^3, respectively, while the particulate concentration was 353 and 32 mg/m^3, respectively. The cold-side tar contained about 83 percent toluene and xylenes, which are typically used as performance enhancers in internal combustion engines. No tar heaver than naphthalene (only 7 percent) escaped the syngas polisher. Fine performance adjustments in the syngas polisher can lead to higher than 95 percent tar capture.

Overall, the performance study revealed that gasification efficiency greater than 80 percent could be achieved for fuel such as railroad ties and high-moisture biomass. The primary advantage of using waste without requir-

ing predrying is envisaged to be a simple system, and moisture could be used as gasification medium.

Subtask 2.2.1 — FT process development

To develop and demonstrate a bench-scale coal-/biomass-to-liquids process, three large batches of an iron-based, Fischer–Tropsch (FT) catalyst, 1 kg each, were prepared and evaluated in a lab-scale FT reactor. After the effectiveness of the catalyst was verified, the catalysts were loaded into the bench-scale FT reactor, which was used to convert coal–biomass derived syngas into FT liquids. The liquids were subsequently upgraded into synthetic isoparaffinic kerosene (SPK) that is compatible with military-grade JP-8 jet fuel.

Further tests were conducted on the FT iron catalyst preparation method to improve the repeatability of catalyst production and the stability and performance of the catalyst. It was determined that, if the catalyst is exposed to atmospheric water vapor for extended periods of time, activity, and selectivity to heavier hydrocarbons will be negatively impacted. Also, the catalyst must be exposed to dry, flowing air during calcining to maximize performance.

The FT iron catalyst was promoted with varying amounts of lanthanum oxide to determine potential effects on catalyst productivity and product selectivity. It may be that small amounts of lanthanum help to improve selectivity to heavy hydrocarbons, but too much may negatively impact catalyst performance. The trials were confounded by excessive variation in iron and potassium loading on the catalyst, and the results of the experiment may be due in large part to the ratio of potassium to iron.

Various FT catalysts were received from a commercial catalyst supplier. These catalysts were tested in the small-scale FT reactor. The performance of the catalyst was evaluated and compared to the FT catalyst developed as part of this work. The results were reported back to the supplier to assist in improving the catalyst formulation for future tests.

Subtask 2.2.2 — Hydrotreated renewable jet fuel process development

A process to convert plant- or animal-derived fats and oils into hydrocarbon fuels was developed. The fuels produced from this process are chemically identical to their petroleum-derived counterparts.

Under ERDC-CERL funding, experiments were conducted to support process scale-up. Laboratory experiments were conducted in continuous process systems, typically run at 0–6 L/hr. Feedstock flexibility was demonstrated. A feedstock-flexible process is less sensitive to specific feedstock prices and, therefore, reduces the economic risks associated with feedstock price volatility. To demonstrate feedstock flexibility, researchers experimented with many different crop oil and fatty acid feedstocks. Feedstock effect on product composition and quality was investigated. The process proved to be extremely feedstock-flexible with the only notable difference, when varying feedstock, being the chain length of the hydrocarbon product.

Operational parameters were also investigated to optimize the process and to reduce overall operating costs. Reactor pressure, oil feed rate, and hydrogen feed rate were varied to determine their effect on product quality. The minimum operating condition was found for each variable. Reaction kinetics were also investigated, and a kinetic model was developed to fit the experimental data. This model showed that the reaction was first order with respect to feedstock concentration and a fractional order with respect to hydrogen partial pressure.

Process integration strategies were investigated. The main conclusion from this analysis was that the high-cetane, low-sulfur, renewable hydrocarbon fuel that is produced from the University of North Dakota Energy and Environmental Research Center (EERC) process could be a valuable product for refineries to blend into their existing diesel pool.

Subtask 2.3 — Development of modular systems for distributed fuels and energy

The EERC performed a brief evaluation of specific renewable technologies focused on the distributed production of fuels and/or energy. Technologies evaluated were biomass gasification coupled with internal combustion engine, biomass gasification coupled with synthetic natural gas (SNG) production, biomass gasification coupled with the FT process, and catalytic hydrodeoxygenation isomerization (CHI).

Based on previous work by the National Renewable Energy Laboratory (NREL), Princeton University, and the EERC, process efficiencies, energy balances, and block diagrams were determined for each process based on a

"normalized" input Btu content of the feedstock, and output quantities and makeup were then derived.

Using these results, these technologies were evaluated for a specific military facility, Grand Forks Air Force Base (GFAFB) located near Grand Forks, ND. Fuel and energy usage information was provided by GFAFB personnel, and each technology was evaluated to determine the potential to offset current fuels or energy usage.

Based on reasonableness of scale, cost, and feedstock availability, three technologies appear to warrant further study: (1) biomass gasification coupled with synthetic natural gas (SNG) production to offset propane usage, (2) diesel production using biomass gasification coupled with FT, and (3) CHI process to offset diesel usage.

Task 3 — Project management and reporting

This task facilitated management of the entire project, including all project management such as tracking deliverables and budgets, monthly and quarterly reporting, final reporting, internal project meetings, project review meetings, and strategic studies.

A second major strategic studies effort involved work done to put together a biomass resource and characterization assessment for the contiguous United States. A report was written that gives the current status biomass availability for conversion to power and fuels. Biomass types considered included agricultural and forest residues and energy crops and urban residuals. Primary data consisted of county-by-county biomass resource types and estimates and also included some data on the chemical and physical properties of those sources. The study included some data and information on national land ownership, climate zones, and biomass-growing conditions. One conclusion drawn from the study is that there is no single ideal biomass source. While some sources may have ideal combustion and cofiring properties, such as wood, other sources are optimal feedstocks for fuel production, such as corn or soybeans. In addition, no type of biomass is uniformly available across the United States or even within individual states.

Table of Contents

List of Figures and Tables

Figures

Figures

Figures

Figures

Tables

Tables

Preface

This study was conducted for Assistant Secretary of the Army for Acquisition, Logistics, and Technology (ASAALT) under Project Requisition No. 137573, "Advanced Tactical Fuels for the Military." The technical monitor was Kristopher Gardner Deputy Director for Technology - C4ISR/Space/Power & Energy. Deputy Director for Command, Control, Communications, Computers, Intelligence, Surveillance, and Reconnaissance; P&E; and Space Technologies for the Office of the Deputy Assistant Secretary of the Army for Research and Technology and Army Chief Scientist

The work was managed and executed by the Energy Branch (CF-E) of the Facilities Division (CF), Construction Engineering Research Laboratory (CERL). The CERL principal investigator was Dr. Chang W. Sohn. The work was contracted by the University of North Dakota Energy & Environmental Research Center (EERC) under Cooperative Agreement No. W9132T-08-2-0014. Franklin H. Holcomb is Chief, CEERD-CF-E, and L. Michael Golish is Chief, CEERD-CF. The associated Technical Director was Martin J. Savoie, CEERD-CV-T. The Director of ERDC-CERL is Dr. Ilker R. Adiguzel.

CERL is an element of the U.S. Army Engineer Research and Development Center (ERDC), U.S. Army Corps of Engineers. The Commander and Executive Director of ERDC is COL Gary E. Johnston, and the Director of ERDC is Dr. Jeffery P. Holland.

Unit Conversion Factors

Multiply	By	To Obtain
British thermal units (International Table)	1,055.056	joules
cubic feet	0.02831685	cubic meters
cubic inches	1.6387064 E-05	cubic meters
cubic yards	0.7645549	cubic meters
degrees (angle)	0.01745329	radians
degrees Fahrenheit	(F-32)/1.8	degrees Celsius
feet	0.3048	meters
gallons (U.S. liquid)	3.785412 E-03	cubic meters
inches	0.0254	meters
inch-pounds (force)	0.1129848	newton meters
pounds (mass)	0.45359237	kilograms
square feet	0.09290304	square meters
square inches	6.4516 E-04	square meters
square miles	2.589998 E+06	square meters
square yards	0.8361274	square meters
tons (force)	8,896.443	newtons
tons (2,000 pounds, mass)	907.1847	kilograms

1 Introduction

Background

Today's Army is heavily dependent on oil and its byproducts as the primary fuel for the force. Yet oil reserves are limited. Current predictions indicate that the decline of oil reserves will coincide with the timeline for implementing Army After Next (AAN) technologies. AAN plans for the year 2025 and beyond call for a more fuel-efficient Army—in particular, making fossil fuel powered vehicles up to 75 percent more efficient.

This work was undertaken to help achieve that objective as part of a multiyear program to develop, optimize, and demonstrate the military viability of a technology for on-demand production of high-pressure hydrogen for fuel cell electric hybrid (FCEH) vehicles. A broad goal of the program was to develop a military logistics fuel-based hydrogen supply scenario that enables battlefield use of hydrogen in highly efficient FCEH vehicles. A second goal of this program was to develop advanced tactical fuels with superior hydrogen-reforming properties, and that may substitute for JP-8 (jet propulsion fuel), from domestic or indigenous fossil feedstocks such as coal, natural gas, and petroleum coke, and renewable feedstocks such as crop oils and biomass.

Objectives

The key objectives of this stage of research were:

- to develop and optimize the HPWR concept for on-demand production of high-pressure PEM fuel cell-quality hydrogen from JP-8 and other feedstocks
- to develop advanced tactical fuels with JP-8 drop-in compatibility and superior hydrogen-reforming properties from domestic or indigenous fossil feedstocks such as coal, natural gas, and petroleum coke and renewable feedstocks such as crop oils and biomass
- to advance the development of FCEH vehicles through demonstration of fuel cell-powered vehicles and hydrogen dispensing and refueling systems at military installations.

Approach

This work was accomplished in three general tasks:

1. Integrated Demonstration of JP-8-Based Hydrogen Production and Dispensing
2. Fuel Production from Alternative Feedstocks
3. Project Management and Reporting.

The appendixes to this report contain supporting material:

- Appendix A identifies and characterizes biomass sources in the United States.
- Appendix B contains summary maps showing agriculture crop yields by county.
- Appendix C contains a listing of urban residuals generation and use by State
- Appendix D contains listings of agriculture production outlook.
- Appendix E contains a listing of wood production outlook.
- Appendix F contains listings of urban residues outlook.
- Appendix G contains sources that external chemical analysis and physical characterization data references.
- Appendix H lists definitions and methods of characterization analysis.

Mode of technology transfer

This report will be made accessible through the World Wide Web (WWW) at URL: http://www.cecer.army.mil

2 Preliminary Work

Since 2006, the following activities have been conducted:

- Preliminary evaluation of the military viability of the high-pressure water reforming (HPWR) concept for on-demand production of high-pressure PEM fuel cell-quality hydrogen from JP-8, resulting in a positive proof-of-concept assessment.
- Completion of the design, fabrication, and shakedown of a pilot-scale (600-standard cu ft/hr [1.5-kg/hr]) HPWR hydrogen production system.
- Completion of required facility upgrades for conducting HPWR system optimization activities.
- Initiation of partnership arrangements with major catalyst suppliers, including CRI International, Johnson Matthey, and Süd Chemie to enable project access to catalysts and/or catalyst combinations with the best potential for generating maximum hydrogen and minimum coke production in the HPWR system.
- HPWR process optimization testing using aromatics- and sulfur-free Syntroleum-produced "S-8" fuel as feedstock. Initial results have demonstrated good hydrogen production, as measured by product gas hydrogen concentrations of up to 56 percent (versus a maximum theoretical concentration of 75 percent), and indicated the need for increased S-8 "cracking" before hydrogen production to achieve a higher overall hydrogen yield.
- Design and construction of a FCEH forklift to operate in the cold winter and hot summer weather of Grand Forks Army National Guard Base (GFARNGB). The forklift was delivered to GFARNGB and demonstrated for over 1 year before being decommissioned and returned to the builder (ePower). Development of an FCEH multipurpose utility vehicle (MPUV) was initiated and then halted after ePower Synergies was unable to meet the performance specification requirements with the first of two Bobcat® MPUVs. Two additional FCEH forklift vehicles were fabricated and delivered to Robins Air Force Base (AFB) for demonstration activities. The FCEH forklift vehicles were delivered to Robins AFB on 18 December 2007, and 27 April 2009.

- In collaboration with Kraus Global Inc. and Airgas, Inc., design, fabrication, shakedown, and installation at GFARNGB of a hydrogen-dispensing system that delivers high-pressure hydrogen. The dispensing system was used at GFARNGB to refuel the ePower-designed FCEH forklift and provided an interim hydrogen supply to support FCEH vehicle demonstration activities in advance of a fully integrated HPWR-based hydrogen production, purification, and dispensing system running on JP-8. The EERC and ePower conducted a training session at GFARNGB on 19 October 2006, to provide instruction to base personnel on the proper and safe operation of the hydrogen refueler and the FCEH forklift.
- Investigation of options for increasing the density of commercially available activated carbon sorbents without reducing their surface areas. The purpose of this work was to create a high-density electrically conductive monolithic adsorber for purifying hydrogen at very high pressures. The monolithic design is necessary whether electrical, pressure, or thermal swinging is used to regenerate the adsorber. Monoliths have been made using mixtures of granular and powdered activated carbon tested at up to 800 psig. They are effective at adsorbing contaminants from the gas stream, leaving pure hydrogen.
- Tests of the regeneration of the monoliths at up to 800 psig using electric currents, which showed significant heating of the monolith, indicating that gas desorption may be due to the heating and not the electric current alone. However, work continues to make more electrically conductive monoliths, which may better show gas desorption due to the electric current before any heating occurs.
- Training of two engineers in high-pressure hydrogen technologies, who subsequently performed a detailed risk assessment of the operation of a 12,000 psi electric swing adsorption (ESA) system operated in an open-bay area with other workers in the facility. The assessment led to design changes to match the safety level equivalent to that of trained operators at a commercial hydrogen-refueling station.
- Design and construction of a 12,000 psi ESA test system capable of purifying 300 scfh of reformed gas. The system is designed for remote computer-controlled operation and has automatically operated safety procedures in case of a gas leak. Two monolith pressure vessels were installed: one for a 1.5-in.-diameter monolith 24 in. long, the other for a 2.5-in.-diameter monolith 36 in. long.

- In collaboration with U.S. military fuel experts and commercial fuel developers, development of a process to produce a renewable biomass-derived turbine fuel with JP-8 "drop-in compatibility" (the ability to meet all JP-8 military specifications and "fit-for-purpose" requirements). Theoretical design, chemical modeling, and bench-scale thermocatalytic processing activities were used to produce a crop oil-derived JP-8—an advanced tactical fuel with excellent properties (zero aromatics and sulfur content) for use as a turbine engine fuel or a feedstock for the HPWR hydrogen production process.
- In collaboration with technology providers and catalyst producers, initiation of development of a process for producing a drop-in-compatible alternative JP-8 from nonpetroleum feedstocks, including coal, natural gas, and biomass. Initial work was focused on enhancing the chemical composition of fossil-based Fischer–Tropsch (FT) fuel as required to meet all military JP-8 specification and fit-for-purpose requirements and serve as a superior feedstock for the HPWR hydrogen production process.
- Design and construction of a bench-scale reactor to convert syngas to liquid fuels, which, on upgrading, meet key JP-8 specification requirements.
- Preparation and evaluation of three large batches of an iron-based FT catalyst, 1 kg each, in the small-scale FT reactor. The large batches were loaded into the large-scale FT reactor, which was used to convert coal–biomass-derived syngas into FT liquids. The liquids were subsequently upgraded into synthetic paraffinic kerosene (SPK) that is compatible with JP-8 jet fuel.
- Further tests on the FT iron catalyst preparation method to improve the repeatability of catalyst production and the stability and performance of the catalyst. It was determined that if the catalyst is exposed to atmospheric water vapor for extended periods of time, activity, and selectivity to heavier hydrocarbons will be negatively impacted. Also, the catalyst must be exposed to dry, flowing air during drying and calcining to maximize performance.
- Promotion of the FT iron catalyst with varying amounts of lanthanum oxide to determine potential effects on catalyst productivity and product selectivity. Small amounts of lanthanum help to reduce the surface acidity of the alumina support, which improves selectivity to heavy hydrocarbons. However, it appears that too much lanthanum negatively impacts catalyst productivity.

- Testing in the small-scale FT reactor of various FT catalysts received from a commercial catalyst supplier. The performance of the catalyst was evaluated and compared to the FT catalyst developed in this work. The results were reported to the supplier to assist in improving catalyst formulation for future tests.

3 Integrated Demonstration of JP-8-Based Hydrogen Production and Dispensing (Task 1)

The Task 1 subtasks and activities comprise optimization of the HPWR-based hydrogen production process and development and optimization of the ESA-based hydrogen purification process. It is anticipated that an integrated hydrogen production, purification, and dispensing system and vehicle demonstration will be conducted at Grand Forks Air Force Base (GFAFB) under a subsequent contract after completion of the design and fabrication of a deployable HPWR–ESA-based hydrogen-refueling system.

Subtask 1.1 – Hydrogen production process optimization

Experimental

A high-pressure hydrogen production system to reform liquid organic feedstocks and water at operating pressures up to 12,000 psi had previously been developed. The advantages of this system include: (1) elimination of energy-intensive hydrogen compression, (2) a smaller process footprint, and (3) elimination of gaseous or liquid hydrogen transport. The objective of the gas cleanup work conducted under Subtask 1.1 was to decrease the load on downstream gas cleanup equipment that will further purify the reformate gas to PEM fuel cell quality. To accomplish the subtask objective, the existing system was optimized through a series of reactor modifications. Thermodynamic modeling was used to determine expected carbon dioxide removals and shakedown, and multiple test runs were conducted.

Results and discussion

A new reactor was designed and constructed to provide better heat transfer to the catalyst bed. The reforming reactions are endothermic, and cold-spots are possible if there is inadequate heat transfer. A high-pressure condensation vessel was also installed downstream of the reactor as a means to remove water and carbon dioxide from the product gas. Shakedown activities were conducted with the new, reconfigured high-pressure reforming system. The unit was run at an increased capacity of approx-

imately tenfold the original system, indicating that the process can be readily scaled up. Table 1 lists typical reactor conditions and Table 2 lists typical reformate gas composition.

Thermodynamic modeling indicated that it should be possible to condense liquid carbon dioxide simply by cooling the high-pressure gas stream. In laboratory tests, however, condensation of carbon dioxide to liquid was not achieved in the cold, high-pressure condensate vessel. To increase the cold surface area in the condensate vessel, steel packing was inserted. Even with the additional condensation area provided by the steel packing, the carbon dioxide concentration of the reformate gas remained unchanged. An alternate approach to removing carbon dioxide from the high-pressure reformate stream involving physical absorption of the carbon dioxide into a proprietary liquid solvent was investigated. The results listed in Table 2 indicate that the physical absorption column was moderately effective at removing carbon dioxide and water from the reformate gas stream. To prevent the absorption vessel solvent from becoming saturated with contaminants, the solution was constantly circulated to a flash drum, where pressure was dropped and contaminant gases were flashed off. Clean absorbent solution was then circulated back to the working absorption vessel. Figure 1 shows a system flow diagram.

Table 1. Typical high-pressure reformer conditions during experiments.

Feedstock	Methanol
Temperature, °C	350–400
Pressure, psig	7500–8500
Methanol flow, lb/hr	2
Water flow, lb/hr	9

Table 2. Typical reformate gas composition from the high-pressure reformer.

Reformate Gas Component	Without CO_2 Absorber, vol% [R50]	With CO_2 Absorber, vol% [R56]
Hydrogen	74.6	83.1
Carbon dioxide	19.1	11.1
Carbon monoxide	2.0	1.7
Methane	1.8	1.0
Other light hydrocarbons (C_xH_y)	0.4	0.2
Water	1.1	0.1

To increase gas–liquid contact time, a taller absorption column was constructed and installed to investigate the effect of increased contact time between reformate gas and absorption liquid on carbon dioxide absorption. This modification did not have a discernible effect on reformate gas composition compared to the shorter absorption column. The experiment indicated that the contact time between the absorbent and reformate gas stream was not limiting carbon dioxide removal, further indicating that the absorption solvent itself may be the limiting factor. It was hypothesized that better carbon dioxide removal would be achieved with an improved absorption solvent. This hypothesis was supported when an improved absorption media was used. Table 3 lists the results from tests using the improved absorption media, a methanol feed rate of 1.25 lb/hr, water feed rate of 6.25 lb/hr, and a pressure of 6000 psi.

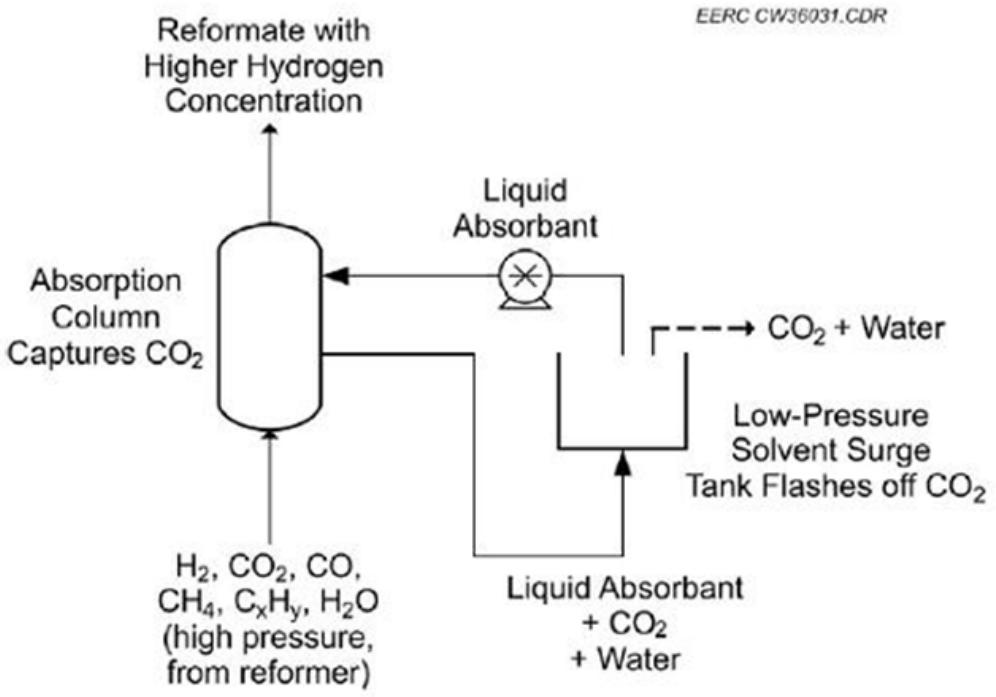

Figure 1. Liquid absorbent circulation system to remove carbon dioxide and water from a high-pressure reformate gas stream.

Table 3. High-pressure reformate gas composition upstream and downstream of an absorption column designed to remove carbon dioxide.

Reformate Gas Component	Concentration (vol%) Upstream of Absorption Column	Concentration (vol%) Downstream of Absorption Column
Hydrogen	76	96
Carbon dioxide	20.8	0.07
Methane	1.5	2.1
Carbon monoxide	1.5	1.8

Accomplishments

Work during this period of performance focused on optimization of the high-pressure production system. The reactor vessel was modified for higher hydrogen production and proof-of-concept testing was conducted for various high-pressure gas cleanup systems. The high-pressure carbon dioxide absorption experiments conducted resulted in promising proof-of-concept data for the high-pressure physical absorption technique of removing carbon dioxide and water. The absorption system will substantially reduce the load on downstream gas purification equipment (Oster et al. 2008).

Subtask 1.2 – High-pressure hydrogen purification process development and evaluation

Multiple activities were included in Subtask 1.2.

Activity 1.2.1 – ESA process development

Experimental

The HPWR process concept consists of converting JP-8 to a hydrogen-rich gas stream at pressures ranging from 3200 to 12,000 psi. To maximize the benefit of generating hydrogen at high pressure, a purification process that can work efficiently at these pressures without significantly reducing the pressure of the hydrogen is required. Separation membranes produce hydrogen with a pressure less than its partial pressure in the HPWR reformate stream. Conversely, adsorption systems produce hydrogen at pressures slightly less than the total gas pressure of the reformate. By producing and purifying hydrogen at the dispensing pressure, the need for high capital cost and energy-intensive hydrogen compression is eliminat-

ed. Currently, pressure swing adsorption (PSA) is the most common hydrogen purification technology in commercial use. In PSA, a pressure drop is used to desorb contaminants from an activated carbon sorbent, and clean hydrogen is used to purge the contaminants from the PSA vessel. Because effecting large pressure variations with hydrogen is expensive, the use of PSA at high pressure is unlikely to be economical. ESA represents a plausible alternative to PSA for hydrogen purification at high pressure, since ESA relies on electrical current variation rather than pressure variation to effect sorbent purging. Under this activity, the EERC evaluated the use of ORNL-developed ESA for purification of hydrogen produced from the HPWR process.

Granular activated carbon is a common sorbent used in both PSA and ESA, but the high intergranular porosity and macroporosity of typical granular activated carbon sorbents (about 80 percent) necessitates the use of large volumes of hydrogen to purge the mass of contaminated gas present within the pore structures. Additionally, granular carbon beds are poor electrical conductors. To address these technical issues, this activity focused on development of an electrically conductive adsorber with a significantly higher density than granular beds. Development of a dense electrically conductive monolithic activated carbon adsorber was accomplished through the use of powdered activated carbon and binder, which was then compressed to create a monolith with a density approximately twice that of the bulk density of powdered activated carbon. Absorptivity of the monoliths was tested by passing a mixture of H_2, CH_4, CO, and CO_2 gases through small cylinders of the material. Delays and breakthroughs of each gas in the mixture were evaluated. Figure 2 schematically shows the gas-mixing system and pressure vessel.

In addition to developing a dense electrically conductive monolithic activated carbon adsorber, a 12,000-psi ESA system capable of testing the purification technology on a standalone basis, separate from the HPWR system, was designed and built.

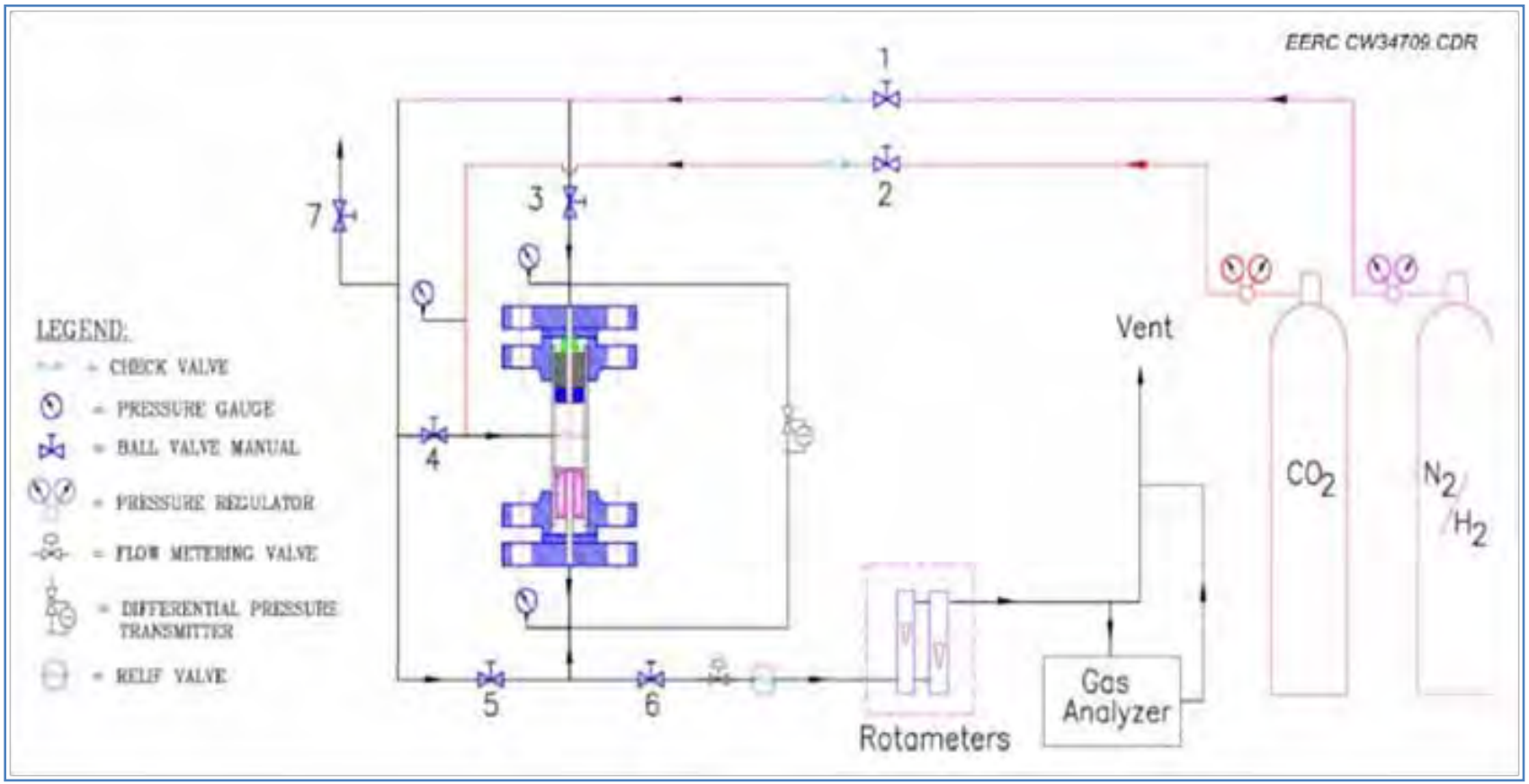

Figure 2. Schematic of the gas mixing system and pressure vessel used for testing the adsorber monoliths at pressures up to 1000 psig.

Results and discussion

High-density electrically conductive activated carbon monoliths were formed using both powdered and granular activated carbons and various binders. Approximately eight different types of activated carbons and five different types of binders were tested. The best first generation monoliths had an electrical resistivity of approximately 1.2 inch-ohms. Refinements in the methodology to produce the monoliths resulted in an increase in density and a decrease in electrical resistance. After the development of activated carbon treatments to reduce resistance, a second-generation monolith with resistivity of approximately one-tenth that of the first generation was developed. The lower resistivity reduces the amount of heating that occurs while driving off the gas.

Efforts were also made to produce activated carbon fiber composite monoliths. The composite material had an even higher density and lower resistivity than the pressed powdered activated carbon monoliths. As reported in last year's quarterly reports, efforts to activate the carbon fiber composites focused on physical activation using compressed carbon dioxide or steam. These attempts were unsuccessful because the pressure vessels could not reach a sufficiently high temperature for activation. In these experiments, chemical activation using potassium hydroxide and potassium carbonate was investigated for the carbon fiber monoliths. The chemical activation was more successful than the previous physical activation; however, the adsorptivity of the chemically activated carbon fiber was significantly lower (1/7) than the powdered activated carbon. As a result, the remainder of the testing focused on the monoliths made of the compressed powdered activated carbon.

Testing of the monoliths with a mixture of H_2, CH_4, CO, and CO_2 to simulate a reformate stream was performed. The order of breakthrough of the gases is H_2, CO, CH_4 and, finally, CO_2. Figure 3 shows typical results. The original concentrations of the different gases in the simulated reformate stream are signified by the horizontal lines in the graph. The data show the breakthrough times for the gases when passed through a 4-in. long cylinder of the monolith at a flow rate and pressure of 1.5 scfh and 200 psig.

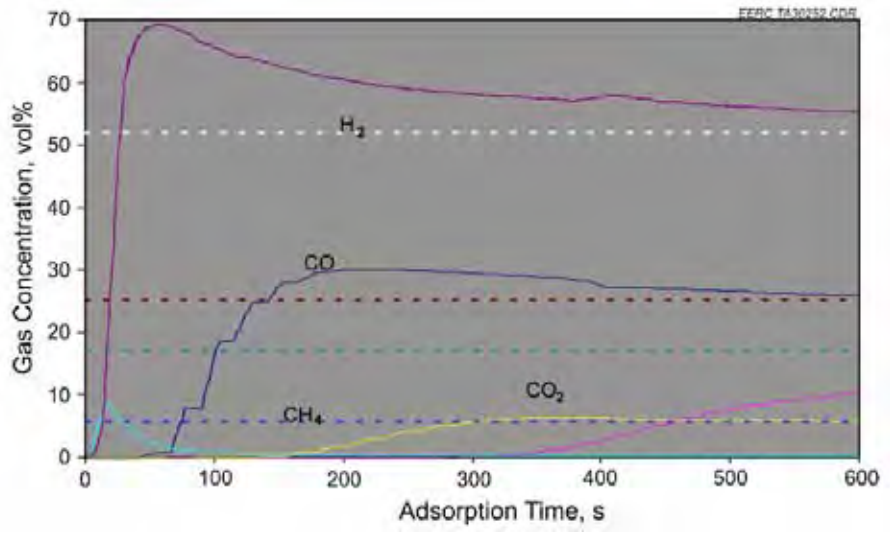

Figure 3. Gas breakthrough curves for a monolith tested at 200 psig with a simulated reformate gas stream.

The light blue line in the graph shows the breakthrough of oxygen that had been adsorbed on the carbon from the air before testing. Nitrogen was not measured directly, but can be calculated by difference. Adsorptivity tests were also performed at 300 and 800 psig. Breakthrough results were similar at the higher pressure. Regeneration of the first-generation monoliths was evaluated at up to 800 psig using electric currents. During the regeneration, significant heating of the monolith was noted, potentially indicating that gas desorption may be due to the heating and not the electric current alone. Regeneration testing of the second-generation monoliths has not yet been performed, but will be performed in future work under this activity.

Work in this activity continued with design and construction of the 12,000 psi ESA test system. Before finalizing the design of the system, project engineers were trained in high-pressure hydrogen technology. Design parameters required a quantifiable risk assessment of the system to ensure safe operation in an open pilot plant setting. Risk needed to be equivalent to that experienced by workers at a commercial hydrogen-fueling station. One engineer was certified as a hydrogen safety engineer.

Figure 4 shows a schematic of the 12,000 psi ESA test system. It is designed to allow mixing of simulated reformate gases from gas cylinders. The gas is then compressed to an operating pressure of 12,000 psi.

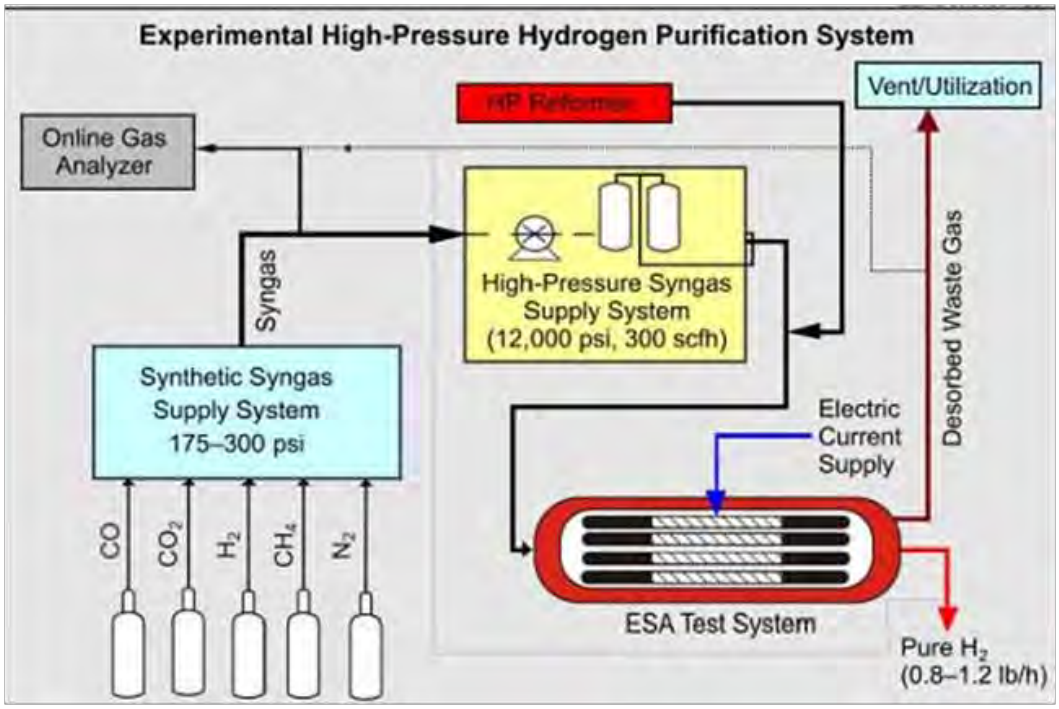

Figure 4. Schematic of the 12,000 psi ESA test system.

The system will be used in future work in this activity to refine operating procedures, determine gas adsorptivity and breakthrough behavior at high pressure, and develop monolith regeneration procedures. The system was designed for remote operation, and all electrical components meet the National Electrical Code Class 1 Division 2 rating for operation in environments that may contain explosive gases. A detailed risk assessment of the system was performed, and the system design modified as needed, to meet the suggested safety requirements of a commercial hydrogen refueling station. The 12,000 ESA test system was constructed and is ready for testing.

Figure 5 shows the two pressure vessels that will house the purification monoliths and valves and a meter for controlling gas flow during the adsorption and desorption cycles. Two monolith pressure vessels were installed: one for a 1.5-in. diameter monolith 24 in. long and the other for a 2.5-in. diameter monolith 36 in. long. The smaller vessel will be used in early development of operating procedures to reduce gas usage.

Figure 6 shows the air-purged box in which all electronic controls and data acquisition connections are made. The gas cylinders will be held in the rack along the right side.

Figure 5. Monolith pressure vessels and valves and regulators that control gas flow during adsorption and desorption testing. The open pilot plant setting can be seen behind the test system.

Figure 6. The air-purged electronics box in which all electronic connections are made.

Figure 7 shows the gas compressor and the back of the board holding gas-blending valves and regulators. The system is capable of blending up to five gases and compressing them from 175 to 300 psi inlet to up to 14,500 psi with a flow rate of up to 500 scfh. However, the standard operation will be for 175 psi inlet, outlet of 12,000 psi, and a flow rate of up to 300 scfh. The EERC technology for producing and purifying hydrogen at high pressures offers several advantages over systems that produce the hydrogen at low pressures and then compress it. The advantages include a smaller footprint, lower cost, lower operation noise, lower weight, and lower energy requirement.

Figure 7. The gas compressor and the back of the board holding gas-blending valves and regulators.

Accomplishments

Activated carbon monoliths were prepared and tested for potential use in the 12,000-psi ESA system.

For the ESA 12,000 psi system, all equipment and parts were received and installed, and computer programs have been written for remote operation and automatic shutdown in case of system failures or leaks.

A technical presentation entitled, "High-Pressure Hydrogen Purification Using Electrical Swing Adsorption," was given at the American Institute of Chemical Engineers' Spring national meeting in Tampa, FL, in March 2008.

Also during this reporting period, a gas analyzer for use in the purification method development work was purchased and received. The analyzer supported hydrogen purification work performed under Task 1.2.1 to determine the selectivity, capacity, and regeneration activity of the gas purification system.

Because of delays in delivery of equipment and required additional work related to safety issues, system shakedown and testing were postponed.

Activity 1.2.2 – Electrochemical hydrogen purification process development

Experimental

Electrochemical hydrogen purification process development work was investigated using simulated reformate gas mixtures and two modified fuel cells with each comprising two metal end plates, two graphite flow field plates, and a high-temperature membrane–electrode assembly (MEA) based on high-temperature polymer proton-conducting membranes. The component development and process optimization were carried out in an electrochemical cell with 5 cm^2 active area and using a single channel serpentine flow field. The process scale-up research was performed in an electrochemical cell with 50 cm^2 active area and using a parallel multichannel serpentine flow field. The two electrochemical cells have a similar structure (Figure 8). Figure 9 shows the two electrochemical cells. During the electrolysis, currents and potentials were controlled by an Autolab potentiostat/galvanostat integrated with a 20-A booster (Figure 10).

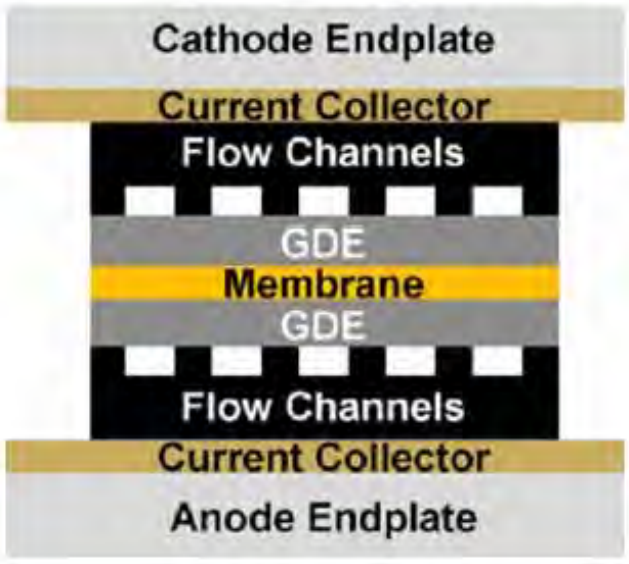

Figure 8. Schematic diagram of an electrochemical cell.

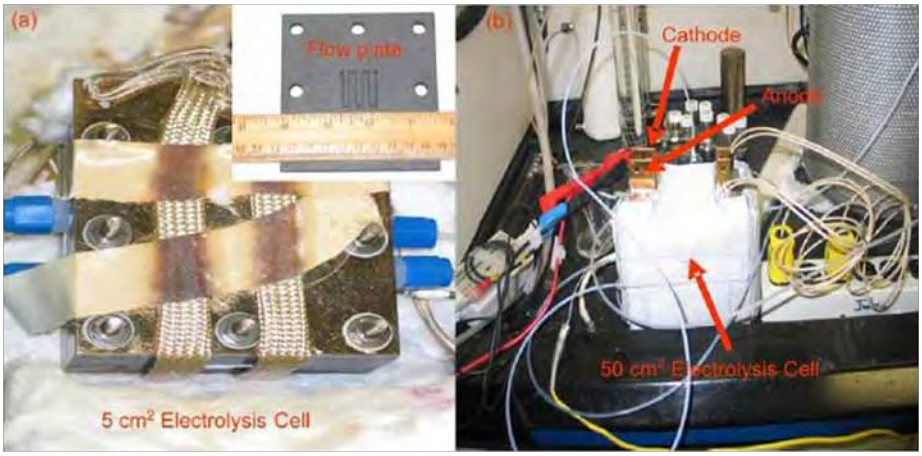

Figure 9. Images of electrolysis cell with an active cell area of 5 cm² (a) and 50 cm² (b).

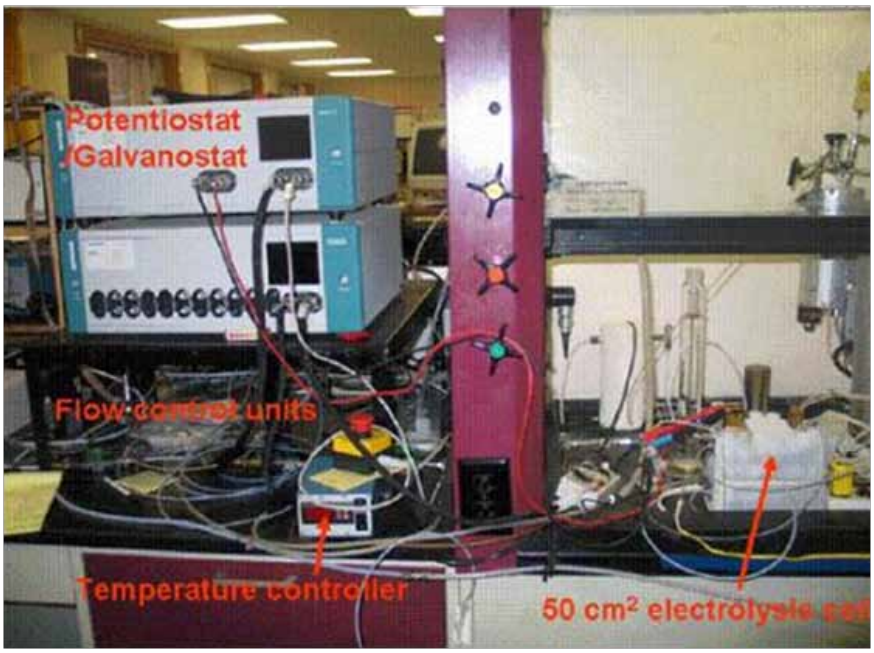

Figure 10. A controlling system for electrochemical hydrogen purification process, which comprises an Autolab potentiostat/galvanostat, mass flow controllers, and temperature control.

The gas streams were supplied directly from commercially available tanks without external humidification, except where humidification is noted. The external humidification was controlled by a water bath held at 60 °C, resulting in approximately 3 percent relative humidity at 160 °C, 6 percent at 140 °C, and 10 percent at 120 °C. The pressure was not regulated and open to the atmosphere. All tests were performed in the temperature range of 140 – 180 °C. The fuels included pure hydrogen and simulated refor-

mate gas (76 percent H_2, 2 percent CO, 2 percent CH_4, and 20 percent CO_2). High-purity nitrogen was fed to the cathode side to carry hydrogen purified for gas analysis using an Agilent 7890A gas chromatograph (GC).

Gas diffusion electrodes with a platinum loading of 1.0 mg/cm^2 were used as the cathode. The MEAs were fabricated by hot-pressing a piece of membrane between the two Kapton-framed electrodes. The MEA was then assembled into a single cell testing hardware.

Results and discussion

Electrochemical hydrogen purification using 5-cm² electrolysis cell.

Initial proof-of-concept work was performed by feeding simulated reformate gas and pure nitrogen gas through the anode chamber and cathode chamber, respectively. Under open-circuit potential (OCP) and at atmospheric pressure and 140 °C, hydrogen permeated the polymer membrane, and CO_2 crossover was too low to be detected by GC analysis. In a constant-current electrolysis mode, only H_2 was detected as an exclusive cathode product, and no CO, CH_4, or CO_2 was detected. For the purpose of comparison, pure H_2 was fed to the anode side in replace of the simulated reformate gas, the similar results were obtained with H_2 produced at the cathode side. The production rates of H_2 from pure H_2 and the simulated reformate were similar under the same constant current conditions. These results indicated the viability of the proposed electrochemical hydrogen purification method at ambient pressure.

The optimization of the hydrogen purification process focused on the MEAs for decreased cell voltage and increased electrochemical reaction rate. The prepared MEAs were evaluated as a function of reaction temperature based on the measured potential-current curves with hydrogen as reactant input through both anode and cathode chambers of a modified fuel cell. At temperatures relevant to the purification process operating conditions, a typical cell voltage is around 0.2 V at a constant current density of 200 mA cm^{-2}, with dry H_2 as the input. This cell voltage was decreased to 0.15 V at the same current density when dry H_2 was switched to wet H_2. This decrease in the cell voltage is mainly caused by the increase in electrolyte membrane conductivity in the presence of moisture. It is expected that the cell voltage could be further decreased at a controlled cur-

rent density via further optimization of the MEAs and operating conditions.

Two approaches were used to improve performance of MEAs for increased current density and decreased cell voltage. Because the high-temperature gas diffusion electrodes used were designed for aqueous electrolyte-based electrochemical processes, no three-dimensional net channels for ion conduction inside the electrodes themselves were developed. Since the electrochemical reactions occur only at the interfacial area between the electrode and the polymer electrolyte membrane, the total electrochemical reaction areas were expected to be low. Because the polyelectrolyte solution is not commercially available, a one-step synthesis of the high-temperature polymer electrolyte was developed. The synthesized polymer solution was used to impregnate the electrode layers for improved reaction areas. The second approach evaluated was the optimization of the hot-pressing process for the preparation of MEAs.

Electrochemical hydrogen purification using a scaled-up electrolysis cell

The optimization of the electrochemical hydrogen purification process at atmospheric pressure was completed. The optimized process was demonstrated using a high-performance, high-temperature MEA with highly developed solid electrolyte and electrode interfaces and dry simulated reforming gas comprising 76 percent H_2, 2 percent CO, 2 percent CH_4, and 20 percent CO_2. At three operating temperatures of 140, 160, and 180 °C, only hydrogen was produced at the cathode. The current efficiency for the hydrogen purification process was greater than 90 percent at the test temperatures noted and at a constant current of 200 mA cm^{-2}. The cell voltage measured at this constant current density was dependent on the operating temperature. At 140 °C, a value of approximately 0.14 V was obtained. This value decreased to approximately 0.06 V when the temperature was increased to 180 °C. The cell voltage remained nearly constant at controlled constant current polarizations (Figure 11).

Electrochemical hydrogen purification using a pressurized scaled-up electrolysis cell

The design and construction of a pressurized electrochemical cell were initialized, and the integration of the controlling system was initiated.

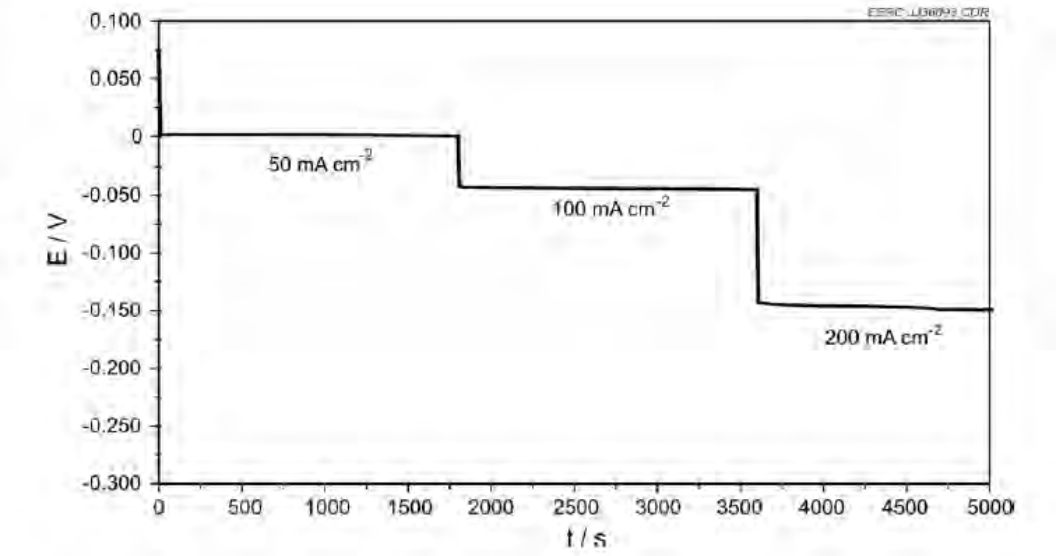

Figure 11. Dependence of cell voltage as a function of reaction time under controlled constant current conditions at 140 °C.

Accomplishments

The purification process was further investigated as a function of process shutdown and restart. Pure hydrogen gas was produced at the cathode. High current efficiency and stable low cell voltage were reproduced. The progress made at atmospheric pressure enabled initialization of work to tailor the process for use at elevated pressure.

The feasibility of electrochemical hydrogen purification process was demonstrated, and the electrochemical process was optimized at ambient pressure. Low cell voltage, high reaction rate, and high current efficiency were achieved for the purification process. Work was initialized on tailoring the process for use at elevated pressure.

The next phase of work will focus on the feasibility demonstration and optimization of high-pressure hydrogen purification processes.

Activity 1.2.3 – Hydrogen production and purification systems integration

The system integration design team has completed a draft piping and instrumentation diagram and has begun specifying equipment for the integrated hydrogen production, purification, and dispensing system. Some pressure vessels will be purchased; however, many components of the current reforming system will be used in the new integrated system. The sys-

tem, when modified, will include hydrogen production, purification, and dispensing in a continuous, integrated process.

Subtask 1.3 – Hydrogen dispensing and use

The objective of this subtask is to advance the development of FCEH vehicles through demonstration of fuel cell-powered vehicles and hydrogen dispensing and refueling systems at military installations.

Experimental

With respect to hydrogen as a tactical fuel, the increased efficiency of an FCEH vehicle (running on onboard-stored hydrogen) versus a comparable-power internal combustion (IC) engine vehicle is well documented. The work performed under this subtask was designed to quantify the actual efficiency increase achievable in specific military applications and to develop vehicle performance and maintenance data. The vehicle performance and maintenance data are critical to assessing the military viability of FCEH vehicles for mobility applications, including applications whereby multiple power-generating assets can be combined, thereby reducing the number of power generators and the complexity of maintaining and operating those assets.

Results and discussion

Technical work focused on ensuring that vehicle design, use, and refueling operations were compatible with hydrogen production and dispensing operations. The following sections describe systems and vehicles developed under this activity.

Mobile hydrogen refueler

In collaboration with Kraus Global and Airgas Inc., a high-pressure (5000 psi) hydrogen-dispensing system was designed and fabricated by the EERC, based on the use of delivered cylinders of 6400 psi hydrogen (Figure 12). The refueling station was operated extensively for over 12 months in cold winter and hot summer weather at GFARNGB.

Figure 12. Mobile hydrogen refueler.

FCEH forklift truck

A 5000-lb capacity FCEH forklift truck was designed and manufactured by ePower Synergies and demonstrated at GFARNGB. This vehicle represented an early application of an electric forklift and plug-and-play fuel cell pack using commercially available off-the-shelf technology. The standard battery pack was removed from a Hyster 50 forklift and replaced with a fuel cell pack produced by General Hydrogen. The General Hydrogen Model FS-0002 Hydricity Fuel Cell Pack consisted of a Ballard 80-V 9-kW fuel cell stack, 5000 psi hydrogen tank capable of holding 1.79 kg of hydrogen and an ultracapacitor system to provide energy storage and transient power. Beginning in 2006, the FCEH forklift and refueling station were operated extensively for over 12 months in cold winter and hot summer weather. In December of 2007, a second forklift was assembled by ePower and delivered to Robins AFB for subsequent use and demonstration.

Hyster forklift truck

In 2009, a third FCEH forklift was assembled based on the Hyster 50 platform (Figure 13). A Hydrogenics HyPX-1-33 fuel cell pack was used to replace the battery pack of the forklift. The Hyster 50 and Hydrogenics fuel cell pack were delivered to the EERC and assembled before being shipped to Robins AFB. The FCEH forklift provided equivalent performance to a standard forklift and had several features that improved operability over the previous forklifts demonstrated in 2006 and 2007. The fuel cell pack possessed a 12-V battery in addition to the ultracapacitors. The 12-V battery works similarly to the battery of an automobile, providing start-up power even when the forklift had sat unused and the ultracapacitors had lost their electrical charge. The Hydrogenics HyPX-1-33 fuel cell provides plug-and-play capability with the Hyster 50 forklift. The only custom fabrication modification performed by the EERC was fabrication and installation of a steel plate under the fuel cell to increase the vehicle weight to that of the original battery-powered vehicle. This increase in weight maintained the forklift lift capacity consistent with the stock battery-powered Hyster 50. This vehicle will continue to be used at Robins AFB under the direction of the Advanced Power Technology Office (APTO).

Figure 13. FCEH Hyster forklift.

Bobcat Toolcat

Following the completion of two FCEH forklift vehicles, ePower worked with GFARNGB and APTO personnel to develop design specifications for a MPUV based on the Bobcat Toolcat vehicle platform. The vehicle was designed and fabricated with a hub motor for each wheel and significant upgrades to the frame and suspension to meet the tow requirements of an aircraft tug vehicle. The Toolcat was delivered to Robins AFB and evaluated by APTO personnel and then shipped to the EERC where staff conducted a detailed inspection in which the systems were reviewed and documented in a series of as-built drawings. Evaluation of the vehicle by APTO personnel and EERC staff determined that the Toolcat was not well suited for use as an aircraft tug. Further design modifications were identified that, if implemented, would allow the vehicle to have performance capabilities similar to a standard diesel-powered Bobcat Toolcat. The vehicle has undergone several modifications in an effort to achieve this standard level of performance using the hydrogen-powered fuel cell system. In its current configuration (Figure 14), the Bobcat Toolcat uses a hydraulic drive system powered by the fuel cell. The vehicle is fully functional, but lacks the efficiency and power that could be achieved with a fully electric drive system. Future work is anticipated in which improvements to the drive system and component integration will take advantage of the efficiency benefits of a hydrogen-powered fuel cell.

Figure 14. Current configuration of the Bobcat Toolcat.

Accomplishments

Several vehicles and a hydrogen-refueling system were designed, built, and tested under a range of hot to cold weather conditions. The refueling system remains in service at GFARNGB. Two hydrogen-powered forklift trucks remain in service at Robins AFB, and the Bobcat Toolcat is fully functional after modifications; however, additional modifications are planned.

4 Fuel Production from Alternative Feedstocks (Task 2)

Task 2 included development of alternative (nonpetroleum) feedstock-based technologies for production of advanced tactical fuels with JP-8 drop-in compatibility and improved properties for use as hydrogen feedstocks.

Subtask 2.1 – Advanced gasifier development for clean syngas generation

Gasification is one of several thermochemical conversion technologies capable of providing advanced fuels and energy to the military using domestic feedstocks such as biomass, coal, municipal solid waste, or field waste. The activities conducted under this subtask were focused on testing an advanced gasifier, designed and fabricated for this project, capable of producing a variety of syngas compositions from a range of feedstocks with diverse physicochemical properties. The objective of this effort was to demonstrate the operational flexibility of the advanced gasification system to accommodate numerous feedstocks to produce different syngas compositions ideally suited for applications such as power generation in IC engine generators, distributed hydrogen production, and liquid fuel synthesis reactions such as FT.

One of the greatest challenges to commercial deployment of distributed gasification systems has been the inability to effectively gasify a variety of fuels with different physical and chemical characteristics. The EERC's advanced gasifier addresses this challenge by providing exceptional operational control allowing the system to accommodate a wide variety of fuels and associated char reactivity while still providing self-sustained steady-state gasification and providing near-complete carbon conversion.

Advanced gasifier system description

The gasifier design philosophy is based on the production of clean syngas with high conversion efficiency and achieving near-zero effluent discharge from the overall system. The production of clean syngas is achieved by

converting the complex organics in the hot zones of the gasifier. The near-zero effluent discharge is achieved by recycling the trace amount of unconverted organics in the syngas into the gasifier hot zones such that the syngas (composition) production is favored.

The main components of the gasifier system include a fixed-bed downdraft gasifier reactor, a fuel feed system, a syngas scrubbing and polishing system, a syngas exhaust system, an auxiliary fuel feed system, a residue extraction system, an induced-draft (ID) fan, and an instrumentation and control system. Figure 15 shows the process flow diagram of the gasification system, which is shown in Figure 16. Figure 17 shows a 3-dimensional representation of the gasifier. The system is classified for Class 1, Division 2, Group B for the operation of electrical components in explosive gas environments.

Chipped fuels are screw-fed from the top of the gasifier. The syngas is removed from the reactor outlet at the bottom of the gasifier. The nominal throughput of the biomass is 33 lb/hr; however, maximum capacity can reach 100 lb/hr depending on the type and size of the fuel, its reactivity, and gasifier operating parameters. The fuel hopper can store about 200 lb of biomass or 400 lb of coal. Gasification air is injected from the top of the gasifier under the suction caused by the ID fan located downstream of the syngas scrubber system. The fuel bed is ignited with the help of a hot air generator especially adapted for the system. After ignition, the reaction front propagates and attains the steady-state exothermic heat profile necessary for maintaining gasification reactions. Steady-state gasification can be achieved within 30 minutes of ignition, depending on the fuel moisture content and fuel reactivity. Specially designed vertical augers are used to extract solid residue and provide the added function of supporting the bed.

Clean syngas is produced in the hot zone of the gasifier by staging the oxidizer to combine devolatilization, partial oxidation, and reduction reactions. The reactor geometry in the upper zone of the gasifier is designed to allow a smooth flow of the chipped fuel and gasification air. The air injection occurs in this zone. The air injection is balanced by forced-draft and ID fans such that the overall gasifier operating pressure is maintained slightly below atmospheric pressure.

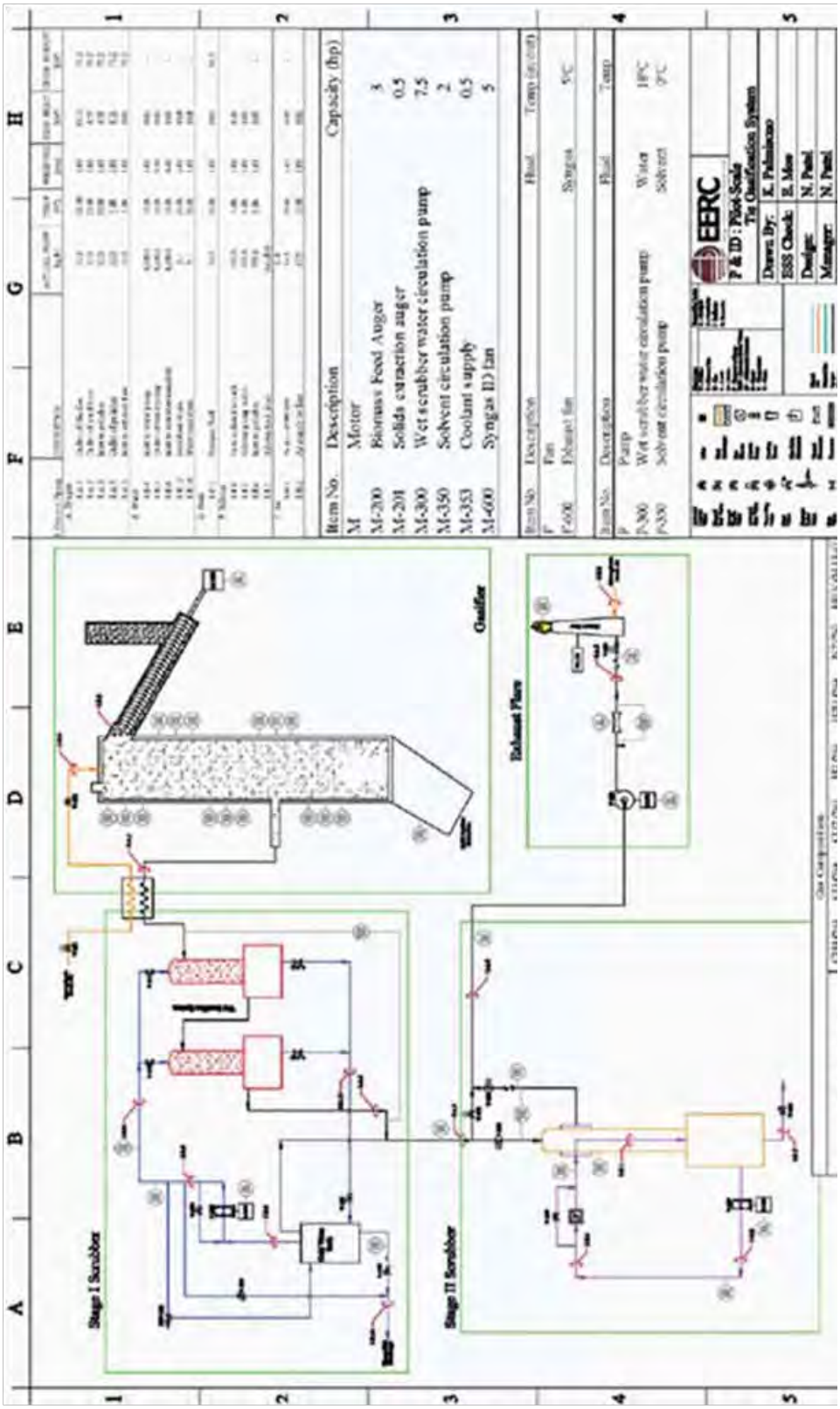

Figure 15. General process flow diagram of the advanced pilot plant gasifier.

Figure 16. Photographs of commissioned advanced fixed-bed gasifier pilot plant.

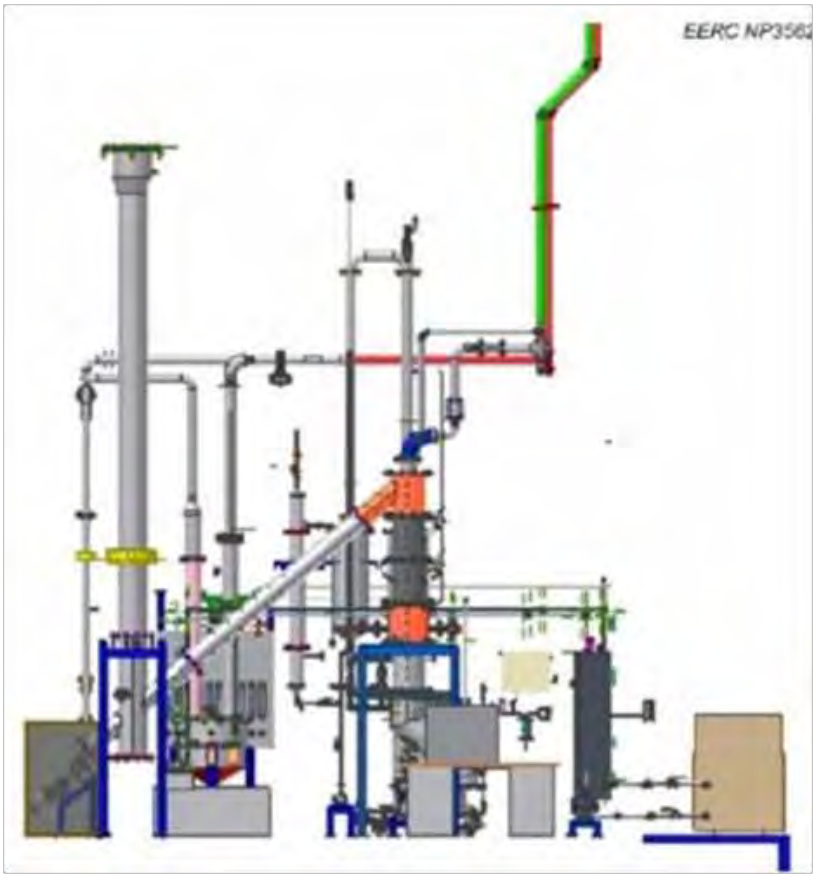

Figure 17. Three-dimensional view of the pilot plant gasifier depicting the major components of the system.

The ID fan located downstream of the syngas cleanup system is sized to overcome the system pressure drop (of about 30–40 in. of water column) at a rated flow rate. The pressure sensor at the inlet controls the forced-draft fan used for injecting gasification air through a preheater. To improve the conversion and thermodynamic efficiency of the system, extractable sensible heat from the syngas is recycled back into the gasifier by using gasification air as a heat carrier fluid.

To achieve near-zero effluent discharge and improve the composition of syngas, the effluent from the scrubber section is injected into the gasifier. The condensed tar and particulate matter along with a small fraction of water are injected into the reactor hot bed such that the hydrodynamics or the reactor temperature profile is not affected. The inert inorganic residue removed from the gasifier is the only disposable material generated from the system.

Syngas, after exiting the reactor, is scrubbed in a two-stage water scrubber and syngas polisher. The first section cools the hot syngas and removes the condensable tars. The second stage effectively scrubs the remaining tars that are typically formed only under high tar loading conditions attained during severe conditions such as high throughput or high fine loading, etc. The final syngas polisher removes carryover tar with a liquid solvent. This syngas polishing system can be bypassed depending on the syngas quality required. Both scrubbers are closed-looped systems to facilitate determination of condensable and soluble organic and inorganic components of the syngas. The solids removed in the scrubbing mediums can be removed in the filtration system.

The flow rate of the syngas and gasification air is measured using orifice flowmeters. The syngas flowmeter is located downstream of the blower; the gasification injection air is measured upstream of the gasifier.

The clean syngas is routed through the enclosed combustor and flared at an elevation of 16 ft from the roof height. The flare in the pilot system has a hot surface igniter; the combustion air is induced by the ejector effect caused by the flow of syngas. A gas-sampling port is available for determining flare emissions.

The clean syngas composition is determined using an online gas analyzer capable of measuring CO, CO_2, O_2, N_2, H_2, CH_4, and higher hydrocarbons. A quasi online GC is used for determining trace hydrocarbon gases in the syngas. Additional sample ports are available for conducting isokinetic sampling of syngas to measure tar and particulate matter according to the modified European Tar Protocol (Neeft et al. 2002) and EPA Method 5. These samples can be obtained from the syngas both before and after syngas cleanup unit operations.

The bed and syngas temperatures are measured at several locations to provide both process control and operational monitoring.

Fuel selection

The gasification experiments were conducted on five fuels that considered most challenging, but that have commercial interest in being used without requiring any preprocessing, including drying or screening fines. Since

these preprocessing efforts are capital-intensive and are not practical for distributed applications because of economic or environmental reasons, the experiments were conducted on the fuels as received. These fuels included high-moisture wood waste, Powder River Basin (PRB) coal, and creosote-treated railroad ties. Figure 18 shows fuel samples used in the pilot plant test. The writing pen shown along with the fuel is to provide an estimation of the relative size of the fuels and the fraction of fines.

Table 4 summarizes the results from proximate and ultimate analysis of these fuels as well as data on typical oak wood and oakwood charcoal.

35 percent moisture pine wood

This fuel consisted of chipped pine lumber collected from a residential roof truss plant in Grand Forks, ND. The average moisture content of the batch of fuel received was about 9.2 percent. The moisture in the pine wood waste was increased to 35 percent by adding water to the batch of 1000 lb to match with the typical moisture content of the fuel stored in the exposed piles outside the plant premises to determine gasifier performance on actual fuel.

Figure 18. Sample of fuels used in the pilot plant test.

Table 4. Comparative fuel analysis of woody biomass wastes, oak and pine wood, PRB coal, and oak wood charcoal used in the experiments.

Fuel	Oak Wood	35% Moisture Pine Wood		Railroad Tie 2		Railroad Tie 4		Marcel Wood Chips		GF Municipal Wood Waste		PRB Coal		Oakwood Charcoal	
	From Literature	Moisture-, Ash-Free	As-Received	Moisture-, Ash-Free	As-Received	Moisture-, Ash-Free	As-Received	Moisture-, Ash-Free	As-Received	Moisture-, Ash-Free	As-Received	Moisture-, Ash-Free	As-Received	Moisture-, Ash-Free	As-Received
Proximate Analysis, wt%															
Moisture	–	9.2	–	31.9	–	23.7	–	33.5	–	43.6	–	22.7	–	5	–
Volatile matter	81.28	76.99	84.97	56.95	85.83	65.73	87.22	51.17	77.47	39.57	71.43	25.6	35.98	19.68	21.1
Fixed carbon	17.2	13.66	15.03	9.38	14.17	9.58	12.78	14.26	22.53	15.84	28.57	45.97	64.02	73.58	78.9
Ash	1.52	0.15	–	1.76	–	0.99	–	0.17	–	0.99	–	5.48	–	1.74	–
Ultimate Analysis, wt%															
Hydrogen	5.38	6.58	6.13	7.85	6.49	7.83	6.9	8.27	6.89	8.34	6.31	5.5	4.78	3.21	2.85
Carbon	49.28	44.67	49.3	40.29	60.72	49.23	65.33	34.45	52.15	32.43	58.55	54.91	76.4	77.93	85.53
Nitrogen	0.035	0.15	0.016	0.27	0.41	0.44	0.59	0.16	0.25	0.28	0.51	0.75	1.04	0.38	0.41
Sulfur	0.01	0.2	0.22	0.12	0.18	0.21	0.27	0.19	0.19	0.01	0.02	0.56	0.77	0	0
Oxygen	43.13	48.26	44.19	49.71	32.19	41.29	26.9	40.23	40.51	57.94	34.61	32.35	17	1.74	0
Heating Value															
MJ/kg	19.42	17.33	19.12	15.79	23.80	18.34	24.34	12.71	19.25	11.85	21.40	21.16	29.44	21.16	34.18
Btu/lb	8349	7451	8223	6790	10,233	7888	10,468	5467	8277	5097	9200	9098	12,659	9098	14,697
C/H ratio	9.16		8.04		9.36		9.47		7.57		9.28		15.98		30.01
C/O ratio	1.14		1.12		1.89		2.43		1.29		1.69		4.49		–
C/C (oak)	1.00		1.00		1.23		1.33		1.06		1.19		1.55		1.74
CV/CV (oak wood)	1.00		0.98		1.23		1.25		0.87		0.97		1.33		1.55

Railroad ties

Creosote-treated railroad ties were also identified as a fuel of commercial interest. This is a complex gasification feedstock containing hardwood and coal-derived creosote used as a treating agent. The creosote is a mixture of different distillation fractions of hard coal tar. The main compounds in the creosote are polycyclic aromatic hydrocarbons (PAHs) and heteroaromatic compounds such as naphthalene, quinoline, acenaphthene, dibenzofuran, fluorene, phenanthrene, anthracene, fluoranthene, and pyrene. To further complicate railroad tie chemistry, this feedstock is exposed to changing environmental conditions, and the ties are often coated with lubricants and fuel. Table 5 lists data from proximate and ultimate analyses conducted on rail ties from two different sources. The differences observed from these two samples can be attributed to differences in creosote used to treat the railroad tie as well as different environmental conditions over the service life of the railroad tie. Tie 2 came from a source in the United States, and Tie 4 from Kamloops, British Columbia, Canada.

Marcel wood chips

This wood waste was obtained from legacy piles or landfill located near a sawmill situated in Marcel, MI. The moisture content of the fuel determined was 33.5 percent, which is about 1.5–25 percent lower than fuel processed during the gasification test.

Grand Forks municipal wood waste

The composition of the municipal waste wood in Table 4 shows 43.6 percent moisture on an as-received basis. However, additional moisture analysis was conducted on this feedstock during testing to gather representative data on fuel chemistry as it was fed to the gasifier. Moisture data collected over the course of 2 test days show a range of moisture content from 51.0–60.6 percent from a single 1500-lb batch of waste wood. Data from the gasification of this fuel were obtained on 19 October 2009 (refer to Table 5), and represent a waste wood fuel possessing, on average, 52.69 percent moisture.

PRB coal

Coal feedstock, one of the fuels of interest for distributed hydrogen production, contained of about 25 percent moisture. The coal was Montana sub-bituminous, commonly known as PRB coal.

Table 5. Grand Forks municipal waste wood moisture.

Sample	Units	10/1/2009	10/12/2009
Sample 1	%	59.6	51.0
Sample 2	%	58.2	53.1
Sample 3	%	61.6	52.2
Sample 4	%	62.9	54.4
Average	%	60.58	52.68
Standard deviation	%	2.09	1.44

Comparative fuel analysis of railroad ties, wood, and PRB coal

Composition data collected for the various fuels were compared to oak wood, which is the type of wood typically used in making railroad ties. Volatile matter was the highest in the two railroad tie feeds; however, similar volatile matter was measured in the oak wood, pine wood, and railroad ties ranging from 81.28 to 87.22 wt% on a moisture- and ash-free basis. The volatile matter of the waste wood chip samples was slightly lower than that of the other wood samples and the PRB coal had the lowest volatile matter, about 35 percent on an ash- and moisture-free basis.

Fuel volatile content is an important parameter in gasification. The fuel particle size and associated heating rate typically determine the yield and devolatilization rate in the gasifier. However, fuels with high volatile contents such as railroad ties, can achieve higher devolatilization rates leading to higher tar concentration in the syngas. A high devolatilization rate may have the effect of reducing gas-phase residence time of volatile product, therefore limiting opportunity to crack the tars in the high-temperature zone. Additionally, the higher devolatilization rate can reduce the gasifier bed temperature because of excessive heat loss caused by convection or endothermic organic devolatilization. The EERC's advanced gasifier has been designed to accommodate fuel with high volatile content, and through proper process control, railroad ties have been gasified while demonstrating improved syngas composition, increased gasification efficiency, and reduced tar formation.

Table 4 lists the comparative data of C/H and C/O ratio of the fuels. C/H values of woody fuels ranged between 7.57 and 9.28, while the values for ties are in a higher range, 9.36 to 9.47, indicating the presence of carbon-rich organics typically found in coal tar or creosote. The C/H of coal and

oak charcoal are 15.98 and 30.01, respectively. At these elevated C/H ratios, fixed-bed gasification would typically produce a CO-rich syngas.

The concentration of oxygen in the fuel is critical in estimating the required oxidizer-to-fuel ratio to attain the desired gasification operation and syngas quality. The ability to adjust process inputs, such as feed or air, ensures effective feed conversion and low tar formation. The C/O ratio of the wood biomass fuels ranged from 1.12 to 1.69. By contrast, the values for railroad ties range from 1.89 to 2.43, and PRB coal had a C/O ratio of 4.5. In response to these feedstock characteristics, a higher oxidizer feed rate was used when testing fuels such as railroad ties and coal.

For comparison, Table 4 lists the carbon content of the different fuels as a ratio of fuel carbon to that present in oak wood. The carbon content in railroad ties is 23 to 33 percent higher than oak wood, while in PBR coal, it is about 55 percent higher than oak wood. The calorific value of the ties and coal are about 25 and 33 percent higher than oak wood, while the oak wood charcoal is about 55 percent higher than dry, ash-free wood.

Oakwood charcoal gasification

During gasifier start-up, charcoal was used as the bed fuel for ignition and reactor heatup. Data were collected during start-up and, for a short period of time, at steady-state operation. The results of the charcoal gasification test are presented to compare the variations in gas composition and bed temperature observed during railroad tie gasification with low-volatile-fraction charcoal. Figure 19 shows test results depicting syngas composition and bed temperature variation with time for three phases of gasification (ignition, devolatilization, and carbon gasification).

A steady-state bed temperature is observed to have been attained soon after sustained ignition occurred. The oxygen concentration reduced to near zero percent, while the concentration of combustible syngas species (H_2, CO, and CH_4) increased. Since the char contains volatiles during the initial gasification phase, the concentration of H_2 and CH_4 species attains peak values.

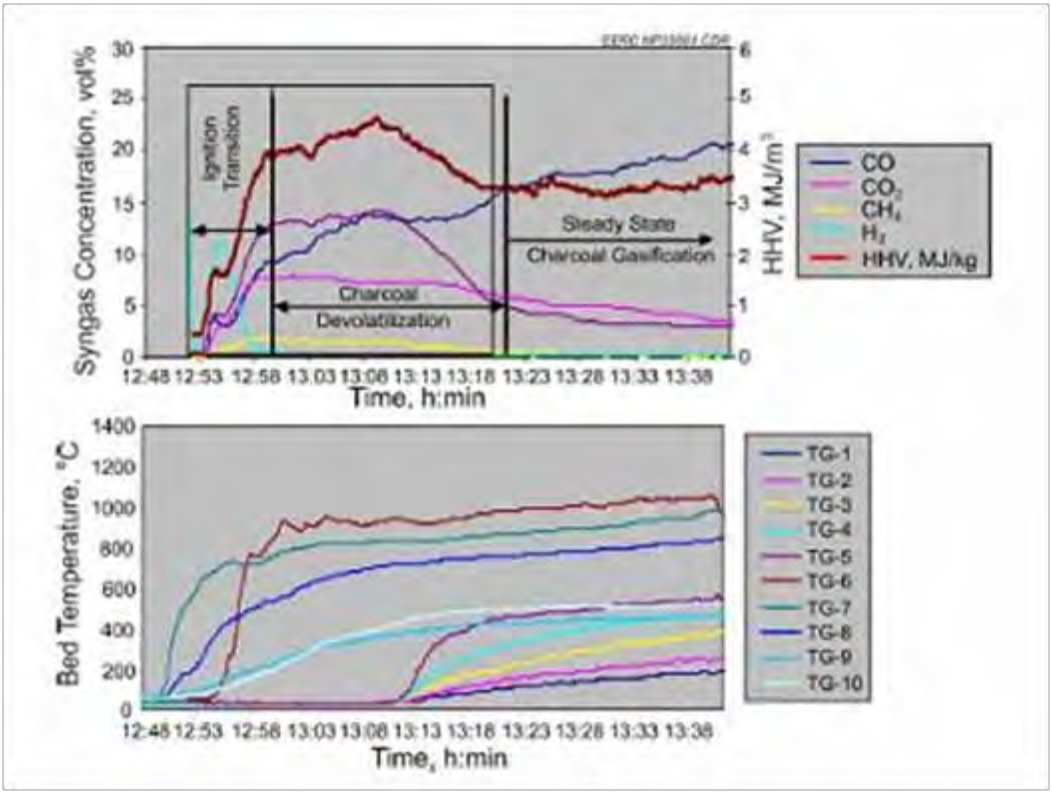

Figure 19. The charcoal gasification test results depicting syngas composition and bed temperature variation with time obtained during ignition, devolatilization, and carbon steady-state gasification.

In this batch mode charcoal gasification experiment, the fuel volatiles depleted rapidly, resulting in reduced H_2 and CH_4 concentrations. Subsequent carbon gasification resulted in an increase in CO concentration, peaking at about 21 percent. The CO_2 concentration decreased during this gasification phase until complete conversion of carbon in the bed occurred. A CO/CO_2 ratio greater than 10 obtained in the gasifier is attributed to the ability of the gasifier to maintain bed temperature profiles such that near-complete conversion of carbon is possible under self-sustained (without external heating) gasifier operation.

35 percent pine wood gasification

This test was conducted with the aim of acquiring steady-state operational data for a full day of operation while operating on high-moisture fuels. The feedstock for this test was a 35 percent moisture content pine wood. The system was operated for a total of 14 hours, 13 hours of which pine wood fuel was being gasified. The gasifier operating condition was unaltered during the test run except for small variation in fuel moisture levels typical of woody biomass stored in open space.

Figure 20 shows results from gasifying 35 percent moisture pine wood waste. The test was ended voluntary after approximately 13 hours of operation on pine wood fuel. The fuel conversion rate was 61 lb/hr. Besides high moisture content, this fuel consisted of about 10 to 15 percent fines, an unacceptably high concentration for commercial downdraft gasifiers. The fuel was continuously injected at a constant rate, and the bed height remained constant. The syngas was cleaned in the pilot plant scrubber system. Fuel ash content was low; therefore, the residue dump system was not operated during the test. The gasifier produced water at a rate of 8.1 L (2.14 gal/hr). The clean syngas was flared.

Table 6 summarizes syngas composition and higher heating value. The average H_2/CO ratio achieved was 1.51; the highest ratio achieved was 2.26. The high concentration of CO_2 was primarily due to water–gas shift reaction. It would be possible to produce a syngas with lower CO_2 concentrations in the current gasifier design using different operating conditions.

The average CH_4 and higher hydrocarbons (C_xH_x) concentration in the syngas was 1.5 and 0.5 percent, respectively. The highest CH_4 concentration measured was 2.2 percent, with a higher hydrocarbon value of 1.2 percent for a total of 3.4 percent total hydrocarbons. These values were observed for a duration of only 3 to 4 minutes during the test. Since instantaneous tar concentration cannot be measured, the CH_4 concentration was used as an indicator of tar production. Generally, a CH_4 concentration greater than 2 percent indicates that heavier tars are being formed.

The bed temperature profile shows a significant variation in the high-temperature zone of the gasifier. The average bed temperature achieved was 850 °C, which is desired for attaining carbon gasification and is indicated by consistent CO and H_2 concentration in the syngas. The upper bed temperature was below 250 °C. Evaporation and devolatilization occur in this upper cold zone before ignition of the particles in the bed. The bed depth was found to be greater (from TG-3 to TG-9) as an effect of higher moisture content in the test fuel. In contrast to this, the upper bed depth for drier fuels such as charcoal and pre-dried tie consisting of 5 percent was small TG3 – TG5 (Figure 20). This feature of the expansion of the cold zone can be compared to the effect of moisture on single particle ignition delay as earlier observed by Patel et al. (1996) in the case of single particle combustion studies performed on distillery effluents consisting of moisture ranging from 0 to 45 percent.

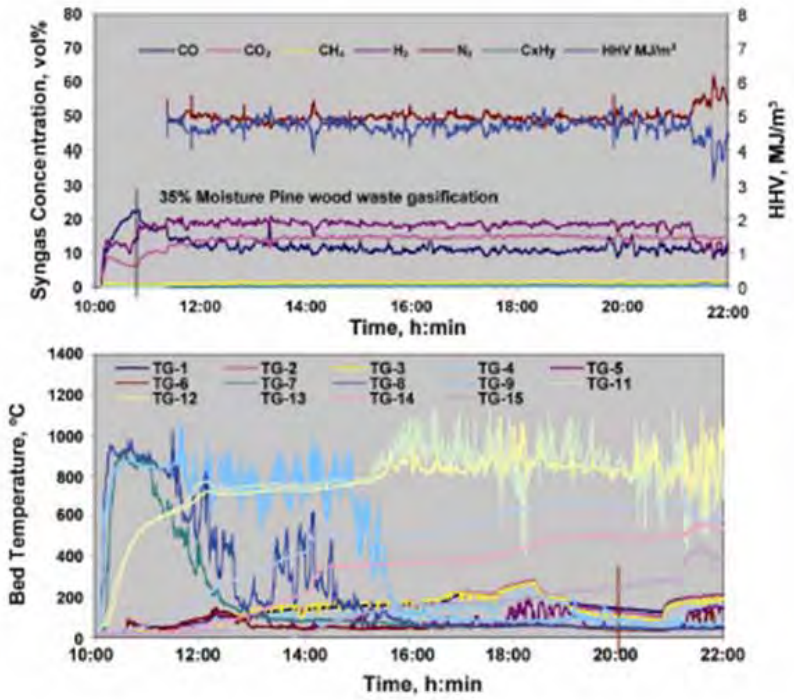

Figure 20. The 35% moisture pine wood waste gasification test results depict syngas composition and bed temperature variation with time obtained during steady-state gasification.

Table 6. Average syngas composition and HHV of the syngas (35%-moisture content pine wood) and standard deviations.

Parameter	CO, %	CO_2, %	CH_4, %	H_2, %	N_2, %	C_xH_y, %	HHV,MJ/m^3
Average syngas composition	12.1	14.1	1.5	17.2	50.3	0.5	4.7
Standard deviation	2.2	1.8	0.4	2.8	2.6	0.2	0.3

The syngas production to biomass feed ratio was 2.57. The flow rate remained almost constant during the experiment. The average higher heating value (HHV) of the gas was 4.7 MJ/m^3, which is acceptable for IC engine operation for electrical generation applications. Inorganics from the fuel did agglomerate into small deposits less with diameters less than 1 in.; however, the bed temperature distribution helped maintain the solid movement and avoid formation of larger deposits.

The concentration of trace gaseous hydrocarbons consisting of ethylene, ethane, propane, and propylene were an order of magnitude lower than the methane concentration (right-hand abscissa). The variation in the trace hydrocarbon concentration is nearly proportional to the variation in the methane concentration. The H_2S and COS concentration time profile shown in Figure 21 shows no direct relationship with the variation in hydrocarbon concentration.

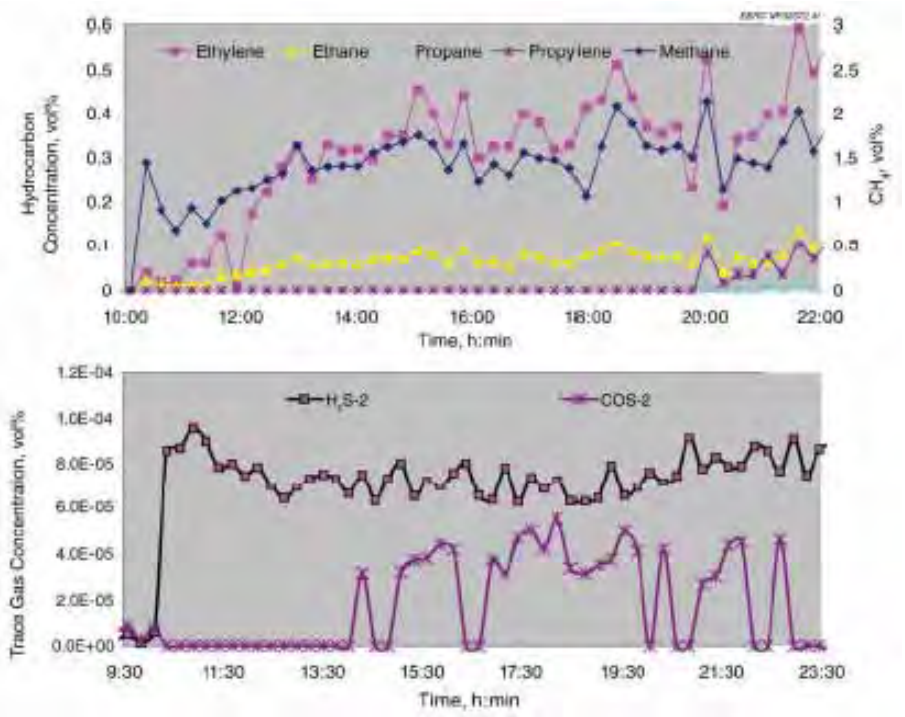

Figure 21. Concentration of hydrocarbon and sulfur containing gases vs. time history obtained during gasification of 35% moisture pine wood waste.

Table 7 lists mass and energy balance and average gasification efficiency based on measured gasification parameters. The gasifier is designed to achieve complete carbon conversion; therefore, except to remove inorganic residue, the extraction screw is not operated.

Grand Forks municipal wood waste gasification

During the previous test in which 35 percent pine waste wood was gasified, hydrogen-rich syngas was produced by promoting the water–gas shift reaction in the gasifier bed. A hydrogen-rich syngas is desirable in some fuel and energy applications; however, when syngas is used for power production in IC engine generators, a CO-rich syngas is preferred. It is possible to adjust operational conditions of the gasifier to reduce N_2 and CO_2 dilution, thereby further increasing hydrogen yield. To test the ability of the gasifier to produce H_2-rich syngas or CO-rich syngas, gasifier operating conditions were varied over the course of the 24-hour period.

Table 7. Gasifier performance: Test 1.

Test duration	787.00 minutes
Biomass throughput	27.94 kg/h
Additional char consumed	1.64 kg/h
Air flow rate	46.48 kg/h
Biomass moisture	35.00%
Biomass calorific value	12.84 MJ/kg
Thermal input (tie)	99.65 kW
Char moisture	3%
Char calorific value	31.30 MJ/kg
Thermal input (char)	13.82
Net thermal input	113.46 W_{th}
Syngas: thermal output	
Higher heating value	4.65 MJ/m^3
Flow rate	72.60 m^3/h
Gas density @18 °C	0.99 kg/m^3
Thermal output (syngas), HHV	92.84 MJ/m^3
Gasification efficiency, HHV	81.8%

A 24-hour test was conducted to gather data on long-term operation of the gasification system and to demonstrate the production of both a hydrogen-rich and a CO-rich syngas. During the 24-hour gasifier operation, two fuels were tested: (1) Grand Forks municipal wood waste and (2) Marcel saw-mill wood waste. During the first half of this 24-hour, test Grand Forks municipal wood waste possessing an average moisture content of 52.68 percent was gasified.

Table 8 lists the average syngas composition and Table 9 lists the trace gas concentration determined by colorimetric tubes.

Table 8. Average syngas composition and HHV of the syngas (GF municipal wood waste) and standard deviations.

Parameter	CO, %	CO_2, %	CH_4, %	H_2, %	N_2, %	C_xH_y, %	HHV, MJ/m^3
Average syngas composition	1.3	14.7	12.0	14.5	57.5	4.5	1.3
Standard deviation	0.5	2.1	1.7	2.5	3.1	0.4	0.5

Table 9. Trace gas concentration determined using colorimetric tubes.

Gas	Cold Side Test Time 9:06 – 10:10 ppmv
Toluene	400.0
COS	Not detected
SO_2	0.5
Xylene	2.5
HCN	0.8
NH_3	Not detected
H_2S	11.0

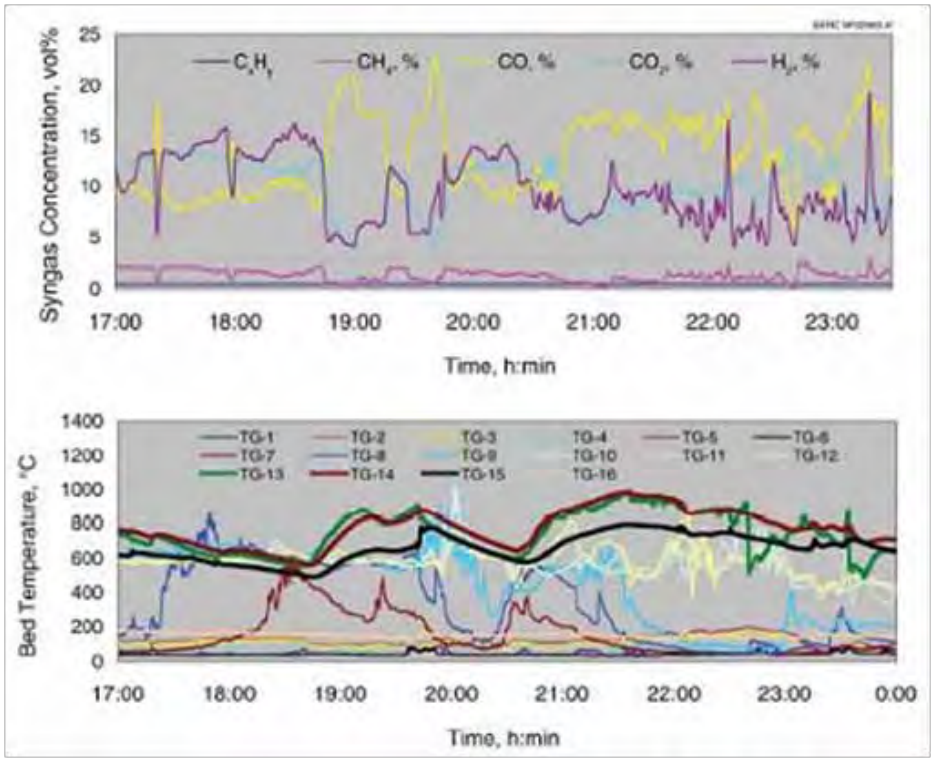

Figure 22. The 52.6% moisture Grand Forks municipal wood waste gasification test results depict syngas composition and bed temperature variation with time obtained during testing to produce CO-rich and high CO/CO_2 syngas.

The syngas composition profile shown in Figure 22 provides a plot of CO and H_2 concentration with time. Although these concentrations vary over the course of the test, the sum of these two gases remains fairly constant. Furthermore, since CO and H_2 have similar calorific values on a volume basis, the syngas calorific value remained constant. The CO/CO_2 ratio throughout the test remained between 2.5 and 5.5, indicating good CO_2

and char conversion. The fuel injection was constant during the experiment, and the pressure drop across the bed was consistent during the entire 24-hr operation. Although this test was successful in achieving the desired syngas composition at the pilot scale, better performance could be obtained by optimizing heat transfer in the reacting packed bed.

Gasification of high-moisture Marcel sawmill wood waste

The fuel used during the second half of the 24-hour test was obtained from the Marcel sawmill. This waste wood was gasified containing an average moisture content of 33.5 percent. During gasification of this fuel, tests were conducted to better understand the range of H_2/CO ratio achievable in the advanced fixed-bed gasifier. Short-duration, steady-state experiments were conducted during the test to observe the range of H_2 and CO achievable. Table 10 lists single measurement values.

Table 10. Measured gas composition achievable during self-sustained gasification of 35%-moisture Marcel sawmill wood waste.

Test Date: 19 November 2009	CO	CO_2	CH_4	H_2	N_2
Highest concentration, vol%	22.8	8.4	1.36	37.4	30

Figure 23 shows the syngas composition and bed temperature vs. time measured during the gasification of Marcel sawmill waste wood. This fuel was gasified for about 5 hours with a throughput of 56.8 lb/hr. Several gasifier operating conditions were tested to estimate conditions for attaining desired syngas composition. As can be seen, the average bed temperature at the gasifier operating condition could gasify the wet biomass, and it was possible to increase bed temperature as desired. The gasifier could be operated at two steady-state conditions such that the syngas composition with either high CO or high H_2 concentration could be obtained (H_2/CO ratio of 0.25 and 1.8). The bed temperature profiles were adjusted with the help of air staging in the advanced gasifier. This special feature allows production of distinct steady-state syngas compositions. The gasifier operating condition, selected for long-duration testing, was a high H_2/CO ratio applicable to liquid synthesis applications.

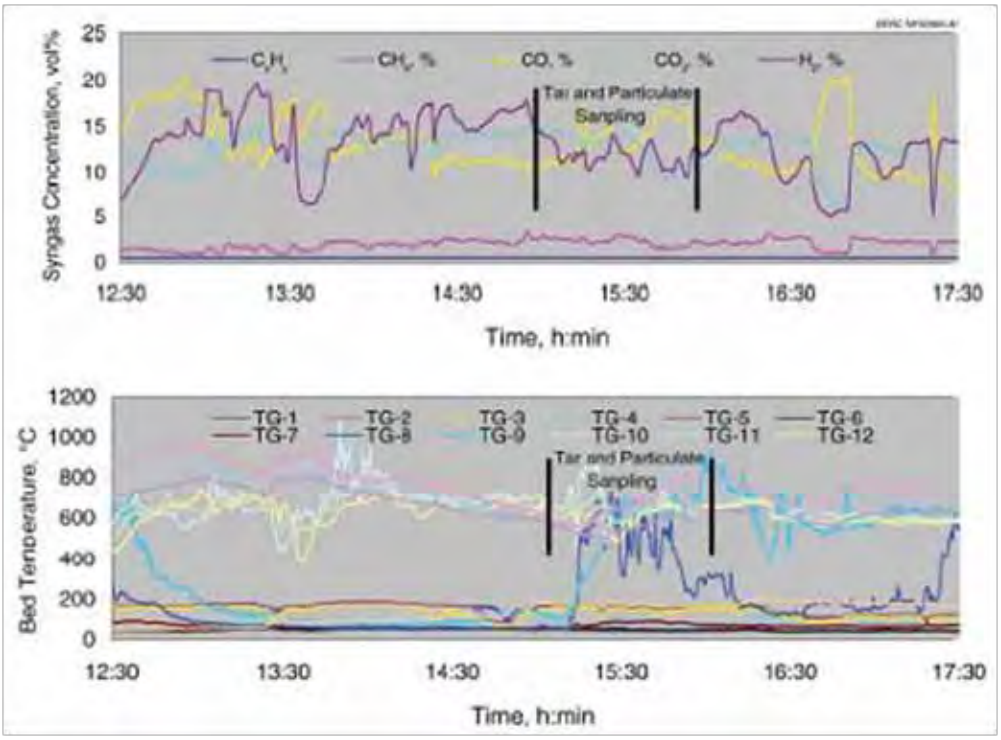

Figure 23. Syngas composition and bed temperature vs. time history of gasification of wet wood received from legacy waste pile from a sawmill located in Marcel, MN. Tar and particulate sampling was conducted during times indicated on the composition and bed temperature plot (24-hr test).

Table 11. Results of calorimetric tube measurement of trace syngas components obtained during gasification of sawmill wood waste from Marcel.

Component	Hot Side Test Time 12:49–13:50 ppmv
Toluene	33.3
COS	Not detected
SO_2	1.0
Xylene	1.7
HCN	0.8
NH_3	Not detected
H_2S	2.0

Table 11 lists that the trace gas concentration in the hot syngas was determined by calorimetric tubes. The COS and NH_3 were not detected; however, trace concentrations of HCN, SO_2, xylene, and H_2S were determined. The toluene concentration was lower than expected. These short point tests are indicative and could be used for planning scrubbing strategies.

The tar and particulate matter concentration in the syngas was determined during the wet wood gasification test. The results of the test are described in a later section.

Railroad tie gasification

Railroad ties are a complex fuel for use in gasification because of the presence of wood with complex hydrocarbon mixtures and associated high volatiles content. Table 4 lists the comparative composition of two different railroad ties. Railroad Tie 2 was obtained from a source in the United States, and Railroad Tie 4 was obtained from British Columbia, Canada. Tie 2 was used in both tests. These ties were pre-dried to 12.6 percent moisture to be tested with the advanced gasifier; for comparison, 35 percent moisture pine wood was also tested.

The railroad tie feedstocks were not modified for the experiment. The variation in syngas composition including variation in trace hydrocarbon gases and reactor bed temperature with time were recorded.

During the first phase of operation, 35 percent moisture pine wood was gasified for a period of 10.6 hr at the rate of 56 lb/hr. Railroad Tie 2 was next fed to the gasifier for 3 hours at the rate of 62 lb/hr. Figures 24 and 25 shows the test results.

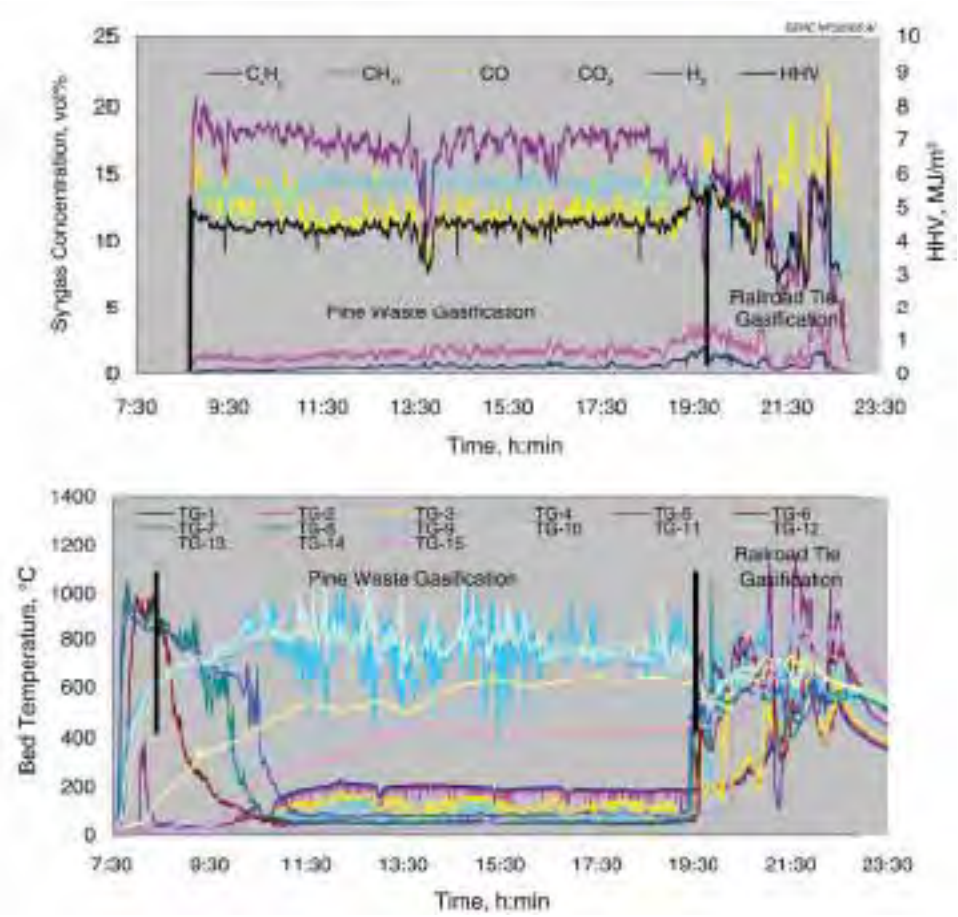

Figure 24. Syngas and bed temperature vs. time history of pine wood waste and railroad tie gasification at 54.5- and 56.1-lb/hr throughput, respectively.

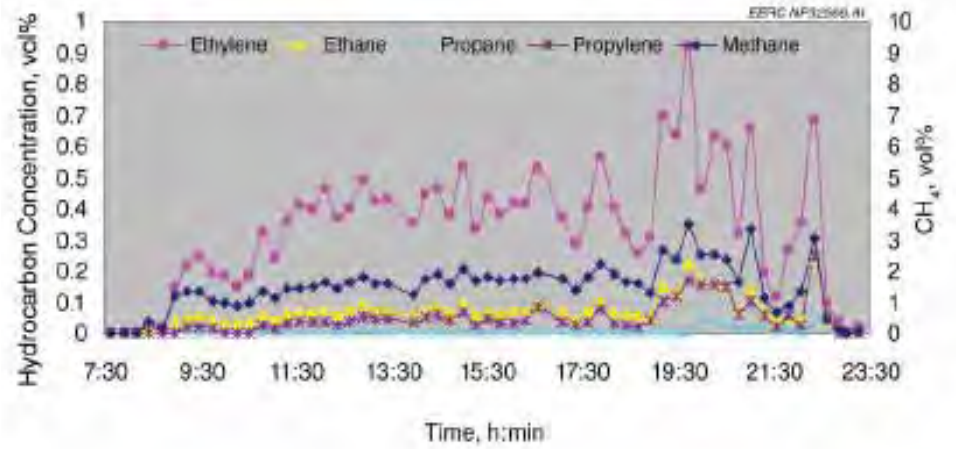

Figure 25. Concentration of hydrocarbon gases obtained during gasification of 35% moisture pine wood waste.

The gasifier performance with pine wood chips was similar to the previous test (see Figure 20). The gas composition and temperature profile were similar until the injection of railroad ties at approximately 18:30. A new

steady state for railroad tie was attained as observed with the distinct lowering of the H_2/CO ratio from greater than 1 to less than 1. In contrast to the pine wood gasification, the bed temperature during the tie gasification spread into the upper zones of the gasifier such that the reacting bed depth increased, resulting in a higher conversion rate. The observable shift in bed temperatures to the upper zone of the gasifier could be attributed to comparatively lower moisture (approximately 12.5 percent) and higher volatile content of the railroad tie fuel. The higher volatile content likely resulted in a higher devolatilization rate, which in turn caused flaming and temperature fluctuations in the bed.

Besides lowering of H_2/CO ratio, the CO_2 concentration also dropped when railroad ties were injected to the gasifier. CO_2 concentration decrease is a direct effect of increased bed temperature and decrease in feed moisture, consistent with the properties of the railroad tie fuel.

The H_2/CO ratio dropped because of a decrease in H_2 concentration as an effect of fuel composition, including low fuel moisture content. A distinct increase in the trace hydrocarbon gas concentration was also observed with the railroad tie fuel.

The second test using Railroad Tie 2 was designed to evaluate the effect of maintaining higher average bed temperatures as compared to the bed temperature in the first test on carbon conversion and the fate of organic material during gasification. The gasifier was operated at its nominal design throughput of 33 lb/hr. Table 12 lists average syngas composition, HHV, and standard deviation obtained during tie performance test. The heating value of the syngas was higher than syngas from pine wood waste. The lower CH_4 concentration as compared to previously observed concentrations greater than 2.5 percent is an indication of relatively better organic conversion. The syngas flow rate was 33.0 scfm and remained constant during steady-state gasifier operation. The tie carbon conversion was complete, and in addition, the bed char above the grate converted at a rate of about 2.4 lb/hr (1.09 kg/hr) (7 percent of the tie throughput). In the gasification efficiency calculation, the thermal energy contribution of the char is added to the net thermal input to the gasifier. It was observed that, because of the higher bed temperature, a large fraction of fuel moisture was converted to syngas. The gasification efficiency calculated as a ratio of thermal energy output in the syngas and input in the tie and char was about 80 to 85 percent (Table 13).

Table 12. Average syngas composition, HHV, and standard deviation obtained during Performance Test 2.

Parameter	CO, %	CO_2, %	CH_4, %	H_2, %	C_xH_y, %	HHV MJ/m^3
Average syngas composition	17.4	11.1	1.8	14.8	1.1	5.29
Standard deviation	2.1	1.5	0.9	5.2	–	1.06

Table 13. Gasifier performance: Tie test.

Test duration	82.00 minutes
Tie throughput	14.60 kg/hr
Additional char consumed	1.09 kg/hr
Air flow rate	37.31 kg/hr
Tie moisture	12.60%
Tie calorific value	20.17 MJ/kg
Thermal input (tie)	81.80 kW
Char moisture	5%
Char calorific value	31.30 MJ/kg
Thermal input (char)	9.48
Net thermal input	91.28
Syngas: thermal output	
Higher heating value	5.29 MJ/m^3
Flow rate	56.00 m^3/h
Gas density @ 18 °C	0.94 kg/m^3
	52.64 kg/hr
Thermal output (syngas), HHV	77.35 MJ/m^3
Gasification efficiency, HHV	84.74%

Figure 26 shows variation of syngas composition, HHV bed temperature, and syngas flow rate variation with time. As was observed, the variation in the syngas composition is due to fuel injection timing, which is consistent with previous observations and characteristic of the fuel. However, the variation in bed temperature was not coupled with fuel injection and maintained an almost constant profile. This effect is primarily due to reduction in the fines (compared to the fines in Test 1) in the fuel and a stable reacting char bed.

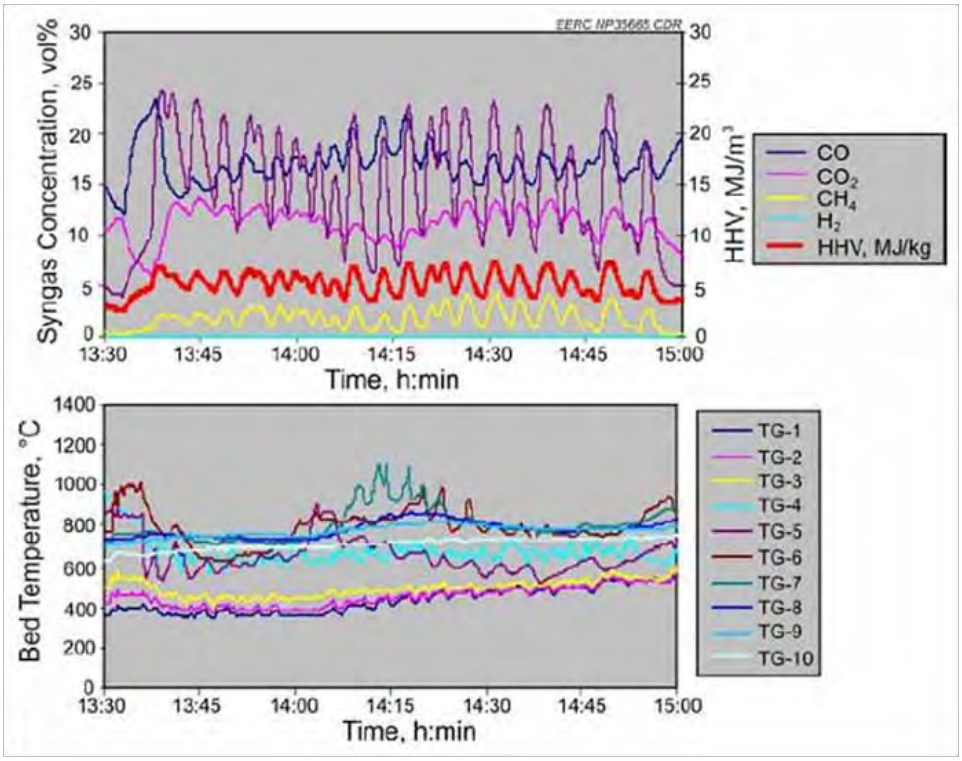

Figure 26. Syngas, bed temperature, and flow rate vs. time history of Tie 2 gasification at 14.6 kg (32.2 lb/hr) throughput obtained during gasifier performance Test 2.

PRB coal gasification

A coal gasification test was conducted to evaluate gasifier operation and syngas quality. The self-sustained gasification test was conducted with a Montana sub-bituminous coal commonly known as PRB coal containing 26.5 percent moisture. The experiment was initiated with the gasification of wood charcoal consisting of 5 percent moisture. Figure 27 summarizes syngas composition and bed temperature data. The coal conversion began as soon as the coal reached the hot charcoal reaction front. Moisture in the coal typically reduces bed temperature and the rate of syngas production (see temperature profile TG-7). Tests conducted with the advanced gasifier resulted in maintaining bed temperature and gas composition ($CO + H_2$). However, the axial location of the hot zone moved downstream in the gasifier char bed.

The conversion of the coal-bound moisture increased the H_2/CO ratio to greater than 1.5: a condition that could be easily maintained for achieving hydrogen-rich syngas. This scenario could avoid coal predrying.

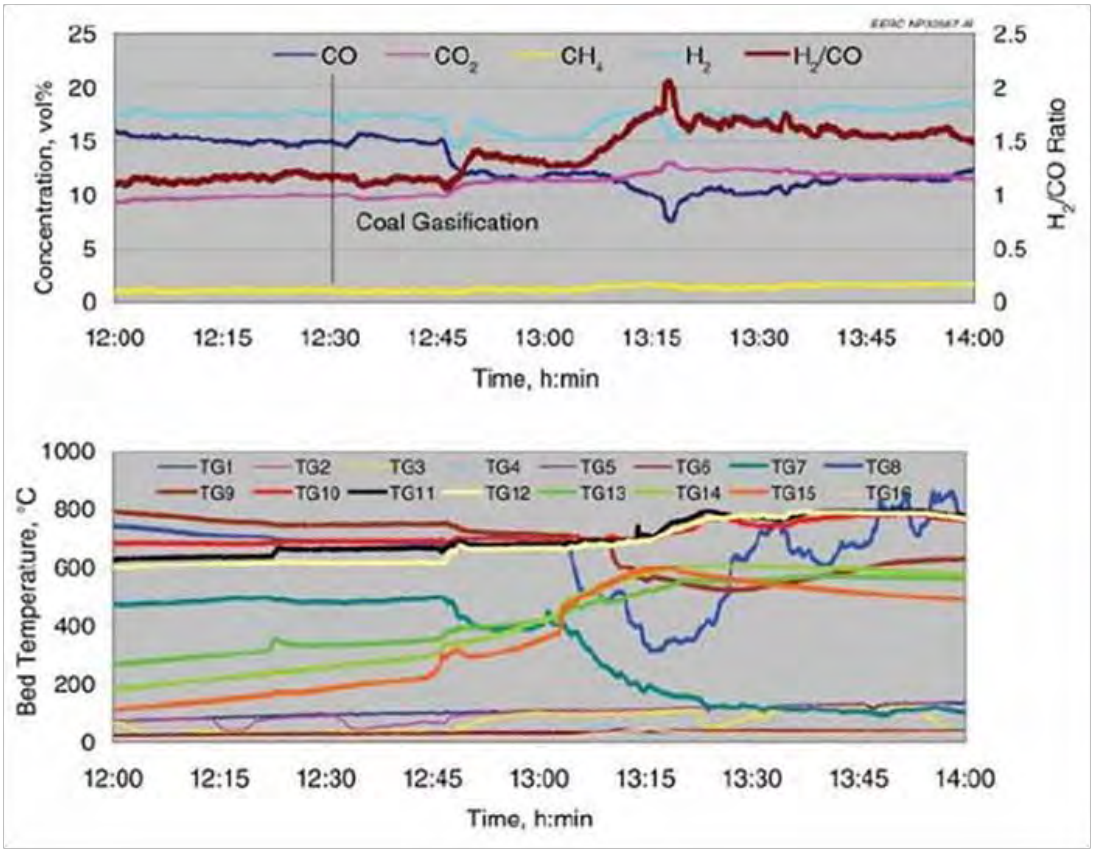

Figure 27. Syngas composition and bed temperature vs. time history of Montana sub-bituminous coal gasification in pilot plant gasifier.

Figure 28 shows the trace gas composition determined by the quasi online GC. The concentration of trace gaseous hydrocarbons consisting of ethylene, ethane, propane, and propylene were an order of magnitude lower than methane concentration (right-hand abscissa). The variation in the trace HC concentration is nearly proportional to the variation in the methane concentration.

To understand the effect of wet coal on the syngas composition, an experiment was conducted in which high-moisture coal was injected during the gasification of dried coal. To simulate this condition, the coal fuel was not fed for a short period of time. During this nonfeed period, the reaction front stabilized on the top surface of the bed, and it was assumed that the moisture was completely evaporated from fuel contained in the gasifier:

$$CO + H_2O \longrightarrow CO_2 + H_2$$

$$CO_2 + C_2 \rightleftharpoons CO$$

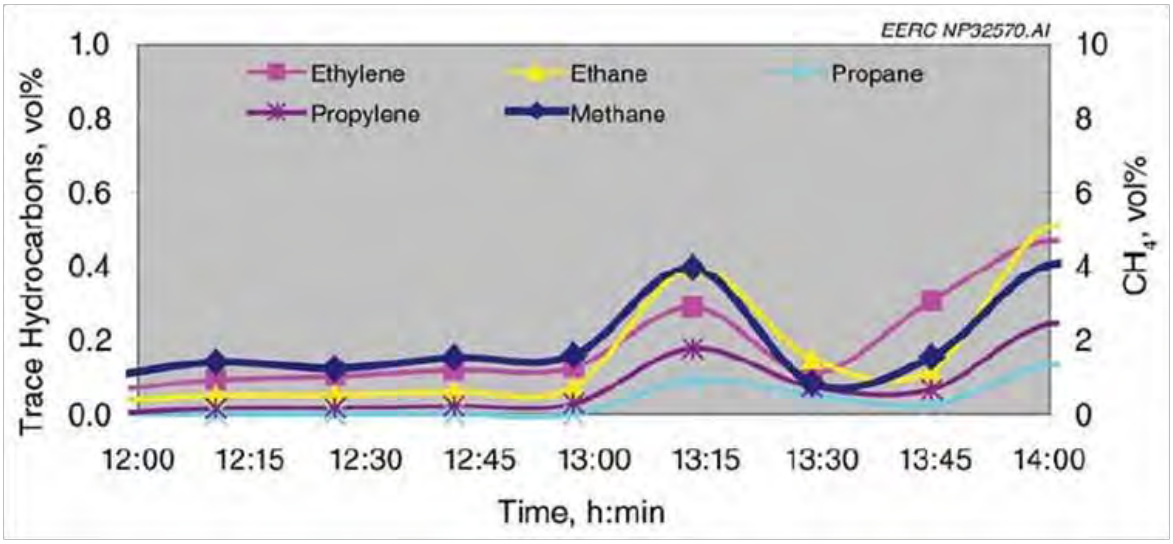

Figure 28. Concentration of hydrocarbon gases obtained during gasification of Montana subbituminous coal gasification in pilot plant gasifier.

Figure 29 shows the syngas composition measured during the dry coal gasification phase. The CO/H_2 ratio was less than 1; however, the production of CH_4 is a clear indication that coal was being gasified and not the char, which is devoid of volatiles. When high-moisture coal was again fed to the gasifier, a sharp increase in H_2 occurred. This change is primarily due to the water–gas shift reaction (first reaction). The increase in CO_2 coupled with a decrease in CO clearly indicates the water–gas shift reaction. The condition of dry coal gasification was recovered once the feeding of wet coal was stopped. The sharp decrease in the local bed (TG-10) is an indication of the localized cooling of the bed because of injection of wet coal.

The bed temperature during the dry coal gasification was favorable for the Boudouard reaction (second reaction); therefore, the resulting CO_2 concentration in the syngas was a relatively low value of about 5 percent (CO/CO_2 ratio was about 5). The pilot plant gasifier is capable of operating at conditions such that rates of both these reactions are high to maintain high H_2/CO and CO/CO_2 ratios. This is desirable for applications requiring production of pure hydrogen and liquid fuel synthesis. These results demonstrate preliminary proof-of-concept for using high-moisture coal as a feedstock for distributed application using air as gasification medium.

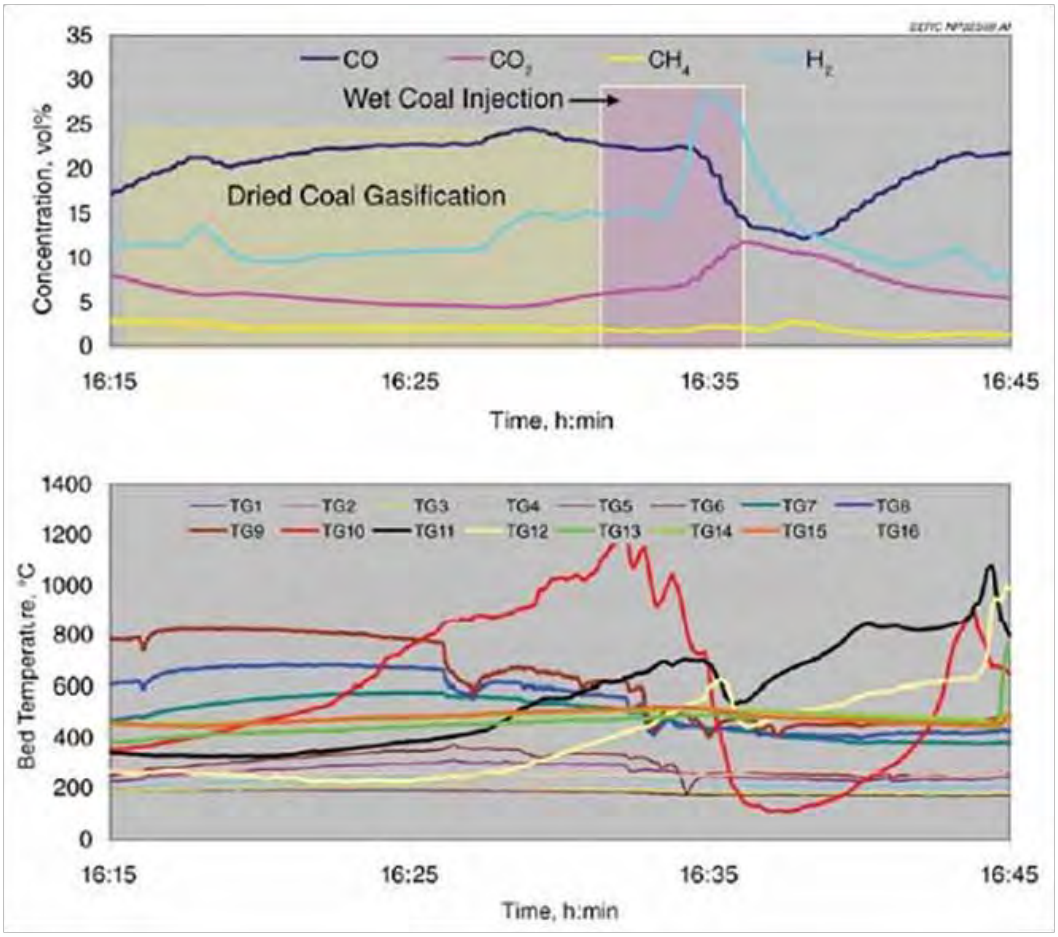

Figure 29. Syngas composition and bed temperature vs. time history obtained during gasification of PRB coal – effect of injection of wet coal on dry coal bed.

Tar and particulate measurement

One of the important performance characteristics of the gasifier is determined by quantifying the tar and particulate matter in the syngas. The condensable tars typically heavier than benzene are considered problematic in the applications such as power generation in the IC engine for distributed application. Toluene and xylenes could be considered as engine performance enhancers; however, the engine manufacturers have yet to characterize the engine performance as a function of the effect of these components. Similarly, the effect of heavier components in the catalytic synthesis of FT liquids or methanol is not clearly understood.

A low concentration of gaseous hydrocarbons in syngas is a qualitative indication of the presence of low contaminants (tar and particulate matter) in the syngas. In practical applications, tar and particulate matter are not determined. As an effort to evaluate the gasifier's ability to minimize pro-

duction of these contaminants as well as the capability of the scrubber system to effectively remove them from the syngas, tar and particulates were determined during the gasification of railroad ties and Marcel sawmill waste wood.

Elaborate tar- and particulate-sampling and analysis procedures have been developed and implemented. A general outline of the procedures is found in the European Tar Protocol (Neeft et al. 2002). Figure 30 shows the tar and particulate sampling system in the pilot plant gasifier. Tar and particulate matter concentrations in the hot (unscrubbed gas) and cold syngas were measured to determine the effectiveness of the upstream scrubber system. The syngas was isokinetically sampled and passed through heated thimbles (Figure 30, Module 2) used for capturing particulate. The tar-laden syngas was passed through a series of impinger bottles (Module 3 and 4) filled with dichloromethane (DCM) in which the tar is captured by dissolution. DCM is an excellent solvent for capturing and analyzing tar by gas chromatographic techniques. Gravimetric tar determination was achieved by evaporating the solvent.

The total volume of sampled syngas was measured using a gas flowmeter in Module 5. This module consists of a pump, a rotameter, a gas flowmeter, stainless steel needle and ball valves, and pressure and temperature indicators to accurately determine the sample gas volume. The gas leaving Module 5 is then vented to the flare.

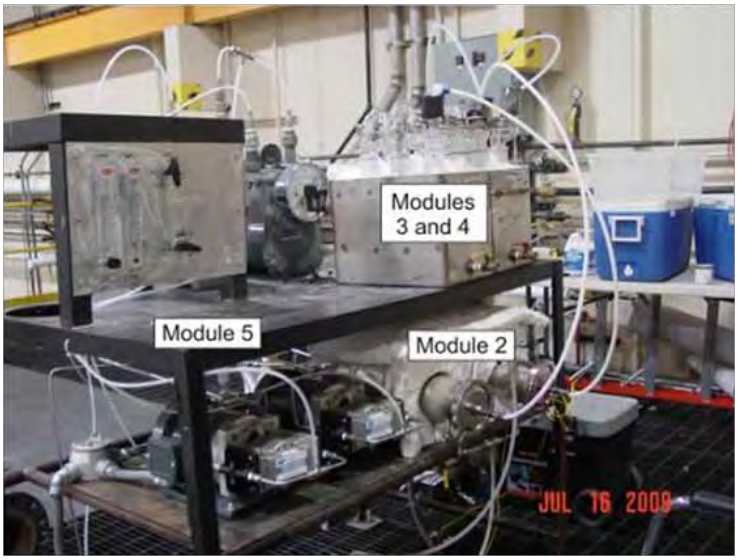

Figure 30. Tar and particulate sampling system in pilot plant gasifier.

Tables 14 and 15 list the differences between the tar concentrations in Test 1 (railroad tie gasification) and Test 2 (Marcel sawmill waste wood), respectively. The optimized gasifier operation, with higher uniform bed temperatures, produced a syngas with tar concentrations to 822 mg/m^3 (see Figures 23 and 26) on the hot side (uncleaned syngas). In the case of biomass gasification, the tar and particulate sampling was conducted at lower bed temperatures to understand the worst-case concentrations on the hot side and the ability of the scrubbing section to remove the condensable tar. Wet biomass was directly fed to the relatively cold char zone (630 °C). The CH_4 concentration was about 2.5–2.9 percent, which is about 1–1.5 percent higher than that observed during higher bed temperature steady-state gasification of wet biomass. This demonstrates that higher CH_4 concentration may provide an indication of higher tar concentration in the syngas.

The scrubber successfully removed all condensable tars heavier than naphthalene from syngas produced with railroad ties, and all condensable tars heavier than acenaphthalene from syngas produced from biomass. It was determined that, in the case of railroad ties, about 93 percent of the naphthalene was removed in the scrubber. Out of the total 200 mg/m^3 of tar in the tie syngas, the organics (about 83 percent) are typical engine performance enhancers, and the remaining condensable tars can be removed in the syngas polisher by adjusting the operation of the system.

Table 14. Summary of the gravimetric analysis of tar (heavier than benzene) and particulate matter (PM) sampled from hot and cold side – Railroad tie gasification with syngas polisher.

	Contaminants			Concentrations in Producer Gas	
Test No.	Particulate Filters, mg	Tar Heavier than Benzene, mg	Total Flow Syngas Volume, Nm^3	Particulate, mg/Nm^3	Tars, mg/Nm^3
2 (hot side)	230	534	0.65	353.3	822
2 (cold side)	21	134	0.65	32.3	200

Table 15. Summary of the gravimetric analysis of tar (heavier than benzene) and PM sampled from hot and cold side – 33.5% Marcel wood waste.

	Contaminants			Concentrations in Producer Gas	
Test No.	Particulate Filters, mg	Tar Heavier than Benzene, mg	Total Flow Syngas Volume, Nm^3	Particulate, mg/Nm^3	Tars, mg/Nm^3
2 (hot side)	106	2317	0.605	175.2	3829.8
2 (cold side)	31	168	0.579	53.5	290.2

Method 5 measurements determined that the installed scrubber system was capable of removing about 85–96 percent of the particulate matter, and it is possible to achieve even higher efficiency. Near-zero carbon conversion could be achieved in the gasifier bed except for a small fraction of carbon recovered during the test to determine its gas adsorption capacity.

Accomplishments

To reduce the gasifier start-up transient period and reduce tar levels during this phase, ignition tests were conducted on cold, warm, and hot charcoal beds. The hot bed had the shortest ignition delay and produced combustible syngas almost instantaneously. The baseline charcoal gasification tests were conducted to understand the difference in syngas composition and temperature vs. time profiles.

A CO/CO_2 ratio greater than 10 is typically achieved during charcoal gasification, while for high-moisture biomass, the value ranged between 2.5 and 5 in this gasifier design. This shows the ability of the gasifier to attain self-sustained gasification conditions with high CO_2 and carbon conversion.

During the 13-hr steady-state gasification of pine wood, hydrogen-rich syngas composition was produced with an achieved average and highest H_2/CO ratio of 1.51 and 2.26, respectively. Such steady-state gasification could be obtained on high-moisture biomass for a commercial syngas-to-liquid production system.

Cold gasification efficiency greater than 80 percent for high-moisture biomass and railroad ties was achieved. Higher gasification efficiency is an indication of higher conversion of organics present in the fuel and near-complete carbon conversion.

Woody biomass containing moisture greater than 50 percent was tested, and desirable syngas composition was achieved for applications of either liquid synthesis process (high H_2/CO ratio) or electricity production (high CO/H_2).

A proof-of-concept using high-moisture coal as feedstock for distributed application such as production of pure hydrogen and liquid synthesis was demonstrated. It was established that the advanced gasifier is capable of operating at conditions such that high H_2/CO and CO/CO_2 ratios in the syngas, as required by these applications, could be produced.

The level of tar during steady-state gasification of railroad tie in the unscrubbed hot syngas and scrubbed syngas was determined to be 822 and 200 mg/m^3, respectively, while the particulate concentration was 353 and 32 mg/m^3 respectively. The cold-side tar contained about 83 percent toluenes and xylenes, which are typically used as performance enhancers in IC engines. No tar heaver than naphthalene (only 7 percent) escaped the syngas polisher. Operational adjustments to the syngas polisher can lead to higher than 95 percent tar capture.

The worst-case tar produced in the case of wet biomass gasification was 3830 mg/m^3 and 290 mg/m^3 in hot and cold syngas, respectively. The particulate matter concentration determined was 175 and 54 mg/m^3 in hot and cold syngas, respectively. The gas cleanup system of the advanced gasifier was able to reduce hydrocarbon levels from 3830 to 290 mg/m^3 and reduce particulate from 175 to 54 mg/m^3.

Subtask 2.2 – Process development for advanced alternative fuels

Subtask 2.2.1 – FT process development

In earlier work, a small-scale FT reactor (Figure 31) was designed and built to test FT catalysts (Zygarlicke et al. 2009). The FT reaction typically requires iron- or cobalt-based catalysts, but previous efforts to acquire commercial FT catalysts had failed. Therefore, work under this activity included development of an FT catalyst to demonstrate the technology. As iron FT catalysts are cheaper and more suitable for converting coal/biomass-derived syngas, it was chosen as the basis for catalyst development. The iron was precipitated onto an alumina pellet for support, and various promoters such as potassium, copper, and lanthanum were added to improve catalyst performance. Several iterations of catalyst formulations, activation procedures, and operating conditions were tested until satisfactory catalyst productivity and product selectivity were achieved.

As part of a separate project, a large-scale FT reactor (Figure 32) was built capable of testing up to 2 kg of catalyst. The reactor was installed in proximity to various coal and biomass gasifiers and was available for use in this activity. Syngas cleanup units to remove contaminants and catalyst poisons were available as well. To fill the large FT reactor with catalyst, the EERC needed to scale up the iron catalyst production process and prepare at least 3 kg of catalyst.

Figure 31. Small-scale FT reactor system for testing small quantities of catalyst with synthetic syngas.

Figure 32. Large-scale FT reactor for testing large batches of catalyst with coal- or biomass-derived syngas.

While a suitable iron catalyst formulation had been developed, further avenues for catalyst optimization were pursued. In particular, it was observed in a repeat test, delayed 4 months after the original test on the same batch of catalyst, that the catalyst activity had declined significantly during storage in the laboratory. The factors that caused this deactivation were investigated. It was also known that lanthanum oxide improved catalyst performance by reducing the surface acidity of the alumina support. The optimum level of lanthanum had not yet been researched, so this variable was also studied more closely.

Continued efforts during this reporting period to acquire FT catalyst from a commercial supplier finally yielded results. A relationship was built with a particular company from another project, and the company agreed to submit small quantities of cobalt- and iron-based FT catalysts. These catalysts were tested in the small-scale reactor, and the results were used primarily as a baseline reference to compare the effectiveness of the EERC FT catalyst.

Coal- and biomass-to-liquids process demonstration

Because it was difficult to obtain large quantities of commercial FT catalyst from vendors with exclusive contracts or closely held intellectual property positions, the EERC developed an in-house, iron-based, supported catalyst formulation for initial testing. This catalyst was developed, tested, and optimized in a laboratory-scale FT reactor using bottled gases to simulate coal-derived syngas. After successful demonstration of the in-house catalyst formulation, a large batch of the catalyst formulation was prepared for loading into a large bench-scale FT reactor system and testing on actual coal-derived syngas from a bench-scale high-pressure fluid-bed gasifier.

Production of EERC iron-based FT catalyst was scaled up using the methodology described in more detail in an earlier report (Zygarlicke et al. 2009). The porous alumina pellets that were promoted with lanthanum were soaked in a solution of iron nitrate, copper nitrate, and urea. Under vacuum, the solution fills the pores of the catalyst rapidly. The excess solution was drained, and the catalyst pellets were heated slowly up to 280 °C. The urea decomposed into ammonia, which then reacted with the iron and copper compounds to precipitate inside the pores of the support.

Three separate, large batches of catalyst were prepared for the large-scale reactor. The iron loading for each batch was targeted to be 10 percent by total weight of the catalyst. The lanthanum weight fraction target was 1 percent, but significant variation was noted between batches (Table 16). A small sample of approximately 7 g was loaded into the small FT reactor. The catalyst was activated under flowing carbon monoxide at a temperature of 300 °C. After several hours, the temperature of the reactor was reduced to 260 °C, and synthetic syngas was introduced to the catalyst with a hydrogen to carbon monoxide ratio of 1:1.33. The flow rate of the syngas was adjusted so that ~15 to 20 percent of the CO was converted.

Each catalyst batch was minimally tested for 250 hrs to allow for steady-state catalyst observations. Liquid and wax product were periodically collected, weighed, and analyzed. Exit gases were collected and analyzed to determine CO conversion rates and light hydrocarbon gas production.

Table 16. Catalyst composition, CO conversion, and product selectivity data for three catalyst batches.

Composition	Measure	AP11A	AP11B	AP11C
Iron	wt%	11.2	9.4	10.1
Copper	wt%	0.29	0.20	0.38
Potassium	wt%	0.22	0.30	0.24
Lanthanum	wt%	0.84	1.7	2.9
CO conversion fraction	% Feed	17.6	17.4	16.2
CO conversion rate	mol CO/kg cat-hr	12.7	13.8	12.4
Light gas selectivity %	CO to HC	18.1	16.1	16.2
Liquid/wax HC productivity	g HC /kg cat – hr	60	72.9	60.3

No major differences were observed in catalyst productivity or selectivity for the three test batches, and although the catalysts did not exhibit performance equivalent to the commercial FT catalyst, they were successful in producing significant amounts of liquid and wax hydrocarbons. AP11B had a slightly higher CO conversion rate and better selectivity to heavier hydrocarbons. Based on this result, it was determined that investigation into the effect of lanthanum on catalyst performance was warranted.

The catalysts were loaded into the large FT reactor. Pressurized syngas exiting the gasification and syngas cleanup systems was routed to the large FT reactor with an estimated maximum liquid production rate of 4 liters (1 gal) per day per reactor bed. The FT reactor system meters up to 100 slpm (3.5 scfm) per bed of clean, pressure-regulated syngas from the gasifier through a preheater and then into a set of downflow parallel packed shell-and-tube reactor beds. Two reactor beds are currently installed on the system, with room for expansion to four. The reactor beds can operate at up to 70 bar (1000 psig) and 300 °C (570 °F), providing flexibility for the potential of methanol or mixed-alcohol synthesis in future tests.

For the initial start-up of the reactor system, the shell-and-tube reactor beds were heated to temperature using a countercurrent flow of Dowtherm oil through the external (shell-side) tube. Syngas passing through the beds was then slowly brought to operating pressure, initiating the exothermic FT reaction. As pressure builds and the beds begin to heat under exothermic reaction, the Dowtherm heater is turned down, and the Dowtherm begins to function as a coolant. Product gas exiting the beds is recycled through preheater coils to the bed inlets. Incoming syngas is diluted, which promotes higher overall conversion efficiencies. Liquid exiting the

bottom of the packed beds was collected in a heated wax trap before passing through a set of water-cooled condensers to remove lighter organic material and water. Hot liquid in the wax trap can be recycled to the top of the reactor to provide further syngas dilution and catalyst cooling, thus bringing the inlet to the packed beds closer to outlet conditions. This design allows the packed beds to function similarly to slurry bed designs more commonly used in large-scale FT synthesis. Unrecycled product gas is depressurized and measured through a dry gas meter, and a slipstream is passed to a laser gas analyzer to provide online comparison of inlet syngas and outlet product gas composition.

Because the entire unit is compact and skid-mounted, it can be readily moved to any of the different gasification systems located at the EERC, or it can be loaded into a truck and coupled to an off-site gasifier. This design flexibility in terms of recycle ratio, operating conditions, heat load or heat removal, and placement makes the FT reactor system a valuable tool for testing catalysts under a wide variety of scenarios.

To produce syngas from coal and biomass, a bench-scale fluid-bed gasifier was used that is capable of feeding up to 9.0 kg/hr (20 lb/hr) of pulverized coal or biomass at pressures up to 70 bar absolute (1000 psig). The externally heated bed is initially charged from an independent hopper with silica sand or, in the case of high-alkali fuels, an appropriate fluidization media. Independent mass flow controllers meter the flow of nitrogen, oxygen, steam, and recycled syngas into the bottom of the fluid bed. Various safety interlocks prevent the inadvertent flow of pure oxygen into the bed or reverse flow into the coal feeder. Coal feed from a K-tron® system drops through a long section of vertical tubing and is then pushed quickly into the fluid bed through a downward-angled feed auger as seen in Figure 33 and Figure 34. Syngas exiting the fluid bed passes through a cyclone before flowing into a transport reactor that uses regenerable sorbent to remove sulfur from the syngas stream.

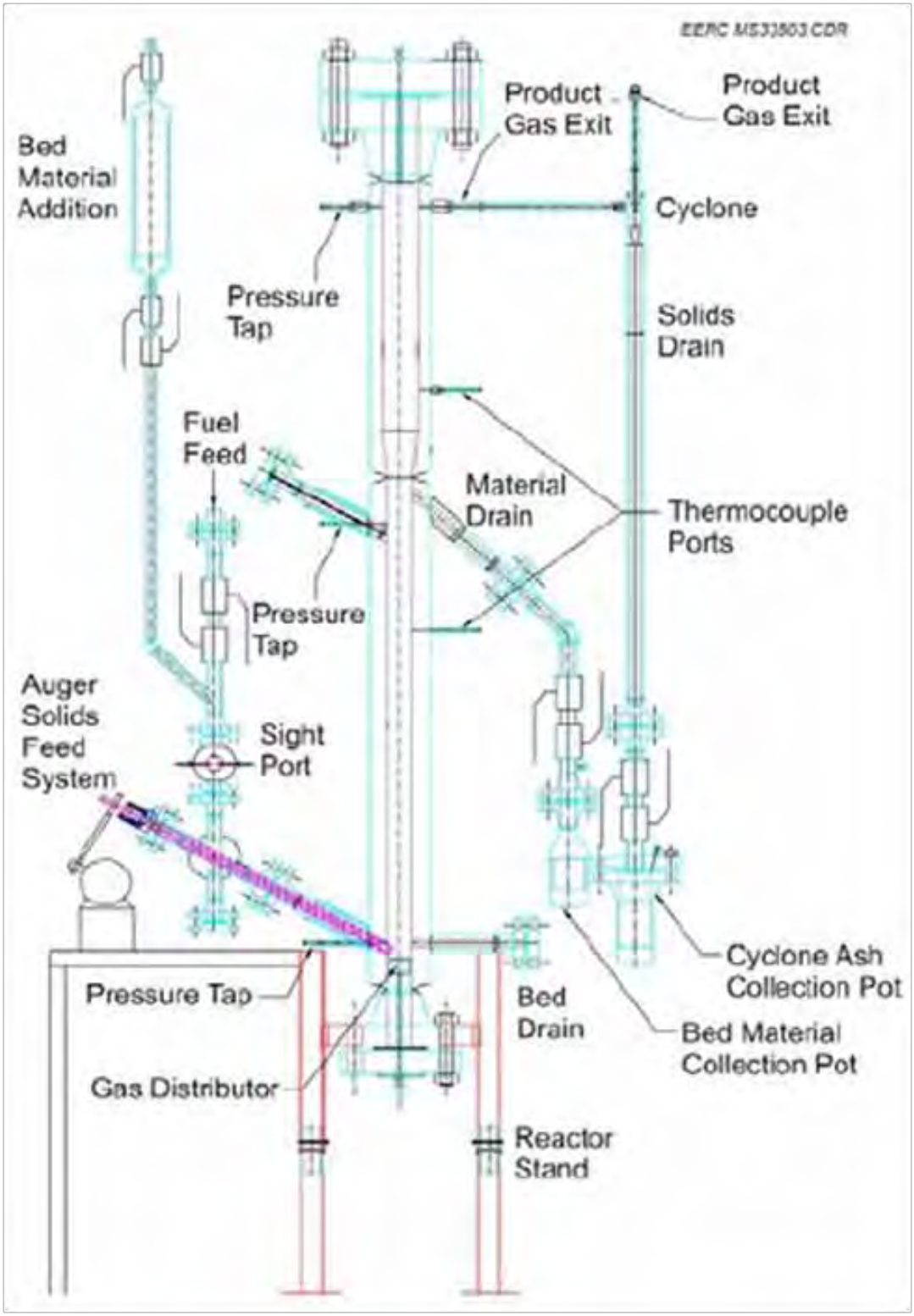

Figure 33. Design drawing of the pressurized, fluidized gasification reactor.

Figure 34. Photograph of the lower section of high-pressure fluid-bed gasifier. Visible at left is the feed auger angled downward into the bed.

The syngas then passes through a hot candle filter to remove fine particulate before entering a series of fixed beds. One bed is a polishing bed of ZnO that removes all remaining traces of sulfur from the syngas. Other beds can be loaded with water–gas shift catalyst, heavy metal sorbent, a chlorine guard, or other sorbents and catalysts. The clean, shifted syngas, still hot and pressurized, is then routed through a series of water-cooled condensers to remove volatile organics and moisture. Syngas can be sampled upstream of the condensers for hot tests. The clean, dry syngas exiting the condensers is then recycled through a compressor to the bottom of the fluid-bed gasifier, and a portion is vented through a control valve to maintain system pressure. The syngas exiting the system passes through a dry gas meter for mass balance. A slipstream of this depressurized, dry gas is also fed to a laser gas analyzer and a GC for online analysis of major gas components and for low-level (ppb) analysis of sulfur species. In addition, operators periodically sample syngas from various points throughout the system using Dräger tubes for H_2S and other trace gases to verify low-level chromatograph data.

Sulfur removal was accomplished by use of two of the fixed beds loaded with regenerable RVS-1® commercial sulfur sorbent. Additionally, two downstream beds were loaded with nonregenerable Actisorb S2® polishing sorbent to capture remaining traces of sulfur compounds from the syngas.

Both sorbents were purchased from Süd-Chemie. Each set of fixed beds was operated one-at-a-time so spent sorbent from one bed could be regenerated or replaced while the system was still running on the second bed.

For the tests described in this section, the gasifier was initially operated using PRB Antelope coal. Target bed temperature was between 816 ° and 843 °C (1500 and 1550 °F), target pressure was 21.7 bar (300 psig), and target bed velocity was 0.30 m/s (1.0 ft/s) or less. Coal, oxygen, steam, and recycle flow rates had no specific target flow rates, but were adjusted to achieve the desired temperature, pressure, and velocity while sustaining flow to the FT reactor. Table 17 lists the results of a laser gas analysis of the syngas composition from the gasifier.

After steady-state gasification had been achieved, clean, dry syngas was passed to the FT system. Both fixed-bed FT reactors were loaded with catalyst, but only one fixed-bed reactor was used for this test. This left the other loaded reactor available in the event that the first reactor was overheated or deactivated because of sulfur breakthrough from the upstream sorbent beds. Target operating conditions for the FT reactor system were 18.9 bar (260 psig), 304 °C (515 °F), 28 slpm (1 scfm) inlet syngas flow, and 140 slpm (5 scfm) recycle product gas flow.

Table 17. Steady-state syngas composition as reported by the laser gas analysis.

Composition	Measure
CO	15.1
H_2O	0.13
H_2S*	0.023
H_2	29.3
N_2	12.9
CO_2	32.7
CH_4	5.1
Hydrocarbons**	0.00

* H_2S reported by laser gas analysis is due to interference from other gas components.

** Hydrocarbons as reported by laser gas analysis is precisely zero due to calibration difficulties. Hydrocarbon composition is lumped with CH4 to give a total light hydrocarbon gas composition.

During the final 24 hours of testing, the gasifier feed was switched from pure PRB coal to blends of 30 percent biomass by weight in PRB coal. Several treated biomass blends were tested sequentially, including leached olive pits, leached and torrefied olive pits, leached dried distillers' grains (DDGs), leached switchgrass, and raw (untreated) DDGs.

Table 18 summarizes the average run conditions for the FT reactor skid. The shell-and-tube Dowtherm heat exchanger successfully removed the heat of reaction, allowing the FT reactor to be operated with the coolant only 3 °C (6 °F) cooler than the catalyst bed. The quench system also performed well, reducing moisture in the exhaust and recycle gas streams to less than 1 percent. On the front end, problems were observed with the syngas metering system (FI901), which had to be taken offline and cleaned out twice as moisture condensed in the regulator. Flow was also intermittent as brief drops in pressure on the back end of the gasifier would quickly affect the FT reactor supply pressure, since the syngas exiting the gasifier was only slightly higher in pressure than the regulated syngas being metered into the FT reactor (PIR900). A small sample conditioner was installed upstream of the pressure regulator to alleviate these problems. This sample conditioner is a metal cylinder with an inlet dip tube and a gas outlet line located at the top of the vessel. By cooling the cylinder in an ice bath, some residual moisture in the syngas is removed, helping to prevent condensation as the syngas expands and cools through the regulator. Moreover, the volume of pressurized gas in the conditioner vessel provides some buffer to the FT reactor, helping to stabilize supply pressure and, therefore, maintain a steady flow rate. In future tests, it is anticipated that higher gasifier pressures will be used, which will also help to maintain a constant flow into the FT reactor.

The CO and H_2 concentration in the FT reactor product gas decreased substantially after the unit was brought to pressure and temperature. All other gas concentrations increased. Perhaps most notably, the concentration of hydrocarbons larger than methane increased from nondetectable levels in the inlet syngas to well over 1 percent in the FT reactor product gas. While the increases in CO_2, CH_4, N_2, and water vapor concentrations in the product gas can be partially attributed to the removal of other gas components (H_2 and CO) from the gas stream, the increase in hydrocarbon concentration is apparently due solely to production by FT reaction.

Table 18. Average run conditions for the FT reactor.

Description	Instrument	Value
Reactor temperatures, °F (°C)		
Inlet syngas temperature	TIR900	77 (25)
Preheated feed gas temperature	TIR901	387 (197)
Top bed temperature	TIR902	473 (245)
Average hot bed temperature	TIR903-909	516 (269)
Wax trap inlet temperature	TIR928	356 (180)
Wax trap outlet temperature	TIR929	309 (154)
Quench system inlet temperature	TIR932	280 (138)
Quench system outlet temperature	TIR935	92 (33)
Recycle syngas temperature (before preheat)	TIR936	88 (31)
Heat exchange temperatures, °F (°C)		
Temperature at Dowtherm heater inlet	TIR943	502 (261)
Dowtherm temperature at reactor inlet	TIR944	513 (267)
Dowtherm temperature exiting reactor	TIR945	510 (266)
Reactor pressures, psig (atm)		
Regulated syngas pressure	PIR900	276 (19.8)
Reactor bed pressure	PIR901	261 (18.7)
Pressure drops, in. H_2O (kPa)		
Pressure drop across reactor	dPIR901	147 (37)
Pressure drop across wax trap	dPIR903	N/A
Flow rates, scfm (slpm)		
Inlet syngas flow rate	FI901	0.88 (25)
Recycle product gas flow rate	FI905	4.8 (137)
Exhaust gas flow rate	FI907	0.57 (16)
Catalyst weight, lb (g)		3.048 (1383)

From calibration before testing, and also from the gas composition reported by both laser gas analyzers before the catalyst was brought to temperature and pressure, it appears that the laser gas analyzer unit used to analyze FT product gas composition gave results in agreement with the laser gas analyzer unit used to analyze syngas composition. Thus reporting errors due to variation between the two instruments may be ignored in calculating syngas conversion efficiency. The nitrogen component in the

syngas does not participate in either the water–gas shift reaction or the FT reaction, and so its composition in the inlet gas may be taken as a standard to determine relative molar flow rates of product gas components. Calibrating product gas nitrogen to inlet gas nitrogen, the average H_2 and CO conversion efficiencies are both approximately 65–70 percent at steady-state.

As seen in Figure 35, the overall conversion efficiency was initially low at around 20 percent (indicating the initial single-pass conversion efficiency), but increased over the course of several hours (perhaps due both to catalyst conditioning and to increasing effect of recycle gas) until it began to reach a plateau.

Another important factor to consider in FT synthesis is selectivity to light gas. This value is simply the ratio of molar increase in total light gaseous hydrocarbons (hydrocarbons + CH_4) divided by the molar consumption of CO on a CO_2-free basis. Once again using nitrogen as a standard to determine relative molar flow rates, the average light gas selectivity over the course of the run was approximately 20 percent. This value remained constant throughout the test duration.

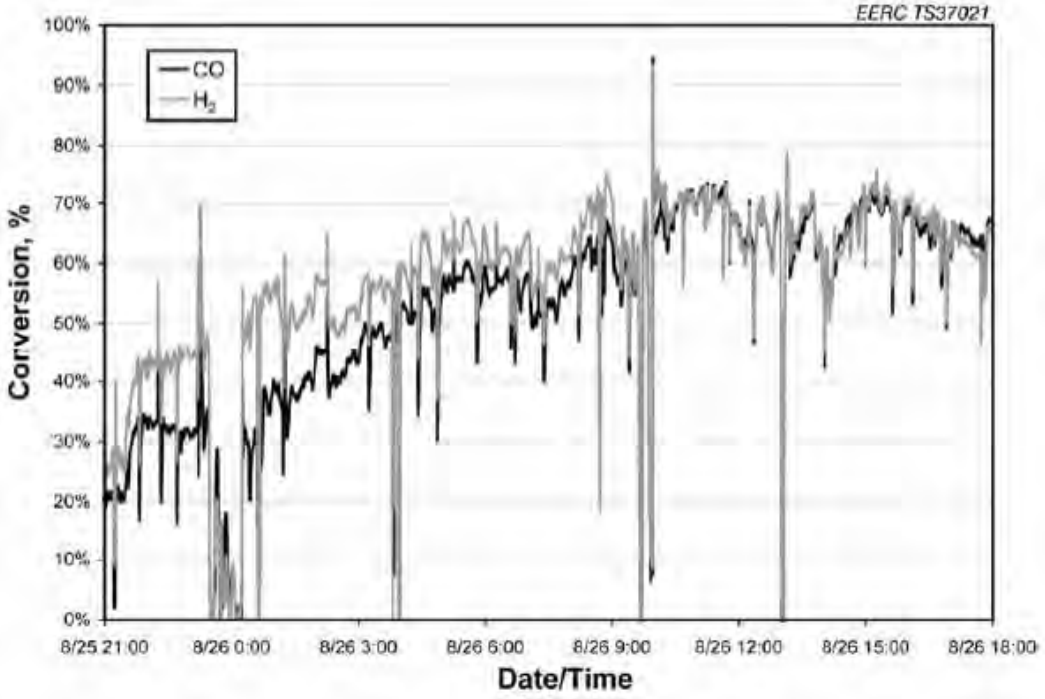

Figure 35. CO and H_2 conversion efficiency during the first 21 hours of FT reactor operation.

The 20 percent selectivity to light gases is slightly higher than was observed in lab testing. The quench pot system used to condense liquid hydrocarbons and product water from the FT reactor product gas is kept at system pressure and drained through a fully enclosed system into a low-pressure pot, from which product can be safely collected. During product collection, it was observed that gas bubbles would form in the low-pressure drain lines. These gas bubbles were likely light hydrocarbons such as butane and propane that were kept in the liquid phase while inside the pressurized quench pots, but then vaporized in the drain line when product was collected. The vent gas exiting the product pot was not analyzed, so the composition of this offgas is unknown. Until a mass balance is completed on the FT reactor, the approximate amount of light gas unaccounted for in the quench system remains unknown.

In addition to the higher light gas selectivity compared to lab test results, wax production was extremely low. Part of this is due to the ineffectiveness of the wax trap to cool the product stream to 150 °C to condense and collect the waxes. The wax product accumulated in the cold traps with the liquids hydrocarbons. Even so, a GC–mass spectroscopy (MS) analysis of the liquid hydrocarbons only showed a moderate increase of heavier hydrocarbons. The overall conclusion is that the hydrocarbon product distribution shifted to lighter products.

This shift was attributed to the syngas composition from the gasifier. The iron-based catalyst had been optimized in the small-scale FT reactor that used only H_2 and CO at a 1:1.33 ratio. The syngas composition (Table 17) contained a significant amount of carbon dioxide. Excess amounts if CO_2 can be a problem for iron catalysts. They are typically tasked with producing more hydrogen via the water–gas shift reaction, and the additional CO_2 present can make the water–gas shift reaction thermodynamically unfavorable. Hydrogen will become a limiting reagent, and the concentration of water will increase because it is not being consumed, which will oxidize catalytically active iron sites and render them inactive.

To verify the effect of CO_2 on the catalysts performance in the small-scale FT reactor, the synthetic syngas composition was altered to approximate the syngas composition from the gasifier. It was shown that from a catalyst operating at steady-state conditions under pure CO and H_2, the liquid and wax productivity dropped by nearly 80 percent when CO_2-laden syngas was introduced. Aqueous productivity dropped somewhat less by 50 per-

cent, which is a crude indication that more light gases were produced. It was clear that CO_2 can significantly hamper the productivity and selectivity of iron catalysts.

FT "syncrude" product must be upgraded to fungible fuels such as diesel, jet, or gasoline. An accomplishment from earlier work (Zygarlicke et al. 2009) was upgrading FT liquids generated from the small-scale FT reactor to synthetic isoparaffinic kerosene (SPK) compatible with military-grade JP-8 jet fuel. FT liquids are hydro-deoxygenated, dewatered, isomerized, and distilled into appropriate fractions. The same process was used to convert coal- and biomass-derived FT liquids into SPK. Figure 36 shows a GC of the raw FT syncrude, which contains a variety of hydrocarbons including paraffins, olefins, alcohols, and isomers. Figure 37 shows a GC of SPK after the upgrading processes.

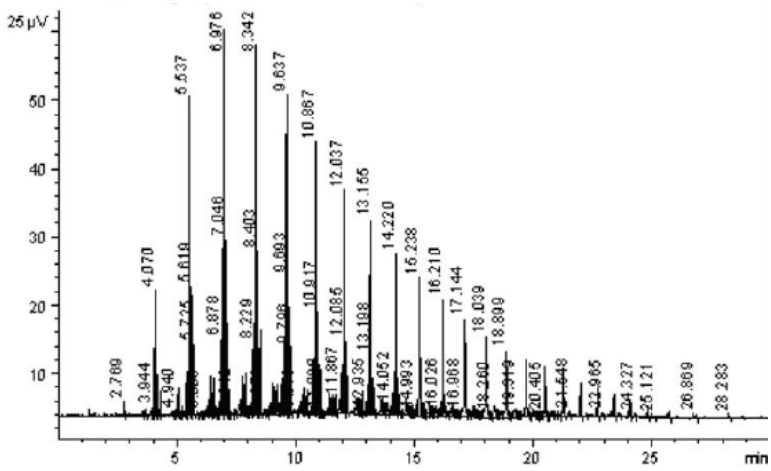

Figure 36. GC of FT syncrude from coal- and biomass-derived syngas.

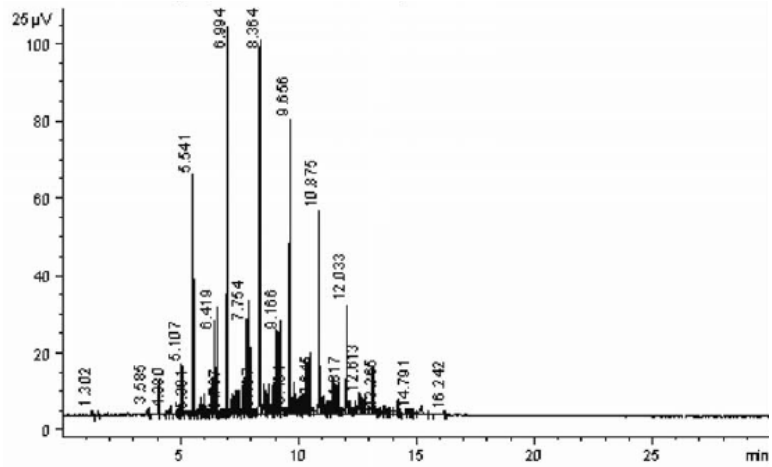

Figure 37. GC of SPK after upgrading.

Effects of water on catalyst activity and selectivity

To determine the repeatability of catalyst testing in the small-scale FT reactor, a second sample of AP11B (designated AP11B 2 in Table 19) was loaded into the reactor approximately 4 months after the catalyst was prepared and originally tested. The activity of the catalyst had decreased by 15 percent, and the selectivity had shifted quite dramatically to lighter hydrocarbons. Selectivity to light gases increased, and wax production decreased by 77 percent. The ratio of waxes to liquid hydrocarbons collected shifted from 0.79 to 0.27.

After preparation and original testing, the catalyst was not immediately loaded into the large-scale FT reactor, and it was stored in the lab. No special precautions were taken to protect the catalyst from the atmosphere in the lab, so it was hypothesized that water vapor from the air hydrolyzed the iron oxide on the catalyst surface, impacting the properties of the active catalytic sites during activation.

To test this hypothesis, another small sample was loaded into the test reactor (AP11B 3.) Before activation with flowing carbon monoxide, the catalyst was heated to 150 °C with flowing nitrogen to completely dehydrate the iron oxide. Activation and operating conditions were then continued as before. The activity of the catalyst recovered somewhat, as the CO conversion rate increased by 8 percent over the previous test. Selectivity to heavier hydrocarbons improved slightly as well, but it did not recover fully to the original catalyst's performance. The catalyst may have been permanently compromised by the exposure to water, perhaps in the form of bonding to the alumina support or the loss of surface area by formation of crystallites.

Table 19. Catalyst productivity and selectivity data for tests on water effects.

Parameter	Measure	AP11B	AP11B 2	AP11B 3	AP18	AP22
CO conversion fraction	% feed	17.4	13.6	15.5	13.2	14.6
CO conversion rate	mol CO/kg cat-hr	13.8	11.7	12.6	12.2	10.7
Light gas selectivity	% CO to hydrocarbon	12.7	15.1	14.8	13.5	11.5
Liquid hydrocarbon productivity	g hydrocarbon/kg cat-hr	40.7	28.0	35.3	34.1	22
Wax hydrocarbon productivity	g hydrocarbon/kg cat-hr	32.2	7.4	12.6	19.2	28.8
Aqueous productivity	g hydrocarbon/kg cat-hr	104.6	81.9	86.4	83.3	55.0
Ratio wax: liquid hydrocarbon		0.79	0.27	0.36	0.56	1.31

A fresh batch of catalyst was prepared (AP18) to duplicate the results of the original trial of AP11B. The catalyst was loaded into the reactor shortly after preparation was completed. The catalyst was not dried with nitrogen, and the activation and operating conditions were otherwise replicated. Productivity and selectivity were slightly better than the AP11B replication trials, but still did not meet that of the original. A review of lab notes revealed that a potentially important lab procedure had been omitted in the preparation of AP18. Flowing air was used during the drying and calcining steps of AP11B, but was not used for AP18. The flowing air perhaps was facilitating the dehydration of iron oxide.

Another batch of catalyst was prepared with flowing air (AP22). In this case, catalyst activity in terms of CO conversion rate was lowest of all the trials, but selectivity to heavier hydrocarbons was much improved. By weight collected, more waxes than liquid hydrocarbons were produced as the wax to liquid hydrocarbon ratio increased to 1.31. Selectivity to light gases decreased to 11.5 percent of all hydrocarbons produced.

It is clear from these five trials that the presence of water on the catalyst during activation can influence the activity and product selectivity. The iron oxide must be completely dehydrated during the drying and calcining preparation steps. This is facilitated with flowing air. After preparation, the catalyst should be stored in a desiccated environment to protect it from re-adsorbing water. The water can be driven off after loading into the reactor with nitrogen, but some catalyst activity cannot be recovered, and selectivity to heavier hydrocarbons is compromised. The original results of AP11B trial could not be fully replicated. It was noted that the concentration of iron was slightly higher in AP22 and that of lanthanum was less. The optimum catalyst composition needed further investigating.

Effects of lanthanum promotion

After the variables related to the hydrolysis of iron oxides that affect catalyst productivity and selectivity were understood and controlled, the effects of lanthanum on catalyst productivity and selectivity were investigated. It is known that the relatively high surface acidity of alumina supports shifts the product distribution toward lighter hydrocarbons. To counter this effect, some researchers have modified the alumina support by adding lanthanum oxide, which reduces the surface acidity. The EERC incorporated this concept into the catalyst formulation by soaking preformed, porous alumina supports in a lanthanum nitrate solution. The

excess solution was drained, and the supports were dried and calcined at a temperature of 600 °C for several hours. The lanthanum nitrate decomposes to lanthanum oxide. The deposition of iron, copper, and potassium then proceeds as described elsewhere.

To vary the amount of lanthanum on the alumina support, the concentration of lanthanum nitrate was varied (Table 20). The composition of catalyst was analyzed by inductively coupled plasma (ICP)–MS. Unfortunately, the lanthanum composition between catalyst batches was not as diverse as was hoped, and the composition of iron and potassium varied more than was expected. Even though a significant difference in catalyst performance was observed between batches, it is difficult to determine what variables caused the effect.

AP25 was targeted to have the lowest lanthanum composition, which it did, but the iron composition of 17.2 percent was much higher than the targeted 10 percent. AP22 was the midrange lanthanum batch, but the composition was only slightly more so than AP25. While the iron was nearly on target, the fraction of potassium was nearly double that of the other two catalysts. AP24 had the highest level of lanthanum as expected, but a weight fraction of 2 percent or higher would have been preferred. Iron and potassium fractions were not unreasonable.

Table 20. Effect of catalyst composition on activity and selectivity.

Parameter	Measure	AP25	AP22	AP24
La_2NO_3 concentration	g/mL	0.1	0.27	0.45
Iron	wt%	17.2	11.5	13.3
Copper	wt%	0.21	0.13	0.13
Potassium	wt%	0.47	0.96	0.31
Lanthanum	wt%	0.68	0.78	1.17
CO Conversion fraction	% feed	14.0	14.6	12.6
CO conversion rate	mol CO/kg cat-hr	11.1	10.7	10.1
Light gas selectivity	% CO to HC	14.1	11.5	12.6
Liquid hydrocarbon productivity	g hydrocarbon/kg cat-hr	29.9	22	24.8
Wax hydrocarbon productivity	g hydrocarbon/kg cat-hr	17.5	28.8	12.5
Aqueous productivity	g hydrocarbon/kg cat-hr	72.4	55.0	67.7
Ratio wax: liquid hydrocarbon		0.58	1.31	0.50

AP22 was the best performing catalyst with the lowest selectivity to light gases and the most productive of heavy hydrocarbons. Conversely, AP24 had the poorest selectivity closely followed by AP25. The activity as measured by carbon monoxide conversion rate was roughly the same for all three batches. The differences in product selectivity between the catalyst batches can be explained by a couple different possibilities, each of which require more data to be proven. The ratio of potassium to iron is four times higher in AP22 because of a smaller weight fraction of iron and much more potassium than the other two batches. Potassium, like lanthanum, is added to the catalyst to decrease acidity, so the significantly improved selectivity of AP22 could very well be due to this. AP25 has a slightly higher ratio of potassium to iron than AP24, and although the light gas selectivity is slightly higher for AP25, it produced more wax than AP24, which lends further support to the effect of potassium on product selectivity.

The other possibility revolves around the original scope of the study on differing amounts of lanthanum. Other researchers have observed that a small amount of lanthanum improves catalyst activity and selectivity, but the effect is not linear, and at a point, an excess of lanthanum will begin to hinder the FT reaction. It is possible that an optimal amount of lanthanum was achieved in AP22, but too much was applied to AP24, which negatively impacted product selectivity. However, it was expected that this deleterious level of lanthanum would be closer to 3–5 percent, not 1.1 percent. Also, the amounts of lanthanum between AP22 and 25 were nearly negligible, yet a rather large difference in product selectivity was observed. The likelihood of potassium composition being the more important variable in this study seems to be greater than that of lanthanum, although more data are required to make a definitive conclusion.

Commercial catalyst testing

During the course of the reporting period, a relationship was built with a commercial catalyst supplier through collaboration on other projects, and the supplier agreed to send samples of its developmental FT catalysts for the purposes of providing a baseline to EERC catalyst performance. Two catalysts were supplied: an iron pellet and a cobalt pellet. The cobalt pellet was later ground into a powder and tested as recommended by the supplier. Under an agreement with the supplier, a detailed composition of the catalyst was not determined, but on visual examination, it appeared that the iron pellet was unsupported. It likely was prepared by forming an iron

precipitate and extruding the powder into pellets. The cobalt pellet appeared to be a supported catalyst, but the support material and composition of cobalt on the support are unknown.

The iron catalyst was of greatest interest for this activity as it would be the most relevant benchmark even though it is an unsupported catalyst. The activation procedure for the iron pellets was provided by the supplier, but the operating conditions such as reaction temperature, pressure, and syngas composition were the same as the other EERC catalyst trials. Table 21 lists the results of the iron pellet trial. The catalyst activity as measured by CO conversion rate is slightly higher when compared to the EERC iron catalyst batch AP22, and selectivity to light gases is a little lower. The major difference between the iron catalysts is the selectivity to heavier hydrocarbons. The supplier's iron pellet produced 70 percent more waxes by weight, and the ratio of waxes to liquid hydrocarbons is significantly higher. The improvement in product selectivity can be attributed to the inherent difference between supported and unsupported catalysts. The EERC catalyst uses a porous alumina support, which increases the surface acidity of the catalyst. This, in turn, reduces the selectivity to heavy hydrocarbons.

The cobalt catalysts were tested at the request of the supplier. The catalyst was received in pellet form. It was loaded into the reactor and activated under flowing hydrogen per the supplier's procedures. Syngas was fed to the reactor in 2:1 hydrogen to carbon monoxide ratio. Reactor temperature was maintained at 220 °C with pressures at 300 psi. The cobalt pellet did not perform well. In general, cobalt catalysts are much more active than iron, but in this case the activity was relatively the same as the iron catalysts. Product selectivity was very poor, with light gas selectivity near 40 percent, and wax production was very marginal as well.

Table 21. Results of commercial supplier catalyst trials.

Parameter	Measure	AP22	Fe Pellet	Co Pellet	Co Powder
CO conversion fraction	% feed	14.6	19.0	39.1	40.7
CO conversion rate	mol CO/kg cat-hr	10.7	12.0	11.5	23.3
Light gas selectivity	% CO to hydrocarbon	11.5	10.1	40.1	13.0
Liquid HC productivity	g hydrocarbon/kg cat-hr	22	19.6	53.8	120.4
Wax HC productivity	g hydrocarbon/kg cat-hr	28.8	48.9	14.3	120.2
Aqueous productivity	g hydrocarbon/kg cat-hr	55.0	33.2	198.8	391.2
Ratio wax: liquid HC		1.31	2.45	0.27	1.0

On review of these results, the catalyst supplier recommended to grind the cobalt pellets and sieve the powder to between 50 and 100 μm. The cobalt powder was diluted with Pyrex glass powder in a 2:1 ratio to better control heat generation in the reactor. Activation and operating conditions were maintained the same as the cobalt pellet. The cobalt powder activity and product selectivity were dramatically improved. CO conversion rate doubled, light gas selectivity dropped to 13 percent, and wax productivity increased nearly 8.5 times. Clearly, in pellet form, the FT reaction was severely diffusion limited, which caused the CO conversion rate to be cut in half and the product selectivity to be significantly shifted toward lighter hydrocarbons. Unfortunately, catalyst in powder form cannot be used in large-scale fixed-bed reactors because of large pressure drops, so the cobalt catalyst requires pelletization not to compromise diffusion.

Conclusions

To demonstrate coal-/biomass-to-liquids technology, the EERC developed an iron-based catalyst to fill a large-scale FT reactor system. Several process variables in catalyst composition, storage protocol, and preparation methods were identified to ensure optimal catalyst activity and product selectivity. Coal and biomass were converted to syngas using a fluidized-bed gasifier. The syngas was cleaned to remove environmental pollutants and catalyst poisons. Clean syngas was fed to the large-scale FT reactor that was loaded with EERC derived catalyst, and liquid hydrocarbons and waxes were produced. The product hydrocarbons were then upgraded into SPK that is compatible with military-grade jet fuel JP-8.

Subtask 2.2.2 – Hydrotreated renewable jet fuel process development

This task developed a technology pathway for converting renewable TAGs (triacylglycerides) such as crop oil, algal oil, animal fats, and waste grease to jet fuel and other liquid fuels. These alternative fuels have chemical and physical properties identical to their petroleum-derived counterparts. Unique from traditional transesterification-based biodiesel technologies, the EERC catalytic hydrodeoxygenation and isomerization (CHI) process yields an oxygen-free hydrocarbon mixture that when distilled produces renewable versions of naphtha, jet fuel, and diesel that can be fully integrated with the current U.S. petroleum fuel infrastructure. In addition to being renewable and fungible, renewable oil-based fuel produced using the CHI technology contains very low levels of sulfur. Sulfur is increasingly being eliminated from petroleum-derived fuels to meet strict U.S. Envi-

ronmental Protection Agency limits. The sub-ppm levels of sulfur present in CHI-based fuels provide a significant advantage to petroleum refiners looking for alternatives to reducing sulfur content in fuel.

Research activities at the EERC have resulted in the production of hundreds of gallons of hydrocarbon samples from a variety of waste fats and oils, and crop oils, including soybean, canola, coconut, cuphea, camelina, crambe, and corn. The primary end product generated via CHI from all of these feedstocks has been aviation fuel (JP-8) that complies with Appendix B of the military specification MIL-DTL 83133F. However, oxygen-free hydrocarbon produced from the CHI technology can readily be converted into any of several petrochemical intermediates used to produce surfactants or plastics in addition to gasoline, jet fuel, or diesel. Figure 38 shows a general block flow diagram outlining the CHI process.

To advance the technology and support implementation of distributed renewable jet fuel production, additional research is necessary to optimize the process. Research conducted during the past year focused on optimizing the hydrodeoxygenation (HDO) step operating conditions and evaluating intermediate product characteristics to support future reactor design and pilot-scale demonstration.

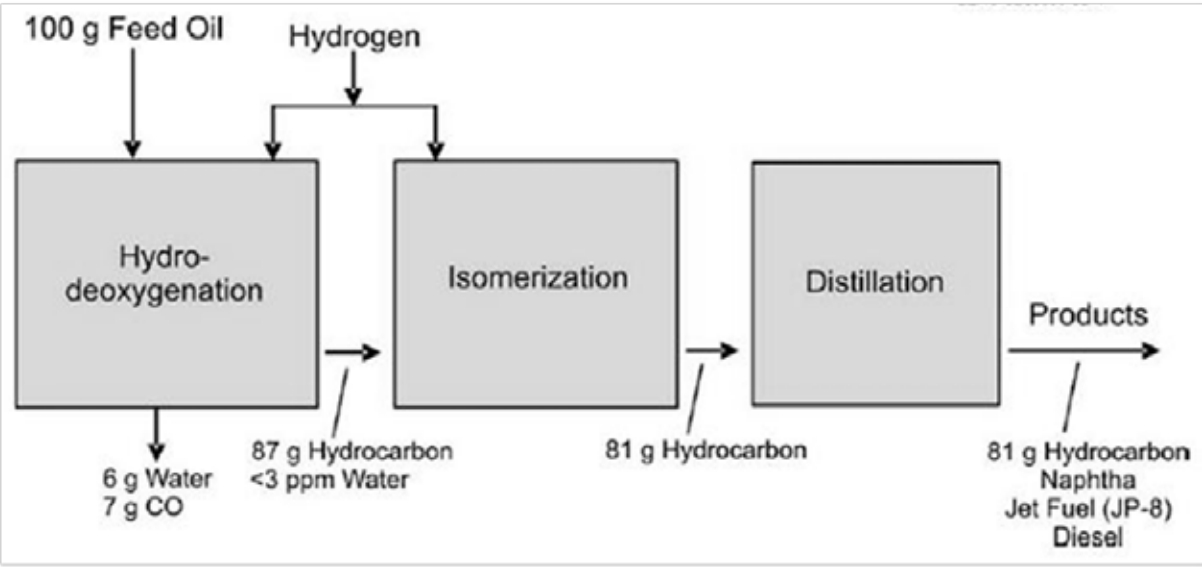

Figure 38. CHI process block flow diagram.

Process chemistry

The HDO reactor converts triglyceride feedstock into hydrocarbon products. By-products of the reaction include water, carbon dioxide, carbon monoxide, and propane. The reaction is heterogeneous and involves the fixed-bed catalyst particle, liquid triglyceride, and gaseous hydrogen. Figure 39 shows the reaction proceeds by one of three reaction pathways. The three reaction pathways are decarboxylation, decarbonylation, and reduction. The decarboxylation reaction produces hydrocarbon, carbon dioxide, and propane. The decarbonylation reaction produces hydrocarbon, carbon monoxide, propane, and water. The reduction reaction produces hydrocarbon, propane, and water. In order of increasing hydrogen consumption, the reactions are: (1) decarboxylation, (2) decarbonylation, and (3) reduction.

Because the triglyceride's glycerol backbone is removed during the HDO step, there is an inherent loss of mass that dictates the maximum theoretical conversion. For example, a theoretical triglyceride molecule consisting of a glycerol backbone and three saturated heptadecane side chains would have a maximum conversion of triglyceride to hydrocarbon of 81 mass percent, assuming that only decarbonylation and decarboxylation occurred. The theoretical maximum conversion value varies depending on molecular weight of the triglyceride feedstock, reaction pathway, and degree of saturation. Free fatty acids have a higher theoretical maximum conversion because the glycerol backbone has previously been removed; therefore, only the fatty acid functionality would be removed by the HDO reactor.

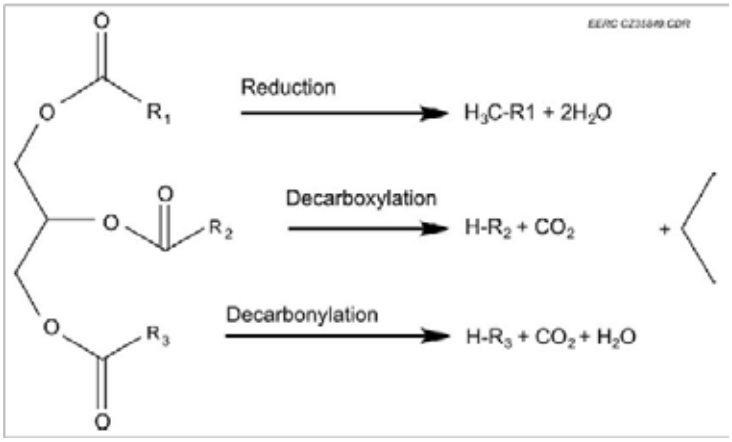

Figure 39. The three deoxygenation reactions that occur in the HDO reactor.

Experimental apparatus

The HDO reactor system consists of a liquid feed pump, a hydrogen gas inlet line, two tubular reactors filled with catalyst, and a product collection system. Both reactors are typically brought online for large sample production runs; however, for certain HDO parametric experiments, only one of the tubular reactors is used, and the other is isolated. Figure 40 shows a picture of the HDO reactor system, taken during its construction.

The ability to process a variety of triglyceride feedstocks is economically advantageous to a commercial-scale fuel production plant. To understand the effect of feedstock composition on product composition, six different feedstocks were processed. Total mass conversion of liquid feedstock to liquid product (water and hydrocarbon), liquid composition (mass% water, mass% hydrocarbon), and hydrocarbon composition (density, acid concentration, water concentration) were measured.

Because of the length of the weeklong, continuous test, it was recognized that there could be drift in the data because of possible catalyst deactivation. To measure catalyst deactivation, the reactor was started up on canola oil, and after processing three different feedstocks, canola oil was processed again midrun, before the remaining two feedstocks were processed. There was no difference between the start-up canola-HDO product and the midrun canola-HDO product, so it was assumed that catalyst activity was constant throughout testing. GSC was used to ensure steady state was achieved before samples of each product were collected for analysis.

Figure 40. HDO reactor system.

Feedstock effect on product composition and quality

Mass conversion of liquid feedstock to liquid product ranged from 88 mass% to 99 mass%. Tests using fatty acid feedstocks resulted in greater mass conversion efficiency because fatty acid molecules do not have the glycerol backbone that triglycerides do. Table 22 lists the mass conversions for each feedstock, as well as the product composition (%water/%hydrocarbon).

All feedstocks produced a fuel with hydrocarbon chain lengths ranging from C-5 (pentane) to C-24 (tetracosane); however, the abundance of each hydrocarbon component varied. Fuel produced from canola oil feedstock (Figure 41), comprised mainly C-16 (hexadecane), 17 (heptadecane), and 18 (octadecane) hydrocarbons. The fuel produced from corn oil (Figure 42) was similar to the canola-derived fuel; however, it contained a slightly higher concentration of C-16 hydrocarbon components. As shown in Figure 43 and Figure 44, the fuel derived from the fatty acids was very similar to the fuel derived from corn oil, with a majority of the hydrocarbon components in the C-16 to C-18 range. The camelina oil-derived fuel (Figure 45) differed from the previous fuels and contained higher concentrations of hydrocarbons in the C-19 (nonadecane) to C-20 (isocane) range with a moderate amount of C-22 (docosane) present. The crambe oil-derived fuel (Figure 46) was similar to camelina oil; however, it contained less C-20 hydrocarbons and significantly higher C-21 (heneicosane) and C-22 components.

Table 22. Mass conversion and product composition when processing various feedstocks.

Feedstock	Mass Conv., %	Liquid Components		Fuel Phase Characteristics		
		Fuel Phase, %	Water Phase, %	Density, g/mL	Acid, mg KOH/g	Water, ppm
Canola oil (start-up)	88	90	10	0.782	0.020	49
Corn oil	92	90	10	0.785	0.029	37
Crambe oil	90	90	10	0.778	0.012	77
Canola oil (midrun)					0.014	37
Soy fatty acid 1	98	89	11	0.783	0.026	41
Soy fatty acid 2	99	89	11	0.785	0.033	48
Camelina oil	94	90	10	0.801	0.044	49

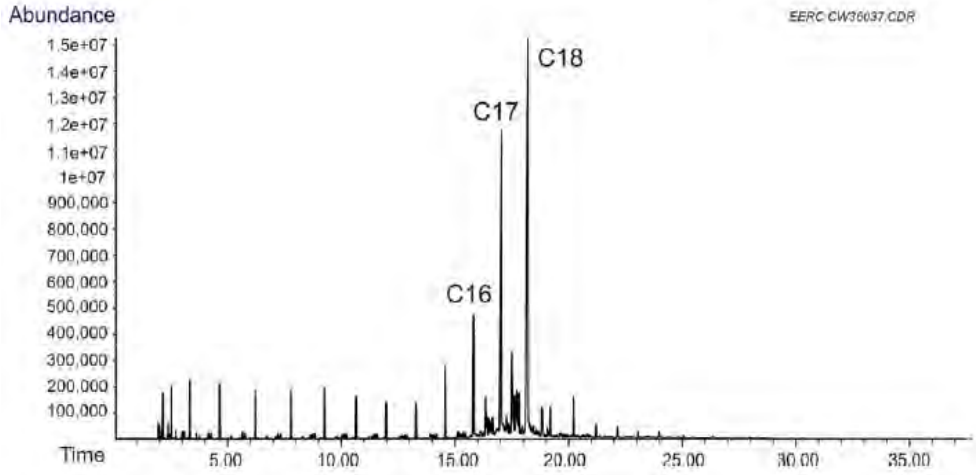

Figure 41. GC chromatogram showing hydrocarbon distribution of canola oil-derived fuel.

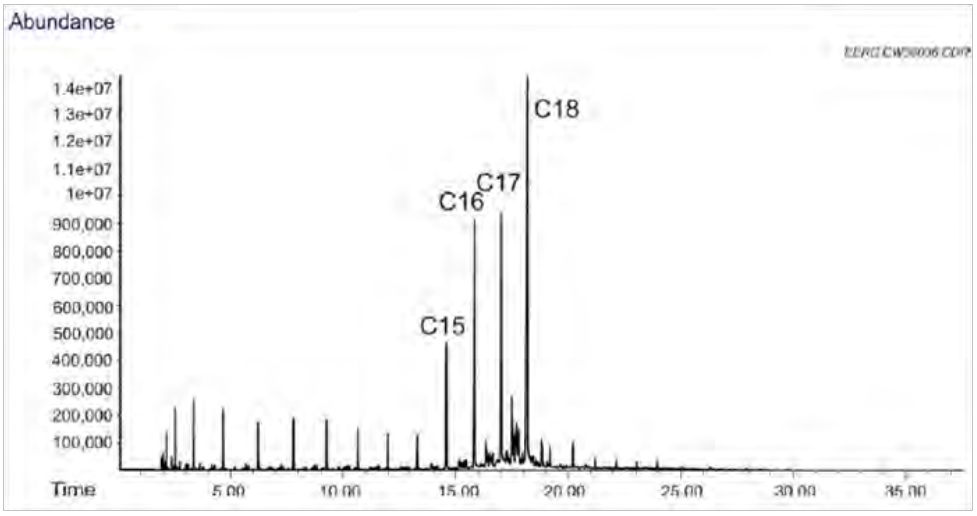

Figure 42. GC chromatogram showing hydrocarbon distribution of corn oil-derived fuel.

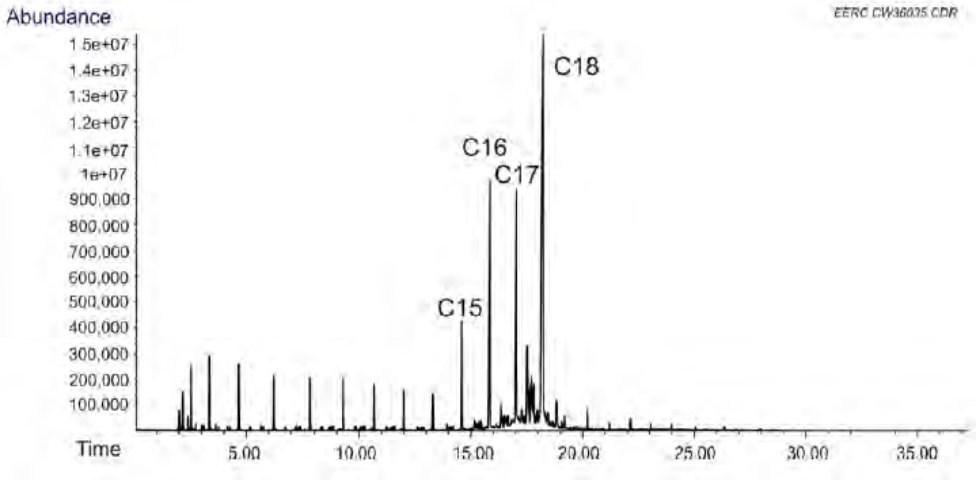

Figure 43. GC chromatogram showing hydrocarbon distribution of fatty acid 1-derived fuel.

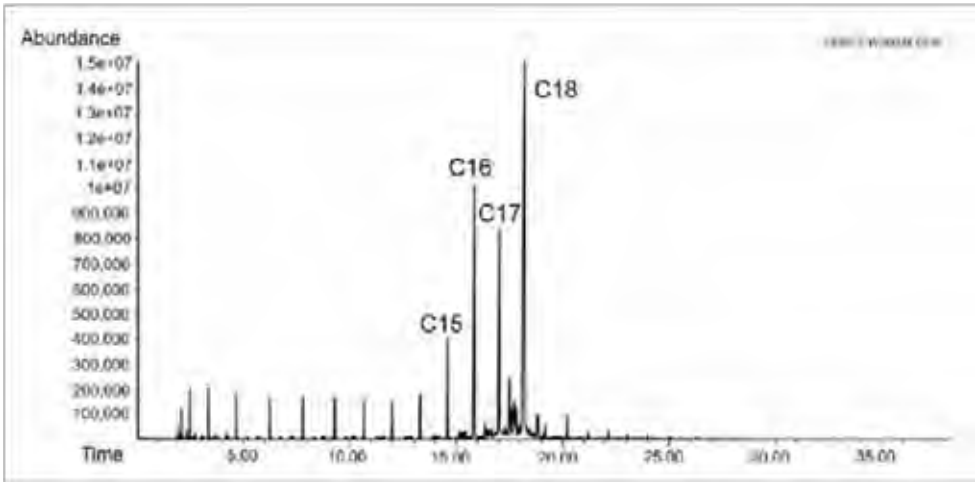

Figure 44. GC chromatogram showing hydrocarbon distribution of fatty acid 2-derived fuel.

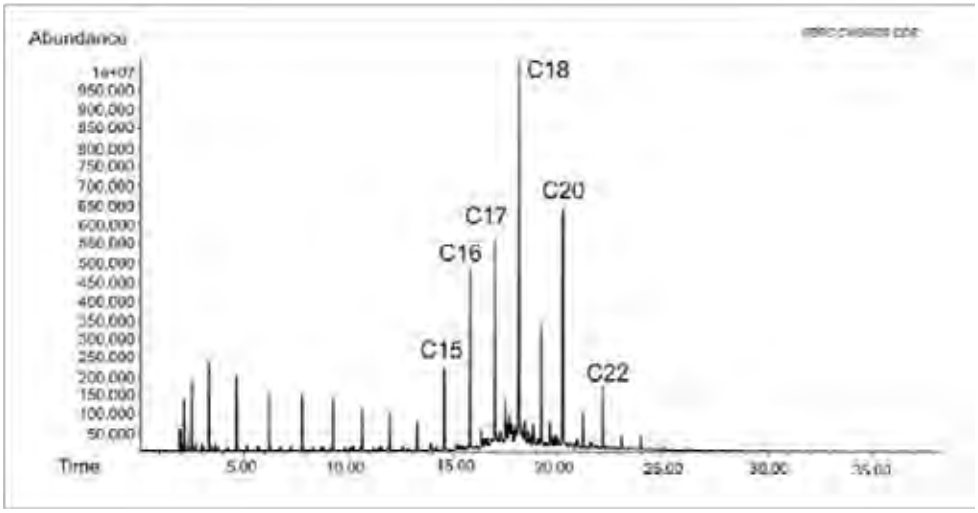

Figure 45. GC chromatogram showing hydrocarbon distribution of camelina oil-derived fuel.

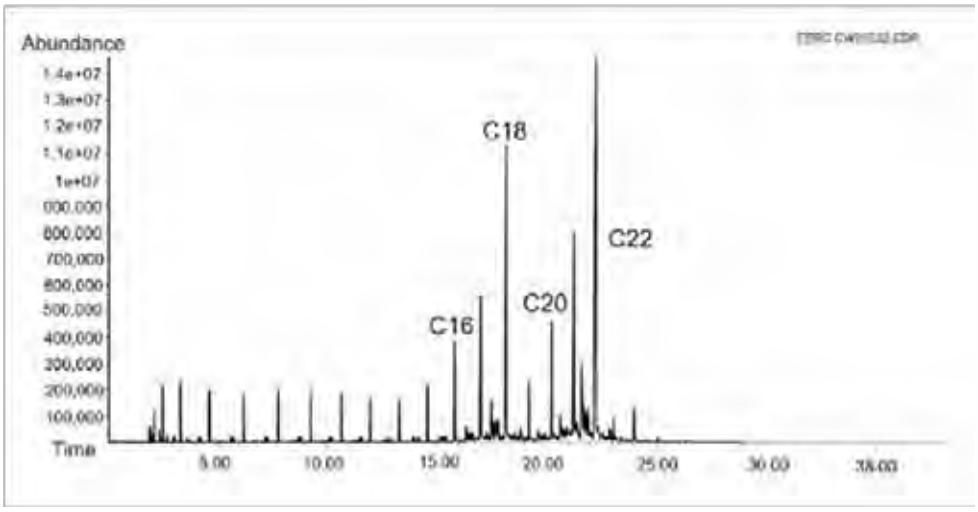

Figure 46. GC chromatogram showing hydrocarbon distribution of crambe oil-derived fuel.

Operational parameters' effect on product composition and quality

Experiments investigating operational parameter effects on product composition and quality were carried out using the continuous tubular reactor (CTR) reactor system.

Feedstock flow rate was investigated using both reactors in series while holding temperature, hydrogen flow rate, and pressure constant conditions. Differences in product quality were not discernible by looking at GC results. Therefore, the acid number, determined by titration and reported in mg KOH/g fuel, was used to measure changes in product quality. Soy fatty acid feedstock was initially fed to the CTR reactor system. Flow rate was incrementally increased, and the initial acid number was measured. The acid number at 1 L/hr was 0.024 mg KOH/g fuel and increased linearly with flow rate up to 3.5 L/hr, where the acid number was 0.1 mg KOH/g fuel. Above a certain flow rate, the acid number increased exponentially. A maximum flow rate at which a relatively low acid number (0.142 mg KOH/g fuel) could be achieved was found. Figure 47 shows the results from variable flow rate experiments.

Pressure experiments were conducted in one of the CTR reactors with a canola oil feedstock. Temperature, feedstock flow rate, and hydrogen flow rate were all held constant. Initially, pressure was set and the reactor was run for 6 hours to ensure steady state. Then, the pressure was decreased incrementally while steady-state acid concentration was measured in the hydrocarbon product. Data from these experiments showed that pressure should be kept above a certain set point to maintain a low acid number (<0.2 mg KOH/g fuel) in the hydrocarbon product. Figure 48 shows results from variable pressure experiments.

The next parameter investigated was hydrogen flow rate. Tests were conducted by maintaining a constant feedstock flow rate, pressure, and temperature while hydrogen flow rate was varied between 30–50 scfh. Figure 49 shows results from variable hydrogen flow rate experiments.

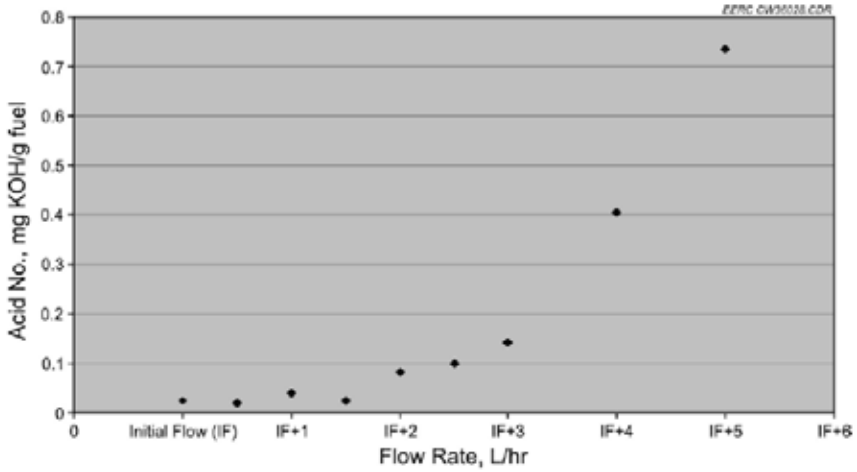

Figure 47. The effect of soy fatty acid feedstock flow rate on hydrocarbon product acid concentration in an HDO reactor.

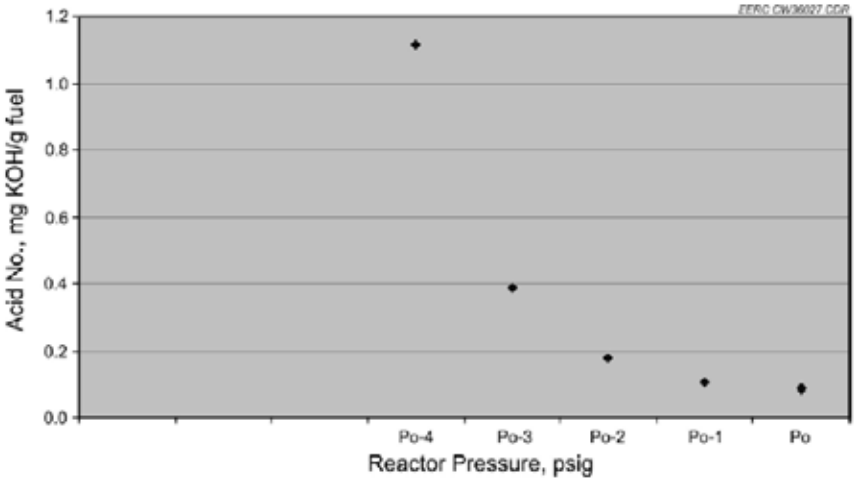

Figure 48. The effect of reactor pressure on hydrocarbon product acid concentration in an HDO reactor.

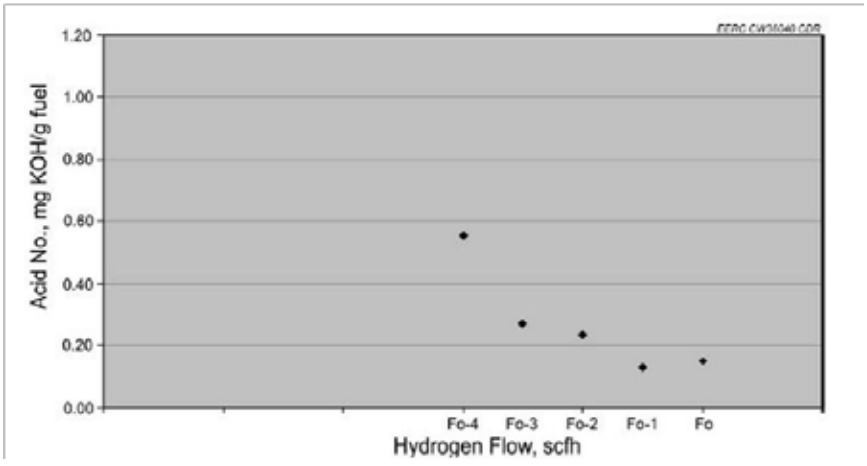

Figure 49. The effect of hydrogen flow rate on hydrocarbon product acid concentration in an HDO reactor.

HDO kinetic rate data

The purpose of the kinetic rate data experiments was to determine the reaction order, with respect to hydrogen partial pressure and fatty acid feed concentration, in a tubular catalytic HDO reactor. This information is useful for process scale-up and provides a better understanding of the HDO reaction.

Experimental setup

EERC's small continuous reactor (SCR) was loaded with 1.2 g of HDO catalyst. The reactor vessel was loaded with glass beads in the area below and above the catalyst bed. The top thermocouple point in the SCR's 4-point thermocouple was located in the catalyst bed for accurate temperature monitoring and control. Figure 50 shows a schematic of the SCR reactor configuration. Figure 51 shows the SCR system.

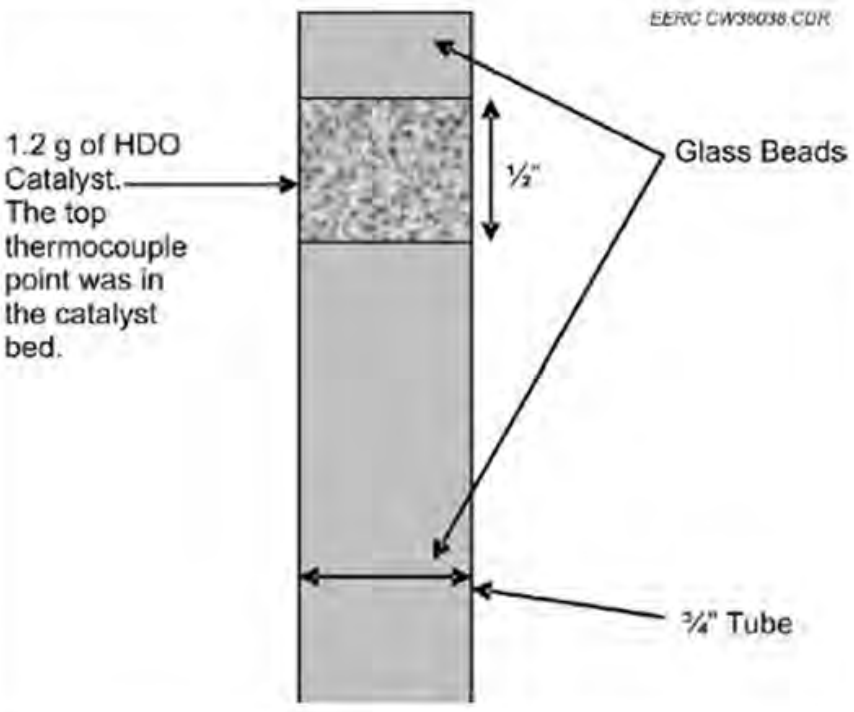

Figure 50. Schematic of the differential reactor used in kinetic rate data experiments.

Figure 51. Small continuous reactor system used for kinetic rate data experiment.

Background and theory

The small catalyst bed loaded into the SCR reactor tube constituted a differential reactor. A differential reactor is "normally used to determine the rate of reaction as a function of either concentration or partial pressure. It consists of a tube containing a very small amount of catalyst usually arranged in the form of a thin wafer or disc" (Fogler 1999). Because the HDO catalyst comes in pellet form, a wafer was not used in these experiments. Instead, the catalyst bed was kept small enough to constitute a differential reactor, but large enough to prevent channeling around the catalyst bed. Figure 52 shows the differential reactor and accompanying mass balance equations, and Equations 1 through 4, respectively (Fogler 1999).

$$\begin{bmatrix}\text{Flow}\\ \text{Rate}\\ \text{In}\end{bmatrix} - \begin{bmatrix}\text{Flow}\\ \text{Rate}\\ \text{Out}\end{bmatrix} + \begin{bmatrix}\text{Rate}\\ \text{of}\\ \text{Generation}\end{bmatrix} = \begin{bmatrix}\text{Rate}\\ \text{of}\\ \text{Accumulaton}\end{bmatrix} \quad \text{Eq. 1}$$

$$[F_{AO}] - [F_{Ae}] + \left[\left(\frac{\text{Rate\_of\_Reaction}}{\text{Mass\_of\_Catalyst}}\right) * \text{Mass\_of\_Catalyst}\right] = 0 \quad \text{Eq. 2}$$

$$F_{AO} - F_{Ae} + (r'_A) * (W) = 0 \quad \text{Eq. 3}$$

$$-r'_A = \frac{F_{AO} - F_{Ae}}{W} \quad \text{Eq. 4}$$

where:

F_{AO} = molar flow rate of fatty acid at the inlet
F_{Ae} = molar flow rate of fatty acid at the outlet
$-r'_A$ = rate of disappearance of fatty acid per mass of catalyst
W = weight of hydrodeoxygenation catalyst (1.2g).

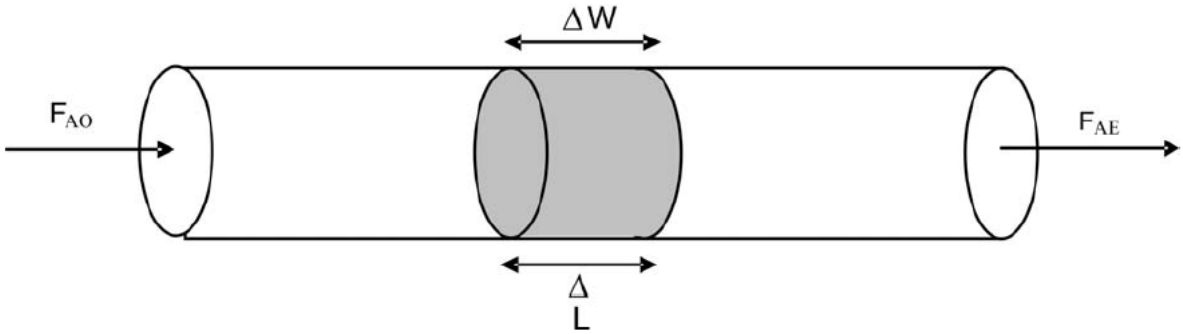

Figure 52. Schematic of a differential reactor. The catalyst bed is kept small, and inlet and outlet concentrations are measured to determine reaction rates.

Rate order with respect to hydrogen

The following rate law was proposed to model the reaction rate of fatty acid conversion to hydrocarbons on the catalyst:

$$r' = k\,[\text{fatty acid}]^a\,[\text{hydrogen}]^b \qquad \text{Eq. 5}$$

where:

r' is the rate at which acid reactant is consumed
a = rate order with respect to fatty acid concentration
b = rate order with respect to hydrogen concentration

At constant fatty acid concentration in the feed:

$$r' = k'\,[\text{hydrogen}]^b \qquad \text{Eq. 6}$$

Because hydrogen concentration is related to the hydrogen partial pressure in the reactor:

$$r' = k''\,[PH_2]^b \qquad \text{Eq. 7}$$

Equation 7 was used to determine the reaction rate order with respect to hydrogen partial pressure. Table 23 lists the experimental design data used to gather hydrogen rate data. The feed for hydrogen experiments was 5 mass% fatty acids and 95 percent Norpar-15. Norpar-15 is a commercially available blend of normal paraffins, concentrated around C-15 (pentadecane). The molar flow rate of fatty acid at the reactor inlet and outlet were determined by titration and known flow rate. Experiments were run in random order to minimize possible error introduced by measurement drift, catalyst aging, etc.

Table 23. Hydrogen rate data experimental design and results.

Run Order	H_2 Pressure, psi	Acid In, gmole/min	Acid Out, gmole/min	r', (gmolAcid)/(gcat*min)	Conversion
5	300	0.00028	0.000139044	0.0001153	50%
2	450	0.00028	0.000107855	0.0001413	61%
3	600	0.00028	0.000110086	0.0001395	60%
1	750	0.00028	0.000100416	0.0001475	64%
4	900	0.00028	0.000103162	0.0001452	63%

Equation 7 was manipulated to graphically determine the reaction order with respect to hydrogen (superscript "b" in Eq. 7). Taking the natural log of both sides of Eq. 7 gives:

$$\ln(r') = \ln(k) + b \ln(PH_2) \qquad \text{Eq. 8}$$

Equation 8 is in the form of the equation for a straight line (y = mx + b). The natural log of the reaction rate, r', was plotted on the y-axis with the natural log of hydrogen pressure on the x-axis. The slope was then "b" in Equation 8, the reaction order with respect to hydrogen.

Figure 53 shows the results from hydrogen rate data experiments; the reaction order with respect to hydrogen was determined to be 0.2. However, the 450 psi data point appeared to be an outlier. The R^2_2 value for the fitted line was 0.77.

Two additional data points were collected at a later date to investigate whether the 450 psi data point was an outlier because of experimental error or some unknown phenomena that occurs at lower pressure. The two additional data points were taken at 400 and 450 psi. Figure 54 shows the results. The two additional data points are shown as red boxes. Because the additional data fell much closer to the trended line, the initial 450 psi data point was dubbed an outlier due to experimental error. Removing the outlier gave the results shown in Figure 55. The reaction rate order with respect to hydrogen was still found to be 0.2; however, the trended line was a better fit, with an R^2 of 0.88.

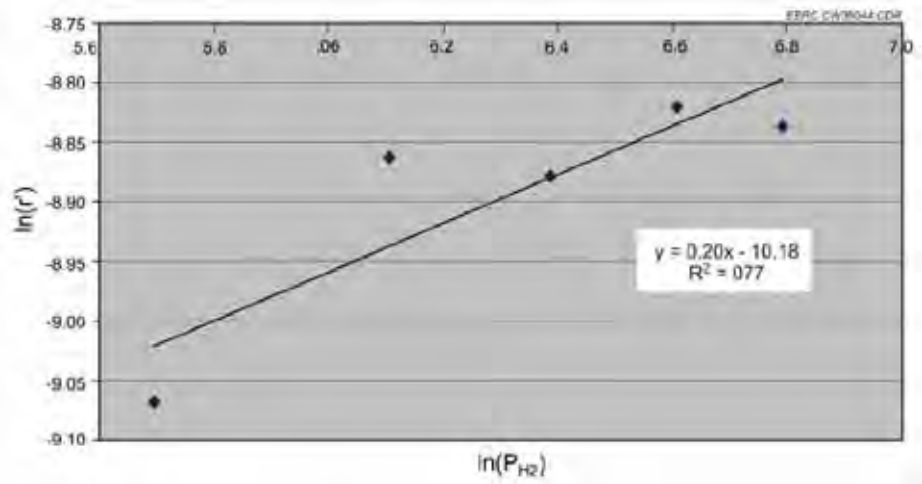

Figure 53. Results from the first five hydrogen rate data experiments.

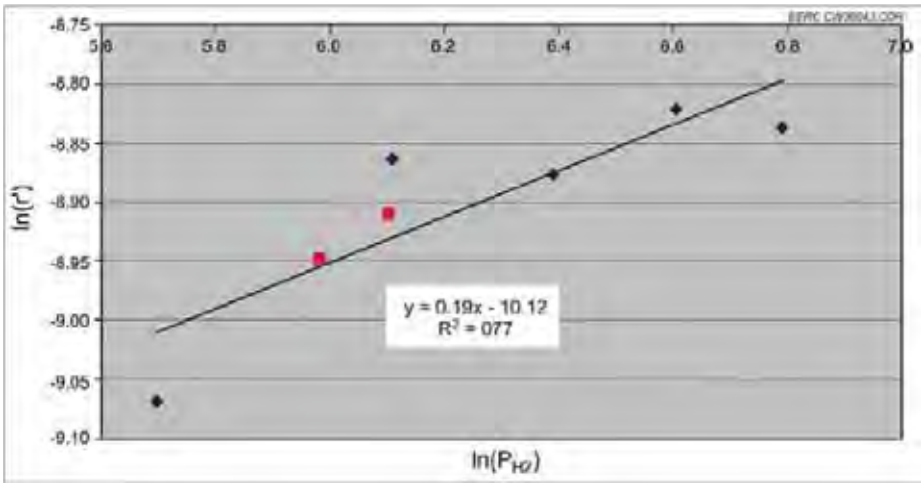

Figure 54. Results from the two additional data points at lower pressure supported the hypothesis that the initial 450 psi data point was an outlier due to experimental error.

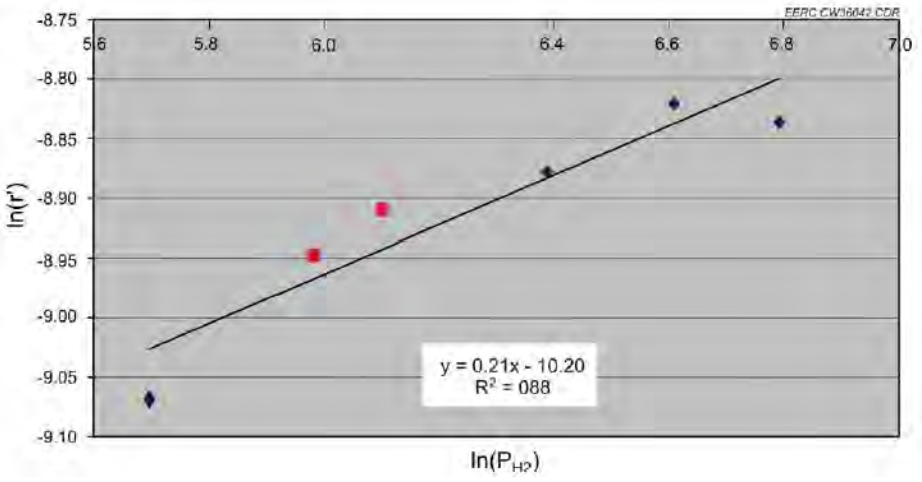

Figure 55. After removing the outlier, the rate order with respect to hydrogen was still found to be 0.2; however, the trend line fitted the data better (R^2 = 0.88).

Rate order with respect to fatty acid concentration

After the rate order was determined with respect to hydrogen, experiments were designed and conducted to determine the reaction rate order with respect to fatty acid concentration. At constant hydrogen pressure, the reaction rate equation (Eq. 5) reduces to:

$$r' = k''' \left[\text{fatty acid}\right]^{a} \quad \text{Eq. 9}$$

As in the hydrogen experiments, taking the natural log of both sides of Equation 9 gives the equation for a straight line (Eq. 10), which can then be used to extract the rate order with respect to fatty acid concentration:

$$\ln(r') = \ln(k) + (a)\ln(\text{fatty acid}) \quad \text{Eq. 10}$$

The feed mixture of fatty acids and Norpar-15 was varied according to the experimental design in Table 24. The run order was again randomized to minimize errors due to drift, catalyst poisoning, etc.

The results from these experiments were fitted very well ($R^2 = 1$) with the trended line shown in Figure 56, strongly supporting the assumption of a power law rate mechanism. The reaction rate with respect to fatty acid concentration was found to be approximately first order (0.92).

Conclusion

These results suggest that the HDO reaction is a first order reaction with respect to fatty acid feed concentration and fractional order (0.2) with respect to hydrogen partial pressure. Equation 11 shows the model:

$$r' = k\left[\text{fatty acid}\right]^{1}\left[\text{hydrogen}\right]^{0.2} \quad \text{Eq. 11}$$

where:

r' = the rate at which fatty acid is consumed (g mol Acid/[g Catalyst*min]).

Table 24. Soy fatty acid concentration rate data experimental design and results.

Run Order	[fatty acid] mass%	Acid In gmole/min	Acid Out gmole/min	r' (gmolAcid)/ (gcat*min)	Conversion
1	1%	0.0000552	0.0000190	0.0000302	66%
3	2%	0.0001105	0.0000393	0.0000594	64%
2	3%	0.0001660	0.0000629	0.0000860	62%
5	4%	0.0002217	0.0000931	0.0001071	58%
4	5%	0.0002774	0.0001153	0.0001351	58%

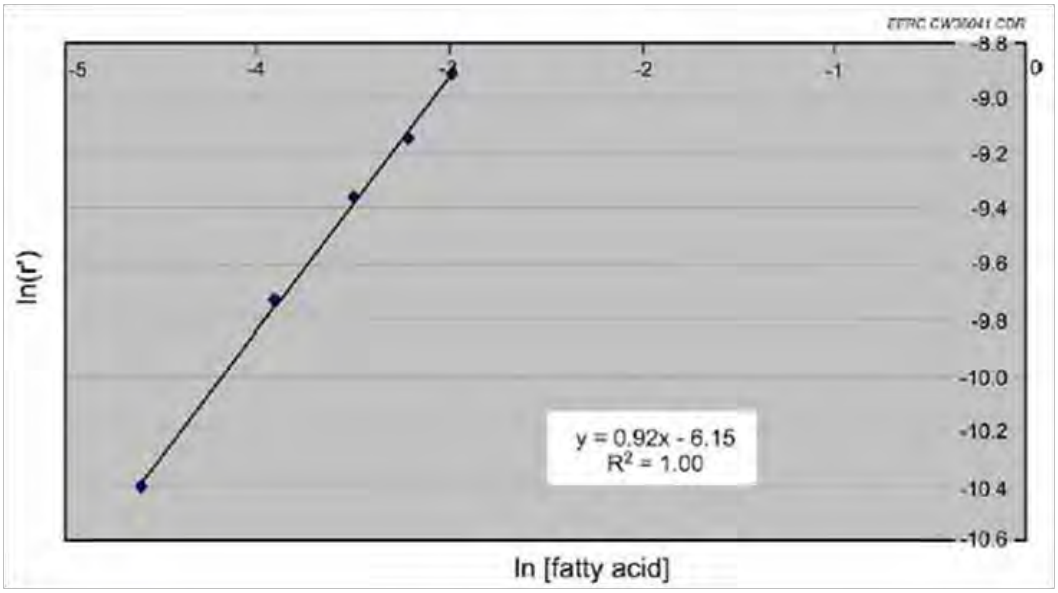

Figure 56. Results from experiments that varied the concentration of fatty acid showed that the reaction rate order with respect to fatty acid concentration was approximately first order.

Isomerization – Intermediate product analysis

To produce a broad distribution of highly isomerized hydrocarbons that can later be distilled into naptha, jet, and diesel fractions, the hydrodeoxygenated product from the HDO reactor is dried and fed to an isomerization/cracking reactor. The isomerization reactor contains a different catalyst than the HDO reactor. Typically, hydrocarbon product is run through the isomerization reactor multiple times to achieve the necessary ratio of straight-chain and branched-chain hydrocarbons. Once sufficient isomerization has been achieved, the product is distilled to provide naphtha, jet fuel, and diesel fuel samples.

Pilot plant integration into existing refinery

Scaling up the renewable fuel process for integration at an existing refinery is an attractive commercial option when compared to a standalone biofuels plant capable of producing specification-compliant fuel from renewable feedstock. The CHI process can be optimally tailored to produce a high cetane, low-sulfur hydrocarbon that can be further processed by existing refinery operations into finished fuel. This scenario takes advantage of existing petroleum refining and distribution infrastructure while providing valuable high-cetane, low-sulfur, and renewable hydrocarbon blendstock to the refinery.

To aid in evaluating the value of an integrated CHI-based process with petroleum refining operations, the EERC conducted a series of experiments to produce a variety of hydrocarbon chemical intermediates and fully fungible, drop-in-compatible liquid fuels from a renewable oil feedstock. Canola oil was processed using the CHI technology, and samples of hydrocarbon were collected from each stage of the process. These samples were analyzed by a contract fuel laboratory to determine physical and chemical properties. Results from these tests are representative of work conducted over the past 2 years in which a variety of feedstocks, including oils from soybean, corn, camelina, canola, crambe, and algae, as well as waste oils, were processed using the CHI technology to produce jet fuel, diesel, and naphtha. Data from these experiments will be used to further evaluate the best integration strategy and pilot plant design basis for the CHI process.

The intermediate renewable hydrocarbon streams have sulfur contents less than 3 ppm and cetane values ranging from 56 to 79. Cetane number trended downward with increased isomerization/cracking. This observation is in agreement with literature reports on cetane number (Santana et al. 2006; Lapidus et al. 2008). Freezing point decreased with increased isomerization. This is the main reason why a high level of isomerization is required to produce a jet fuel that meets specifications. Specific gravity decreased with increased isomerization/cracking. Tables 25 and 26 list fuel analysis results for canola oil, hydrodeoxygenated canola oil (HDO), incrementally isomerized products, and product distillate fractions.

Subtask 2.3 – Development of modular systems for distributed fuels and energy

Introduction

Military facilities and the personnel stationed there, like any other "community," have requirements for performance of its daily operation. These needs fall into two categories: personnel subsistence and mission-specific requirements. Personnel subsistence needs include electricity, water for consumption and washing, sewer systems (both septic and storm), and heating and cooling. The requirements to carry out a mission, although facility-specific, include electricity, water, and fuel needs (both ground and air vehicles).

Table 25. Fuel analysis results.

Parameter	Canola	HDO	Isom 1	Isom 2	Isom 3	Isom 4	Isom 5	Isom 6	Naphtha	Jet	Distillate Bottoms
Vol% aromatics		16.7	1.2	3.4	1.6	1.9	0.8	0.8	NA	0.5	1.8
Vol% olefins		9.9	0.2	0.7	0.6	1.9	0.5	0.3	0.04	0.5	1.8
Vol% saturates		73.4	98.6	95.9	97.8	96.2	98.7	99	NA	98.9	96.4
API gravity @60 °F		46.9	48.6	49.8	50.9	51.7	53.3	55.2	67.3	53	48.6
Specific gravity	0.916	0.7936	0.7857	0.7805	0.7758	0.7724	0.7657	0.7579	0.7118	0.7669	0.7857
IBP, °F		140.5	142.5	144.9	149.2	149.2	135.9	145.4	114.6	287.4	450
FBP, °F		752.2	705.6	607.3	608.5	586	568.8	547.9	374.7	523	562.3
Flash, °F	315	<68	<68	68	<68	<68	<68	<70	NA	102	222.8
Freezing, °F		60.8	32	28.4	8.6	-4	-22	-41.8	NA	-79.8	NA
Cloud smoke, °F		59	42.8	28.4	8.6	-2.2	-29.2	-43.6	NA	<-76	-25.78
Smoke, mm		25	25	25	25	25	25	NA	NA	22	NA
Water content, ppm		49	41	40	34	15	23	39	47	52	<10
Nitrogen, ppm	<3	<1	<1	<1	<1	2	<1	<1	<1	<1	<1
Sulfur, ppm	3.287										
Sulfur, mg/kg		<3	<3	<3	<3	3.4	<3	<3	<3	<3	<3
Cetane		74.3	76.7	77.8	78.9	64.4	62.3	56.3	NA	56.3	73.8
Viscosity @ 104 °F (cst)		0.9800	1.3240	1.0270	0.8995	0.8281	0.5650	0.8011	NA	0.6298	1.0660
Viscosity @ 25 °C (mPa*s)	57.569										

Table 26. Metals content detectable (≥5 ppb) in canola oil derived fuel (all samples).

Metal	Ranges, ppb
Aluminum	24–386
Boron	40–50
Calcium	20–24
Iron	10–13
Lead	100–110
Magnesium	26–38
Silicon	120–226
Titanium	6–8
Zinc	7–14

Figure 57 shows a simplified diagram of the utility inputs and outputs of the facility as a whole.

The U.S. Department of Defense (DOD) and, equally, each armed services branch, is aggressively evaluating the energy and fuel usage at military facilities for a variety of reasons, including vulnerability, sustainability, and environmental impact (i.e., carbon footprint) to name a few. With this focus in mind, the EERC performed a brief evaluation of specific technologies targeted at the production of fuels and/or energy. The technologies evaluated included biomass gasification coupled with IC engine, biomass gasification coupled with synthetic natural gas production, biomass gasification coupled with the FT process, and CHI. Each of these technologies is discussed in greater detail in the following sections, but Table 27 of the technology and primary end product.

Figure 57. Military facility utility inputs/outputs.

Table 27. Summary of technology processes.

Feedstock	Technology Process	Primary End Product
Biomass	Gasification w/SNG[a] production and IC engine	Electricity
Biomass	Gasification w/SNG production	Natural Gas, Propane
Biomass	Gasification w/FT process	JP-8, Gasoline, Diesel
Renewable-derived oils	CHI	JP-8, Gasoline, Diesel

Biomass gasification

Gasification of biomass is the initial step in three of the processes evaluated and, therefore, is discussed in greater detail in this section. Biomass can be gasified into a syngas that can then be converted into electricity, synthetic natural gas, or liquid fuels. This report presents a mass and energy balance for each scenario. Depending on the unique needs at a given military installation, one form of energy may be more desirable than another. The energy efficiency of producing syngas, electricity, synthetic natural gas, and liquid fuels from biomass will be discussed.

According to a National Renewable Energy Laboratory (NREL) subcontractor report (NREL 2004), the energy efficiency for syngas production from a rice straw gasifier is 70 percent, where energy efficiency is defined as the energy content of the product syngas divided by the total energy inputs.

Biomass gasification to syngas

The NREL report (NREL 2004) describes experimental results from a 4.8-ton-per-day biomass gasifier. The simplified block diagram in Figure 58 summarizes that report. Table 28 lists inputs, outputs, and energy efficiency.

For the purpose of clarity and consistency, the Btu content of the feedstock input for each of the processes discussed in the following section was normalized to a common Btu content of 100 MMBtu, while ratioing the energy input and resulting output proportionally.

[a] Synthetic natural gas.

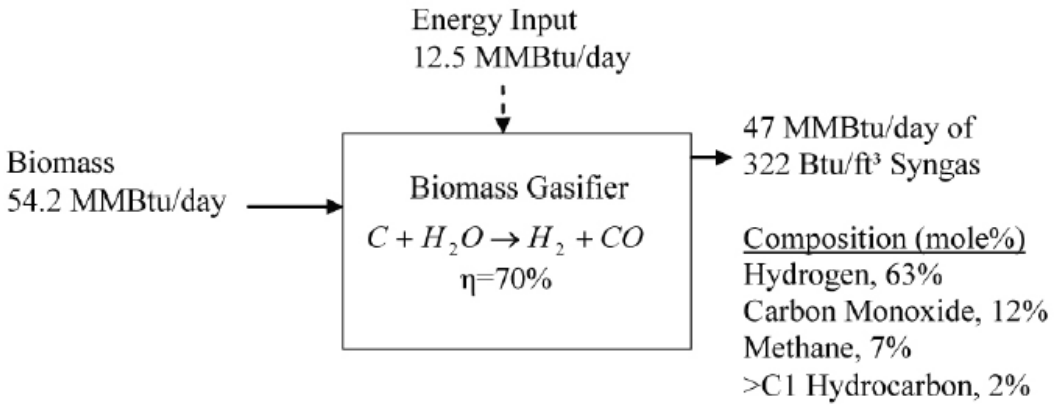

Figure 58. Simplified block flow diagram of a rice straw biomass gasifier.

Table 28. Biomass gasification data (NREL 2004).

Stream Name	Mass per Day, lb	Heating Value, MMBtu	Energy Efficiency
Rice Straw	9600	54.2	(47/[54.2+9.76+2.71])=70%
Natural Gas	–	9.76	
Electricity	–	2.71	
Water (steam)	1728		
Syngas	9886	47	

Biomass gasification to electricity

Biomass-derived syngas can be used in an electrical generator. The average thermal efficiency for a modern IC engine operating on syngas fuel with an energy content ≥ 300 Btu/ft³ is 40 percent. Figure 59 shows the biomass-to-electricity scenario. The overall system efficiency of converting biomass to electricity equates to 28 percent.

Biomass gasification to synthetic natural gas

As an alternative to producing electricity, SNG could also be produced from bio-derived syngas. An analysis was conducted, based on wood gasification, by Jurascik et al. (2009). The analysis calculated the efficiency of gasifying a wood feedstock and subsequently converting the syngas to SNG. Assuming that 10 percent of the woody biomass was not converted to syngas and remained as char, the efficiency, defined as the energy contained in SNG divided by total energy inputs, was 54.2 percent. The overall efficiency of converting biomass to SNG equates to 61 percent. The block flow diagram in Figure 60 shows the energy balance for such a system.

The Center for Energy and Environmental Studies at Princeton University studied the energy balance for a system that converts biomass into liquid fuels (Larson and Jin 1999). The study found the overall efficiency of converting biomass to liquid products to be 49 percent. The liquid products were 25 percent, by energy, naphtha (C_5-C_9), 50 percent kerosene (C_{10}-C_{12}), and 25 percent diesel (C_{13}-C_{18}). Figure 61 shows a flow diagram of the biomass F-T process, on the basis of 100 MMBtu of biomass feedstock.

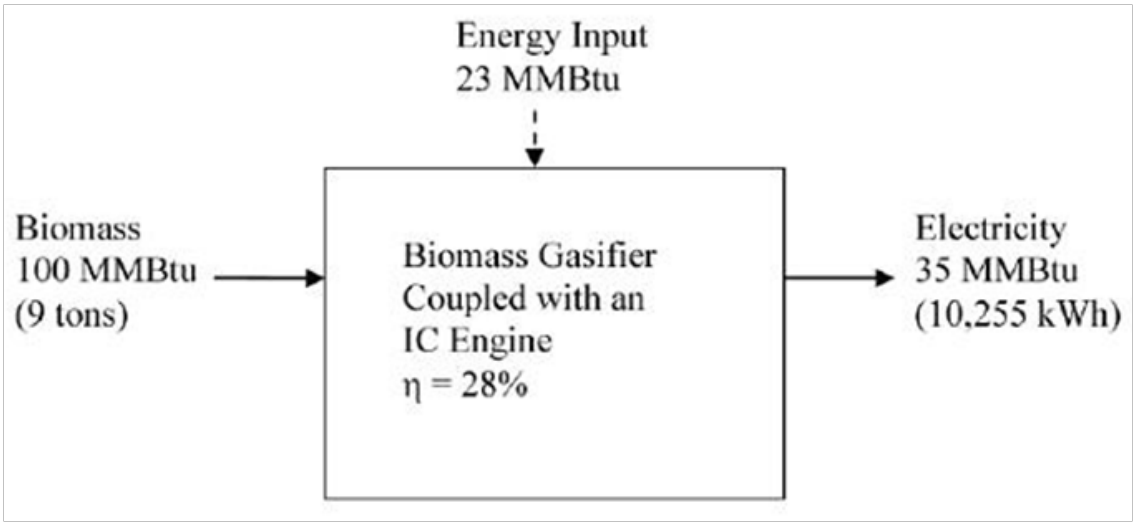

Figure 59. Block diagram for electricity production from biomass.

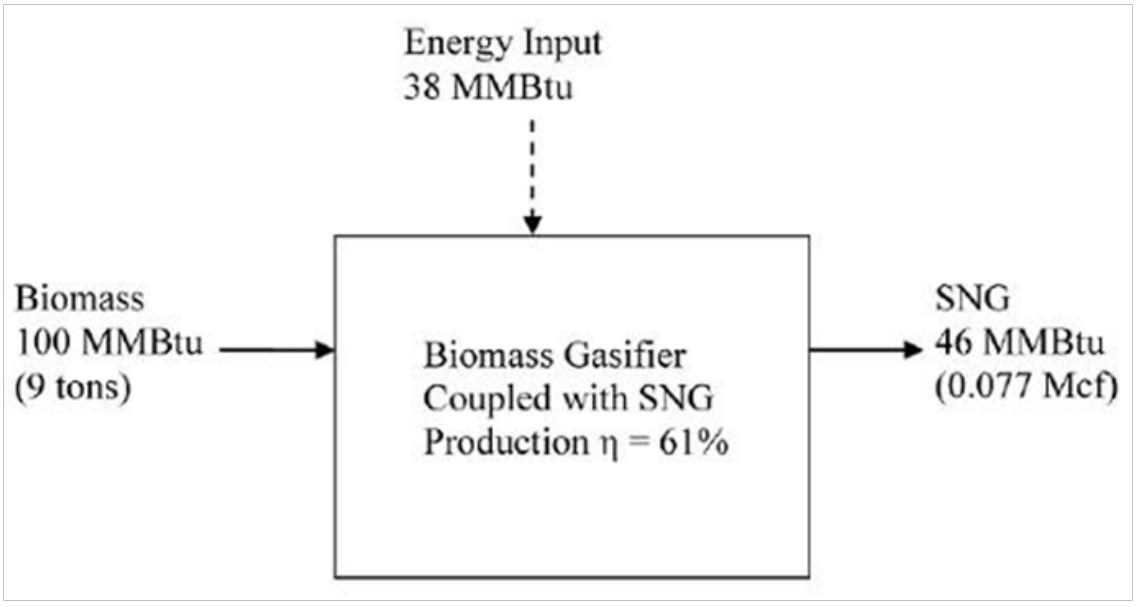

Figure 60. Block diagram for SNG production from biomass.

Biomass gasification to liquid fuels

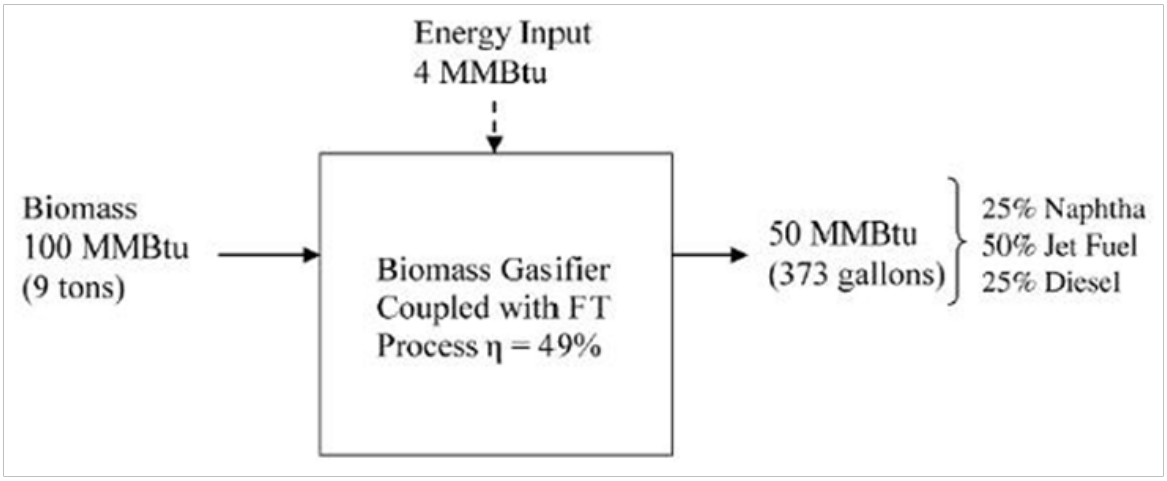

Figure 61. Block diagram for liquid fuels production from biomass.

Catalytic hydrodeoxygenation — Isomerization

The CHI technology uses catalyst, heat, and pressure to react hydrogen and renewable TAG to form hydrocarbon products. The TAG can come from crop oils, algal oils, or animal fats. Multiple TAG and fatty acid feedstocks have been assessed at the EERC and converted into specification-compliant fuels. By varying the degree of processing and the distillation cut points, it is possible to provide a slate of fuel products. Typically, JP-8-grade SPK has been the desired end product for EERC fuel production efforts. The renewable SPK product is then blended with ~20 percent aromatics to produce a specification-compliant JP-8. Aromatics are blended to increase the physical density of the fuel and for their lubricity properties. (Note that a specification-compliant JP-8 requires ~80% jet range isoparaffins, from the CHI process, and ~20% blended aromatics.) Figure 62 shows the inputs and outputs of the CHI process.

By varying the degree of processing in the CHI unit and changing the distillation parameters, it is possible to optimize the process for a different desired product (example: maximize naphtha or maximize diesel).

Oils that have been processed include soybean oil, canola oil, corn oil, crambe oil, camelina oil, soy fatty acids, coconut oil, palm oil, yellow grease, fatty acids from animal fats, and various algal oils. Feedstock flexibility is a major process advantage and allows the CHI technology to use the most convenient and/or inexpensive TAG source available.

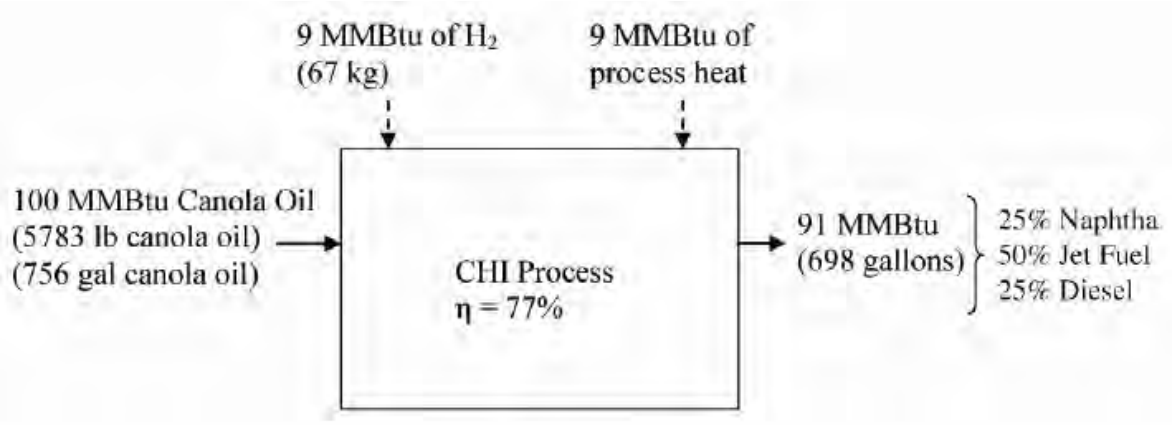

Figure 62. Inputs and outputs for the CHI unit that converts crop or algal oils into fuel products.

When selecting a modular energy production system, it is important to consider the system's utility requirements. The CHI process requires four process inputs: TAG feedstock, hydrogen, cooling water, and electricity. Steam could be used instead of electricity for some process heating requirements if it is available and less expensive. The major product from the CHI process is liquid hydrocarbon fuel (i.e., naphtha, jet fuel, diesel fuel). Light gases (methane, ethane, propane, carbon dioxide, carbon monoxide) are also produced along the water from the reduction reaction. The light gas stream can be used for heating. The produced water would likely have to be treated before disposal.

Technology summary

Biomass and renewably derived oils are a suitable feedstock for the production of electricity, SNG, and/or liquid fuels. In order of increasing efficiency, the four processes are ranked: electricity production from biomass, liquid fuels production from biomass, SNG production from biomass, and CHI. These technologies vary in technical maturity and scalability and would each require detailed technical and economic evaluation on a case-by-case basis.

Grand Forks Air Force Base — ND

Introduction

In an effort to perform a brief technology evaluation to put the scale of these processes in perspective, the EERC requested and obtained information from GFAFB in North Dakota. The information was related to fuel

and utility commodity usage for both mission-critical operations and personnel subsistence requirements.

Facility information

Information in this section serves as the basis for all technology evaluations and feasibilities. GFAFB is located in northeastern North Dakota and performs its mission with approximately 3200 personnel. The closest town is Emerado, ND (population: 500). The nearest population center is Grand Forks, ND, with a population of approximately 50,000 people. Figure 63 shows GFAFB utility inputs and outputs.

Total electrical usage at the GFAFB is approximately 61,000 MWh annually for the entire installation, with a peak electrical demand of slightly greater than 11 MW. Electricity for the facility is provided by Nodak Rural Electric Cooperative, a distribution utility under Minnkota Power Cooperative.

GFAFB primarily uses natural gas for heating, which is provided by a local utility (Xcel Energy). Some natural gas is used to generate steam for humidification (steam requirements are covered in a later section). Annual consumption of natural gas is approximately 327,000 Mcf.

The peak demand month is January since natural gas demand was primarily for space heating. GFAFB indicated that a natural gas steam generator is operated on the facility, and the steam is used for humidification. Propane use is limited to space heating and amounts to approximately 203,000 gal annually.

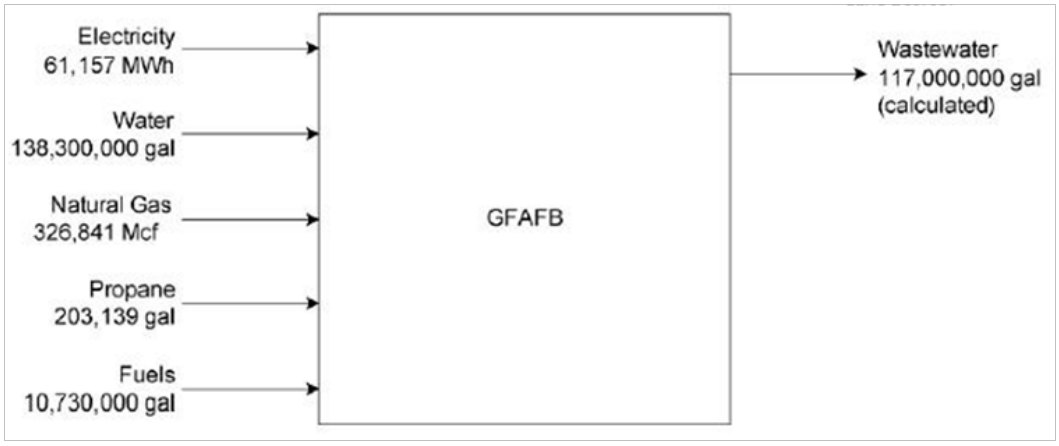

Figure 63. GFAFB utility inputs/outputs.

The water supply for GFAFB is provided under contract with the local rural water district (Agassiz Water Users, Inc.) and the city of Grand Forks. The annual water consumption at GFAFB is approximately 138 million gal per year (MGY) or 378,000 gal per day (gpd). Peak water demand occurs in August with a peak daily demand of slightly more than 1 million gal.

GFAFB operates and maintains its own wastewater treatment facility to manage wastewater discharge from the facility. Information regarding the wastewater treatment facility was not provided. Using accepted estimates for per capita discharge, total wastewater discharge would be approximately 320,000 gpd or 117 MGY, assuming 100 gal per capita per day for the 3200 base personnel.

The GFAFB current mission is to provide refueling support to the U.S. Air Force with a fleet of KC-135 Stratotankers. The annual fuel usage for the GFAFB consists of 10,580,000 gal of JP-8, 87,000 gal of gasoline, and 63,000 gal of diesel fuel (No. 1). Note that the GFAFB mission is currently changing to one of unmanned aerial vehicles (UAV), but for the purposes of this report and given the availability of data, analysis was performed on the GFAFB's mission at the time of writing and does not included fuel usage of the UAV mission.

GFAFB technology evaluation

Each process evaluated for the GFAFB focused on a primary target end product listed in Table 29. In some cases, such as the FT and CHI processes, other usable end products are produced in addition to the target product. The "nontarget" end products are not listed in Table 29, but are discussed in the process summaries described in the following sections.

Table 29. Technology evaluation.

Target Product	Applicable Technology	GFAFB Usage	Feedstock Required
Electricity	Biomass gasification with SNG production and IC engine	61,157 MWh/yr	53,000 tons/yr biomass
Natural gas	Biomass gasification with SNG production	326,841 Mcf/yr	38,000,000 tons/yr biomass
Propane	Biomass gasification with SNG production	203,139 gal/yr	2000 tons/yr biomass
JP-8	Biomass gasification with FT process	10.58 Mg/yr	509,000 tons/yr biomass
Diesel	Biomass gasification with FT process	0.063 Mg/yr	6100 tons/yr biomass
JP-8	CHI	10.58 Mg/yr	84,000 tons/yr canola oil
Diesel	CHI	0.063 Mg/yr	2500 tons/yr canola oil

Biomass gasification to electricity

Based on the information presented in previous sections, gasifying biomass to produce syngas that is, in turn, burned in an IC engine at GFAFB would result in the following scenario. Approximately 53,000 tons of biomass would be required to be gasified a year to meet the annual GFAFB electrical usage of approximately 61,000 MWh.

Biomass gasification to synthetic natural gas

The biomass gasification to SNG scenario was analyzed for displacement of two different currently used products: natural gas and propane. A system to displace the natural gas usage (327,000 Mcf) at the GFAFB would require greater than 38 million tons, while a system operated to displace propane usage (200,000 gal) would require approximately 2000 tons.

Biomass gasification to FT liquids

To meet the JP-8 demand at the GFAFB (11,000,000 gal) would require operation of a biomass gasification to FT liquids system capable of processing of approximately 509,000 tons of biomass, resulting in 5 million gal of both naptha and diesel. Table 30 summarizes biomass gasification to FT.

This same process operated to displace diesel demand would require 6000 tons of biomass gasified annually and would also produce 63,000 gal of naptha and 127,000 gal of JP-8.

CHI process to fuels

The CHI process operation can be adjusted to selectively produce a greater percentage of the target fuel. In testing performed at the EERC, the CHI was operated to maximize JP-8 production, which resulted in an end product mixture of 33 percent naptha, 52 percent JP-8, and 13 percent diesel. Scaling this system up to meet GFAFB's annual JP-8 demand of approximately 11,000,000 gal would require a system capable of processing approximately 84,000 tons of renewably derived oil (in this case, canola oil) annually. In addition, approximately 2,000,000 kg of hydrogen would also be required as a process input. As by-products, the system would also produce approximately 7 million gal of naptha and 3 million gal of diesel a year.

Table 30. Summary of biomass gasification to FT scenarios.

Target Product	Target Quantity	Feedstock Required	By-Product	By-Product Quantity
JP-8	10,580,000 gal	509,000 tons of biomass	Naphtha	5,000,000 gal
			Diesel	5,000,000 gal
Diesel	63,000 gal	6000 tons of biomass	JP-8	127,000 gal
			Naphtha	63,000 gal

Operating the CHI process to maximize diesel production would result in an end product fuel of approximately 20 percent naptha, 40 percent JP-8, and 40 percent diesel. A 40 percent diesel scenario would require approximately 2500 tons/yr of canola oil and would result in approximately 63,000 gal of JP-8 and 32,000 gal of naptha. This scenario would require approximately 15,000 kg of hydrogen a year. Table 31 summarizes these scenarios.

Summary of GFAFB evaluation

Although several technologies can be used to displace energy and fuels used at GFAFB, only a few appear remotely reasonable from an economic feasibility, scale, and feedstock resource perspective: (1) propane displacement using biomass gasification, (2) diesel production using biomass gasification to FT, and (3) diesel displacement using CHI. The scale and cost of the other process scenarios make them unlikely to be implementable at GFAFB.

The evaluation of GFAFB scenarios was performed as a cursory review of available technologies and their potential implementation. To fully determine both technical and economic feasibility would require a thorough analysis.

Table 31. Summary of CHI scenarios.

Target Product	Target Quantity	Feedstock Required	By-Product	By-Product Quantity
JP-8	10,580,000 gal	84,000 tons of canola oil	Naphtha	7,000,000 gal
			Diesel	3,000,000 gal
Diesel	63,000 gal	2500 tons of canola oil	JP-8	63,000 gal
			Naphtha	32,000 gal

5 Project Management and Reporting (Task 3)

Task 3 facilitated management of the entire project, *Production of JP-8-Based Hydrogen and Advanced Tactical Fuels for the U.S. Military*, under Cooperative Agreement No. W9132T-08-2-0014. The overall project manager was Chris J. Zygarlicke, who worked primarily with principal investigators in charge of major technical activities in Tasks 1 and 2. Responsibilities of Task 3 included all project management such as tracking deliverables and budgets, monthly and quarterly reporting, final reporting, internal project meetings, project review meetings with ERDC-CERL staff, and strategic studies. Strategic studies involved developing new ideas and providing forward planning and new technical ideas that enhance the overall goals of this project, working on critical publications and resource assessments, and networking with other researchers and project managers to gain collaborative relationships and valuable technical information. The project period of performance was from 1 July 2008 to 19 December 2009.

An initial internal meeting was held with all principal investigators involved in the new project and milestones, and project experimental plans were discussed and compared with proposal plans. Work was done to finalize the contract with ERDC-CERL and to justify the need for foreign nationals to work on the project. Discussions were held with contract specialists both at EERC and ERDC-CERL to determine reporting and other requirements for the project.

The kickoff meeting was held at the Tank Automotive Research, Design, and Engineering Center (TARDEC) facilities in Warren, MI, on 19 October 2008. Present were Chris Zygarlicke; EERC principal investigator leads including Bruce Folkedahl, John Hurley, and Ben Oster; Franklin Holcomb from ERDC-CERL; and Harold Sanborn, Patsy Muzzell, and several other individuals from TARDEC who stopped in during the course of the meeting for collaborative and information sharing purposes. The meeting agenda included an overview of EERC projects in energy and fuels that relate to military applications, a general review of progress of the current FY07 project, plans for the new FY08 project, and various presentations by TARDEC personnel on their current work related to military power and

fuels. Principal investigators for Task 1 described their work plan for hydrogen production and purification technology development and vehicle development and demonstration. Lead investigators for Task 2 discussed plans to develop alternative (nonpetroleum) feedstock-based technologies for production of advanced tactical fuels with JP-8 drop-in compatibility and improved properties for use as hydrogen feedstocks. Reporting, publications, and collaborations with other DOD agencies and researchers were also discussed. Since then, a collaborative relationship has continued with Ms. Muzzell and her team regarding FT and catalytically cracked hydrotreated diesel and jet fuels.

During this reporting period, Dr. Chang Sohn from ERDC-CERL became the primary contact for this project, and a conference call was held between all project principal investigators, Chris Zygarlicke, Franklin Holcomb, and Dr. Sohn to introduce the project and provide technical background. Dr. Sohn also visited the EERC on 6 May 2009, to further acquaint himself with the project, to get to know EERC engineers, and to tour pilot and analytical facilities, especially those being developed and used in the project. Technical activities on the recently completed FY07 and current FY08 projects were summarized in a PowerPoint presentation, and a full 1-day agenda was organized to review the project with Dr. Sohn. Discussions were also held with Dr. Chang Sohn on supplying more detailed information from the University of North Dakota (UND) billing office along with monthly and quarterly reports regarding costs for labor, fringe benefits, and supplies/equipment. The EERC worked with the billing office at UND and accommodated this additional information.

Although a hydrogen vehicle demonstration was not part of this FY08 project, several management-level discussions were held concerning the future of demonstrating hydrogen fuel cell vehicles, with great interest in providing continued support, but not designing and building such systems. Strategic planning and management were also applied toward finding a reasonable solution to ePower not delivering on two fully functional hydrogen fuel cell-powered utility vehicles for ERDC-CERL and Robins Air Force Base (AFB). EERC upper management sent letters to ePower bringing to its attention that Robins AFB and APTO had rejected the Toolcat fuel cell-powered MPUV that ePower had delivered as part of a separate contract with ERDC-CERL; a contract that, although not appropriated through the EERC, was being executed through the EERC. Scott Slyfield and his staff at APTO determined that the vehicle did not meet the specifi-

cation developed between ePower and APTO, and as such, APTO asked that the vehicle be removed from Robins AFB. The EERC then worked with California Motors, APTO, and ERDC-CERL to define a corrective action plan that would satisfy the requirements of the scope of work within the short amount of time remaining on the contract (26 April 2009). California Motors was unable to repair or modify the existing Toolcat such that the contracted statement of work could be met. Alternatives for providing APTO with a functioning fuel cell electric vehicle were pursued. EERC disassembled the Toolcat to conduct a system/component inventory and was able to reassemble the vehicle to at least get the system to mobilize and start and stop safely. The vehicle was still not satisfactory according to what ePower was supposed to deliver; therefore, the EERC submitted a request for contract modification to ERDC-CERL to eliminate the delivery of the two Bobcat vehicles and add delivery of a new fuel cell-powered forklift. Franklin Holcomb gave approval, and the EERC procured, tested, and delivered a Hyster forklift with a Hydrogenics fuel cell pack. APTO confirmed that the vehicle was performing flawlessly at Robins AFB, and the contract was considered complete.

Several meetings and conferences were attended and participated in by EERC to broaden applicability of technologies being developed in hydrogen, distributed generation and advanced tactical fuels; to network with other researchers and project managers; to gain collaborative working relationships and cost-share partners; and to simply gain valuable technical information that could benefit the technical research activities. An invited presentation and abstract entitled “Biofuels and Bioenergy on U.S. Military Bases” were presented at the U.S. Army Corps of Engineers Net-Zero Energy (NZE) Installation and Deployed Bases 2-day Workshop on 2–4 February 2009, in Colorado Springs. CO. The event had about 140 in attendance, including representatives from U.S. military or defense research departments and defense contractors. Discussions were held with several DOD and nonFederal contractors on potential EERC support research in areas related to energy efficiency and renewable energy for military installations in addition to current work that is focused on hydrogen, distributed generation, and advanced fuels production. Other potential EERC areas of research support that could aid military installations include heating, cooling, materials, design, combined heat and power facilities (CHP), renewable energy systems, microgrids and all many aspects of energy efficiency, building efficiency, and communitywide renewable energy and energy efficiency integration, which may be of future benefit to ERDC CERL.

Several good potential collaborative contacts were made with commercial industry, researchers, and military personnel at the Renewable Energy World conference in Las Vegas, NV, 10–12 March 2009, and at the National Hydrogen Association Conference and Hydrogen Expo, 30 March–3 April 2009. The particular collaborative areas are related to energy efficiency, renewable energy, communitywide renewable energy and energy efficiency integration, fuel cell systems, and hydrogen production. Many of these systems have applications for military installations.

Discussions were held in several round-table meetings at the National Hydrogen Association's (NHA's) Annual Conference and Expo in Columbia, SC, on 30 March – 3 April 2009. Informal presentations, addresses, and discussions were employed to facilitate ideas and programs between the NHA and universities to advance hydrogen production and applications, including military applications.

A presentation related to EERC work in developing oil seed energy crops for conversion to hydrocarbon fuels for military and commercial use was given at the Biomass '09 International Conference and Tradeshow in Portland, OR, on 28–30 April 2009.

Meetings and presentations on coal and biomass conversion to FT liquid fuels, biomass combustion and gasification for power production, municipal waste to power, and hydrogen production were attended and facilitated at the 34th International Technical Conference on Coal Utilization & Fuel Systems in Clearwater, FL, on 31 May – 4 June 2009. A particular emphasis of discussion and information gathering was directed toward indirect and direct coal and biomass liquefaction for fuel development and catalyst production and catalytic processes for gas-to-liquid fuel production. A follow-on planning meeting was attended in Des Plaines, IL, to develop panel discussions, tutorials, and keynote addresses that address needs for liquid and gaseous alternative fuels and hydrogen from coal or coal–biomass mixtures for the 35th International Technical Conference on Clean Coal & Fuel Systems that will take place in June 2010. The meetings included a tour of gasification and fuel development research at Gas Technology Institute.

Numerous discussions were held with key experts working in thermochemical approaches to biomass-to-liquid technologies at the tcbiomass2009 conference in Chicago, IL. Especially pertinent to EERC work

were discussions related to converting biomass to pyrolysis liquids or synthetic gases, with subsequent conversion to hydrocarbon fuels or ethanol. A trip report was prepared for principal investigators for review of certain presentations, meetings, discussions, and posters. Of particular interest to the EERC was the gas cleanup technology developed by Research Triangle Institute (RTI) (United States) and Energieonderzoek Centrum Nederland (Netherlands Energy Research Foundation) for biomass gasification systems similar to the gasifier designs worked on by the EERC for the ERDC-CERL project. Potential collaborations may ensue.

Work was done to help facilitate the 4th Biomass Summit: Feedstock, Cofiring, Finance, and Investment in Washington, DC, held in October 2009, an important venue for discussing real-world biomass fuels and power with applicability to Federal and military agencies, financial entities, and industry. Especially pertinent was the sustainability of biomass feedstocks to military installations for power production.

A summit meeting was attended in nearby Fargo, ND, on 28–30 August 2009, that was put together by Senator Byron Dorgan and involved several national labs, the U.S. Department of Energy, and the National Science Foundation. It was called the Sustainable Energy Innovations Summit and involved discussions on new developments in the production of jet and vehicle alternative fuels, hydrogen, and sustainable energy and marketable products in general. Also, at the EERC, discussions were held with Mr. Jay Otten, Manager, Technology and Innovation at BASF Corporation – Wayandotte, MI. Although primarily in the chemicals business, BASF has been helpful to the EERC/ERDC-CERL projects in supplying materials and expertise. Discussions centered on catalysts for direct and indirect liquefaction of coal and biomass to diesel and jet fuel products; potential production of engine additives, green diesel experience and technology developments in Europe, and cellulose biofuels in general. Discussions were held with Tesoro at the EERC with regard to potential military interests in green diesel and renewable jet fuel production from biobased feedstocks. Finally, fruitful discussions were held with Select Engineering Services (SES) to possibly supply research, development, and technical service work as collaborators with SES on upcoming contractor projects SES may have with TARDEC.

Task 3 facilitated and managed all reporting activities, including quarterly reports and a semiannual report. Also, a project management plan was

prepared for ERDC-CERL as part of contractual reporting requirements, which contained project objectives, work tasks, milestones, and the overall schedule. All reports were prepared and formatted in accordance with U.S. Army Corps of Engineers ERDC Technical Report Guidelines.

In the area strategic studies and publications, a special ERDC-CERL technical report was initiated and completed to a draft copy. The technical report is entitled "Development and Demonstration of Hydrogen Production and Purification Systems for U.S. Military Fuel Cell Vehicles." It was reviewed internally by four EERC principal investigators and Chris J. Zygarlicke. The report summarizes activities to date related to the development of the high-pressure hydrogen production, purification, refueling, and vehicle demonstration work. A copy of the draft report will be given to ERDC-CERL for review and inclusion, if possible, of an ERDC-CERL author. The document should be completed, finalized, and published in the next few months.

A second major strategic studies effort involved work done to put together a biomass resource and characterization assessment for the contiguous United States. In addition to funds from this project, funds from an industrial partner supported the effort. The final report entitled "Identification and Characterization of Biomass Sources in the United States" is cited in the "References" section of this technical report. The aim of the report was to determine the current and future availability of agricultural and forest residues, energy crops, and urban residuals as biomass sources in the United States for power and fuels. The study included some data on the chemical and physical properties of those sources and information on national land ownership, climate zones, and biomass-growing conditions. The project produced a detailed report that included county-by-county biomass resource types and estimates and also included some biomass properties data. The large dataset collected as a result of this study will be used to evaluate the feasibility of specific biomass utilization opportunities. One conclusion drawn from the study is that there is no single ideal biomass source. While some sources may have ideal combustion and cofiring properties, such as wood, other sources are optimal feedstocks for fuel production, such as corn or soybeans. In addition, no type of biomass is uniformly available across the United States or even within individual states.

The best source for a particular energy production scenario will depend on multiple factors that will need to be assessed on a case-by-case basis. These factors include the following:

- local resource availability
- resource costs
- resource physical and chemical properties and intrinsic fuel values
- plant size, feed ratio with coal (for cofiring scenarios)
- resource processing requirements (drying, shredding, pulverizing, separating), storage options
- local geography and climate (which will impact biomass properties)
- availability of process utilities for conditioning as-received resources.

When specific biomass utilization applications are considered, it is imperative to verify the information on a local level and test the specific biomass source to be used. Each application will also require a thorough technoeconomic assessment and analysis of available feedstocks before a candidate biomass being selected for energy generation or product development.

Finally, this management task was heavily involved in all of the day-to-day contract negotiations that took place related to obtaining approval for foreign nationals to work on the project, securing changes to budget structures for purchasing equipment necessary for technical research, securing no-cost project extensions, securing cost-share funding, and other such project and contract modifications.

6 Conclusion

This work successfully completed the following tasks:

1. Developed and optimized the HPWR concept for on-demand production of high-pressure PEM fuel cell-quality hydrogen from JP-8 and other feedstocks, which included:
   a. Complete optimization of the HPWR hydrogen production system
   b. Complete optimization of the ESA hydrogen purification system
   c. Initiate design and fabrication of a fully integrated HPWR–ESA-based system for on-demand production, purification, and dispensing of high-pressure PEM fuel cell-quality hydrogen from JP-8.
2. Develop advanced tactical fuels with JP-8 drop-in compatibility and superior hydrogen-reforming properties from domestic or indigenous fossil feedstocks such as coal, natural gas, and petroleum coke and renewable feedstocks such as crop oils and biomass, which included:
   a. Optimization of a bench-scale FT reactor
   b. Optimized catalyst production
   c. Development of a proof-of-concept system for novel EERC-designed two-stage gasifier
   d. Continued development of modular distributed energy and fuel production systems.

The third stated objective of this stage of work, "to advance the development of FCEH vehicles through demonstration of fuel cell-powered vehicles and hydrogen dispensing and refueling systems at military installations," was not be achieved since the working MPUV that was delivered did not meet customer specifications. (Note the discussion on pp 105-106.)

Work continues on the design and fabricate a laboratory-scale ESA system for process optimization, and ESA optimization, with the goal of advancing the technology sufficiently to enable purification of HPWR-generated hydrogen to PEM fuel cell-quality.

References

Agricultural Utilization Research Institute (AURI). 2009. Agricultural Renewable Solid Fuels Data. AURI Fuels Initiative (accessed Jan 2009) http://forum.iburncorn.com/wiki/index.php/BTU_Values

Arsova, L.; R. van Haaren, N. Goldstein, S. M. Kaufman, and N. J. Themelis. 2008. The state of garbage in America." BioCycle. 49(12):22 (accessed Feb 2009) http://www.jgpress.com/archives/_free/001782.html#more

Austin, A. 2009. Sugarcane bagasse could benefit Brazil energy matrix. Biomass Magazine January 2009 (accessed Feb 2009) http://www.biomassmagazine.com/article.jsp?article_id=2299

Bevill, K. 2009. Forest products industry studies biomass impact. Biomass Magazine. October 2008 (accessed Feb 2009), http://www.biomassmagazine.com/article.jsp?article_id=2074&q=forest%20products%20industry

Buckley, Tera D., Joshua R. Strege, Kerryanne M. B. Leroux, and Wesley D. Peck. September 2009. Identification and characterization of biomass sources: Final technical report. Report No. 2009-EERC-09. Grand Forks, ND: University of North Dakota Energy & Environmental Research Center (EERC).

California Energy Commission. 2008. An Assessment of Biomass Resources in California. Draft Report, Contract No. 500-01-016. March 2008.

Center for Energy and Environment. 2007. BioPower evaluation tool. Minneapolis, MN.

Chang, N. B., and E. Davila. 2008. Municipal solid waste characterizations and management strategies for the lower Rio Grande Valley, Texas. Waste Management. 28:776–794.

Combs, S. 2008. The energy report. Texas Comptroller of Public Accounts. May 2008 (accessed Feb 2009), http://www.window.state.tx.us/specialrpt/energy/pdf/96-1266EnergyReport.pdf

Davis, M., D. Johnson, S. Deutch, F. Agblevor, J. Fennell, and P. Ashley. 1995. Variability in the composition of short rotation woody feedstocks. Proceedings of the 2nd Biomass Conference of the Americas. Portland, OR, pp 216–225.

Dick, R. 2009. Biomass Fueled Power Plants – An Overview. Presented at the Minnesota Society of Professional Engineers.

Eidman, V. R. 2007. Commercialization of first generation biofuels. Presented 21 August 2007.

Ellis, R. P. 2009. Biomass-fueled power plants: An overview. Utility Engineering Corporation (accessed Jan 2009), http://www.ue-corp.com/news/wp_biomass.pdf.

Energy Information Administration. 2009a. Annual energy outlook 2009: Early release overview. (accessed Feb 2009a), http://www.eia.doe.gov/oiaf/aeo/pdf/earlyrelease.pdf.

Energy Information Administration. 2009b. Annual energy review 2007; Renewable energy production and consumption by primary energy source. (accessed March 2009b), http://www.eia.doe.gov/emeu/aer/renew.html

FirewoodResource.com. Tree species for firewood and Btu chart. (accessed Jan 2009), http://firewoodresource.com/firewood-btu-ratings/

Fogler, S. H. 1999. Elements of chemical reaction engineering, 3d ed. Upper Saddle River, NJ: Prentice-Hall.

Food and Agriculture Policy Research Institute (FAPRI). 2008. U.S. and world agriculture outlook database (accessed Feb 2009), http://www.fapri.iastate.edu/tools/outlook.aspx

Gunderson, C. A., E. B. Davis, H. I. Jager, T. O. West, R. D. Perlack, C. C. Brandt, S. D. Wullschleger, L. M. Baskaran, E. G. Wilkerson, and M. E. Downing. 2008. Downing. Exploring potential U.S. switchgrass production for lignocellulosic ethanol. Report No. ORNL/TM-2007/183 prepared by Oak Ridge National Laboratory, Oak Ridge, TN, under Contract No. DE-AC05-00OR22725 for the U.S. Department of Energy.

Haynes, R.W.; D. M. Adams, R. J. Alig, P. J. Ince, J. R. Mills, and X. Zhou. 2007. The 2005 RPA timber assessment update. PNW-GTR-699. U.S. Department of Agriculture, Forest Service, Pacific Northwest Research Station: Portland, OR.

Headquarters, Department of the Air Force (HQ AFPET/AFTT). 2008. Detail specification: Turbine fuel, aviation, kerosene type, JP-8 (NATO F-34), NATO F-35, and JP-8+100 (NATO F-37), MIL-DTL-83133F.

Ince, P. J. 1979. How to estimate recoverable heat energy in wood or bark fuels. Forest Products Laboratory, Forest Service, U.S. Department of Agriculture, General Technical Report FPL 29, 1979 (accessed Jan 2009), http://www.fpl.fs.fed.us/documnts/fplgtr/fplgtr29.pdf

Johnson, D., P. Ashley, S. Deutch, M. Davis, and J. Fennell. 1995. Compositional variability in herbaceous energy crops. Proceedings of the 2nd Biomass Conference of the Americas. Portland, OR, pp 267–277.

Juraščík, M., A. Sues, and K. J. Ptasinski. 2009. Exergy analysis of synthetic natural gas production method from biomass. J. Energy 2009, 7, 31, http://www.mam.gov.tr/bigpower/fullpaperS/11.pdf

Kentucky Pollution Prevention Center. Undated. Introducing industrial solid waste reduction. University of Louisville (accessed Jan 2009), http://www.deq.state.mi.us/documents/deq-ess-retap-tm_SolidWaste-att2.pdf

Lapidusa, A. L, V. M. Bavykin, E. A. Smolenskii, and I. V. Chuvaeva. 2008. Cetane Numbers of hydrocarbons as a function of their molecular structure. Doklady Chem., 420(2):150–155.

Larson, E., and H. Jin. 1999. Biomass conversion to Fischer–Tropsch liquids: Preliminary energy balances. In Proceedings of the 4th Biomass Conference of the Americas. Oxford, UK: Elsevier Science, Ltd.

Lawton, Captain Marc, and Captain Tacildayus Andrews. 1999. Fueling the Force in the Army After Next—Revolution or Evolution? Website, accessed 21 August 2010, http://www.almc.army.mil/alog/issues/JulAug99/MS406.htm

Meeker, D. L., and C. R. Hamilton. *An Overview of the Rendering Industry* (accessed Feb 2009), http://assets.nationalrenderers.org/essential_rendering_book.pdf

Milbrandt, A. 2005. A geographic perspective on the current biomass resource availability in the United States. Final Technical Report NREL/TP-560-39181 Prepared for U.S. Department of Energy under Contract No. DE-AC36-99-GO10337.

Miles, T. R., L. L. Baxter, R. W. Bryers, B. M. Jenkins, and L. L. Oden. 1995. Alkali deposits found in biomass power plants, A preliminary investigation. Summary Report Prepared for National Renewable Energy Laboratory.

National Agronomy Manual, 3d ed. 2002. 190-V-NAM. Washington, DC: U.S. Department of Agriculture, National Resources Conservation Service.

National Renderers Association (accessed July 2008), http://nationalrenderers.org

National Weather Service. JetStream – Online School for Weather (accessed March 2009), http://www.srh.weather.gov/srh/jetstream/global/climate_max.htm

National Wilderness Institute. Public Land Ownership by State. 1995 (accessed March 2009), http://www.nrcm.org/documents/publiclandownership.pdf

Neeft, J. P. A., H. A. M. Knoef, U. Zielke, K. Sjöström, P. Hasler, P. A. Simell, M. A. Dorrington, C. Greil. 2002. Tar Protocol: Development of a Standard Method for the Measurement of Organic Contaminants ("Tar") in Biomass Producer Gases. Petten, Netherlands: Energy Research Centre of the Netherlands, http://www.eeci.net/project-info/pdf/paper-sevilla.pdf

North Dakota sugar beet processor. 2008. Personal Communication, Sept 2008.

Oak Ridge National Laboratory. 2006. Biomass energy data book, Appendix C – Assumptions, Ed. 1; ORNL/TM-2006/571 (accessed Feb 2009), http://cta.ornl.gov/bedb/appendix_c.shtml

Oster, Benjamin G., Ronald C. Timpe, Ted R. Aulich, Mike C. J. Lin, and Franklin H. Holcomb. November 2008. On-demand hydrogen via high-pressure water reforming for military fuel cell applications. Journal of Fuel Cell Science and Technology. 5(4).

Patel, N. M.; P.J. Paul, H.S. Mukunda, and S. Dasappa. 1996. Combustion studies on concentrated distillery effluent. In Twenty-Sixth Symposium (International) on Combustion. Pittsburgh, PA: The Combustion Institute, pp 2479–2485.

Reardon, J., A. Lilley, K. Browne, K. Beard, J. Wimberly, and J. Avens. 2001. Demonstration of a small modular biopower system using poultry litter. Community Power Corporation. DOE SBIR Phase-I Final Report, Contract: DE-FG03-01ER83214 (accessed Jan 2009), http://www.osti.gov/bridge/servlets/purl/794292-6l279H/native/794292.pdf

Santana, R. C.; P.T. Do, M. Santikunaporn, W. E. Alvarez, J. D. Taylor, E. L. Sughrue, and D. E. Resasco. Evaluation of different reaction strategies for the improvement of cetane number in diesel fuels. Fuel 2006, 85(5–6):643–656.

Smith, M., S. Carlson, M. Wiedenhoeft. 2006. Weed management in flax production, on-farm trials – 2005. Iowa State University, University Extension.

Soil Conditioning Index. SCI Spreadsheet, version 25. sciver25.xls (accessed March 2009), ftp://ftp-fc.sc.egov.usda.gov/SQI/web/

Summers, M. D., P. R. Hyde, B. M. Jenkins. Yields and property variations for rice straw in California. University of California (accessed Feb 2009), http://www.brdisolutions.com/pdfs/bcota/abstracts/1/305.pdf

The Prairie Agricultural Machinery Institute. 1995. Using straw as a farm heating fuel. ISSN 1188-4770, Group 2 (i), July 1995 (accessed Jan 2009), http://www1.agric.gov.ab.ca/$department/deptdocs.nsf/all/eng3127/$file/719.pdf?OpenElement

TSS Consultants. Gridley ethanol demonstration project utilizing biomass gasification technology: Pilot plant gasifier and syngas conversion testing. CA Report; August 2002–June 2004, NREL/SR-510-37581, 2005.

U.S. Census Bureau, Population Division. 2005. Interim State Population Projections (accessed Feb 2009), http://www.census.gov/population/www/projections/projectionsagesex.html

U.S. Department of Agriculture National Agricultural Statistics Service (accessed Jan 2009a), http://www.nass.usda.gov/QuickStats/indexbysubject.jsp?Pass_group=Crops+%26+Plants

U.S. Department of Agriculture National Agricultural Statistics Service. 2007 Census of Agriculture (accessed March 2009b), http://www.agcensus.usda.gov/Publications/2007/Online_Highlights/Ag_Atlas_Maps/index.asp

U.S. Department of Agriculture National Resources Conservation Service. 2009. National Engineering Handbook, Part 651, Animal Waste Management, Chapter 4; 210-VI, NEH-651, June 1999 (accessed Jan 2009c), http://www.wsi.nrcs.usda.gov/products/W2Q/AWM/handbk.html

U.S. Department of Agriculture. Forest Service Forest Inventory Data Online (FIDO) Tool (accessed March 2009a), http://www.fia.fs.fed.us

U.S. Department of Agriculture. Timber Product Output Database (accessed Jan 2009b), http://srsfia2.fs.fed.us/php/tpo2/tpo.php

U.S. Department of Agriculture. 2008. USDA Agricultural Projections to 2017, Long-Term Projections Report OCE-2008-1. Feb 2008.

U.S. Department of the Interior, Office of Surface Mining. Revised Universal Soil Loss Equation (RUSLE) – AH 703, Appendix D; Parameter Values for Major Agricultural Crops and Tillage Operations, pp 349–361 (accessed March 2009), http://www.techtransfer.osmre.gov/NTTMainSite/Library/hbmanual/rusle/ah703apd.pdf

Wiltsee, G. Urban wood waste resource assessment. 1998. Valencia, CA: Appel Consultant, Inc.

Zygarlicke, C.J., J.P. Hurley, T.R. Aulich, and B.C. Folkedahl. August 2009. *Production of JP-8-Based Hydrogen and Advanced Tactical Fuels for the U.S. Military*. Final Report for U.S. Army Corps of Engineers, Engineer Research and Development Center, Cooperative Agreement No. W9132T-05-2-0024. Grand Forks, ND: University of North Dakota Energy & Environmental Research Center (EERC).

Zygarlicke, C. J., D.P. McCollor, K. E. Eylands, M. D. Hetland, M. A. Musich, C. R. Crocker, J. Dahl, and S. Laducer. Impacts of cofiring biomass with fossil fuels. 2001. Final Report (1 April 1999 – 31 March 2001) for U.S. Department of Energy Contract No. DE-FC26-98FT40320; EERC Publication 2001-EERC-08-03; Energy & Environmental Research Center: Grand Forks, ND.

Acronyms and Abbreviations

Term	Spellout
AAN	U.S. Army after Next
AEO	Annual Energy Outlook
AFB	Air Force Base
BAA	Broad Agency Announcement
CEERD	U.S. Army Corps of Engineers, Engineer Research and Development Center
CERL	Construction Engineering Research Laboratory
CHI	catalytic hydrodeoxygenation isomerization
CHN	carbon, hydrogen, nitrogen
CHNOS	carbon, hydrogen, nitrogen, oxygen, sulfur
CO	carbon monoxide
DC	District of Columbia
DOE	Department of Energy
EDS	energy-dispersive spectrometer
EERC	[University of North Dakota] Energy and Environmental Research Center
EIA	Energy Information Administration
EPA	Environmental Protection Agency
ERDC	Engineer Research and Development Center
ESA	electrical swing adsorption
FAPRI	Food and Agriculture Policy Research Institute
FCEH	fuel cell electric hybrid
FIDO	Federal Interagency Databases Online
FT	Fischer–Tropsch
FY	fiscal year
GC	Gas Chromatograph
GF	Grand Forks (North Dakota)
GFAFB	Grand Forks Air Force Base
GFARNGB	Grand Forks Army National Guard Base
HDO	Hydrodeoxygenation
HHV	Higher Heating Value
HPWR	high-pressure water reforming
JP-8	Jet Propellant 8
LLV	lower heating value
MEA	membrane-electrode assembly
MPUV	multipurpose utility vehicle
MSW	municipal solid waste
NASS	National Agriculture Statistics Service
NRCS	National Resources Conservation Service
NREL	National Renewable Energy Laboratory

Term	Spellout
NWRR	Northwestern Wheat and Range Region
ODDR&E	Office of the Director, Defense, Research, and Engineering
ORECCL	Oak Ridge Energy Crop County-Level Database
ORNL	Oak Ridge National Laboratory
PEM	Proton Exchange Membrane
PM	particulate matter
POLYSYS	Policy Analysis System
PRB	Powder River Basin
RFS	Renewable Fuel Standard
RPS	renewable portfolio standard
SCI	Soil Conditioning Index
SNG	synthetic natural gas
SPK	synthetic isoparaffinic kerosene
TR	Technical Report
URL	Universal Resource Locator
USDA	U.S. Department of Agriculture
WDS	wavelength-dispersive spectrometer
WTE	waste to energy
WWW	World Wide Web
XRF	x-ray fluorescence

Appendix A: Identification and Characterization of Biomass Sources in the United States

Tera D. Buckley, Joshua R. Strege, Kerryanne, M.B. Leroux, and Wesley D. Peck

University of North Dakota
Energy & Environmental Research Center
15 North 23rd Street, Stop 9018
Grand Forks, ND 58202-9018

Introduction

Biomass is a renewable fuel derived from organic matter contained in plants and animals. Renewable energy comprises 7 percent of the total energy consumption in the United States Figure A1. At 53 percent of the total renewable energy consumption (or 4.45 percent of the total energy output), biomass is the largest renewable energy resource. Wood and wood-derived fuels supply 60 percent of the biomass energy consumed, followed by biofuels at 28 percent and urban residuals at 12 percent (Energy Information Administration [EIA] 2009b).

According to the EIA Annual Energy Outlook (AEO) 2009 reference case (EIA 2009a), energy production from biomass sources is projected to double to 8.85 percent by 2030.* This expected increase in biomass energy production is due in a large part to recently enacted policies and concerns over energy security, greenhouse gas emissions, volatile energy prices, and limited fossil fuel resources.

This study seeks to provide an objective evaluation of biomass sources available in the United States. It has four primary sections:

1. Quantification of major biomass resources
2. Calculation of energy content for common biomass types
3. Estimation of projected biomass production yields
4. Presentation of chemical analysis and physical characterization data of biomass resources

* The EIA AEO 2009 reference case assumed the Federal subsidies for renewable generation were to expire as enacted. Their extension would have a large impact on the future of renewable energy generation.

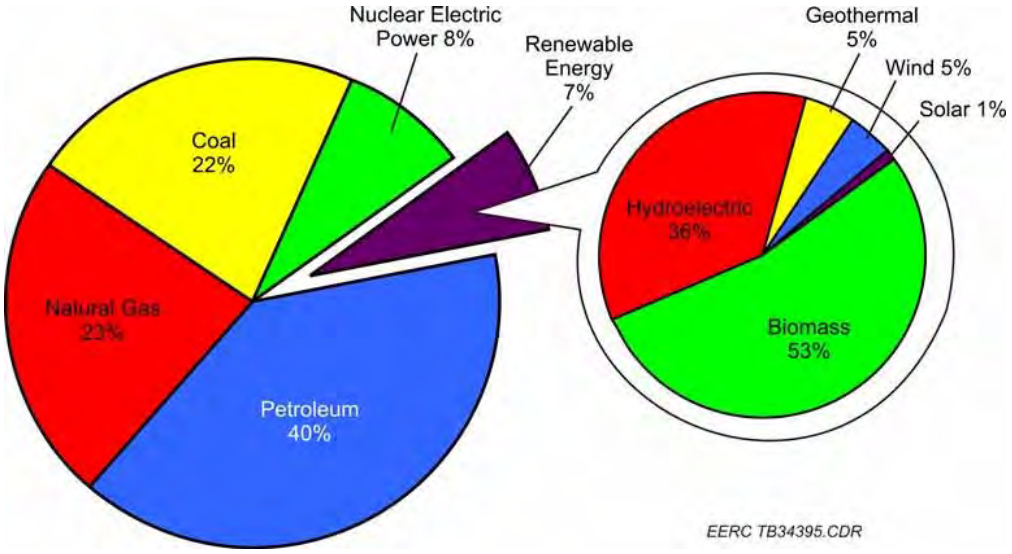

Figure A1. U.S. renewable energy as a share of total primary energy consumption (EIA 2009b).

Quantification of major biomass resources in the United States

Figure A2 shows U.S. biomass resources as classified into three primary categories for this study: agricultural, wood, and urban residuals. The primary categories were further defined into subcategories. The following section presents methods used to obtain county-level data for these subcategories, as well as summary statistics and data limitations. Concentrations of biomass resources varied because of population distribution, climate, and geography.

Agricultural crops

Agricultural crops are specific goods raised on land for sale to markets such as food, feed, or biofuels and include alfalfa, barley, beans, canola, corn, cotton, flax, forage, oats, peanuts, potatoes, rice, rye, safflower, sorghum, soybeans, sugar beets, sunflowers, tobacco, wheat, and other vegetable and fruit crops.

National crop acreages and yields by county were obtained from the U.S. Department of Agriculture (USDA) National Agricultural Statistics Service (NASS) database (USDA NASS 2009a), which is considered to be the definitive source for agriculture production statistics in the United States.

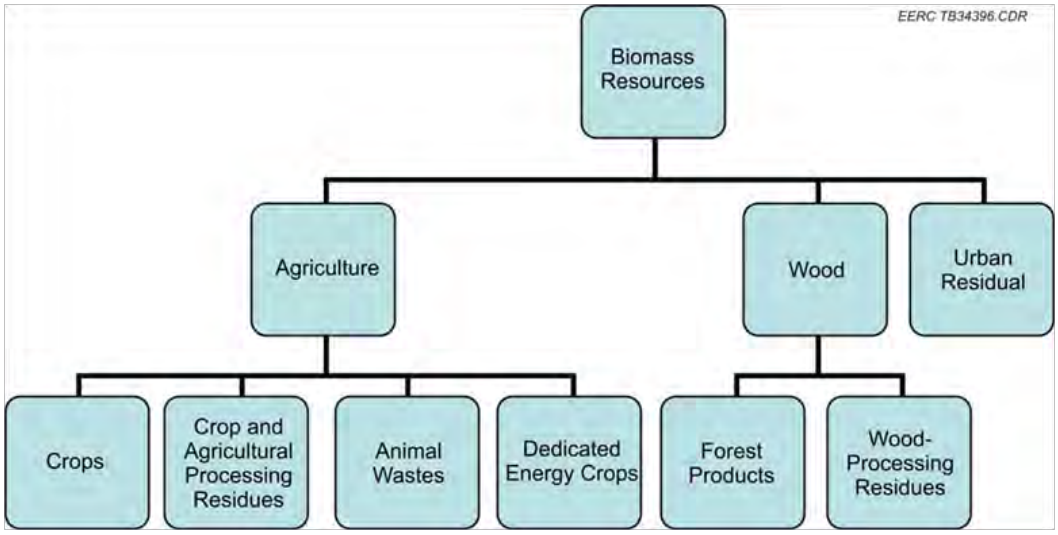

Figure A2. Major biomass resources in the United States.

Some data sets date back to 1970. NASS records yields on an as-reported basis without making moisture or quality adjustments. Production in counties with less than 1000 acres of a crop is generally combined with other counties in the same Crop Reporting District, and their totals are reported as "other counties" to protect the privacy of producers who are distinctive enough in their counties to be clearly identifiable. Summary maps of agriculture crop production by county are provided in Appendix B to this report based on the 2007 Census of Agriculture (USDA 2009b). Figure A3 shows total crop production by county.

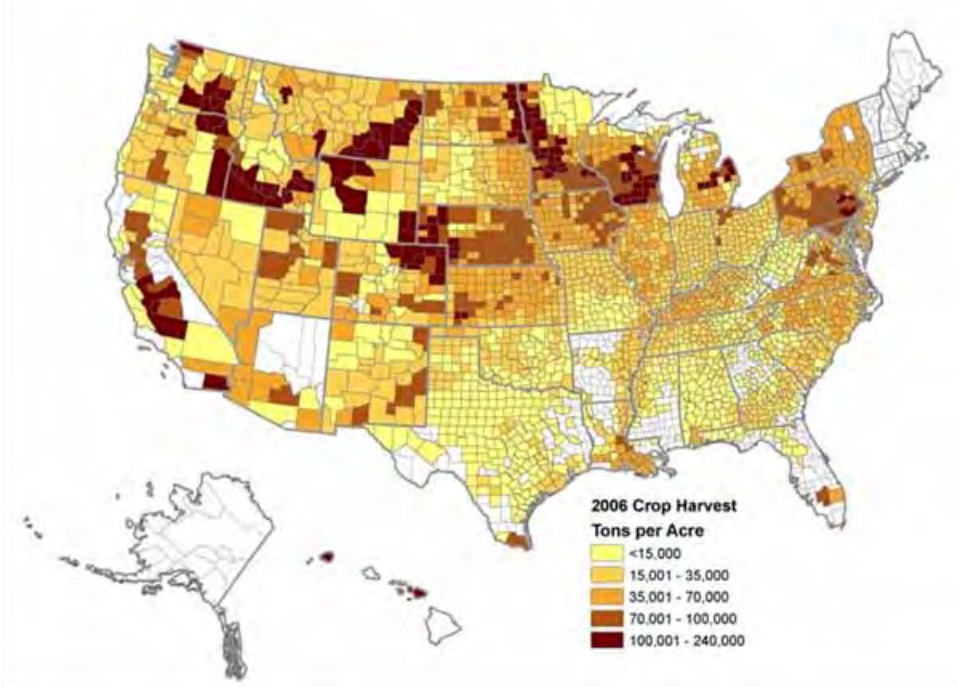

Figure A3. Crop production by county.

Agricultural crop and processing residues

Appendix A: Crop and agricultural processing residues include wastes from the field, such as leaves, straws, stems, and stalks, as well as processing by-products. Specific residues listed in this category include alfalfa stems; corncobs, stalks, and stover; distillers grains; hay; pits, shells, hulls, and pulp from beet and citrus; straw from barley, flax, mint, oat, rice, and wheat; sunflower stalks; and other vegetable-processing residues. Figure A4 shows agricultural crop residues by county.

Using nominal industry rules of thumb, common multipliers can be identified or derived for estimating crop and processing residue yields. Factors used are provided in Table A1. These data have been estimated from the Soil Conditioning Index (SCI) RUSLE2 database for all crops except dry edible peas, cigar tobacco, and a few bean varieties (SCI 2009; National Agronomy Manual 2002). The conversion factors given are multiplied by the yield of the grain crop to achieve the estimated residual yield. For example, about 1 ton of corn stover can be expected for every ton of corn grain harvested. Likewise, if a chosen acre produced 26 tons of sugar beets, about 1.3 tons of pulp could be expected following sugar processing. A number of crops do not have any usable residues because they have an established market, such as animal feed, or the residue is not harvestable (e.g., stubble or twigs). These include apples, peaches, hay, all types of forage, corn used for silage, and sorghum used for silage. Different residue factors for wheat and barley grown in the Northwestern Wheat and Range Region (NWRR), which includes parts of Washington, Oregon, and Idaho, were also noted.

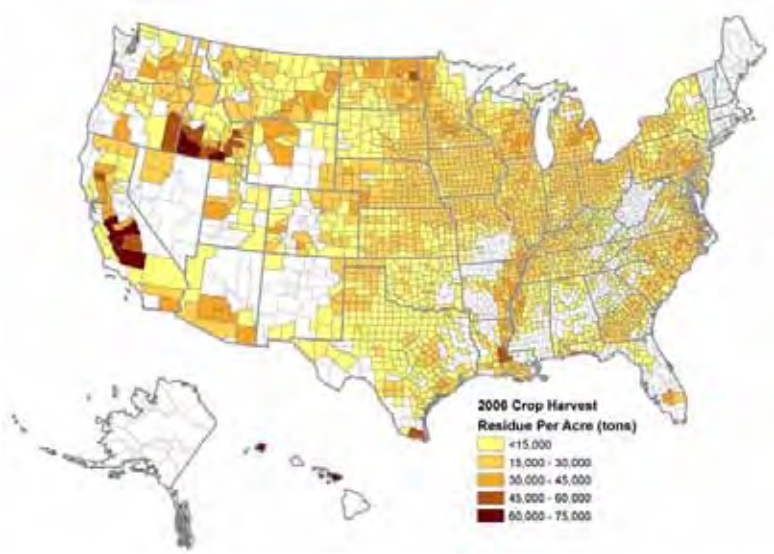

Figure A4. Agricultural crop residues by county.

Table A1. Factors for yield estimation of various agricultural residues (SCI 2009).

Crop Name	Crop Residue, lb/lb	Processing Residue, lb/lb	Comments
Apples	0.0	–	0.03[a]
Barley	1.5	–	
NWRR	1.0	–	1.0 for spring barley, 1.3 for winter barley
Beans, dry edible	1.0	–	
Beans, lima	0.2	–	
Beans, other dry edible	1.0	–	
Beans, pinto	1.0	–	
Canola	2.0	–	
Chickpeas (garbanzo)	2.2	–	
Corn (grain)	1.0	–	AH703[b]
Corn (silage)	0.0	–	0.01[a]
Cotton (American pima and upland)	4.5	–	AH703
Flaxseed	1.3	–	1.3,[c] 1.4-SCI
Forage	0.0	–	
Green Peas for Processing	0.2	–	
Hay	0.0	–	
Lentils	1.2	–	
Mustard	1.2	–	Average for spring and winter residues
Oats	2.0	–	AH703
Peaches	0.0	–	0.03[a]
Peanuts (for nuts)	1.3	–	
Peas, Austrian winter	1.0	–	
Potatoes	0.1	–	value for Irish
Rice	1.0[d]	0.2[c]	
Rye	1.3	–	1.0 for winter, 1.3 for spring, 1.5 for cereal
Safflower	1.5	–	
Snap beans for processing	0.4	–	Lower for hand-picked
Sorghum (grain)	1.0	–	AH703[c]
Sorghum (silage)	0.1	–	
Soybeans	1.5	–	AH703 for south
Sugar Beets	0.1	0.05[e]	
Sugarcane for sugar	0.1	0.3[f]	
Sunflowers	2.2	N/A[g]	
Sweet corn for processing	0.3	–	
Sweet potatoes	0.1	–	
Tobacco, air-cured dark	0.3	–	
Tobacco, air-cured light burley	0.1	–	

Crop Name	Crop Residue, lb/lb	Processing Residue, lb/lb	Comments
Tobacco, air-cured light southern	0.1	–	Value for light burley
Tobacco, fire-cured	0.3	–	Value for flue-cured
Tobacco, flue-cured	0.3	–	
Tomatoes for Processing	0.0	–	0.02[a]
Wheat, durum	1.3	–	AH703 for spring wheat
NWRR	1.4	–	
Wheat, other spring	1.3	–	AH703
NWRR	1.4	–	
Wheat, winter	1.7	–	AH703
NWRR	1.4	–	

[a] Value in parenthesis is reported in SCI RUSLE2 database, taken to be zero for all practical purposes.
[b] U.S. Department of the Interior. 2009 (noted as AH703).
[c] Smith et al. 2009
[d] Summers et al. 2009
[e] North Dakota sugar beet processor 2008.
[f] Austin 2009.
[g] Sunflowers used for oil will have processing residues, but the amount of residue generated in processing is unknown.

Animal wastes

Manure

Animal wastes are manure generated by livestock including beef, dairy, horse, poultry, sheep, and swine. Although NASS does not collect animal waste data, accurate estimates of manure production can be made by multiplying livestock inventories from the Census of Agriculture by manure factors from the National Resources Conservation Service National Engineering Handbook (USDA NRCS 2009c). An alternative method to estimating manure availability is to use county-level U.S. Department of Energy (DOE) National Renewable Energy Laboratory (NREL) data on methane production from manure management (Milbrandt 2005).

The state of Minnesota was used as an example to test both methods. The 2005 county-level data from DOE NREL gives methane production rather than manure collection (Milbrandt 2005). To estimate manure availability, it was assumed that every 100 tons of manure generates 26.7 tons of methane. This is based on the approximate stoichiometry of anaerobic digestion. County-level estimates of manure production in Minnesota were made by multiplying estimated animal weights from the 2007 Census of Agriculture data by appropriate manure production factors. When com-

pared to the estimates made from methane production, it was found that the estimates made from NASS data were almost 20 times higher than the estimates made from methane production data.

Because the data from NASS, the National Engineering Handbook, and DOE NREL are all considered reliable, the most likely reason for this discrepancy is that only 5 percent of the available manure in Minnesota is managed for methane production. The remainder is either used as fertilizer or is not collected, especially if it is produced by grazing animals. Neither source of manure is a good candidate for energy production. Fertilizer is too expensive to be used as fuel and is difficult to transport. Furthermore, the qualities that make good fertilizer (high levels of moisture and ash) make poor fuel. Manure from grazing animals is left where it falls, both because it provides nutrients back to the soil and because it is difficult to efficiently collect from the field. Only the manure that is currently collected for methane production could realistically be used for energy production. Figure A5 shows a map of methane produced annually by manure management.

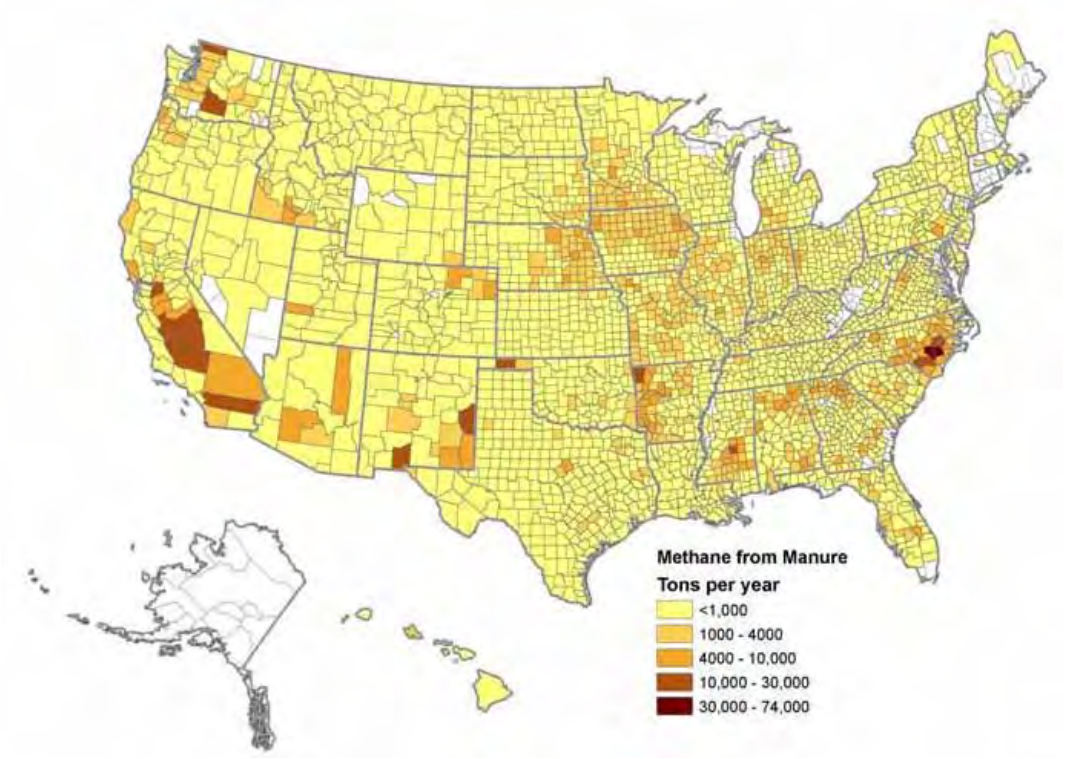

Figure A5. Methane emissions from manure management by county.

Animal by-products

Generally, animal fats are products derived from meat-processing facilities and are solid at room temperature. They include tallow from beef processing, lard, choice white grease from pork processing, and poultry fat from poultry processing. U.S. rendering companies are estimated to produce about 7 billion tons of rendered fat a year (Table A2). Production statistics on a state and county level are available, but would require contacting approximately 300 North American rendering facilities.

Table A2. U.S. supply of waste oil and animal fat (Eidman 2007).

Waste Oil and Animal Fat Type	million tons
Yellow grease and other grease	1.3
Lard	0.5
Edible tallow	0.9
Inedible tallow	1.8
Poultry fat	2.1
Total	6.8

Although there is a large supply of oils and fats in the United States, competing uses for these products keeps supplies tight and prices competitive. About 85 percent of waste animal fat processed by rendering companies is used as animal feed ingredients. Applications for rendered fats in the chemical, metallurgy, rubber, and oleochemical industries account for the second largest market, with over 3000 industrial uses identified. The manufacture of soaps and personal care products remains a major use for animal fats, especially tallow; however, use in biofuel production is increasing (Meeker and Hamilton 2009). Use of rendered fats for biofuel production was estimated at 32.7–87.2 million pounds (3–8 percent of total production) in early 2008 (National Renderers Association 2008).

Dedicated energy crops

Dedicated energy crops are raised for the sole purpose of producing energy in the forms of electricity and/or heat and include short-rotation woody crops, like hybrid poplar and willow, and herbaceous crops, like switchgrass, reed canary grass, and miscanthus. The standard reference for energy crop production potential by county is the Oak Ridge Energy Crop County-Level (ORECCL) Database. This database was prepared in 1996 and gives an estimated upper limit of energy crop production in each county of the United States. Figures A6 and A7 show switchgrass and total energy crop yields, respectively.

Figure A7 shows significantly lower energy crop yields in the western United States. This is not due to a lack of data, but rather because the ORECCL authors determined that most of the western United States was not suitable for economical energy crop growth. All data are reported as the yield after a 2-year establishment period. If the yield in year 3 is expected to be less than 2 dry tons/year/acre, the area is designated unsuitable. Some energy crops may still be grown in the western United States, but the sustainable yields will be much lower than in the eastern United States.

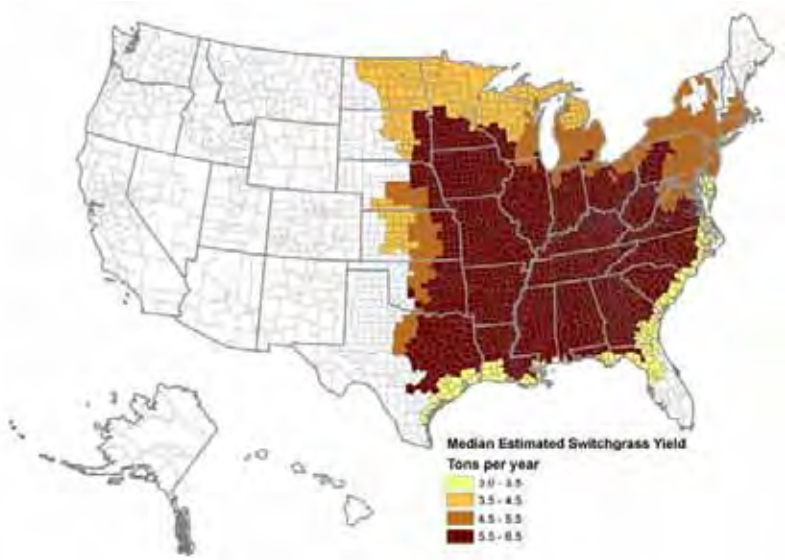

Figure A6. Switchgrass crop yield by county.

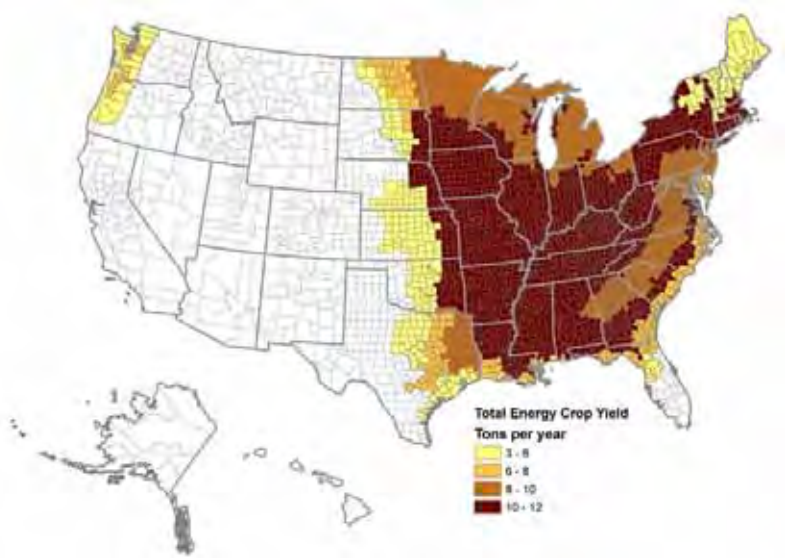

Figure A7. Total energy crop yield by county.

Note that ORECCL is no longer publicly available, as an improved database is being developed to account for better measurements and revised economics from the last decade. The new Policy Analysis System (POLYSYS) model is currently being tested at the University of Tennessee Knoxville and should be available to the public before the end of 2009. This model will provide much more realistic estimates for production of various energy crops than any effort the EERC could achieve at this time and will also provide estimates of the effects of crop prices, policies, and other variables on projected energy crop costs and availability. Also note that Oak Ridge National Laboratory (ORNL) published a report presenting estimated switchgrass growing potential at a resolution of 400 m, which is significantly better than county-level resolution (Gunderson et al. 2008). The interested reader is strongly encouraged to examine both the ORNL report and the POLYSYS model when it becomes available.

Forest products

Specific forest products include all wood grown, such as aspen timber, hardwood timber, softwood timber, brushland, and shrubland. Data on forest products were gleaned from the USDA Forest Service, which performs inventories; collects and analyzes data; and publishes detailed statistics on forest growth, both logging and timber harvesting, and primary wood products industry activities. A rigorous methodology is used to collect and analyze data, updating on a regular basis. The Forest Service statistics are recognized for their completeness and reliability.

Data for this report were generated using the Forest Inventory Database Online (FIDO 2.0) tool (USDA 2009a). To ensure reliability of the generated data, a comparison was made to data generated for the state of North Dakota using the Forest Service data. The level of detail available from the Forest Service is such that the fate of individual trees of 2-inch-diameter or greater, including exact species, growth, disease, and harvest, can be tracked with time. These data become more manageable when used for statistical purposes such as estimating average hardwood forest cover by county or average yearly wood growth. While the EERC has assembled an incredibly vast data set including all available Forest Service data for multiple years, these data are not included in the report, but can be accessed online at:

http://199.128.173.17/fiadb4-downloads/datamart.html

or

http://fiatools.fs.fed.us/fido/index.html.

Figures A8–A11 show the FIDO data and annual cubic feet of wood produced by living trees per acre of county land (cu ft/acre/year), percent of county land covered by softwood forest, percent of county land covered by hardwood forest, and percent of county land covered by all forest types. Total forest coverage includes mixed forests, not the sum of softwood and hardwood forest coverage. Also, because forest coverage is calculated using statistical estimates based on sample plots, the estimated coverage is greater than 100 percent in some cases.

This report offers only the total forested land, rather than breaking down the results to show what portion of forested land includes timberland for each county. Many forests (especially in protected areas) may have high yields, but cannot realistically be harvested or constitute trees that are not amenable to harvest. Any data older than 2000 will have a higher percentage of timberland, because some forested areas not suitable for timber were not included in measurements.

All forest data were derived on an acre-basis, as reported by the 2000 U.S. Census and does not include any water landcover. Values are reported as a percentage of county land rather than of forested area to avoid inflating the importance of large counties with small, but productive forests. One consequence of this approach is that heavily forested, small counties give the false impression of high tree volume. For example, Douglas County, NV has high forest coverage per unit area, but the small size of the county means that the total available forest resource is actually quite small.

Although the sampling method used to collect data from tree plots is universal across every state, there are variations in the types of data collected and in the frequency with which data are collected. In many states, limited regional Forest Service personnel cannot complete all samples in a single year, so statewide estimates depend on the results collected over cycles of years. Some states either do not collect or do not report any data. For instance, New Mexico statewide data are available only for 1989 and 1999 through the FIDO interface. Although the raw data downloaded from the Forest Service includes individual plot measurements for later years, these data either cannot be used to represent the full state of New Mexico or are not available to FIDO. Hawaii is the one state in which no data appear to be publicly available for any sample year. Note that the standard methods used to sample and report data were changed significantly in the 1990s, so data older than 10 years cannot always be compared to more recent data.

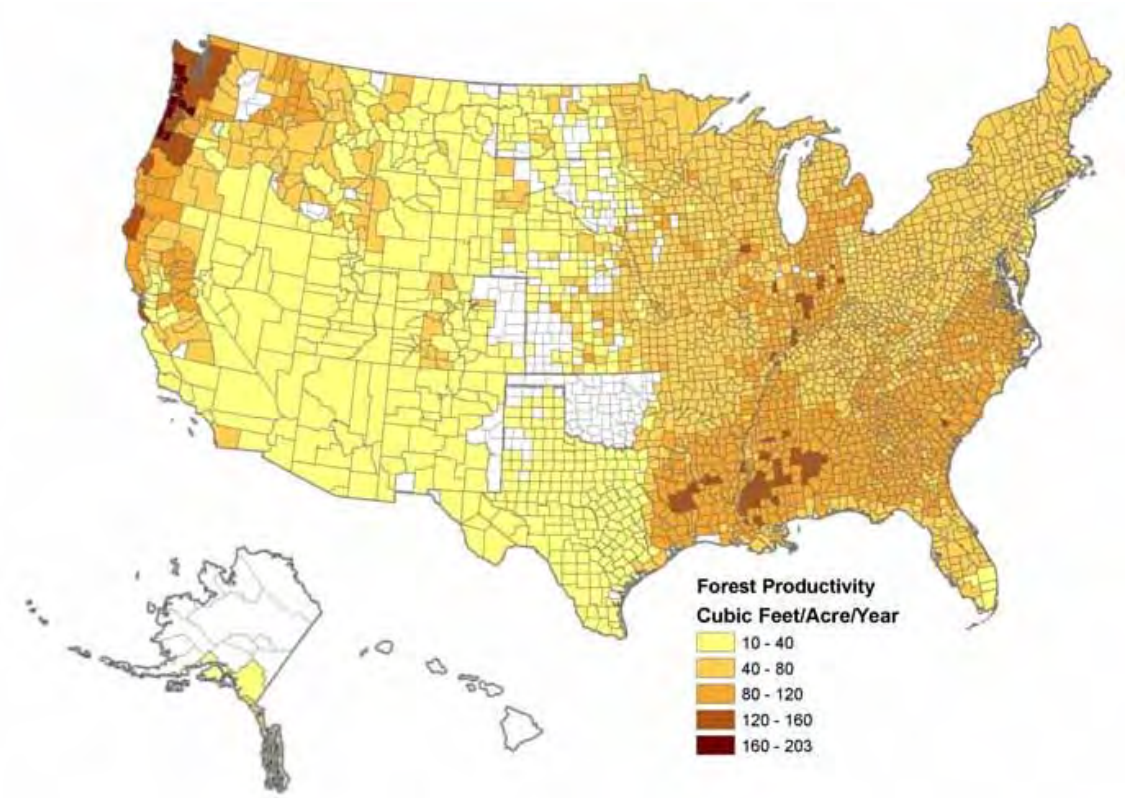

Figure A8. Volume of wood produced by living trees.

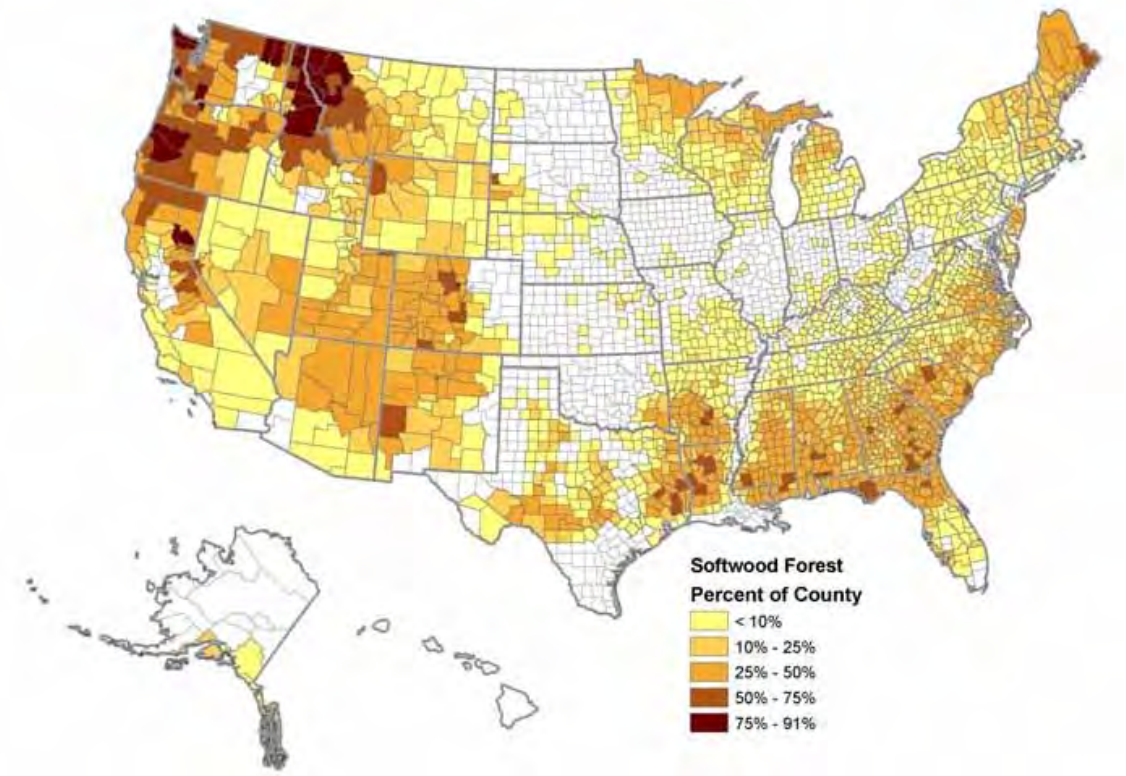

Figure A9. Percentage of county land covered by softwood forest.

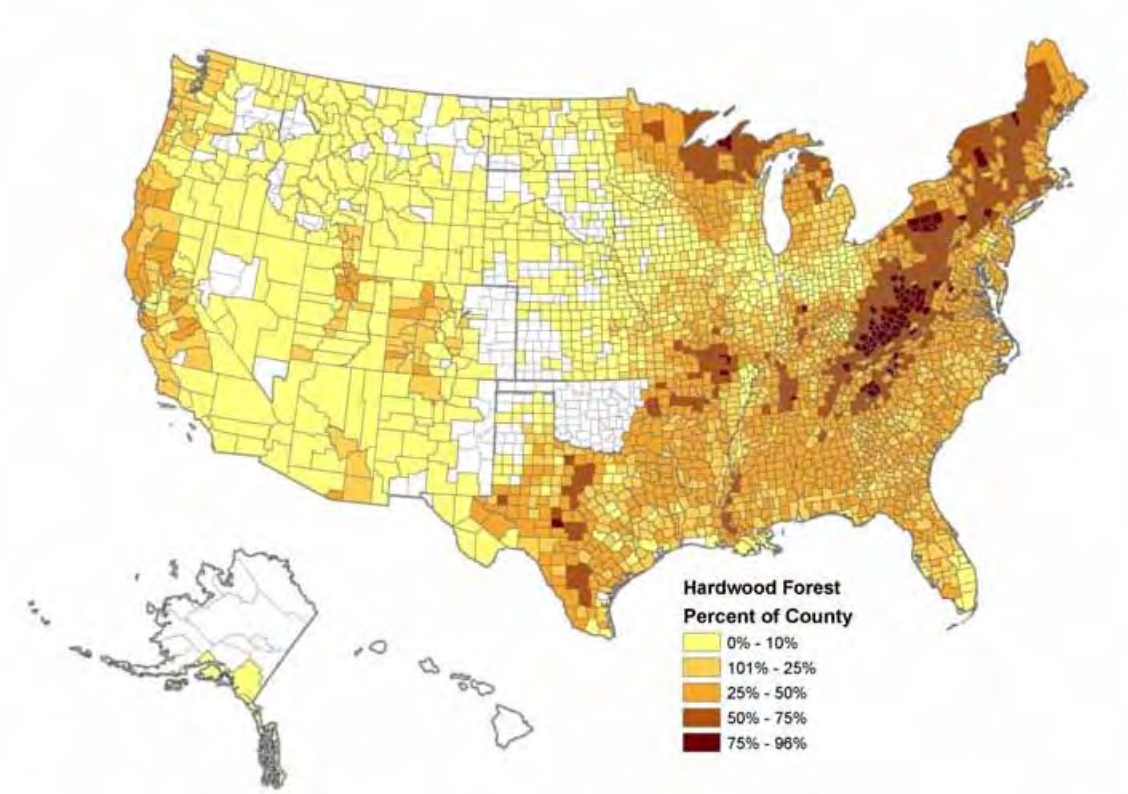

Figure A10. Percentage of county land covered by hardwood forest.

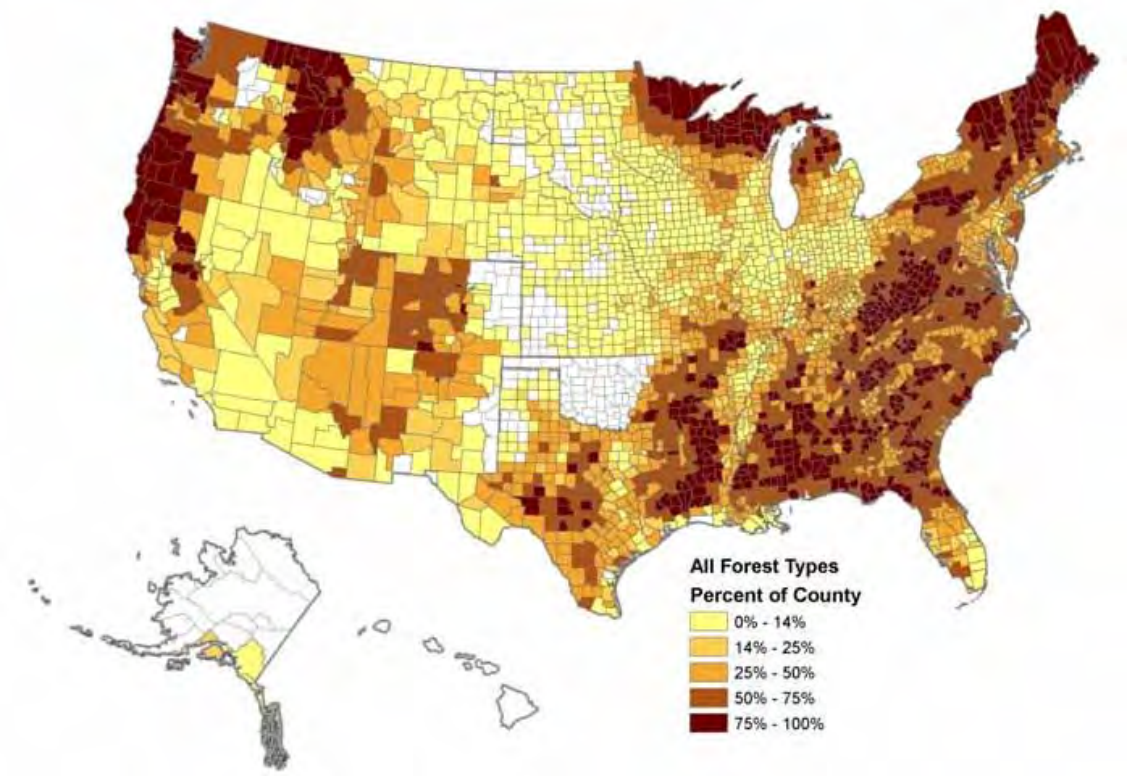

Figure A11. Percentage of county land covered by all forest types.

Given these limitations, it was not possible to use consistent data for every state. Where possible, multiyear data with a cycle ending in 2007 were used. When these were not available, multiyear data from within the last 5 years were used. When these were not available, the most recent available single-year data were used. For New Mexico and Oklahoma, the most recent available data were from 1999 and 1993, respectively. For Wyoming, the most recent available data set is from 2000. These years may not reflect all of the changes made to the collection method during the 1990s.

Data used to estimate productivity (Figure A8) are based on weighted averages of forest growth. FIDO only reports classes of growth, with Class 1 representing the highest productivity (>225 cu ft/acre/year) and Class 7 being the lowest (0–19 cu ft/acre/year). Table A3 lists each class and defined productivity range. The average of each range was used to convert these class categories into values that could estimate county-level average productivity. The average yield for each class was then multiplied by the acres of respective forest classification, summed for the forested area within each county, and divided by the number of total county acres. This gave the approximate yearly growth in cubic feet per acre of county land.

Wood-processing residues

Wood-processing residues result from processing timber to create high-value products and include logging residues, primary mill residues (bark, chunks, slabs, edgings, sawdust/shaving), and urban wood waste. Waste from paper and pulp manufacturing is also included in this category.

Table A3. FIDO classes of forestry growth (USDA 2009a).

Forest Productivity Class	Description (cu ft/acre/year)	Assumed Average Yield (cu ft/acre/year)
1	225+	250
2	165–224	195
3	120–164	143
4	85–119	103
5	50–84	68
6	20–49	35
7	0–19	10
Unknown Productivity Class		0

Reliable information on logging and primary wood product residues is either directly available or can be readily derived from Forest Service data. This leaves a very small amount (~2 percent) of unused primary mill material available for energy. However, not all types of wood residues or waste are available from the Forest Service database, other government agencies, or other organizations. These other types can be described as wood residues and wastes produced in the secondary wood products industry or further along in the production process.

Residues are also generated at secondary processing mills (e.g., millwork, furniture, flooring, containers, etc.) (ORNL 2009). Figure A12 shows mill residue data downloaded by state and county from the Forest Service's Timber Product Output database (USDA 2009b). Because primary mill residues tend to be clean, uniform, concentrated, and low in moisture, most of these materials are already used for generating by-products or boiler fuel at the mills. The Forest Service estimates current usage by type as follows:

- Bark – 80 percent used as fuel and 13 percent used in products
- Coarse residues – 85 percent used in products and 13 percent as fuel
- Fine residues – 55 percent used as fuel and 42 percent in products.

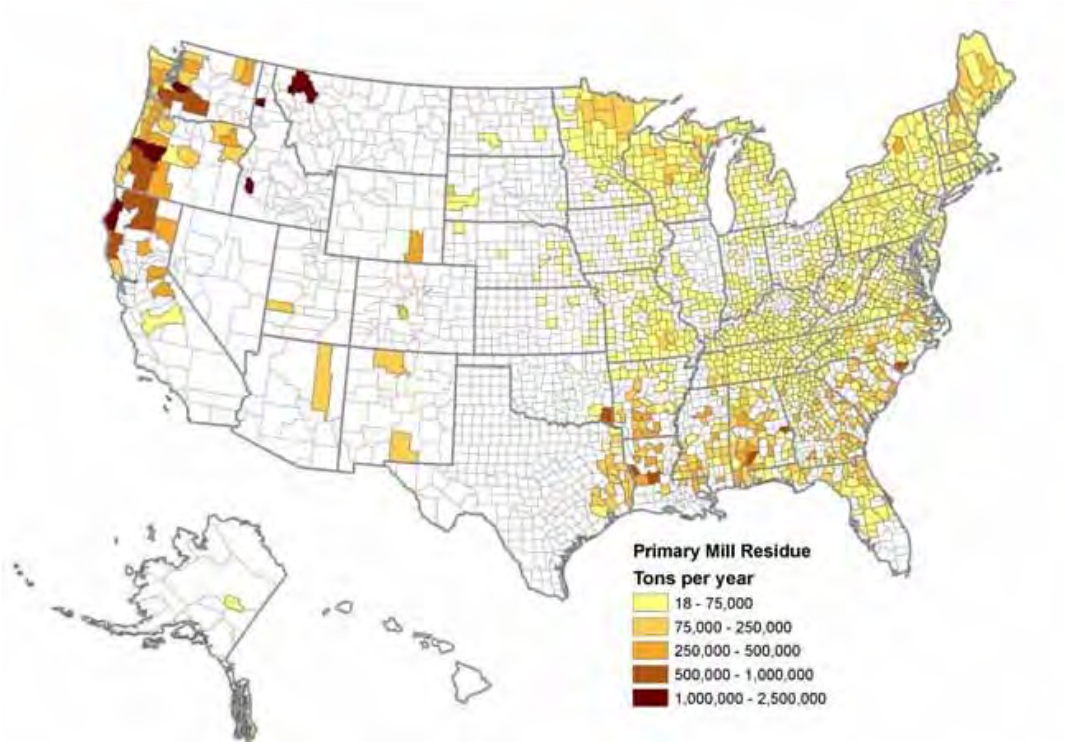

Figure A12. Primary mill residues by county.

Secondary mill residues include wood scraps and sawdust from woodworking shops— furniture factories, wood container and pallet mills, and wholesale lumberyards. Secondary mill residue data are not collected by the Forest Service or any other Federal agency (ORNL 2009), but were estimated in a 2005 NREL study (Milbrandt 2005).

The following business categories were included in the Milbrandt (2005) analysis:

- furniture factories: wood kitchen cabinet and countertop, nonupholstered wood household furniture, wood office furniture, custom architectural woodwork and millwork, and wood window and door manufacturers
- millwork: cut stock, resawing lumber and planing, and other millwork (including flooring)
- truss manufacturing
- wood container and pallet manufacturing
- lumber, plywood, millwork, and wood panel wholesale companies.

Data on the number and size (number of employees) of businesses were gathered from the U.S. Census Bureau 2006 County Business Patterns (Figure A13). According to the Wiltsee study (1998), pallet and lumber companies generate about 300 tons a year, and a small woodworking company typically generates between 5 and 20 tons a year of wood waste.

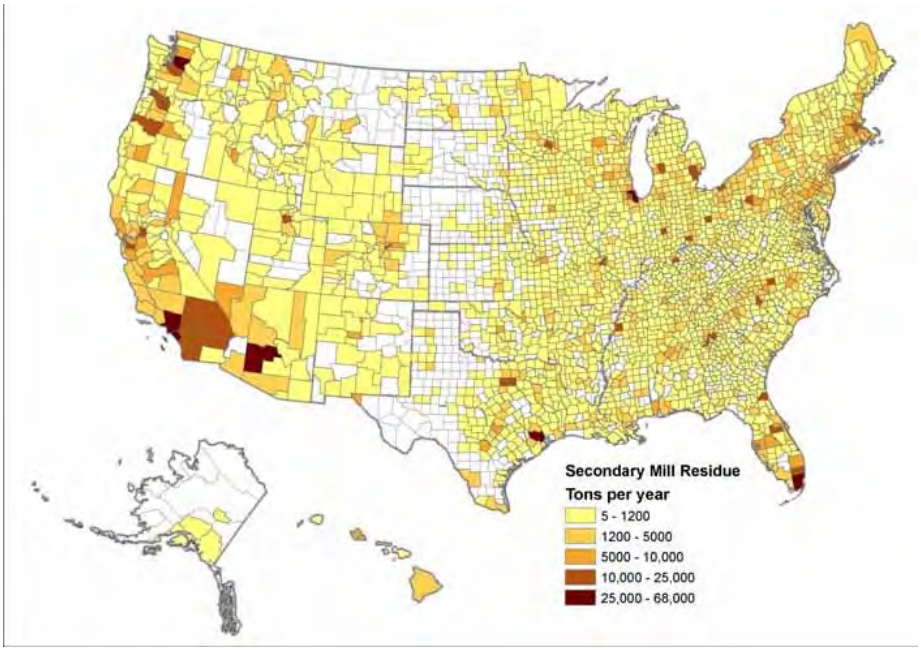

Figure A13. Secondary mill residues by county.

Urban residuals

Urban residuals or municipal solid waste (MSW) include construction and demolition debris, mixed paper, railroad ties, refuse-derived fuel (RDF), residential MSW, scrap tires, and yard waste.

The 2008 State of Garbage in America survey, produced by BioCycle (Arsova et al. 2009), provides a picture of how MSW is handled throughout the United States. The survey collected 2006 data from individual states where available. Reported tonnages were adjusted to exclude non-MSW such as construction and demolition debris and industrial waste. The study concluded that of the over 413 million tons of MSW generated, 28.6 percent is recycled and composted, 6.9 percent is combusted in waste-to-energy plants, and 64.5 percent is landfilled. The per capita estimated generation is 1.38 tons/person/year. Figure A14 shows MSW tonnage for each state and the percentage of MSW recycled, the percentage used for waste-to-energy (WTE) production, and the percentage landfilled. Appendix C to this report provides the actual MSW tonnage by state based on type of waste and the per capita MSW generation rate based on 2006 population.

Projected biomass production yields

In determining projected biomass yields, one must heavily consider demand for renewable energy. The forecasted population size coupled with government influences and consumer behavior patterns creates a measureable demand for biomass resources.

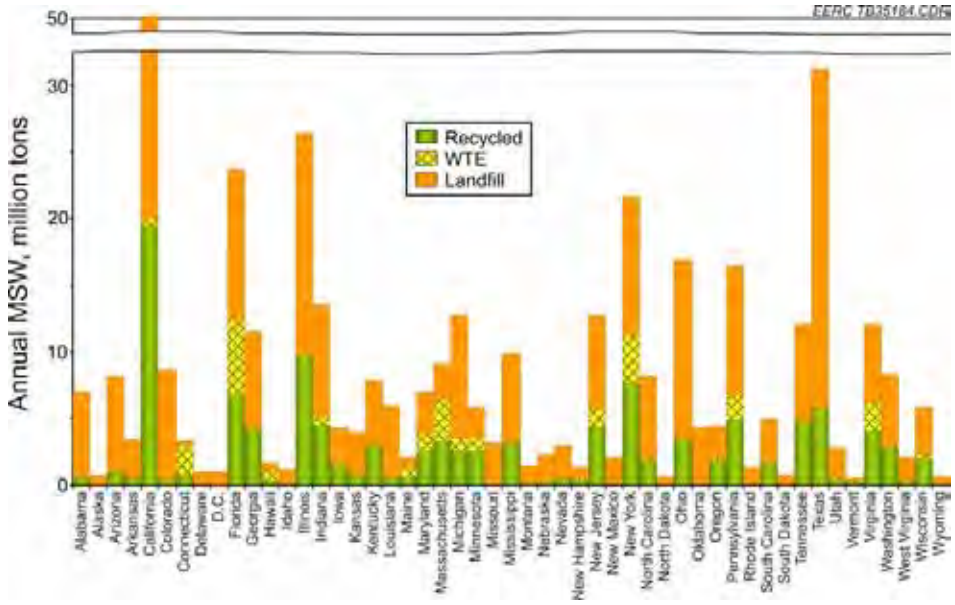

Figure A14. MSW generation and use by state (Arsova et al. 2009).

Population growth is a key determinant of future energy demand, with fluctuations in energy use per capita resulting from variations in climate and economic factors. The U.S. population is expected to increase 24 percent from 2007 to 2030; over the same period, energy consumption will increase by only 11 percent (EIA 2009a). The result is a decrease in energy consumption per capita at an annual rate of 0.05 percent per year. The decline in energy consumption is a result of increased interest in energy conservation induced by higher energy prices (EIA 2009b).

The EIA Early Release Outlook for 2009 anticipates biomass consumption to more than double over the next two decades (2009a), from 2.5 quadrillion Btu of biomass power in 2007 to 5.52 quadrillion Btu by 2030. Rapid growth in the consumption of renewable fuels results mainly from the implementation of the U.S. Environmental Protection Agency's (EPA's) Renewable Fuel Standard (RFS) for transportation fuels and state renewable portfolio standard (RPS) programs for electricity generation. Electricity generation from renewable resources increased in response to minimum renewable generation requirements in more than one-half of the states. Thus growth in renewable electricity (excluding hydropower) represents 33 percent of the growth in electricity demand between 2007 and 2030. This portion may increase if existing production tax credits scheduled to expire in 2009 are extended, or if policies are implemented to limit greenhouse gas emissions (EIA 2009a).

The EIA reference case assumed that Federal subsidies for renewable generation will expire as enacted, but their extension would have a large impact on renewable generation. Because of the great uncertainties in any energy market projection, particularly in periods of high price volatility or rapid market transformation, the reference case results should not be given undue weight (EIA 2009b).

Agriculture production outlook

The USDA report "Agricultural Projections to 2017" and the Food and Agriculture Policy Research Institute (FAPRI) "2008 U.S. and World Agriculture Outlook Database" provides the most current, reputable projected agricultural yields (USDA 2008, FAPRI 2009). Figures A15 and A16 show average projected agriculture crop and animal waste production, which predicts a gradual increase in overall agriculture production to 2017.

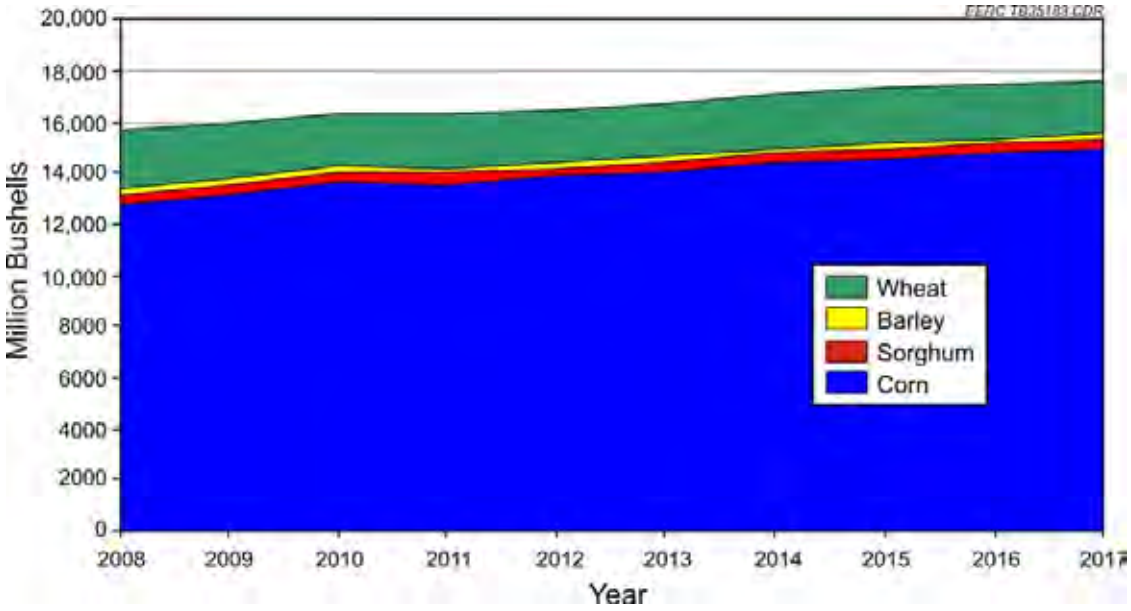

Figure A15. Average projected agriculture crop production to 2017 (USDA 2008; FAPRI 2009).

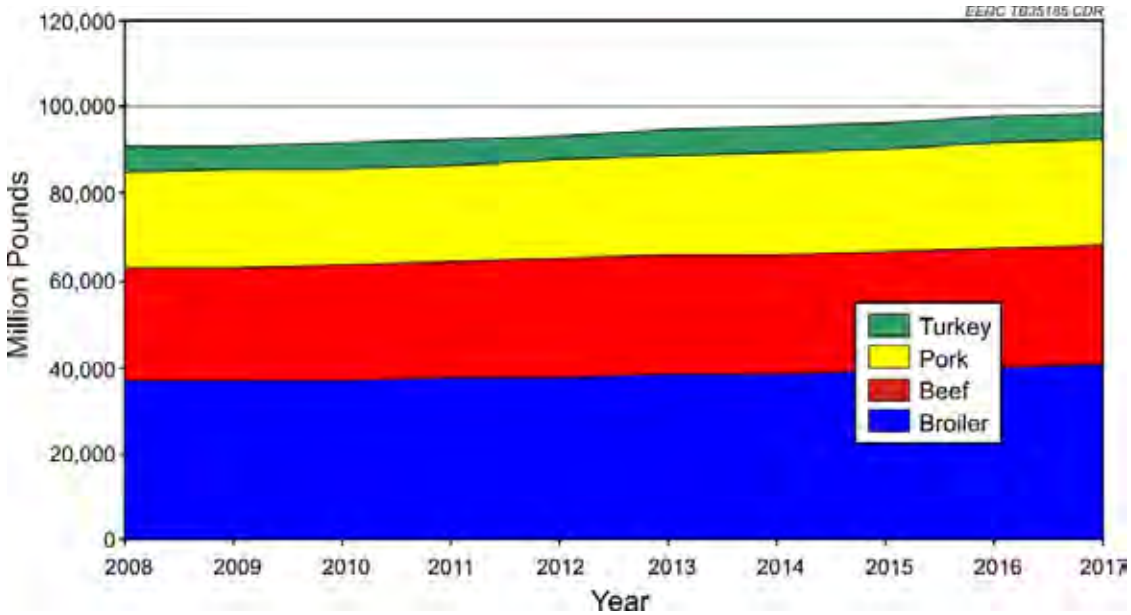

Figure A16. Average projected animal waste production to 2017 (USDA 2008; FAPRI 2009).

Tabular data from both sources is given in Appendix D to this report. The gradual increase in agricultural production across nearly all categories is a result of projected steady domestic and international economic growth. Additionally, the projections reflect continued high crude oil prices and increased demand for biofuels, particularly in the United States and the European Union. Note that the USDA (2008) and FAPRI (2009) sources were generated before the major downturn in the U.S. economy, which will likely influence the agricultural outlook.

Although the results were similar, assumptions varied slightly in each source. The projections in both reports are based on macroeconomic conditions, policy, weather, and international developments. Changes in crop varieties, farming practices, prices, and other variables that can impact the area planted, yields, and total production in a given year were not explicitly factored into the analysis of either of these sources, but are implicitly reflected by the historic trends forming the basis for future projections. Both reports assumed no shocks due to abnormal weather, further outbreaks of plant or animal diseases, or other factors affecting global supply or demand. The USDA projections assumed the Farm Security and Rural Investment Act of 2002, the Energy Policy Act of 2005, and the Agricultural Reconciliation Act of 2005 would remain in effect through the projection period. The FAPRI baseline assumed provisions of the Farm Security and Rural Investment Act of 2002 and incorporated the conditions of the Energy Independence and Security Act (enacted December 2007).

Wood production outlook

Prospective trends in demands and supplies of timber, and the factors that affect these trends, include changes in the U.S. economy, salvage of British Columbia beetle-killed timber, and strength of the U.S. dollar. Other prospective trends that might alter the future timber situation include changes in U.S. timberland area, reductions in southern pine plantation establishment, impacts of climate change on forest productivity, increased restoration thinning on western public lands, and the impact of programs to increase carbon sequestration through afforestation. Data obtained from the USDA Forest Service report "The 2005 RPA Timber Assessment Update" (Haynes et al. 2007) is an update to the 2003 report "Analysis of the Timber Situation in the United States," which reflects these trends.

The USDA Forest Service projected increases in softwood and hardwood harvests from forestland in the contiguous states, by region, through 2050 (Figures A17 and A18). The 2005 update base projection envisions a 38 percent expansion in total U.S. forest product consumption to 27 billion cubic feet per year by 2020. Softwood timber harvest is projected to increase further in high-productivity regions in the southeast and south-central parts of the United States to meet growing demand in pulpwood; however, other regions will remain relatively stable. Hardwood timber is expected to see stable increases in productivity to 2050 in most regions, again as a result of pulpwood demand. Appendix E to this report includes the tabular data supporting the charts shown in Figures A17 and A18.

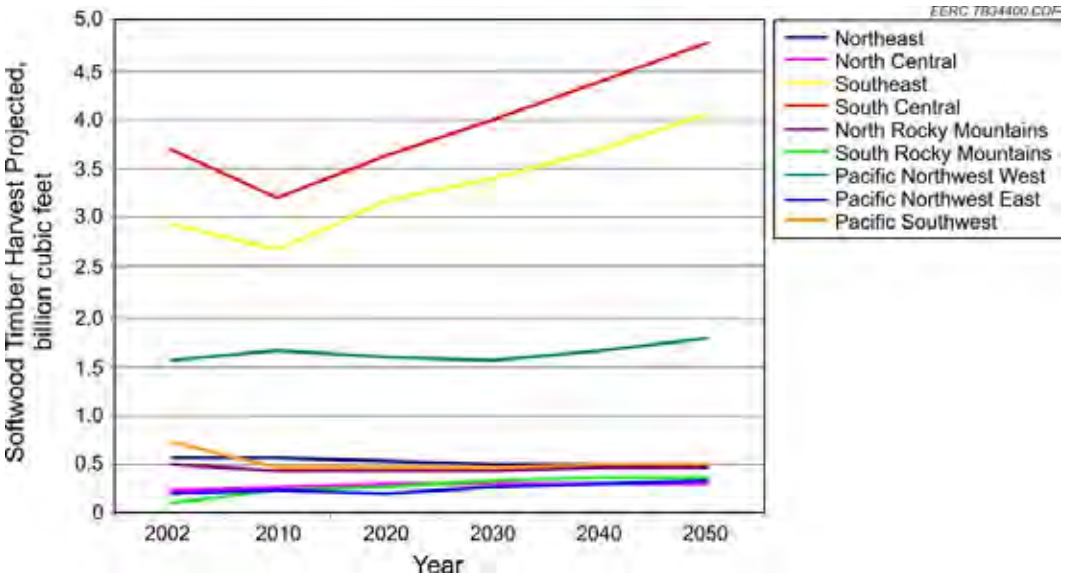

Figure A17. Forest Service softwood timber harvest projections by region 2002–2050 (Haynes et al. 2007).

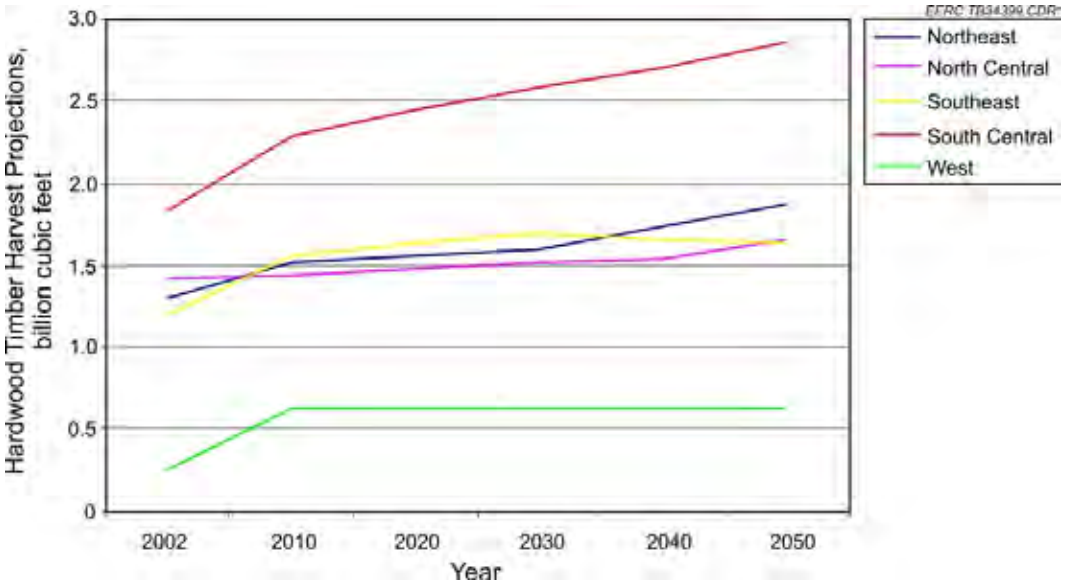

Figure A18. Forest Service hardwood timber harvest projections by region 2002–2050 (Haynes et al. 2007).

Despite the overall increase expected in timber production, it will not be sufficient to solely meet the demands of the emerging biomass industry. An article in *Biomass Magazine* (Bevill 2009) by RISI, Inc., titled "The Emerging Biomass Industry: Impact on Woodfiber Markets" examined the availability of woodfiber supply in comparison to the accelerating demands for advanced biofuel production as mandated by the RFS and RPS. It was determined that use of wastewood (including logging residue, sawmill residue, urban waste wood, and short-cycle energy crops such as poplar trees) could contribute up to one-third of the projected demand needed

to meet RFS and RPS mandates, doubling overall woodfiber demand by 2023. Thus the current supply of U.S. woodfiber is capable of supporting both the forest products industry and the biomass industry in the short term; however, that supply will be severely strained in the long-term. The combined demand of biomass and forest products would require additional growing stock removals from U.S. forests, putting the nation's forests at risk for depletion. Possible solutions to meet the growing demand include:

1. A massive shift from traditional forest products production
2. Changes in RFS and RPS mandates
3. Policy mandates met by greater use of other forms of nonwood biomass, such as dedicated energy crops, and other types of renewable energy, including solar and wind power.

Urban residues outlook

Urban residue (or MSW) generation can be directly attributed to population size. MSW generation per capita estimated by state (Arsova et al. 2009) was combined with U.S. population projections by state (U.S. Census Bureau 2009) to calculate increases in generation of urban residues. Figure A19 shows national results, estimating over 500 million tons of MSW generated annually, or an increase of 25 percent from 2006 levels. Current consumption patterns and recycling programs were assumed to remain unchanged. Individual state statistics are available in Appendix F to this report.

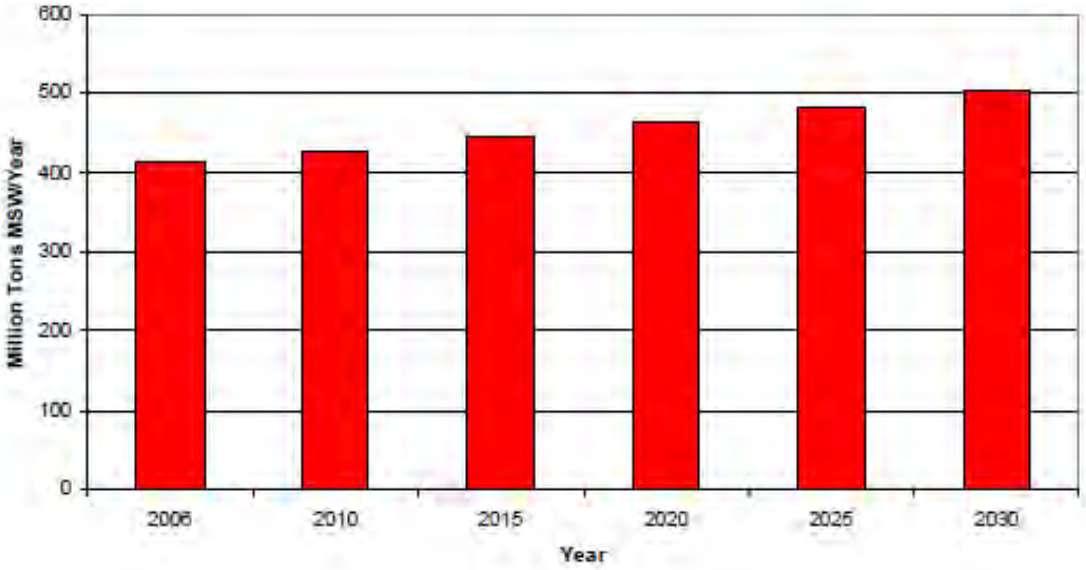

Figure A19. U.S. projected MSW generation to 2030 (U.S. Census Bureau 2009; Arsova et al. 2009).

Government influence on biomass demand

The increase in energy demand creates a need for biomass energy, but Federal and state government initiatives, incentives, and mandates create the immediate demand.

Perhaps the most influential Federal law impacting biomass demand is EPA's RFS, requiring the blending of renewable fuels in transportation fuel. As a result, fuel suppliers blended 9.0 billion gallons of renewable fuel into gasoline in 2008, with annual increases to 36 billion gallons in 2022. The expanded RFS also specifically mandates the use of advanced biofuels, defined as fuels produced from noncorn feedstocks with 50 percent lower lifecycle greenhouse gas emissions than petroleum fuel, starting in 2009. The RFS creates a guaranteed advanced biofuels market and is expected to continue stimulating biomass growth and consumption.

Tax incentives also provide demand for biomass, such as the $1.00/gallon production tax credit for biodiesel and renewable diesel produced solely from biomass. Diesel fuel created by coprocessing biomass with other feedstocks (e.g., petroleum) is eligible for the $0.50 per gallon tax credit for alternative fuels. These Federal tax credits were scheduled to expire on 31 December 2008, but were extended for 1 year through 31 December 2009. The long-term continuation of this tax credit is uncertain.

The passing of the Food, Conservation, and Energy Act of 2008 (H.R. 6124), ("The Farm Bill") assists in the development of agricultural biomass resources. Several grant and loan programs are anticipated, such as the Biomass Crop Assistance Program, which supports sustainably-grown energy crops. These programs will be administered by the USDA and will also impact biomass demand.

In addition to Federal programs, 29 states and the District of Columbia (Figure A20) have implemented regulatory policies (varying by state) requiring the increased production of renewable energy. Many states offer end users tax incentives, in addition to Federal incentives, to encourage the use of biomass. To further economic development and the use of state biomass resources, some states also offer grants, or loans to companies willing to locate biomass-based companies within their state.

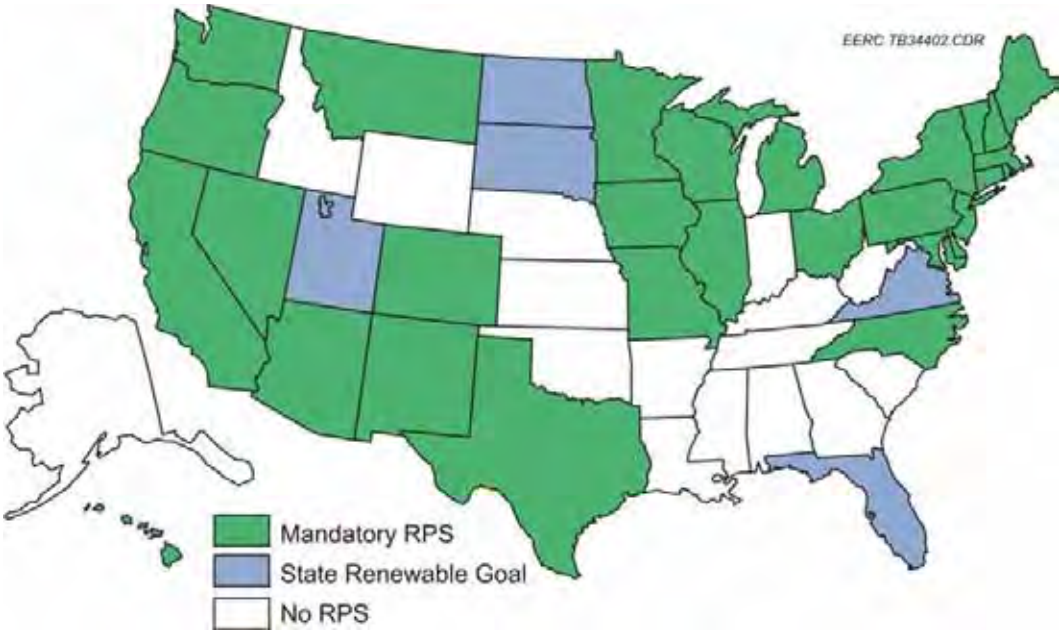

Figure A20. States having renewable performance standards (Dick 2009).

Biomass chemical analysis and physical characterization

An extensive literature search was conducted to obtain biomass chemical analysis and physical characterization data. Major sources included data generated through past EERC biomass research efforts and the U.S. DOE Energy Efficiency and Renewable Energy Biomass Feedstock Composition Database. International biomass composition databases such as the Phyllis Biomass Composition Database; IEA BioBank; and the University of Technology, Vienna, BIOBID database were not used because they were believed to contain mostly data from biomass sources outside the United States. It was discovered that a limited amount of original biomass characterization exists in published literature, oftentimes citing other work without evaluating specific biomass sources. Therefore, differing sample collection, handling, and preparation techniques and scientific methodologies were used to generate the data procured for this study, and values varied widely across regions and states. Because of these variations, it is imperative to evaluate the specific biomass feedstock to be used for a given application.

Only samples that are clearly untreated wood, grass, stalk residue (straw, hay, and stover), or hard processing residue (shells, hulls, and pits) are presented in this section. To account for differing collection methods and allow standard comparison, “as-determined” or air-dry moisture content was assumed to represent total moisture, leaving other results (volatiles, ash, Btu/lb, etc.) unadjusted. The correction does not make a great impact

as air-dry losses were generally low (<1 percent). References for external data are noted in Appendix G to this report. Definitions and methods of characterization analyses for the datasets are presented in Appendix H to this report.

The energy content or heating value of wood and hard processing residues was observed to be greater than grass and stalk residues on average. Figure A21 shows the biomass energy data, displayed as frequency distributions of incremental analytical results. For instance, nearly 45 percent of the analytical data procured for grasses had energy densities 7000–7500 Btu/lb. The average energy of stalk residue is about 7000 Btu/lb, as well. Wood and hard processing residues tend to be >8000 Btu/lb.

Figures A22–A25 show (and Table A4 lists) proximate, ultimate, and ash oxide data as frequency distributions of analytical results with values given in logarithmic increments. For example, the first column of each graph shows the number of samples found with a given property fraction of <0.1 percent, while the final column shows the number of samples with content >46 percent.

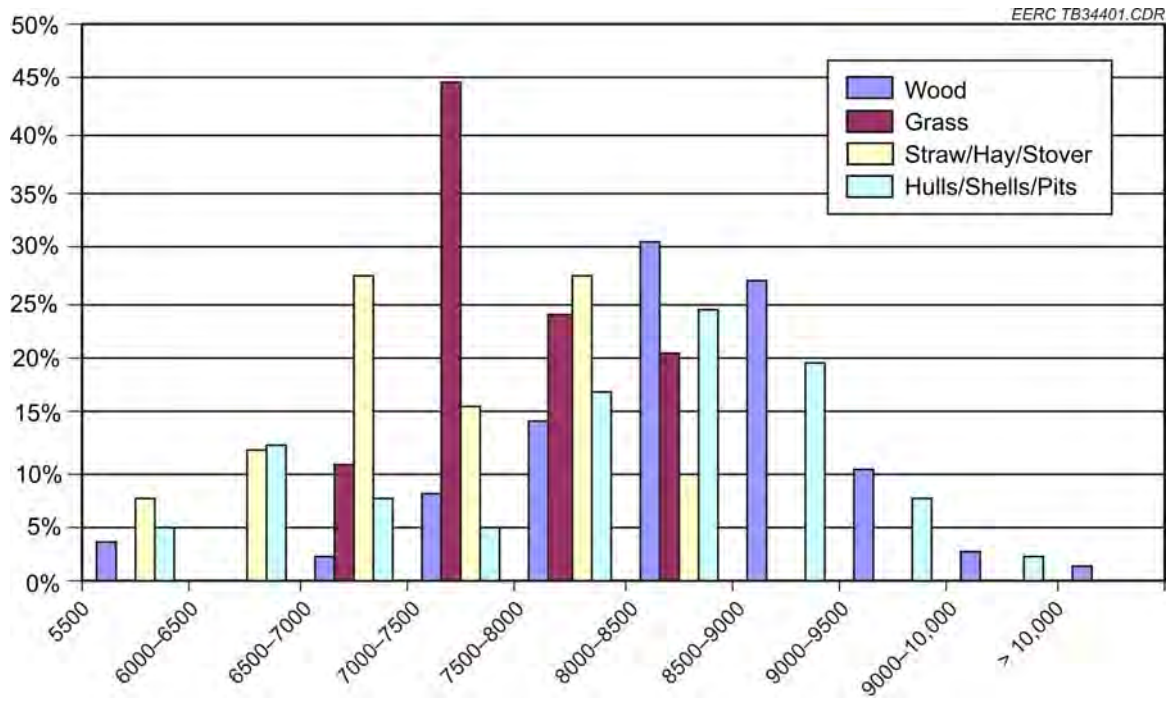

Figure A21. Summary of biomass heating values (Btu/lb).

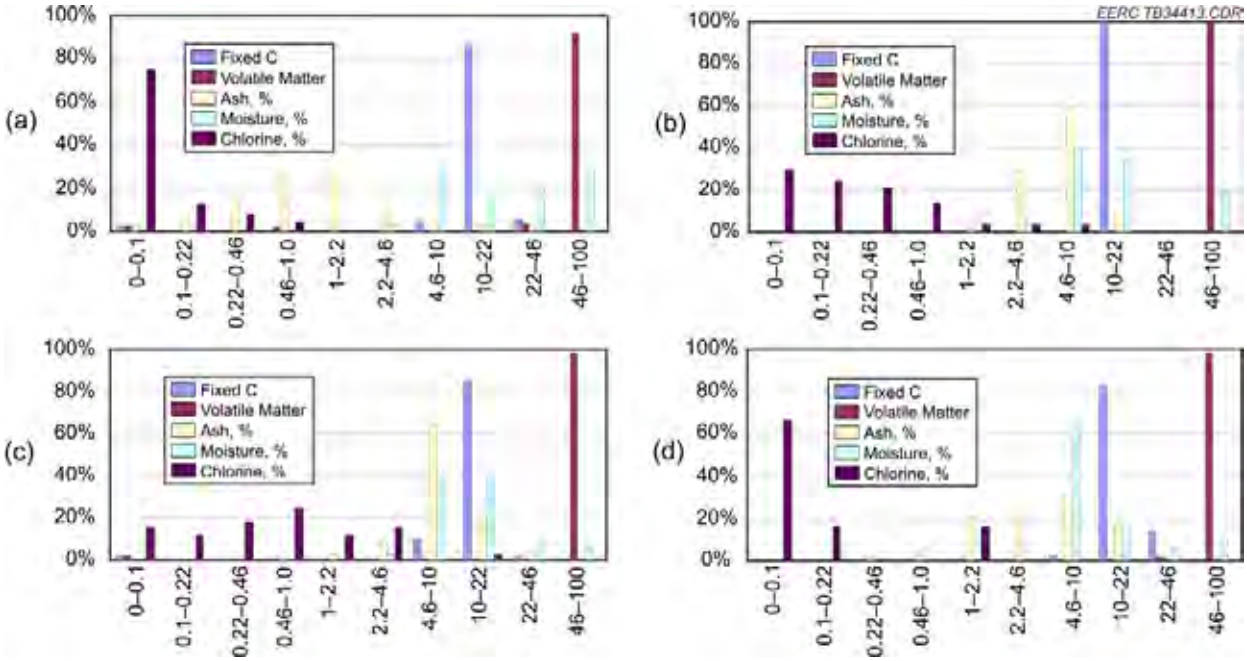

Figure A22. Summaries of proximate analyses: (a) wood, (b) grasses, (c) straw/hay/stover, and (d) hulls/shells/pits.

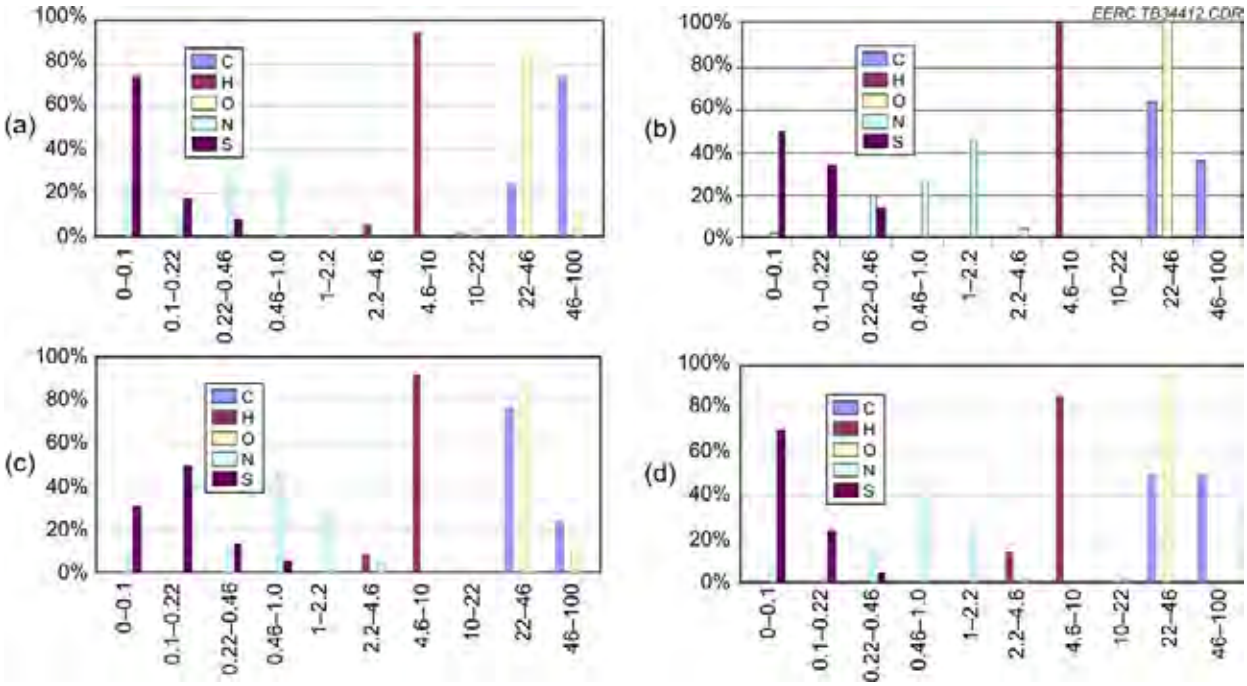

Figure A23. Summaries of ultimate analyses: (a) wood, (b) grasses, (c) straw/hay/stover, and (d) hulls/shells/pits.

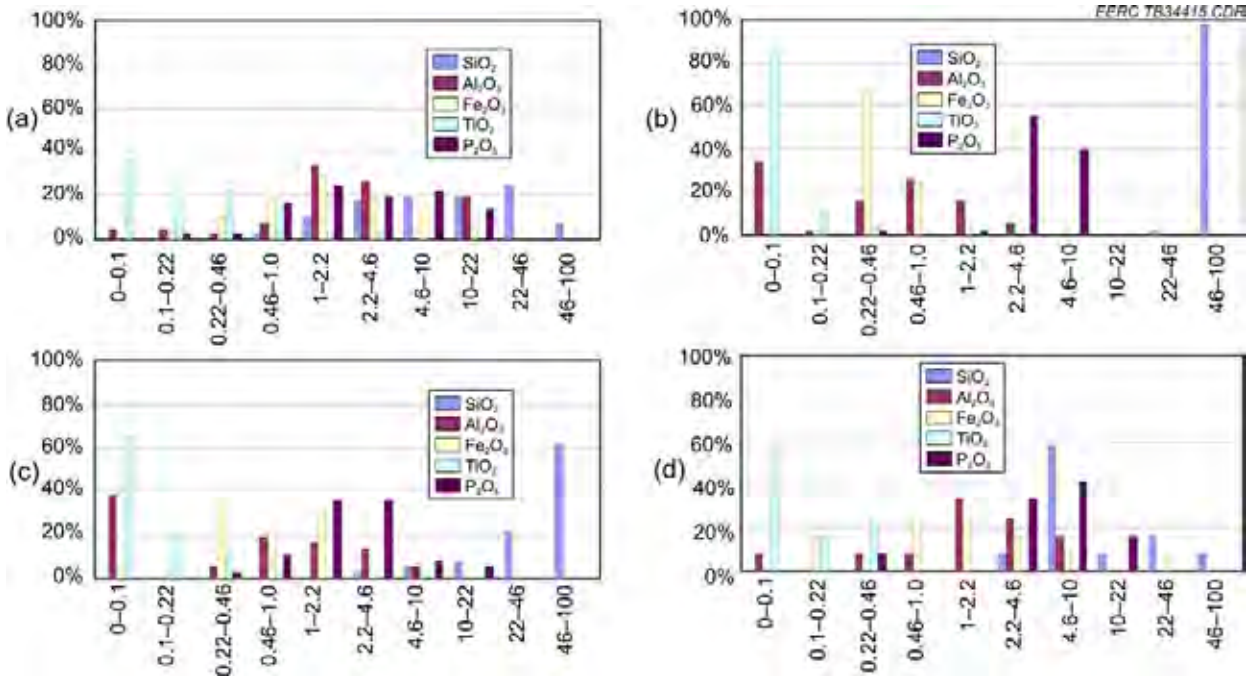

Figure A24. Summaries of major element ash oxide composition (% in ash): (a) wood, (b) grasses, (c) straw/hay/stover, and (d) hulls/shells/pits.

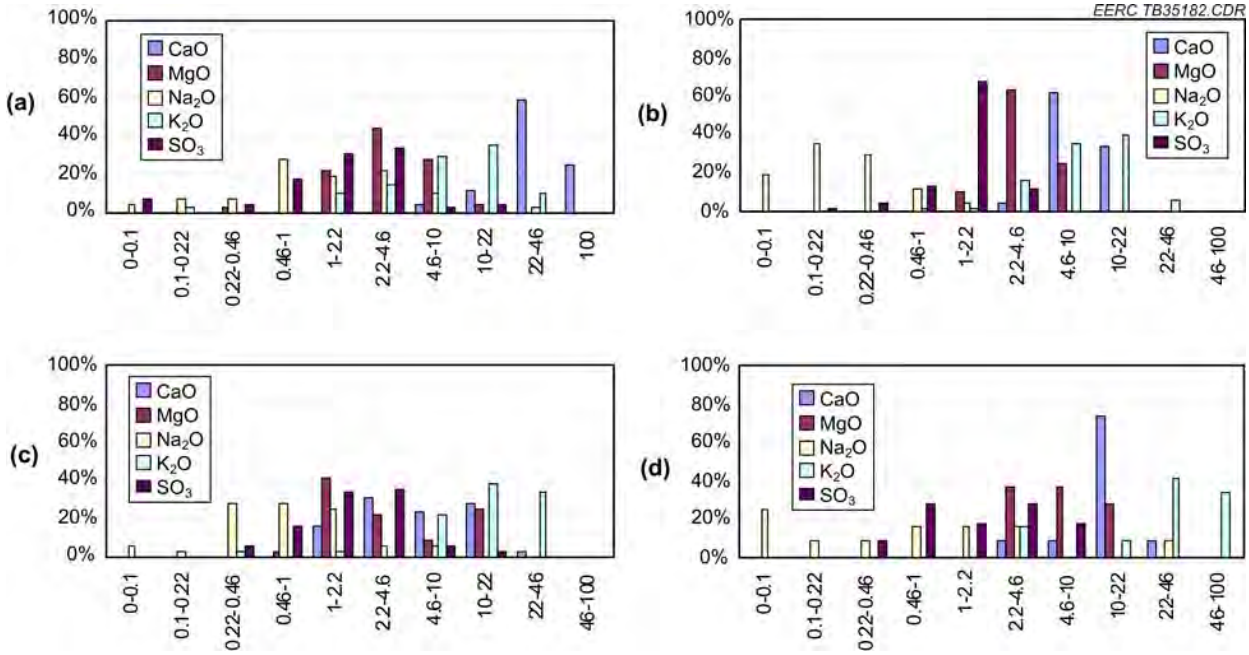

Figure A25. Summaries of major element ash oxide composition (% in ash), continued: (a) wood, (b) grasses, (c) straw/hay/stover, and (d) hulls/shells/pits.

Table A4. Estimated average elemental oxide values (ash basis).

	Wood	Grass	Straw/Hay/Stover	Hulls/Shells/Pits
SiO_2	13–24	65–70	43–58	10–26
Al2O3	2.6–5.6	0.5–1.0	0.6–1.8	1.9–3.6
Fe2O3	1.9–3.7	0.4–0.6	0.6–1.3	1.5–7.7
TiO_2	0.2–0.5	0–0.1	0.1–0.2	0.1–0.2
P2O5	3–5	4–5	2–4	5–8
CaO	30–40	8–10	6–10	11–15
MgO	4–6	3–4	3–7	7–9
Na_2O	1.2–3.6	0.2–0.4	0.6–1.9	1.1–6.1
K_2O	8–13	9–13	14–20	28–41
SO_3	1.5–3.0	1.3–1.7	1.8–3.4	1.8–3.0

Figure A22 shows that wood contains less ash on average than other biomass types, although the average moisture content may be slightly higher. Lower ash levels cause less abrasion or agglomeration during combustion. Fixed carbon and volatile matter are similar for the biomass types shown. Chlorine appears to be lower for wood and hard processing residues, with a majority of samples containing less than 0.1 percent. It can also vary widely in absolute quantity because of its higher solubility, e.g., levels in grasses and stalk range 0–10 percent. Chlorine is notorious for causing boiler ash deposition and corrosion.

Figure A23 shows the biomass types shown to be similar in ultimate composition. Hard processing residues contain slightly more carbon than stalks or grasses, and wood contains more carbon still. This is to be expected, as it coincides with the higher energy potential from combustion of hard processing residues and wood. On average, wood also contains slightly less nitrogen.

A large majority of the grasses and stalk residue ash characterization data collected contains more than 46 percent silica (SiO_2) (Figure A24, Table A4. This is likely the result of silica-based phytoliths in the stalk material of plants. Phytoliths are hardened mineral deposits that are incorporated into the cell walls of plants to add structure and support, and as such, they are common in the stalks of grassy plants. Silica is much less prevalent in hard processing residues, with well more than half of the data collected containing less than 10 percent silica. Because seeds do not provide support to the plant, they incorporate less phytolithic material. The significant presence of phosphorus in biomass combustion ash (~5 percent P_2O_5 average) without potential contaminants (e.g., mercury), generates an inert waste and a suitable fertilizer.

Figure A25 shows that hard processing residues have higher levels of potassium than the other biomass types. Potassium is an important nutrient for plants. The large EERC switchgrass data set may have affected potassium averages for grass data, showing similar levels as wood. Most literature seems to agree that herbaceous plants such as grasses and straws will have higher levels of potassium, >20 percent K_2O in combustion ash. The figures also show that wood contains higher calcium levels on average than the other plant materials, as it is more common to find calcium-based phytoliths in wood. Also of interest is the relative consistency of magnesium in all biomass types shown, an average ~5 percent MgO in combustion ash. Magnesium is the chelated metal in chlorophyll that plants use for photosynthesis so there is little variance in the magnesium levels.

Many factors can interact with feedstock characteristics, affecting the suitability of biomass as a resource for a given application. For example, wood and grasses contain less total alkali (sodium-Na_2O and potassium-K_2O) than stalk or hard processing residues. High alkali concentrations in feedstock ash can cause slagging or deposits on combustion heat-transfer surfaces. Potassium specifically interacts with silica and alumina material, lowering the ash melting temperature and causing agglomeration issues. Table A4 lists this "slag potential," suggesting wood to be more amenable to combustion than other biomass types.

Transportation costs will also likely be the determinant of acceptable moisture or energy content for a given biomass application. A strong inverse relationship exists between moisture content and heating value for selected biomass samples, suggesting low-moisture feedstocks to be preferable (Figure A26). If the radius of procurement for a dry biomass resource is significantly greater than the radius of wetter feedstock, then the wet biomass may be preferable over dry because of lower transportation costs per Btu. Wet feedstock may also be dried by process heat recovery; all factors should be evaluated when choosing a biomass feedstock.

Viability of biomass

Geographic and seasonal factors can significantly impact biomass growth. These factors also affect the elemental uptake of plants, which varies between plant species. Thus the plant environment will affect the inorganic content of biomass. This variability is of interest for elements that give rise to slagging, fouling, and particulate emissions when the biomass is used as an energy source in combustion systems. Yet, the extent of the impact of geographic and seasonal factors depends largely on the biomass type.

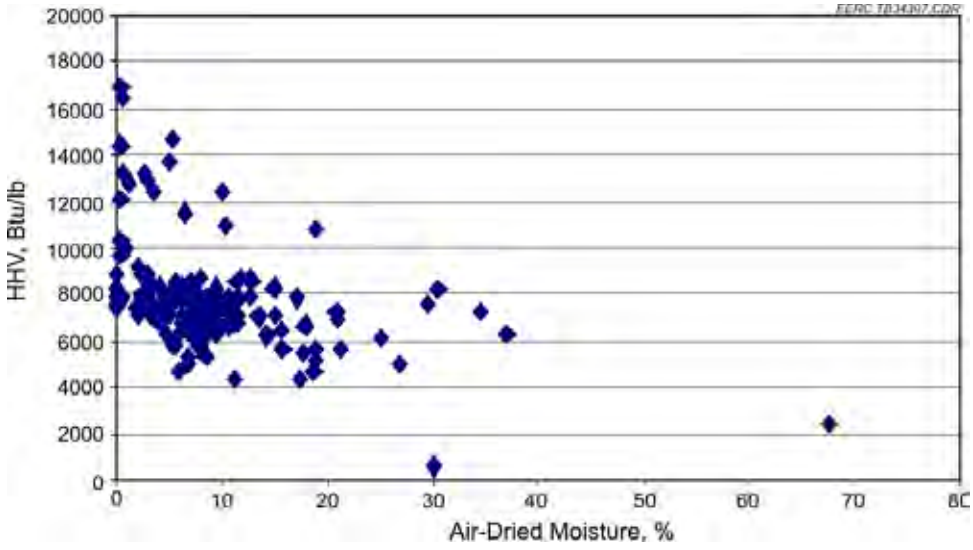

Figure A26. Energy versus moisture for selected biomass samples (HHV = higher heating value).

Studies have been performed on the variability of short rotation woody feedstocks (such as hybrid poplar or willow) and have found minimal compositional variation due to clonal, geographical, and environmental factors, indicating that they are a consistent and stable feedstock for biofuels production (Davis et al. 1995). Compositional variability has also been assessed for herbaceous energy crops. In this case, large differences in composition were found between stems and leaves, with leaves containing much higher concentrations of nonstructural components. The geographic location of where the plants were grown was found to affect the composition even more than differences between varieties (Johnson et al. 1995).

The EERC conducted an in-depth study to evaluate the geographic and climatic factors influencing the elemental composition of switchgrass. Factors evaluated included temperature, solar radiation, moisture supply, soil, and time of harvest. The analysis was performed on switchgrass samples from 10 different farms in south-central Iowa (Zygarlicke et al. 2001).

Figure A27 shows variability of switchgrass from two farms in southern Iowa over several months. Note that ash and alkalinity (both features that increase agglomeration tendency) are several times higher in early fall than in mid- to late-spring. There appears to be a correlation between extra moisture in the spring and the increase in aluminum oxide (Al_2O_3). However, potassium oxide (K_2O) was lowest in spring, which will tend to offset the high Al_2O_3 content. Since this trend is the result of seasonal variations, the extent of variation shown will likely also vary by environmental conditions specific to geographical location. (Zygarlicke et al. 2001).

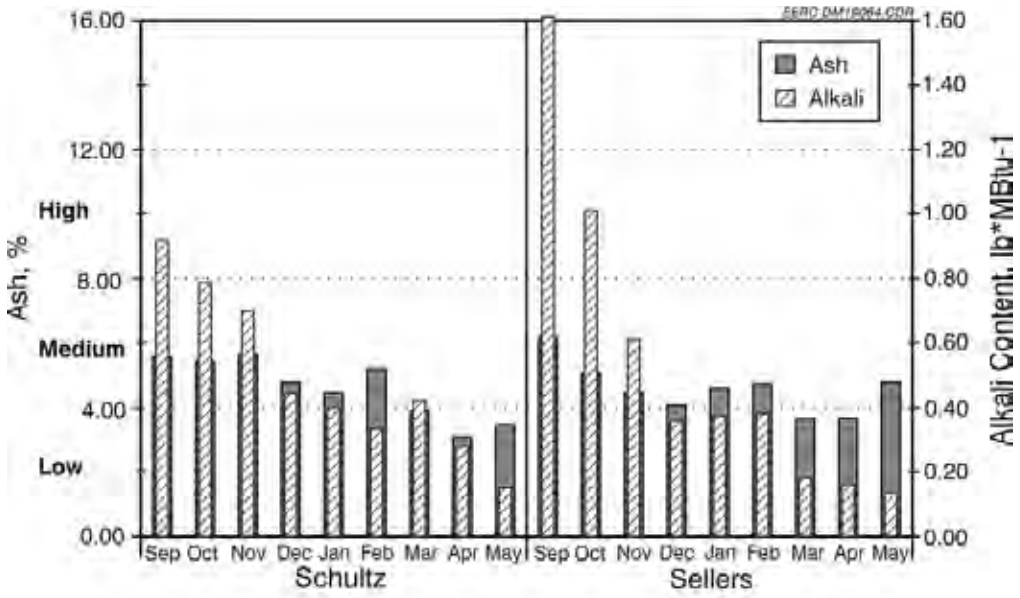

Figure A27. Ash and alkali content for unharvested switchgrass in southern Iowa (Zygarlicke et al. 2001).

Calculation of energy content per acre

Biomass energy density or heating values average about 8000 Btu/lb without moisture and 6500 Btu/lb when accounting for the presence of water. Table A5 lists individual heating values on both a dry and wet basis for the major biomass sources defined in the previous sections. The heating values are multiplied by a chosen biomass yield to estimate the potential energy available per acre. Since biomass resources are typically not dried at their location, the heating values adjusted for moisture content were used. For example, the energy potential of a region growing hybrid poplar trees would be approximately 120 MMBtu per acre with a yield of 8 tons/acre and an energy density of 2600 Btu/lb on a wet basis.

Table A5. Typical energy content for various biomass types.

Biomass Source	Btu/lb, dry	Btu/lb, wet	Ref.*
Agricultural-Based	7700	6500	
Harvest Residuals	*7600*	*6600*	
Wheat Straw	7700	6800	1
Rice Straw	6500	6000	1
Flax Straw	8600	6600	2
Cornstalks (aka stover)	7800	7100	3
Processing Residuals	*8000*	*7300*	
Rice Hulls	6800	6100	1
Sugarcane Bagasse	8200	7300	1
Almond Shells/Hull	8200	7700	1
Olive Pits	9300	8700	1
Sugar Beet Pulp	7300	6600	3
Animal Wastes	*7300*	*4500*	

Biomass Source	Btu/lb, dry	Btu/lb, wet	Ref.*
Poultry Litter	6000	4700	4
Feedlot Wastes	8500	4300	5
Forest Products	7900	5200	
Logging Residuals	*8600*	*4300*	
Cull Trees	8700	4300	6
Tops	8700	4300	6
Dead Wood	8400	4200	6
Small-Diameter Stock	8700	4300	6
Primary Wood-Processing Residuals	*7500*	*5700*	
Sawdust	8600	5800	1
Leaves and Grass Clippings	6500	2600	7
Bark	8800	7900	6, 8
Edgings	6800	6100	6
Slabs	6800	6100	6
Secondary Wood-Processing Residuals	*7700*	*5900*	
Sawdust	8600	5800	1
Edging	6800	6100	6
Urban Wastes	8600	7100	
Residential	*8700*	*7700*	
MSW	7500	6100	9
RDF	6700	6400	1
Mixed Paper	8900	8200	1
Yard Waste	7000	4300	1
Demolition Wood Waste	7900	7200	1
Scrap Tires	14,000	14,000	6, 10
Urban and Landscape Residuals	8500	6100	
Chipped and Unchipped Wood	8500	6300	1
Construction and Demolition Waste	7900	7200	1
Pallets/Scrap	8400	4200	6
Railroad Ties	9200	6800	11
Dedicated Energy Crops	**8600**	**7400**	
Grasses	*7900*	*7000*	
Switchgrass	7900	7000	1
Native Grasses	7900	7100	1
Trees	*8400*	*6900*	
Willow	8400	7500	1
Cottonwood	8700	5600	12
Hybrid Poplar	8200	7600	1
Others	*9500*	*8400*	
Alfalfa Stems	8000	7300	1
Specialty Crops*	11,000	9500	6

References:

1. Miles et al., 1995.
2. The Prairie Agricultural Machinery Institute, 2009.
3. Agricultural Utilization Research Institute, 2009.
4. Reardon et al., 2009.
5. Combs, 2009.
6. Center for Energy and Environment, 2007.
7. California Energy Commission, 2008.
8. Ince, 2009.
9. Chang and Davila, 2008.
10. Kentucky Pollution Prevention Center, 2009.
11. Ellis, 2009.
12. FirewoodResource.com, 2009.

* Average of corn, soybeans, and canola.

Discussion

This report aims to provide a comprehensive, up-to-date, quantitative assessment of the availability of various biomass resources, including material quantities as produced on site (e.g., energy crops, agricultural residues, annual forestry growth) and material generated as a by-product of human consumption (e.g., MSW, mill residues, methane from manure management). Data collection methods erred on the side of overreporting rather than underreporting. While the tactic of collecting all available data has led to the compilation of a fairly comprehensive data set, an unavoidable result is that most resources are counted more than once. For example, estimates of annual forestry growth include all wood grown in a year regardless of its purpose or availability. Some of this wood will be harvested for timber, and its by-product will be mill residues, which are reported in a separate section of the report. Forestry harvest thus impacts mill residue availability. Similarly, energy crops can only be grown in the absence of forests or agricultural crops; therefore, a county cannot yield significant energy crops while maintaining its agricultural and forestry output. These examples demonstrate one of the limits of how these data can be used, and each section must be assessed individually.

The biomass resource assessment quantifies feedstock growth and production on a county-level where available. Although these data are believed to be the most comprehensive and up-to-date available, they are mostly based on estimates and may vary from actual values. Wherever possible, these estimates were made using well-documented standard formulas and techniques.

Many biomass sources are already used in other applications and may not be accessible or economical to use as an energy source. As an example, agricultural residues are generally difficult to harvest and are composted in the field to maintain soil quality. It is unlikely that the total agricultural residues presented can be economically harvested.

Also not reflected in the quantification of biomass sources are new crop species and higher yielding crops that may emerge as the country moves to reduce consumption of fossil fuels by increasing efficiency and use more renewable resources for energy. Dedicated biomass crops for energy, fuels, chemicals, and other bioproducts may develop with sufficient market and government incentives and improved agronomic practices. Waste streams may find some application as commercial products or fuel (as has already happened with fly ash and most food industry processing residues). In the

ever-changing world of developing energy technologies, it is impossible to estimate what resources will be valuable for energy production until those resources are discovered. Therefore, continued monitoring of the energy industry is necessary to ensure that the data reported here remain up-to-date.

The chemical and physical analysis data also have limitations. The samples were collected and prepared using different methods, derived from different locations, and tested using different techniques. Analysis of many hundreds of biomass samples shows that biomass properties vary widely, even within the same species. Based on data sets from within the same laboratories or using the same methods, a valid conclusion can be drawn that biomass combustion properties will likely vary dramatically by species, location, and agricultural practices. This is especially true for resources such as MSW that have no well-defined composition.

Conclusions

The primary conclusion that can be drawn from this study is that there is no single ideal biomass source. While some sources may have ideal combustion and cofiring properties, such as wood, other sources are optimal feedstocks for fuel production, such as corn or soybeans. In addition, no type of biomass is uniformly available across the United States or even within individual states. The best source for a particular energy production scenario will depend on multiple factors that will need to be assessed on a case-by-case basis. These factors include local resource availability, resource costs, resource physical and chemical properties and intrinsic fuel values, plant size, feed ratio with coal (for cofiring scenarios), resources processing requirements (drying, shredding, pulverizing, separating), storage options, local geography and climate (which will impact biomass properties), and availability of process utilities for conditioning as-received resources. When specific biomass utilization applications are considered, it is imperative to verify the information on a local level and test the specific biomass source to be used. Each application will also require a thorough technoeconomic assessment and analysis of available feedstocks prior to a candidate biomass being selected for energy generation or product development.

Appendix B: Agriculture Crop Yields by County – Summary Maps

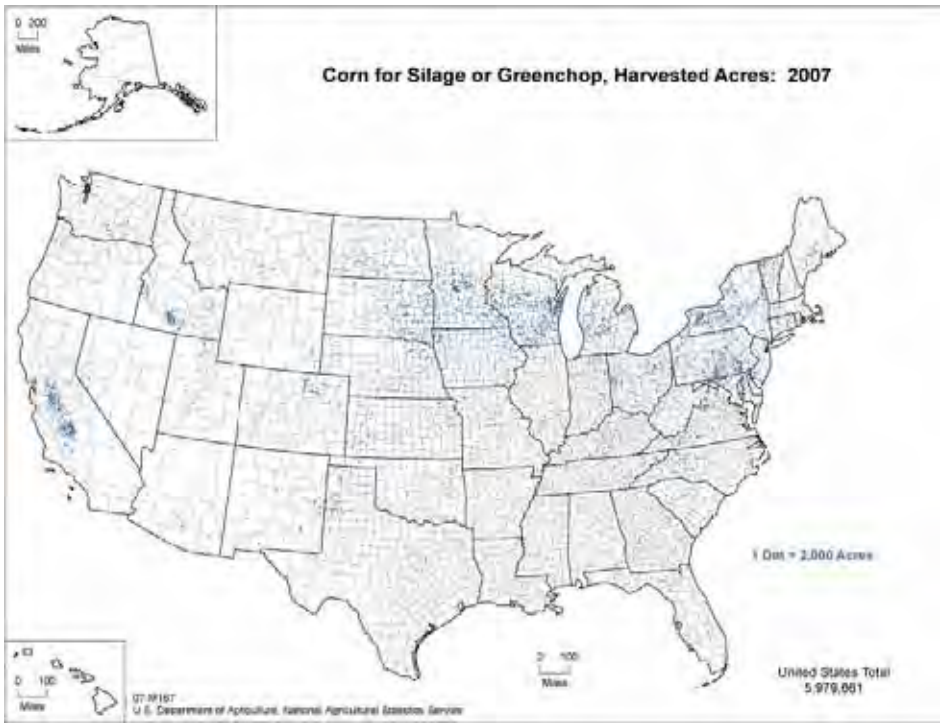

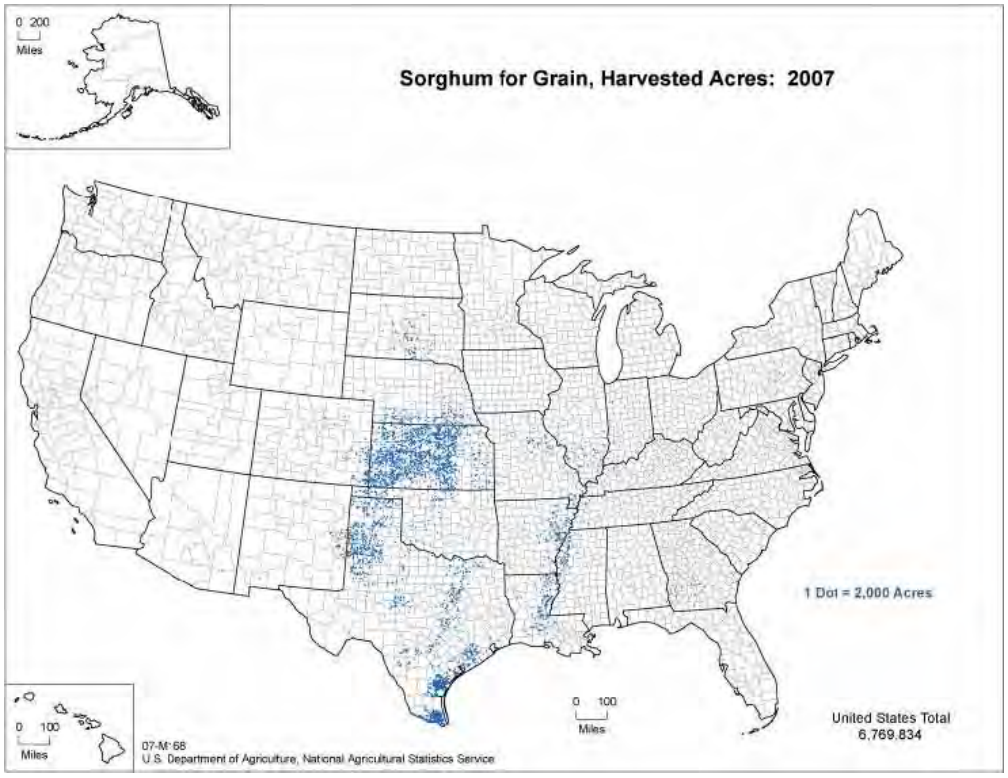
Sorghum for Grain, Harvested Acres: 2007
0 200
Miles
1 Dot = 2,000 Acres
0 100
Miles
United States Total
6,769,834
0 100
Miles
07-M-68
U.S. Department of Agriculture, National Agricultural Statistics Service

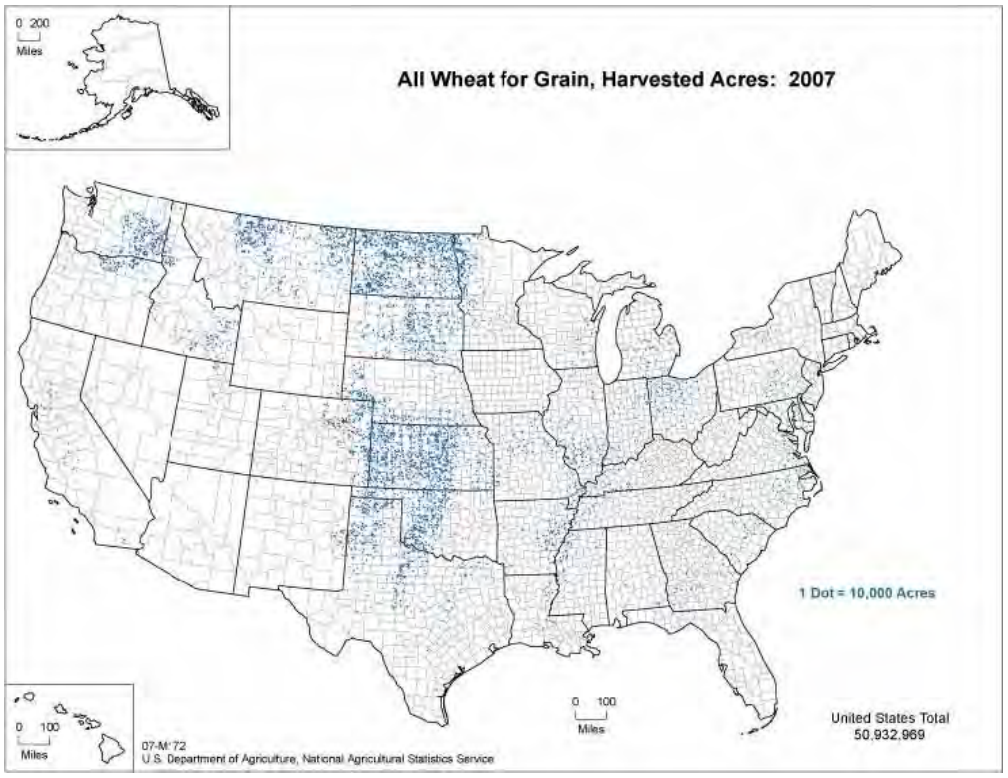
All Wheat for Grain, Harvested Acres: 2007
0 200
Miles
1 Dot = 10,000 Acres
0 100
Miles
United States Total
50,932,969
0 100
Miles
07-M-72
U.S. Department of Agriculture, National Agricultural Statistics Service

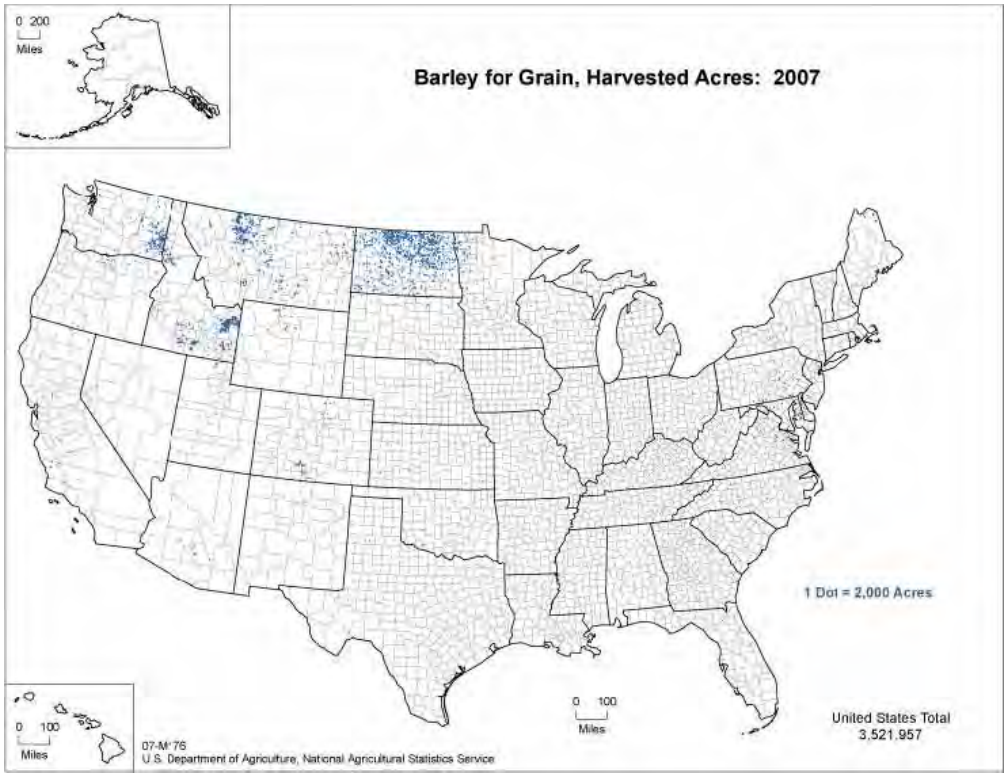
0 200
Miles
Barley for Grain, Harvested Acres: 2007
1 Dot = 2,000 Acres
0 100
Miles
United States Total
3,521,957
0 100
Miles
07-M-76
U.S. Department of Agriculture, National Agricultural Statistics Service

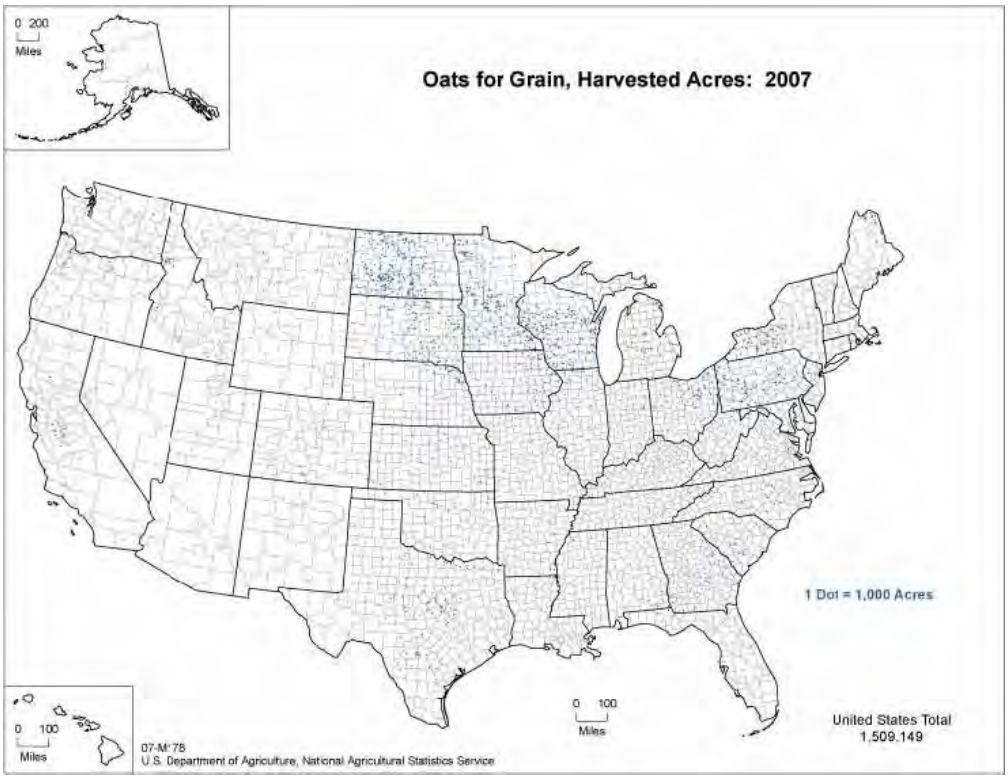
0 200
Miles
Oats for Grain, Harvested Acres: 2007
1 Dot = 1,000 Acres
0 100
Miles
United States Total
1,509,149
0 100
Miles
07-M-78
U.S. Department of Agriculture, National Agricultural Statistics Service

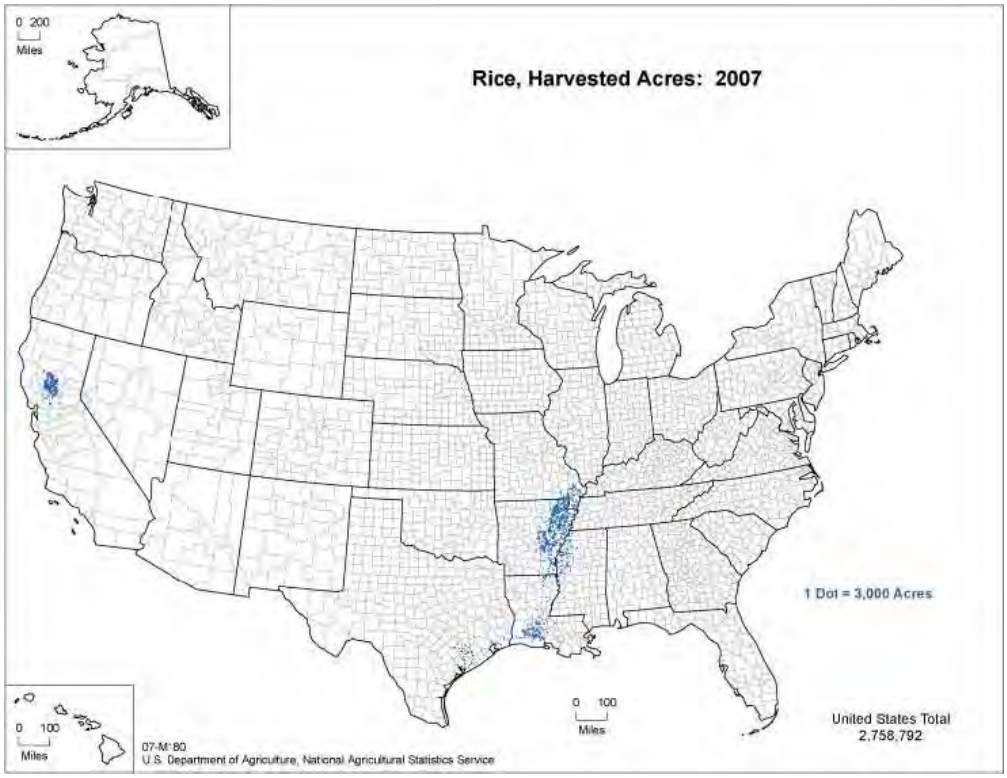
Rice, Harvested Acres: 2007
0 200
Miles
1 Dot = 3,000 Acres
0 100
Miles
United States Total
2,758,792
0 100
Miles
07-M-80
U.S. Department of Agriculture, National Agricultural Statistics Service

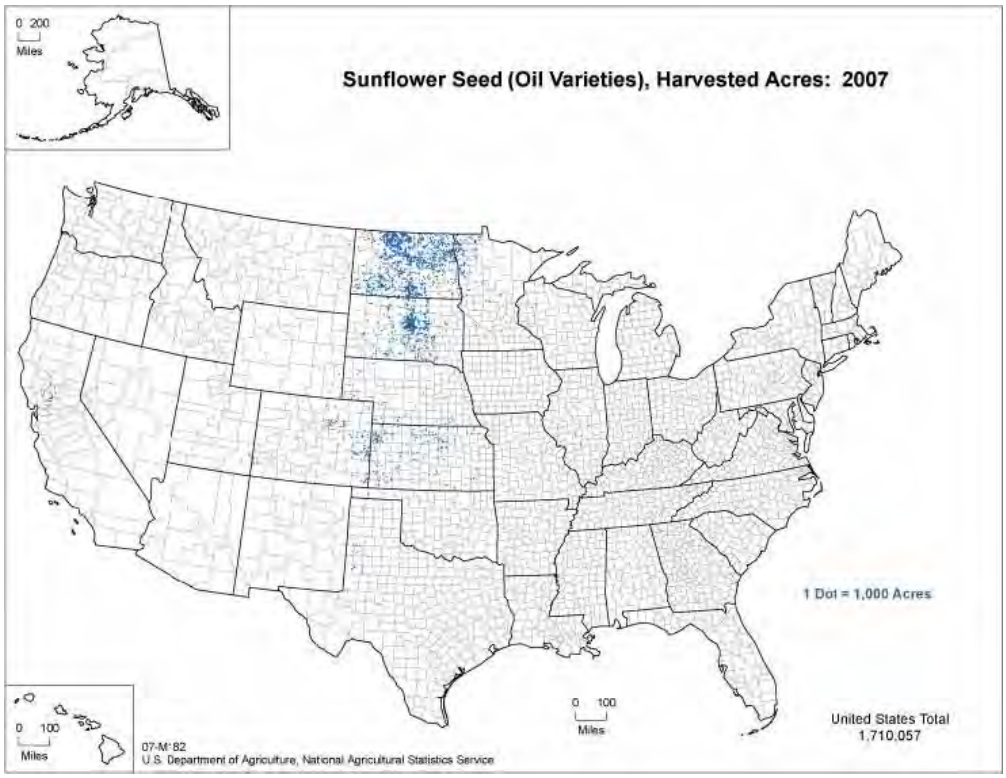
Sunflower Seed (Oil Varieties), Harvested Acres: 2007
0 200
Miles
1 Dot = 1,000 Acres
0 100
Miles
United States Total
1,710,057
0 100
Miles
07-M-82
U.S. Department of Agriculture, National Agricultural Statistics Service

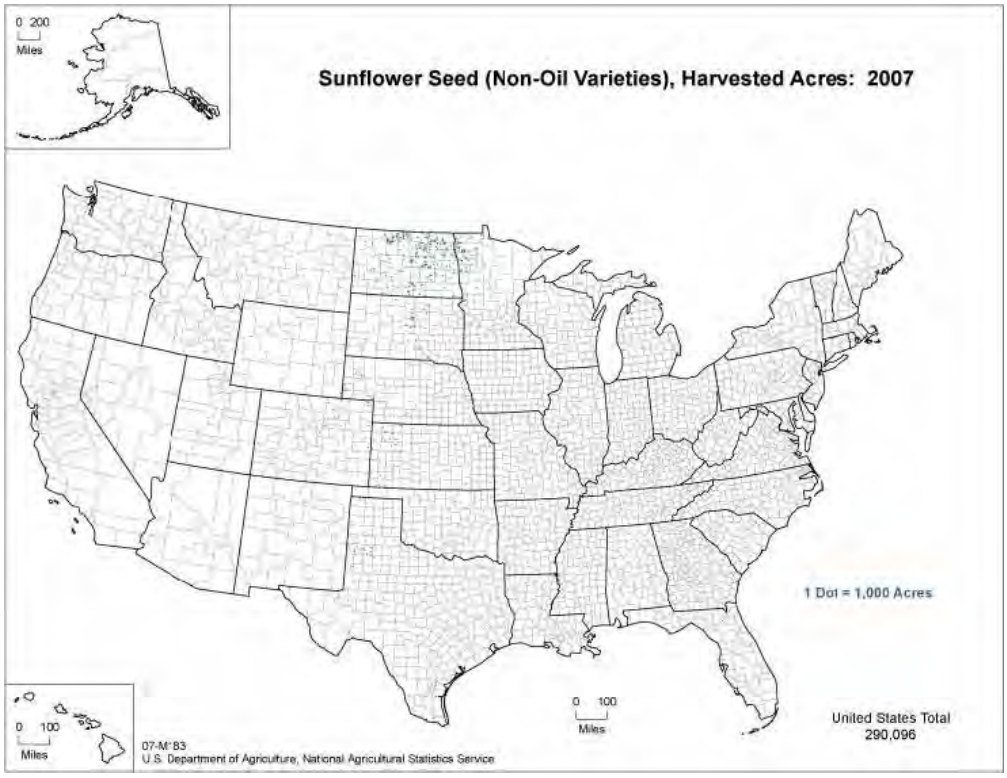
Sunflower Seed (Non-Oil Varieties), Harvested Acres: 2007
0 200
Miles
1 Dot = 1,000 Acres
0 100
Miles
0 100
Miles
United States Total
290,096
07-M-83
U.S. Department of Agriculture, National Agricultural Statistics Service

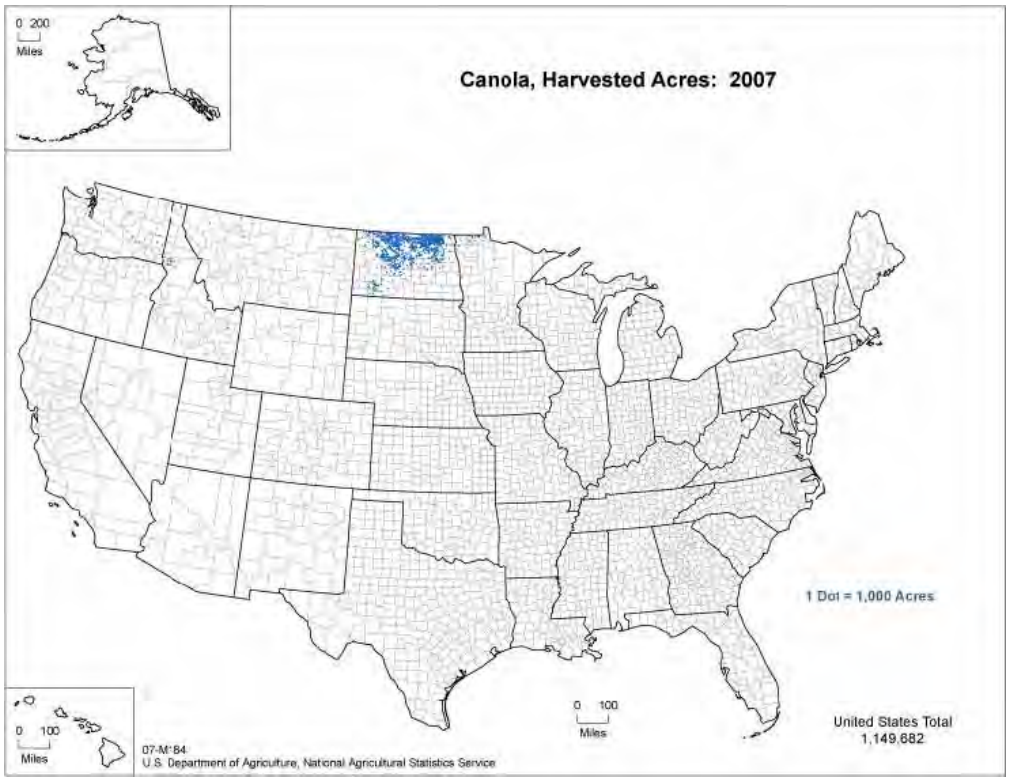
Canola, Harvested Acres: 2007
0 200
Miles
1 Dot = 1,000 Acres
0 100
Miles
0 100
Miles
United States Total
1,149,682
07-M-84
U.S. Department of Agriculture, National Agricultural Statistics Service

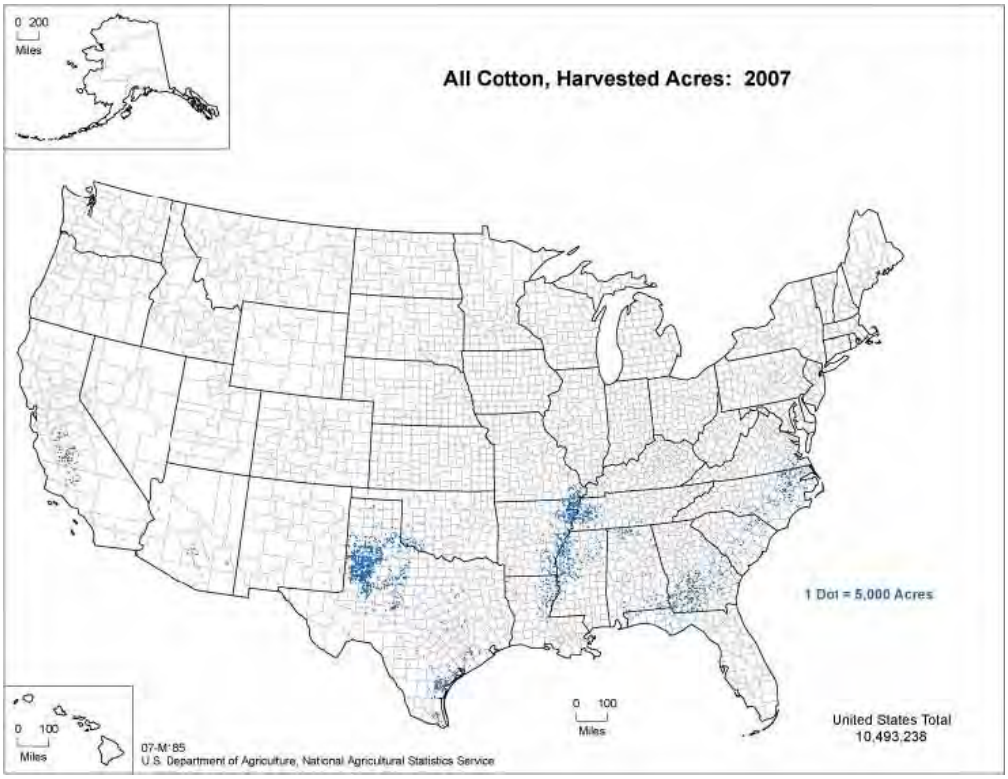
All Cotton, Harvested Acres: 2007
0 200
Miles
1 Dot = 5,000 Acres
0 100
Miles
United States Total
10,493,238
0 100
Miles
07-M-85
U.S. Department of Agriculture, National Agricultural Statistics Service

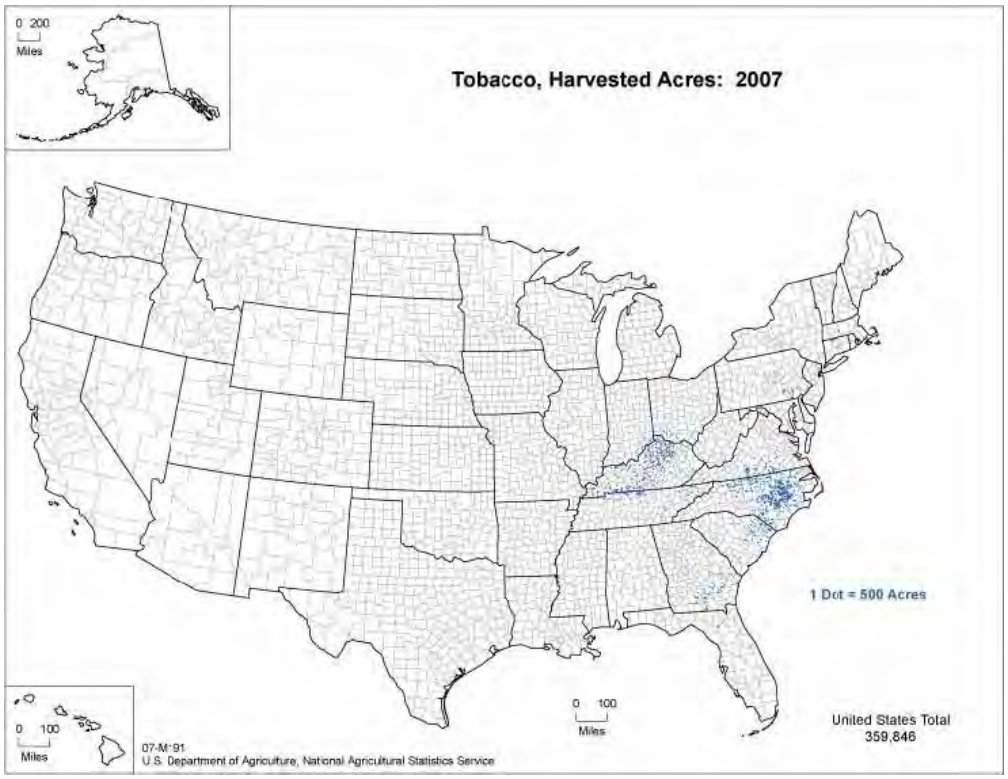
Tobacco, Harvested Acres: 2007
0 200
Miles
1 Dot = 500 Acres
0 100
Miles
United States Total
359,846
0 100
Miles
07-M-91
U.S. Department of Agriculture, National Agricultural Statistics Service

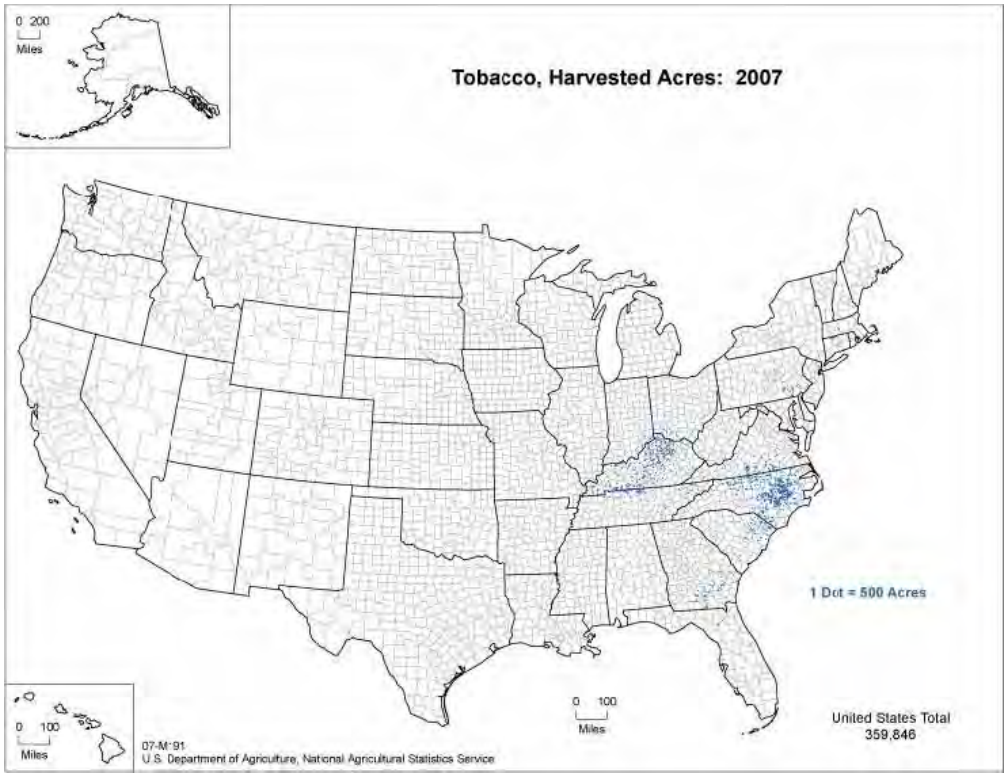
0 200
Miles
Tobacco, Harvested Acres: 2007
1 Dot = 500 Acres
0 100
Miles
0 100
Miles
United States Total
359,846
07-M-91
U.S. Department of Agriculture, National Agricultural Statistics Service


0 200
Miles
Soybeans for Beans, Harvested Acres: 2007
1 Dot = 10,000 Acres
0 100
Miles
0 100
Miles
United States Total
63,915,821
07-M-93
U.S. Department of Agriculture, National Agricultural Statistics Service

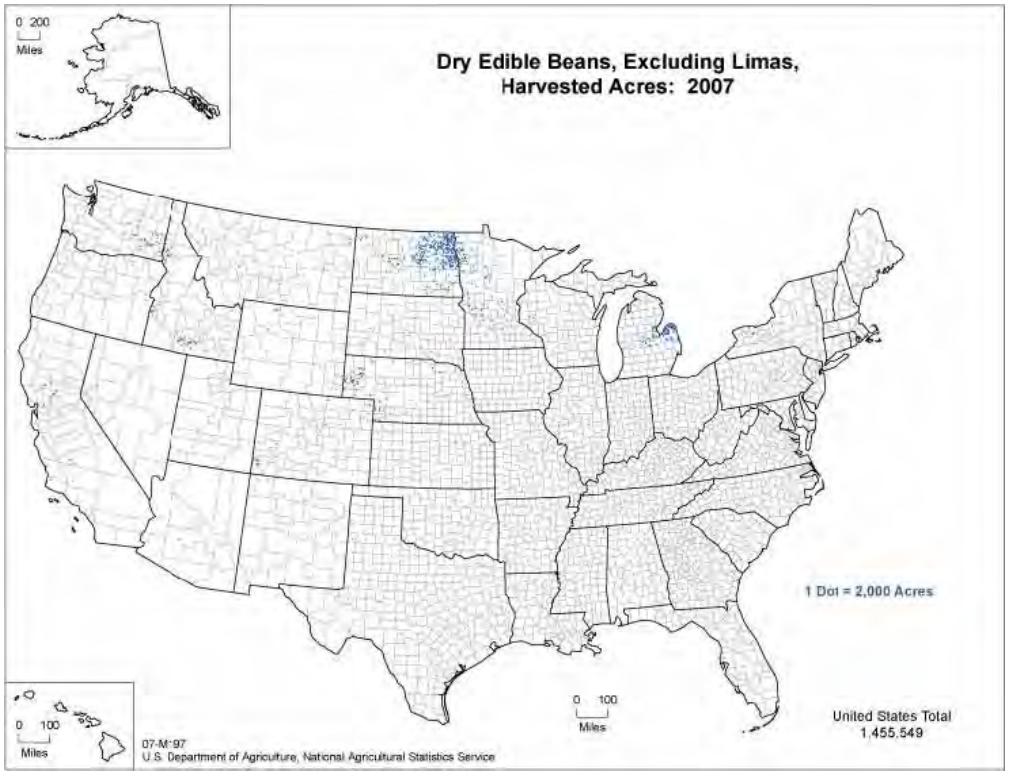
Dry Edible Beans, Excluding Limas,
Harvested Acres: 2007
0 200
Miles
1 Dot = 2,000 Acres
0 100
Miles
United States Total
1,455,549
0 100
Miles
07-M-97
U.S. Department of Agriculture, National Agricultural Statistics Service

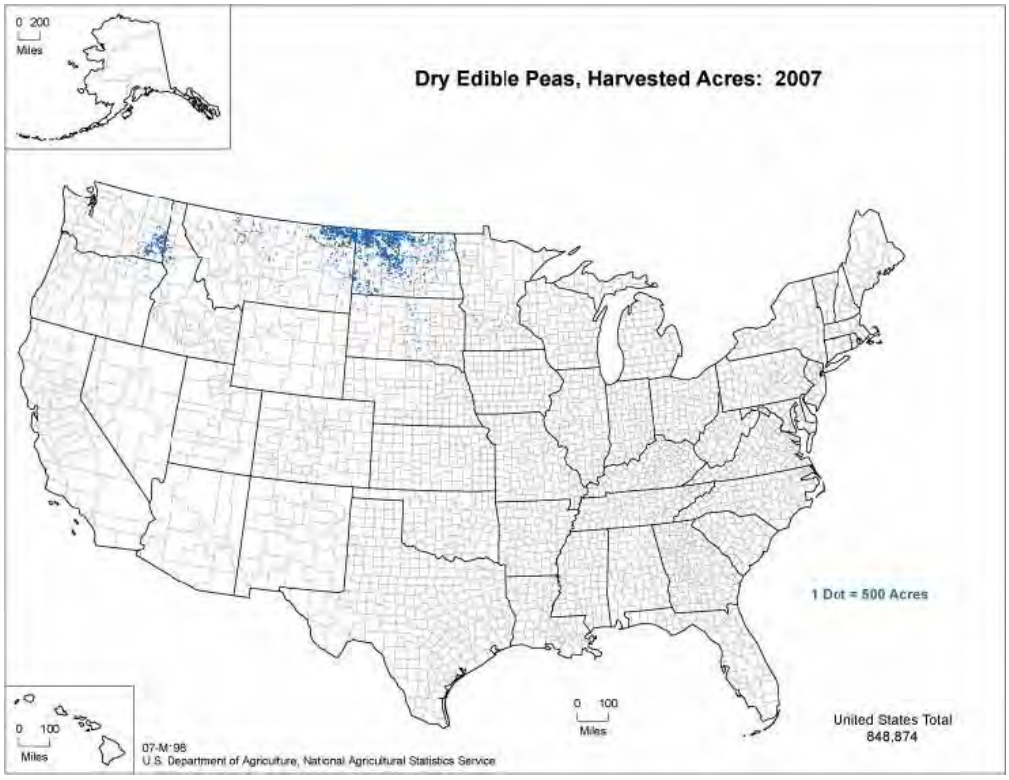
Dry Edible Peas, Harvested Acres: 2007
0 200
Miles
1 Dot = 500 Acres
0 100
Miles
United States Total
848,874
0 100
Miles
07-M-98
U.S. Department of Agriculture, National Agricultural Statistics Service

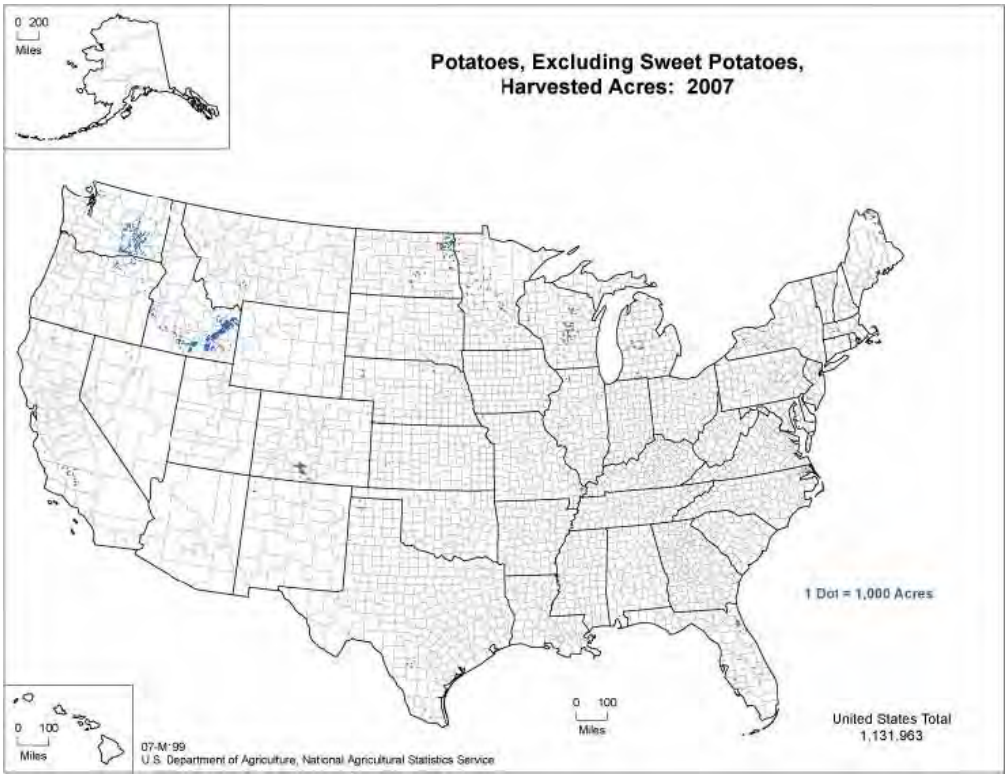
0 200
Miles
Potatoes, Excluding Sweet Potatoes,
Harvested Acres: 2007
1 Dot = 1,000 Acres
0 100
Miles
United States Total
1,131,963
0 100
Miles
07-M 99
U.S. Department of Agriculture, National Agricultural Statistics Service

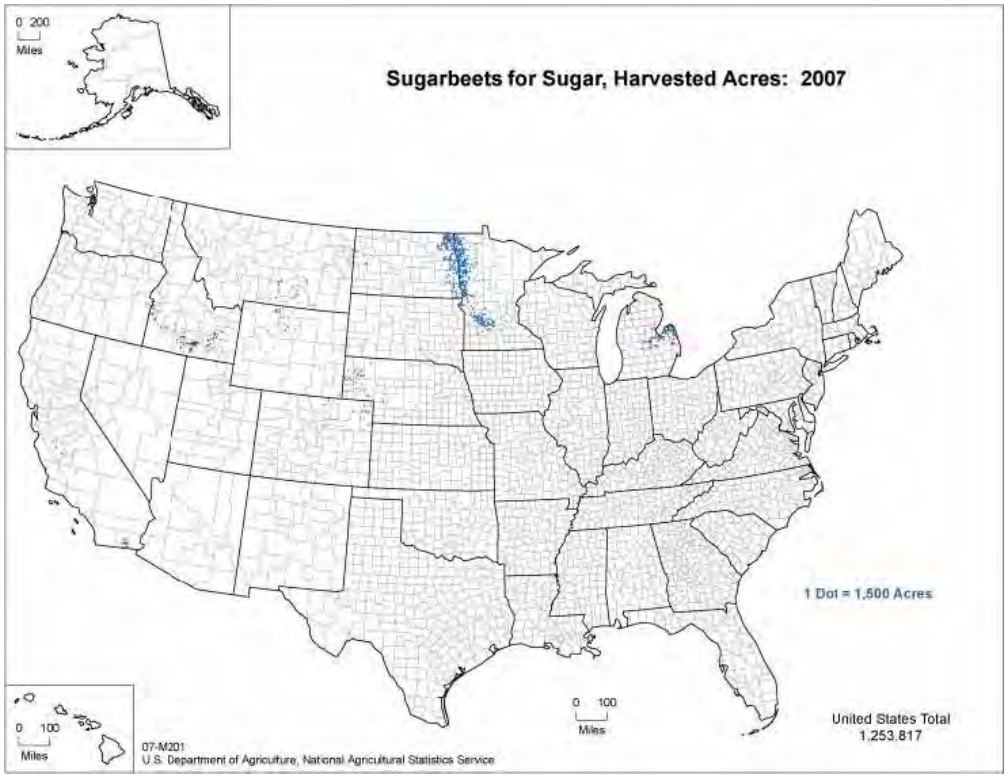
0 200
Miles
Sugarbeets for Sugar, Harvested Acres: 2007
1 Dot = 1,500 Acres
0 100
Miles
United States Total
1,253,817
0 100
Miles
07-M201
U.S. Department of Agriculture, National Agricultural Statistics Service

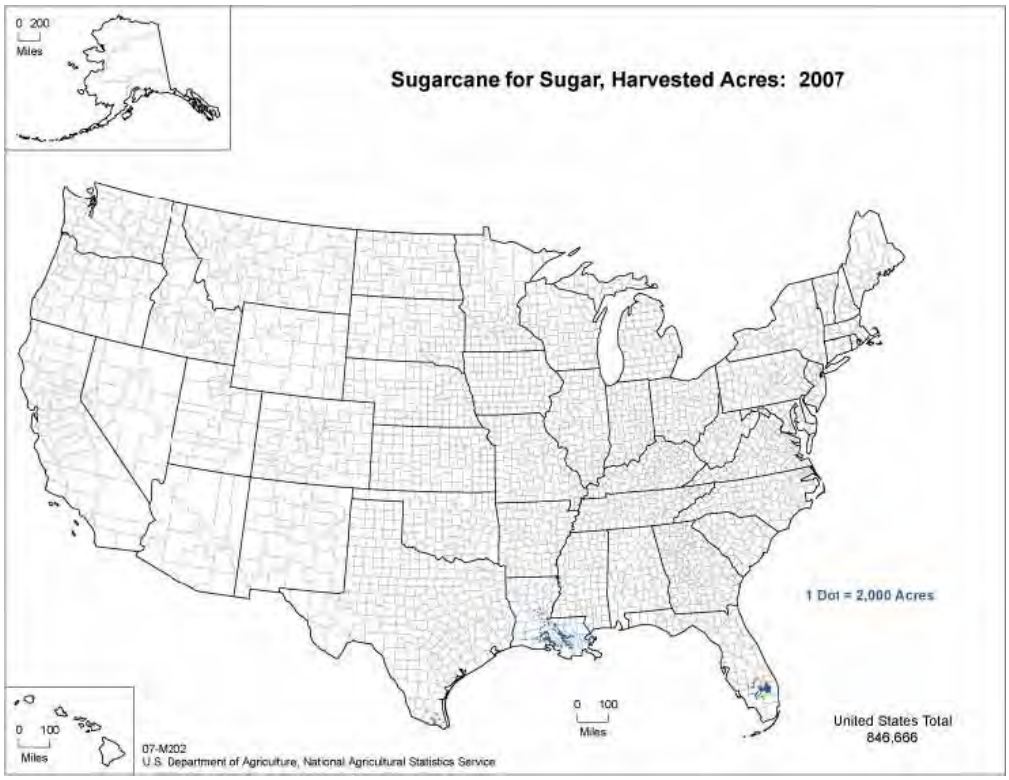
0 200
Miles
Sugarcane for Sugar, Harvested Acres: 2007
1 Dot = 2,000 Acres
0 100
Miles
0 100
Miles
United States Total
846,666
07-M202
U.S. Department of Agriculture, National Agricultural Statistics Service

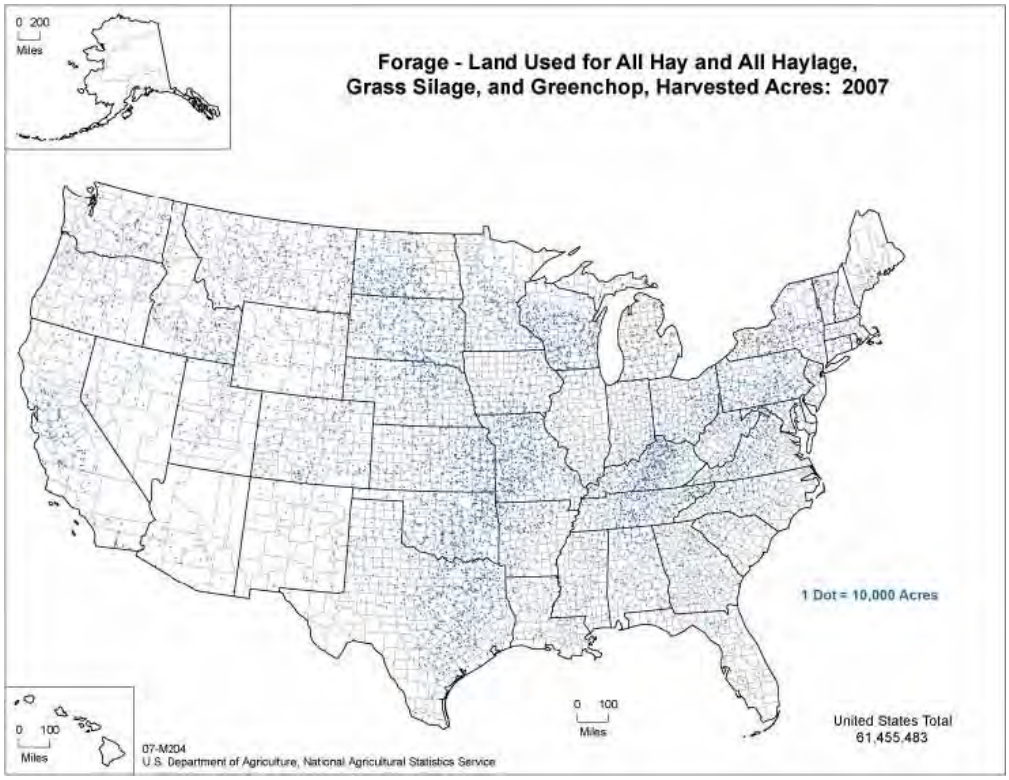
0 200
Miles
Forage - Land Used for All Hay and All Haylage,
Grass Silage, and Greenchop, Harvested Acres: 2007
1 Dot = 10,000 Acres
0 100
Miles
0 100
Miles
United States Total
61,455,483
07-M204
U.S. Department of Agriculture, National Agricultural Statistics Service

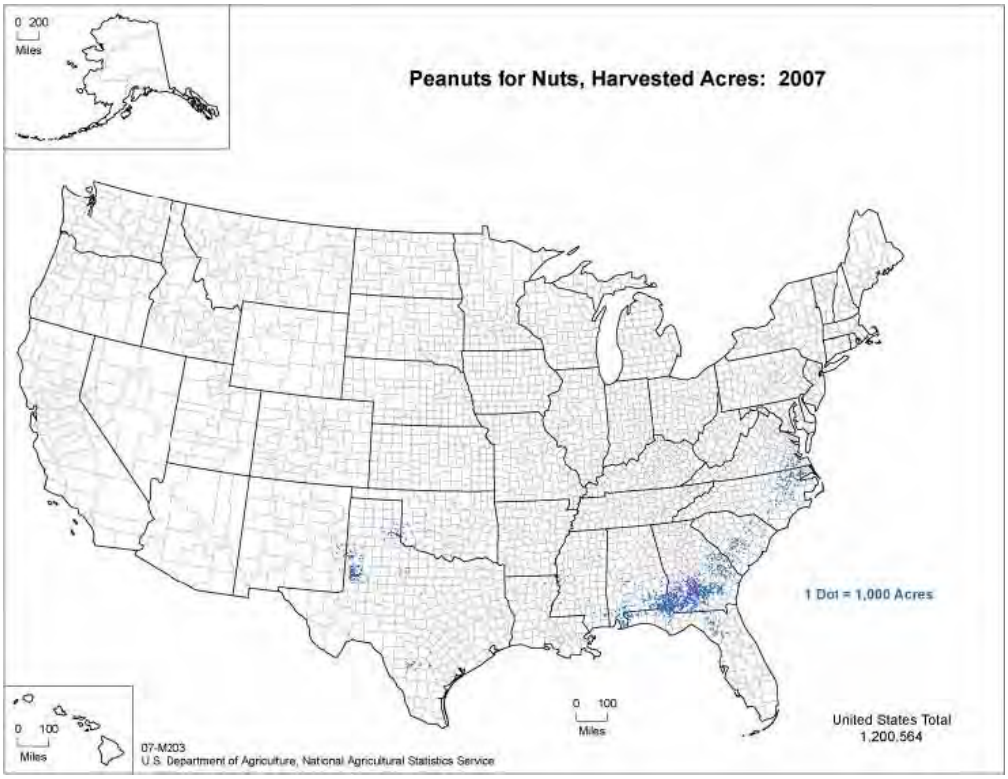
0 200
Miles
Peanuts for Nuts, Harvested Acres: 2007
1 Dot = 1,000 Acres
0 100
Miles
0 100
Miles
United States Total
1,200,564
07-M203
U.S. Department of Agriculture, National Agricultural Statistics Service

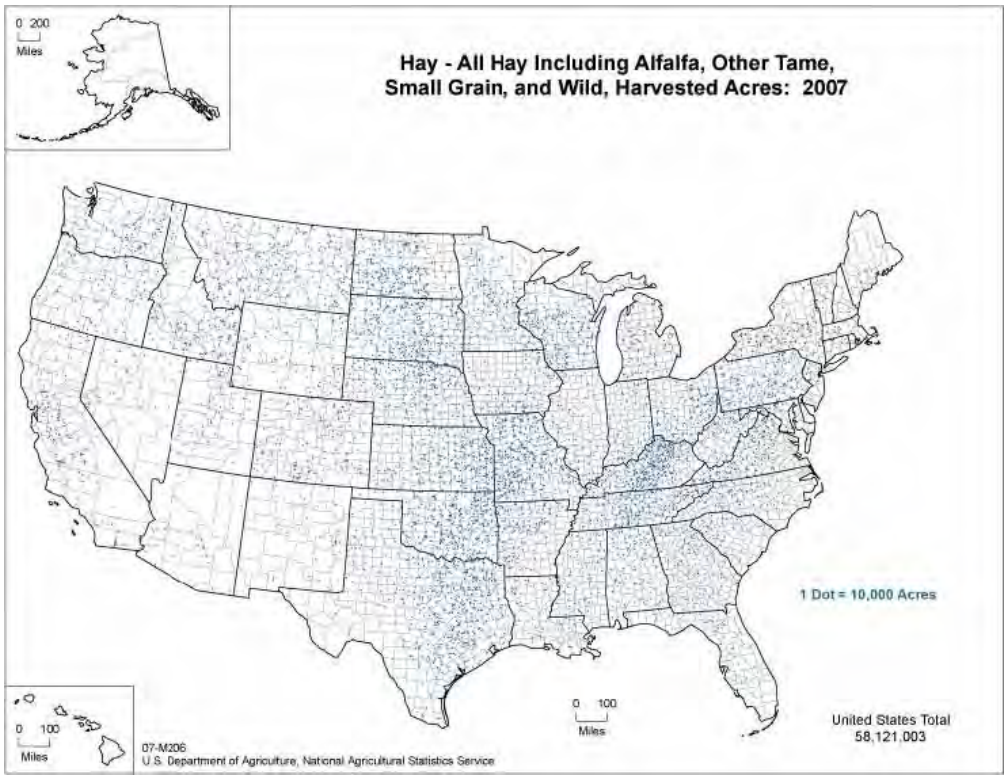
0 200
Miles
Hay - All Hay Including Alfalfa, Other Tame,
Small Grain, and Wild, Harvested Acres: 2007
1 Dot = 10,000 Acres
0 100
Miles
0 100
Miles
United States Total
58,121,003
07-M206
U.S. Department of Agriculture, National Agricultural Statistics Service

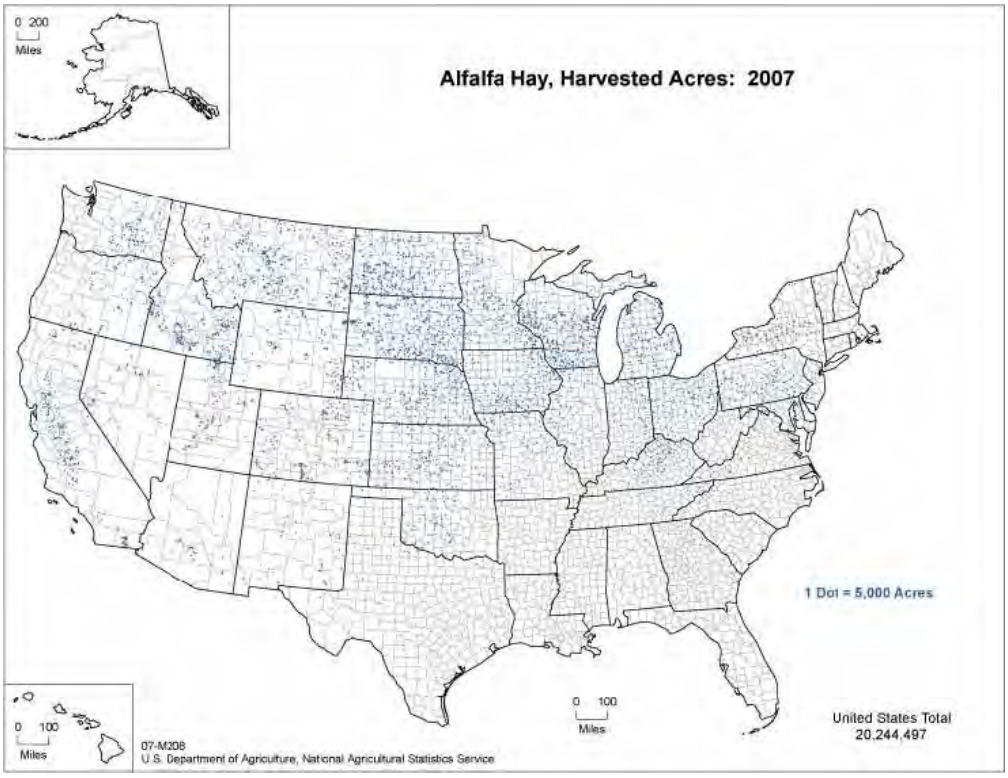
Alfalfa Hay, Harvested Acres: 2007
0 200
Miles
1 Dot = 5,000 Acres
0 100
Miles
0 100
Miles
United States Total
20,244,497
07-M208
U.S. Department of Agriculture, National Agricultural Statistics Service

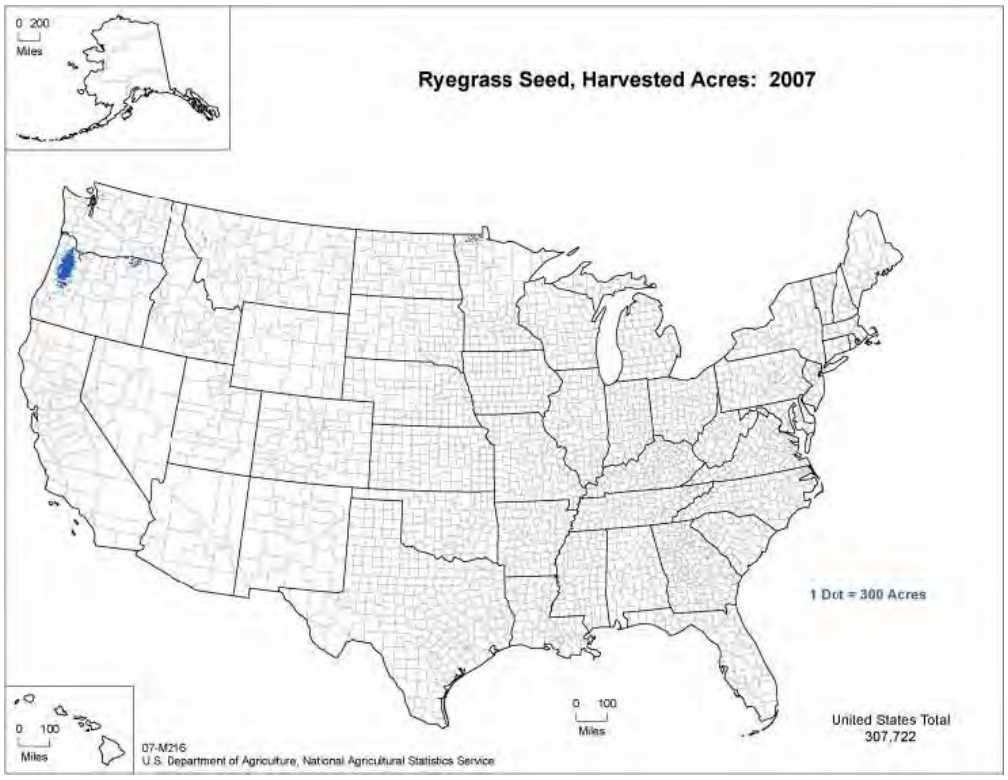
Ryegrass Seed, Harvested Acres: 2007
0 200
Miles
1 Dot = 300 Acres
0 100
Miles
0 100
Miles
United States Total
307,722
07-M216
U.S. Department of Agriculture, National Agricultural Statistics Service

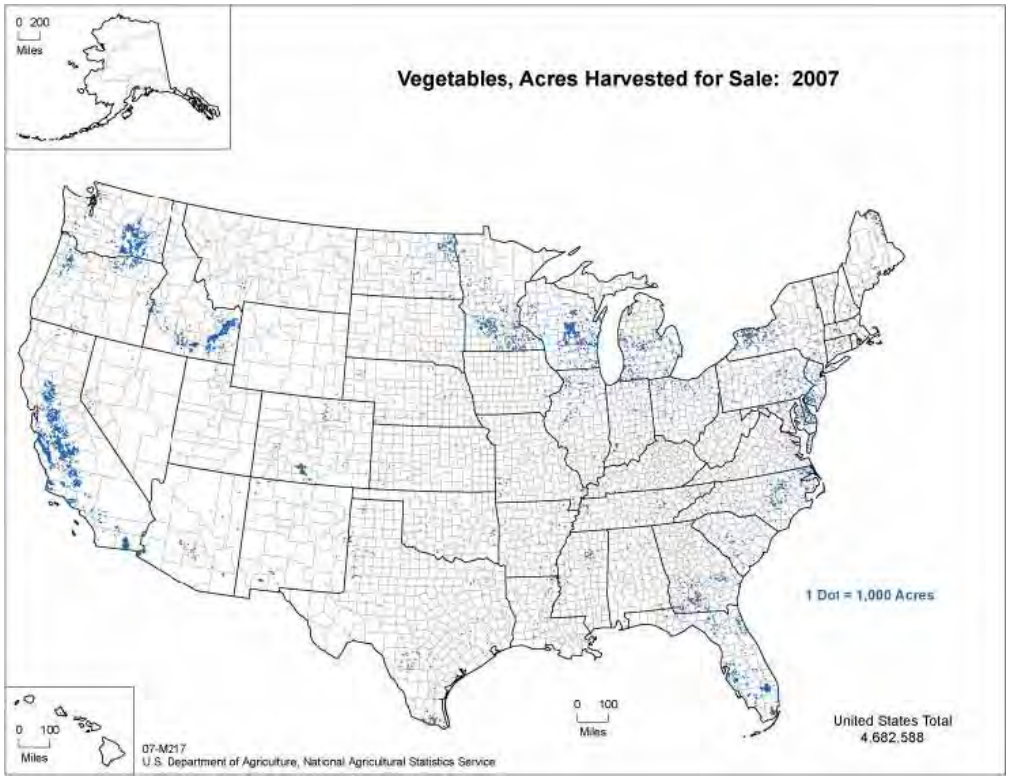
0 200
Miles
Vegetables, Acres Harvested for Sale: 2007
1 Dot = 1,000 Acres
0 100
Miles
0 100
Miles
United States Total
4,682,588
07-M217
U.S. Department of Agriculture, National Agricultural Statistics Service

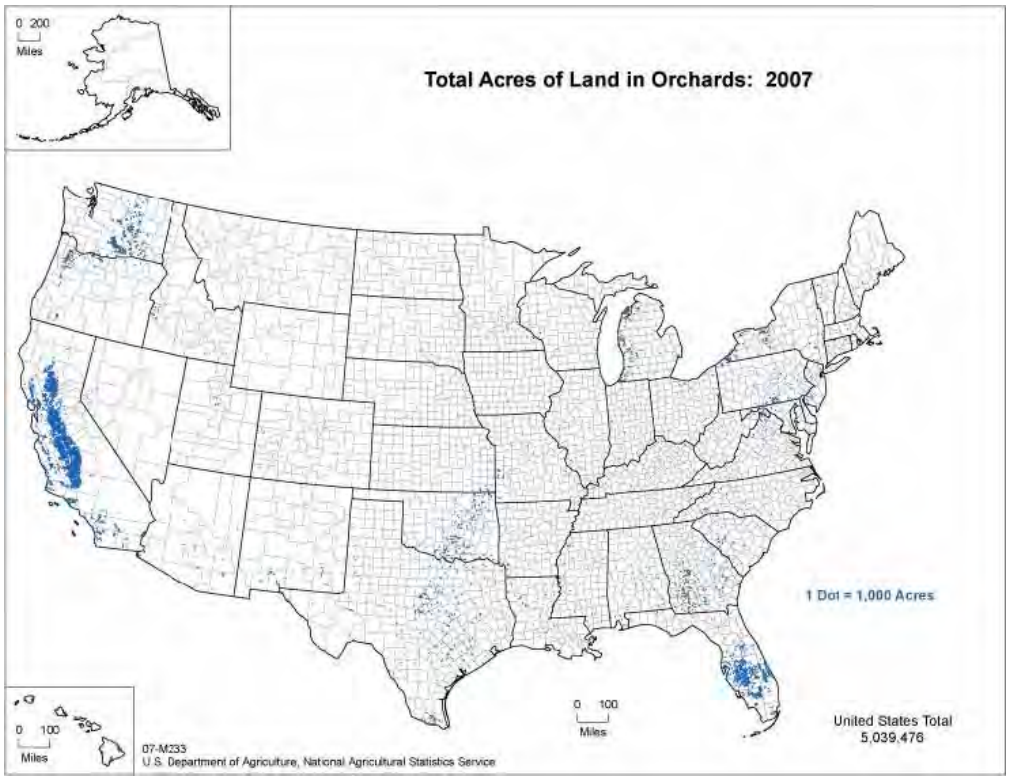
0 200
Miles
Total Acres of Land in Orchards: 2007
1 Dot = 1,000 Acres
0 100
Miles
0 100
Miles
United States Total
5,039,476
07-M233
U.S. Department of Agriculture, National Agricultural Statistics Service

Appendix C: Urban Residuals Generation and Use by State

State	Population (2006)	Estimated MSW Generation, tons/yr	MSW Recycled, tons/yr	MSW to WTE,[1] tons/yr	MSW Landfilled, tons/yr	Per Capita Estimated Generation, tons/person/yr	Number of MSW Landfills	Number of WTE Plants	Glass, tons/yr	Paper, tons/yr	C&D,[2] tons/yr	Steel, tons/yr	Plastic, tons/yr	Aluminum, tons/yr	Other Metals, tons/yr	Wood, tons/yr	Tires, tons/yr	Organics, tons/yr	Total Other, tons/yr
Alabama	4,590,240	6,996,343	591,608	194,039	6,210,696	1.52													
Alaska	677,450	765,354	28,646	3,000	733,708	1.13	300	1											
Arizona	6,165,689	8,197,591	1,025,591	0	7,172,000	1.33	40	0											
Arkansas	2,809,111	3,468,842	532,689	35,464	2,900,689	1.23	62	3	2,646	148,851		72,264	33,876	76,293		55,878	34,508	79,068	5,622
California	36,249,872	49,926,000	19,409,000	591,000	29,926,000	1.38													
Colorado	4,766,248	8,690,005	481,598	0	8,208,407	1.82			2,557	308,209	4,227		1,076		7,457	12	32,022		14,339
Connecticut	3,495,753	3,360,933	830,264	2,158,292	372,377	0.96	2	6	32,182	460,056		11,959	13,067	733	75,507			233,029	236,754
Delaware	852,747	988,433	103,150	0	885,283	1.16	3	0											
District of Columbia	585,459	1,031,083	21,142	12,791	997,150	1.76			5,538	14,066		404	876	258					
Florida	18,057,508	23,631,947	6,775,329	5,796,339	11,060,279	1.31	50	11	164,965	1,780,993	2,668,057	312,730	69,425	44,247	2,066,703	1,525,048	607,000	1,440,745	
Georgia	9,342,080	11,549,889	n/a	81,535	7,195,075	1.24	56	1											
Hawaii	1,278,635	1,649,000	410,000	756,000	483,000	1.29													
Idaho	1,463,878	1,238,394	99,590	0	1,138,804	0.85													
Illinois	12,777,042	26,420,364	9,773,194	0	16,647,170	2.07	49	0											
Indiana	6,302,646	13,570,231	4,531,056	569,263	8,469,912	2.15	35	1											
Iowa	2,972,566	4,341,454	1,464,395	54,496	2,822,563	1.46	59	1											
Kansas	2,755,817	4,089,591	817,818	0	3,271,773	1.48	52	0	27,854	267,852		39,435	5,633	5,194	118,749	62,343	12,787	76,592	20,712
Kentucky	4,204,444	7,887,748	2,996,565	63,700	4,827,483	1.88	34	2	4,688	231,326		1,437,226	4,617	12,295	102,751		942,361	258,752	2,546
Louisiana	4,243,288	6,051,158	500,000	0	5,551,158	1.43	27	0											
Maine	1,314,910	2,178,339	695,580	701,811	780,948	1.66	12	4	52,172	286,055	24,830	81,853	15,646	2,185	92,219	94,518	30,678	30,371	9,883
Maryland	5,602,017	7,009,905	2,536,633	1,371,970	3,101,302	1.25	22	9	58,992	938,992	155,967	532,583	34,815		619,247	209,140	29,925	898,777	42,549
Massachusetts	6,434,389	9,160,000	3,410,000	3,100,000	2,650,000	1.42	18	7	420,000	1,240,000	3,060,000		60,000		920,000	6,000		734,000	30,000
Michigan	10,102,322	12,768,089	2,594,940	1,039,389	9,133,760	1.26	50	3											
Minnesota	5,154,586	5,894,933	2,523,635	1,170,841	2,200,457	1.14	21	9	122,274	932,501		24,778	47,845	24,778	406,604	103,837	18,646	179,043	825,937
Mississippi	2,899,112	3,194,368	145,000	0	3,049,368	1.1	17	0											
Missouri	5,837,639	9,939,008	3,183,864	23,300	6,731,844	1.7	21	7											
Montana	946,795	1,430,049	240,510	0	1,189,539	1.51	79	0	1,024	56,698	28,971	135,172	260	1,733				31,135	4,963
Nebraska	1,763,765	2,360,861	260,514	0	2,100,347	1.34	23	0	8,457	231,058		1,935	6,895	8,549					3,620
Nevada	2,492,427	3,007,000	619,000	0	2,388,000	1.21													
New Hampshire	1,311,821	1,269,774	406,693	206,873	656,208	0.97	9	2	9,251	50,870	304,657	24,909	2,086	823	1,232			30,387	287,135
New Jersey	8,666,075	12,756,058	4,400,000	1,397,094	6,958,964	1.47	12	5	300,521	1,364,156		593,276	75,160	79,474		159,433	37,327	1,723,466	
New Mexico	1,942,302	2,125,052	191,601	0	1,933,451	1.09	33	0	541	88,162		21,528	1,760	3,672			866	65,137	3,935
New York	19,281,988	21,686,509	7,694,160	3,491,700	10,500,649	1.12	27	10	333,181	2,603,911	6,319,191	1,381,104	205,107	60,680		70,179	39,124	856,642	522,679
North Carolina	8,869,442	8,205,475	1,877,277	107,837	6,220,361	0.93	40	1	51,883	305,615	40,352	7,516	19,373	5,808	28,382	60,399	187,273	570,994	69,041
North Dakota	637,460	660,552	83,404	0	577,148	1.04	14	0											
Ohio	11,463,513	16,885,677	3,530,328	0	13,355,349	1.47	42	0	40,112	1,029,617		409,862	43,739	124,485	4,834	193,783	106,772	1,311,497	265,627
Oklahoma	3,577,536	4,394,393	170,000	0	4,224,393	1.23	38	0											
Oregon	3,691,084	4,426,431	1,820,063	203,103	2,403,265	1.2	33	1	96,619	790,363	14,332	339,360	42,412	21,521	8,398	87,645	16,557	391,213	52,959
Pennsylvania	12,402,817	16,486,254	4,868,115	1,951,447	9,666,692	1.33	48	6	57,447	557,578	404,745	19,074	56,625	47,603	1,062,090	191,032	49,730	557,691	2,269,246
Rhode Island	1,061,641	1,351,454	166,962	1,995	1,182,497	1.27	2	0	14,980	57,847		5,696	4,909	1,027				76,242	403
South Carolina	4,330,108	4,974,679	1,510,409	224,506	3,239,764	1.15	18	1	11,090	822,026	1,093,459	4,415	20,379	6,606	190,220	44,127	62,765	604,699	348,779
South Dakota	788,467	861,576	83,476	0	778,100	1.09	15	0											
Tennessee	6,074,913	12,211,686	4,798,402	0	7,413,284	2.01	34	0	5,196	85,387	65,020	10,643	4,274		25,727	369,962	72,902	148,330	5,113
Texas	23,407,629	31,212,927	5,900,000	0	25,312,927	1.33	215	1											
Utah	2,579,535	2,864,492	438,873	123,912	2,301,707	1.11	34	1											
Vermont	620,778	644,226	229,953	47,286	366,987	1.04	4	0											
Virginia	7,640,249	12,210,991	4,140,457	2,135,407	5,935,127	1.6	60	5	39,278	922,024	123,998		30,159		704,127	296,165	70,210	860,133	237,769
Washington	6,374,910	8,313,340	2,725,310	325,398	5,262,632	1.3	16	3	90,992	570,802	2,295,278	1,048,885	38,262	14,951	135,976	289,612	23,528	1,000,040	
West Virginia	1,808,699	2,110,381	337,661	0	1,772,720	1.17	19	0	777	22,165		3,217	688	623	105				
Wisconsin	5,617,744	5,881,023	1,886,545	454,321	3,540,157	1.05	35	2	103,527	921,125	46,000	25,973	29,424	7,959	17,231		31,500	537,600	212,206
Wyoming	512,757	684,690	73,200	0	611,490	1.34	51	0											

Appendix D: Agriculture Production Outlook

USDA Agricultural Projections to 2017 (USDA 2009).

Item	Unit	2006	2007	2008	2009	2010	2011	2012	2013	2014	2015	2016	2017
Corn Yield	bushels/acre	149.1	153	155.3	157.3	159.3	161.3	163.3	165.3	167.3	169.3	171.3	173.3
Corn Production	million bushels	10535	13168	12515	13150	13635	13645	13650	13820	14070	14240	14405	14660
Sorghum Yield	bushels/acre	56.2	76.8	66.1	66.5	67	67.4	67.9	68.3	68.8	69.2	69.7	70.1
Sorghum Production	million bushels	278	515	395	365	340	345	340	340	335	340	340	345
Barley Yield	bushels/acre	61.1	60.4	65	65.6	66.2	66.8	67.4	68	68.6	69.2	69.3	70.4
Barley Production	million bushels	180	212	255	230	200	200	200	205	205	210	210	210
Oats Yield	bushels/acre	59.8	60.9	63.1	63.5	63.9	64.3	64.7	65.1	65.5	65.9	44.9	66.7
Oats Production	million bushels	94	92	100	100	100	105	105	105	105	105	105	105
Wheat Yield	bushels/acre	38.7	40.5	42.5	42.8	43.1	43.4	43.7	44	44.3	44.6	44.9	45.2
Wheat Production	million bushels	1812	2067	2350	2185	2140	2120	2100	2110	2110	2125	2120	2135
Rice Yield	lb/acre	6868	7247	7222	7284	7351	7419	7481	7543	7608	7666	7725	7784
Rice Production	million hundredweight	193.7	197.9	201	210	215.5	221.2	226.8	232.4	236.3	240	243.8	247.6
Upland Cotton Yield	lb/acre	806	845	860	875	885	895	905	915	925	935	945	955
Upland Cotton Production	million bales	20.82	18.05	17.4	18.8	19.5	20.1	20.6	20.8	21.2	21.6	22.1	22.5
Soybean Yield	bushels/acre	42.7	41.3	42.1	42.6	43	43.5	43.9	44.4	44.8	45.3	45.7	46.2
Soybean Production	thousand tons	3188	2594	2950	2920	2930	2935	2970	3000	3005	3035	3065	3095
Sugarbeet Yield	tons/acre	26.1	25.4	26.3	26.6	26.8	27.1	27.3	27.5	27.7	27.9	28.1	28.3
Sugarbeet Production	million short tons	34.1	31.6	31.6	30.7	30.7	30.4	30.3	30.6	30.9	31.2	31.5	31.8
Sugarcane Yield	tons/acre	33	34.7	34.2	34.3	34.5	34.6	34.7	34.8	34.9	35	35.1	35.2
Sugarcane Production	million short tons	28	28.9	28.6	28.1	25.9	26	26.1	26.2	26.3	26.4	26.5	26.6
Citrus Fruit	million lb	23490	20528	24960	25334	25841	26358	27017	27692	28246	28811	29243	29682
Noncitrus Fruit	million lb	40378	40436	40746	41058	41372	41689	42008	42330	42654	42981	43310	43642
Tree Nuts	million lb	3186	3628	3664	3745	3827	3911	3997	4085	4175	4267	4361	4457
Fresh Market Vegetables	million lb	42738	43000	44052	44555	45063	45578	46098	46624	47157	47696	48241	48793
Processing Vegetables	million lb	38915	42800	40500	40865	41232	41603	41978	42356	42737	43121	43510	43901
Potatoes	million lb	44135	44797	45155	45517	45881	46248	46618	46991	47367	47746	48128	48513
Specialty and Minor Vegetables	million lb	8000	8120	8242	8365	8491	8618	8748	8879	9012	9147	9284	9424
Beef, Commercial Production	million lb	26153	26135	26000	25565	25515	26017	26273	26365	26373	26586	26893	27132
Beef, Farm Production	million lb	105	105	105	105	105	105	105	105	105	105	105	105
Pork, Commercial Production	million lb	21055	21754	22265	21884	21866	21737	21904	22230	22623	23004	23372	23756
Pork, Farm Production	million lb	20	20	20	20	20	20	20	20	20	20	20	20
Broiler Production	million lb	35369	35442	36456	36722	36906	37090	37350	37748	38312	38888	39484	40098
Turkey Production	million lb	5612	5815	5862	5863	5879	5896	5910	5946	5998	6076	6176	6306
Dairy Cows	number of cows, 1000 head	9112	9148	9215	9230	9195	9160	9130	9105	9075	9040	9015	8985

FAPRI Agricultural Projections to 2017 (FAPRI 2008).

Item	Unit	2007	2008	2009	2010	2011	2012	2013	2014	2015	2016	2017
Corn Yield	bushels/acre	151.1	153.5	155.5	157.8	159.9	162.1	164.3	166.4	168.6	170.8	173
Corn Production	million bushels	13074	12910	13214	13661	13541	13968	14298	14697	14862	15142	15212
Sorghum Yield	bushels/acre	74.2	64.6	64.6	64.9	65.2	65.4	65.6	65.8	66.1	66.3	66.6
Sorghum Production	million bushels	505	430	371	390	379	382	377	376	373	372	369
Barley Yield	bushels/acre	60.4	62.9	63.5	64.1	64.8	65.4	66	66.6	67.3	67.9	68.5
Barley Production	million bushels	212	227	241	239	232	233	232	232	230	229	226
Oats Yield	bushels/acre	60.9	61.9	62.2	62.6	62.9	63.3	63.6	63.9	64.2	64.6	64.9
Oats Production	million bushels	92	81	85	88	88	87	86	84	84	83	83
Wheat Yield	bushels/acre	40.5	42.7	42.9	43.2	43.5	43.9	44.2	44.5	44.9	45.2	45.5
Wheat Production	million bushels	2067	2244	2103	2111	2126	2136	2138	2146	2157	2163	2177
Rice Yield	lb/acre	7185	7074	7161	7216	7282	7332	7396	7451	7511	7571	7634
Rice Production	million hundredweight	197.5	204.3	188.7	204.5	203.9	215.9	215.4	227.2	228.8	230	237.1
Upland Cotton Yield	lb/acre	857	830	840	847	855	862	870	877	885	892	900
Upland Cotton Production	million bales	18.21	14.69	17.31	17.09	17.2	16.96	16.81	16.53	16.55	16.55	16.49
Soybean Yield	bushels/acre	41.2	42.5	42.9	43.4	43.8	44.3	44.7	45.1	45.6	46	46.5
Soybean Production	thousand tons	2585	2913	3082	3006	3118	3095	3130	3134	3183	3201	3262
Hay Yield	tons/acre	2.44	2.48	2.52	2.54	2.55	2.56	2.57	2.58	2.59	2.61	2.62
Hay Production	million tons	150.3	153.3	154.6	155.1	155.8	156.5	157.2	157.8	158.3	158.8	159.3
Sunflower Seed Yield	lb/acre	1437	1376	1389	1403	1418	1432	1446	1461	1475	1490	1505
Sunflower Seed Production	million **b**	2889	2785	2781	2878	2937	2922	2953	2974	3022	3069	3114
Canola Seed Yield	lb/acre	1250	1431	1449	1467	1485	1503	1521	1539	1557	1575	1593
Canola Seed Production	million **b**	1464	1933	1872	2125	2150	2110	2197	2252	2321	2388	2481
Peanut Yield	lb/acre	3130	3034	3062	3087	3114	3141	3169	3196	3223	3250	3276
Peanut Production	million **b**	3741	3783	3962	4027	3965	4003	4004	3998	4026	4027	4053
Sugarbeet Yield	tons/acre	25.59	23.93	24.14	24.3	24.45	24.61	24.78	24.93	25.1	25.26	25.41
Sugarbeet Production	1,000 tons	31912	26386	28323	28850	28723	28697	29081	28845	29302	29322	29258
Sugarcane Yield	tons/acre	34.99	34.72	34.89	35.2	35.3	35.45	35.8	36.04	36.29	36.51	36.63
Sugarcane Production	1,000 tons	29101	27977	28078	28933	28469	28262	28752	28793	28977	29088	28773
Beef Production	million **b**	26515	26465	26811	27388	27861	28336	28455	28485	28482	28440	28450
Pork Production	million **b**	21959	22692	22786	22751	22836	23174	23675	24167	24509	24699	24887
Broiler Production	million **b**	35492	36354	36812	37119	37583	38059	38531	38989	39525	40104	40741
Turkey Production	million **b**	5825	5841	5800	5785	5801	5838	5882	5927	5977	6032	6094
Dairy Cows	number of cows, 1000 thousand head	9153	9245	9186	9187	9195	9199	9196	9184	9171	9161	9156

Appendix E: Wood Production Outlook

Timber harvests from forest land in the contiguous states, by region 2002, with projections through 2005.

		Projections				
	2002	2010	2020	2030	2040	2050
			Billion cubic feet			
Softwoods:						
Northeast	0.58	0.58	0.53	0.51	0.50	0.51
North Central	0.26	0.28	0.30	0.30	0.30	0.30*
Southeast	2.92	2.67	3.17	3.41	3.70	4.06
South Central	3.69	3.21	3.64	4.00	4.39	4.79
North Rocky Mountains	0.50	0.44	0.43	0.44	0.46	0.46
South Rocky Mountains	0.10	0.25	0.28	0.32	0.35	0.36
Pacific Northwest West	1.55	1.65	1.58	1.57	1.65	1.78†
Pacific Northwest East	0.20	0.24	0.20	0.29	0.31	0.34‡
Pacific Southwest	0.72	0.46	0.47	0.47	0.49	0.49§
Softwoods Total Harvests	10.51	9.77	10.67	11.31	12.15	13.11
Hardwoods:						
Northeast	1.29	1.51	1.55	1.59	1.73	1.87
North Central	1.42	1.43	1.47	1.51	1.53	1.65
Southeast	1.19	1.55	1.63	1.70	1.66	1.64
South Central	1.84	2.28	2.44	2.58	2.70	2.86
West	0.25	0.63	0.62	0.62	0.62	0.62
Hardwoods Total Harvests	5.99	7.40	7.70	7.99	8.24	8.65

Source: The 2005 RPA Timber Assessment Update

* Includes the Great Plains States: Kansas, Nebraska, North Dakota, and eastern South Dakota.

† Excludes Alaska. Includes western Oregon and western Washington and is also called the Douglas fir subregion.

‡ Includes eastern Oregon and eastern Washington and is also called the ponderosa pine subregion.

§ Excludes Hawaii.

Appendix F: Urban Residues Outlook

State	Census April 1, 2000	Per Capita Estimated Generation (tons/ person/yr)*	Projections July 1, 2010	Estimated MSW Generation (tons/yr), 2010	Projections July 1, 2015	Estimated MSW Generation (tons/yr), 2015	Projections July 1, 2020	Estimated MSW Generation (tons/yr), 2020	Projections July 1, 2025	Estimated MSW Generation (tons/yr), 2025	Projections July 1, 2030	Estimated MSW Generation (tons/yr), 2030
Alabama	4,447,100	1.52	4,596,330	6,986,422	4,663,111	7,087,929	4,728,915	7,187,951	4,800,092	7,296,140	4,874,243	7,408,849
Alaska	626,932	1.13	694,109	784,343	732,544	827,775	774,421	875,096	820,881	927,596	867,674	980,472
Arizona	5,130,632	1.33	6,637,381	8,827,717	7,495,238	9,968,667	8,456,448	11,247,076	9,531,537	12,676,944	10,712,397	14,247,488
Arkansas	2,673,400	1.23	2,875,039	3,536,298	2,968,913	3,651,763	3,060,219	3,764,069	3,151,005	3,875,736	3,240,208	3,985,456
California	33,871,648	1.38	38,067,134	52,532,645	40,123,232	55,370,060	42,206,743	58,245,305	44,305,177	61,141,144	46,444,861	64,093,908
Colorado	4,301,261	1.82	4,831,554	8,793,428	5,049,493	9,190,077	5,278,867	9,607,538	5,522,803	10,051,501	5,792,357	10,542,090
Connecticut	3,405,565	0.96	3,577,490	3,434,390	3,635,414	3,489,997	3,675,650	3,528,624	3,691,016	3,543,375	3,688,630	3,541,085
Delaware	783,600	1.16	884,342	1,025,837	927,400	1,075,784	963,209	1,117,322	990,694	1,149,205	1,012,658	1,174,683
District of Columbia	572,059	1.76	529,785	932,422	506,323	891,128	480,540	845,750	455,108	800,990	433,414	762,809
Florida	15,982,378	1.31	19,251,691	25,219,715	21,204,132	27,777,413	23,406,525	30,662,548	25,912,458	33,945,320	28,685,769	37,578,357
Georgia	8,186,453	1.24	9,589,080	11,890,459	10,230,578	12,685,917	10,843,753	13,446,254	11,438,622	14,183,891	12,017,838	14,902,119
Hawaii	1,211,537	1.29	1,340,674	1,729,469	1,385,952	1,787,878	1,412,373	1,821,961	1,438,720	1,855,949	1,466,046	1,891,199
Idaho	1,293,953	0.85	1,517,291	1,289,697	1,630,045	1,385,538	1,741,333	1,480,133	1,852,627	1,574,733	1,969,624	1,674,180
Illinois	12,419,293	2.07	12,916,894	26,737,971	13,097,218	27,111,241	13,236,720	27,400,010	13,340,507	27,614,849	13,432,892	27,806,086
Indiana	6,080,485	2.15	6,392,139	13,743,099	6,517,631	14,012,907	6,627,008	14,248,067	6,721,322	14,450,842	6,810,108	14,641,732
Iowa	2,926,324	1.46	3,009,907	4,394,464	3,026,380	4,418,515	3,020,496	4,409,924	2,993,222	4,370,104	2,955,172	4,314,551
Kansas	2,688,418	1.48	2,805,470	4,152,096	2,852,690	4,221,981	2,890,566	4,278,038	2,919,002	4,320,123	2,940,084	4,351,324
Kentucky	4,041,769	1.88	4,265,117	8,018,420	4,351,188	8,180,233	4,424,431	8,317,930	4,489,662	8,440,565	4,554,998	8,563,396
Louisiana	4,468,976	1.43	4,612,679	6,596,131	4,673,721	6,683,421	4,719,160	6,748,399	4,762,398	6,810,229	4,802,633	6,867,765
Maine	1,274,923	1.66	1,357,134	2,252,842	1,388,878	2,305,537	1,408,665	2,338,384	1,414,402	2,347,907	1,411,097	2,342,421
Maryland	5,296,486	1.25	5,904,970	7,381,213	6,208,392	7,760,490	6,497,626	8,122,033	6,762,732	8,453,415	7,022,251	8,777,814
Massachusetts	6,349,097	1.42	6,649,441	9,442,206	6,758,580	9,597,184	6,855,546	9,734,875	6,938,636	9,852,863	7,012,009	9,957,053
Michigan	9,938,444	1.26	10,428,683	13,140,141	10,599,122	13,354,894	10,695,993	13,476,951	10,713,730	13,499,300	10,694,172	13,474,657
Minnesota	4,919,479	1.14	5,420,636	6,179,525	5,668,211	6,461,761	5,900,769	6,726,877	6,108,787	6,964,017	6,306,130	7,188,988
Mississippi	2,844,658	1.1	2,971,412	3,268,553	3,014,409	3,315,850	3,044,812	3,349,293	3,069,420	3,376,362	3,092,410	3,401,651
Missouri	5,595,211	1.7	5,922,078	10,067,533	6,069,556	10,318,245	6,199,882	10,539,799	6,315,366	10,736,122	6,430,173	10,931,294
Montana	902,195	1.51	968,598	1,462,583	999,489	1,509,228	1,022,735	1,544,330	1,037,387	1,566,454	1,044,898	1,577,796
Nebraska	1,711,263	1.34	1,768,997	2,370,456	1,788,508	2,396,601	1,802,678	2,415,589	1,812,787	2,429,135	1,820,247	2,439,131
Nevada	1,998,257	1.21	2,690,531	3,255,543	3,058,190	3,700,410	3,452,283	4,177,262	3,863,298	4,674,591	4,282,102	5,181,343
New Hampshire	1,235,786	0.97	1,385,560	1,343,993	1,456,679	1,412,979	1,524,751	1,479,008	1,586,348	1,538,758	1,646,471	1,597,077
New Jersey	8,414,350	1.47	9,018,231	13,256,800	9,255,769	13,605,980	9,461,635	13,908,603	9,636,644	14,165,867	9,802,440	14,409,587
New Mexico	1,819,046	1.09	1,980,225	2,158,445	2,041,539	2,225,278	2,084,341	2,271,932	2,106,584	2,296,177	2,099,708	2,288,682

State	Census April 1, 2000	Per Capita Estimated Generation (tons/person/yr)*	Projections July 1, 2010	Estimated MSW Generation (tons/yr), 2010	Projections July 1, 2015	Estimated MSW Generation (tons/yr), 2015	Projections July 1, 2020	Estimated MSW Generation (tons/yr), 2020	Projections July 1, 2025	Estimated MSW Generation (tons/yr), 2025	Projections July 1, 2030	Estimated MSW Generation (tons/yr), 2030
New York	18,976,457	1.12	19,443,672	21,776,913	19,546,699	21,892,303	19,576,920	21,926,150	19,540,179	21,885,000	19,477,429	21,814,720
North Carolina	8,049,313	0.93	9,345,823	8,691,615	10,010,770	9,310,016	10,709,289	9,959,639	11,449,153	10,647,712	12,227,739	11,371,797
North Dakota	642,200	1.04	636,623	662,088	635,133	660,538	630,112	655,316	620,777	645,608	606,566	630,829
Ohio	11,353,140	1.47	11,576,181	17,016,986	11,635,446	17,104,106	11,644,058	17,116,765	11,605,738	17,060,435	11,550,528	16,979,276
Oklahoma	3,450,654	1.23	3,591,516	4,417,565	3,661,694	4,503,884	3,735,690	4,594,899	3,820,994	4,699,823	3,913,251	4,813,299
Oregon	3,421,399	1.2	3,790,996	4,549,195	4,012,924	4,815,509	4,260,393	5,112,472	4,536,418	5,443,702	4,833,918	5,800,702
Pennsylvania	12,281,054	1.33	12,584,487	16,737,368	12,710,938	16,905,548	12,787,354	17,007,181	12,801,945	17,026,587	12,768,184	16,981,685
Rhode Island	1,048,319	1.27	1,116,652	1,418,148	1,139,543	1,447,220	1,154,230	1,465,872	1,157,855	1,470,476	1,152,941	1,464,235
South Carolina	4,012,012	1.15	4,446,704	5,113,710	4,642,137	5,338,458	4,822,577	5,545,964	4,989,550	5,737,983	5,148,569	5,920,854
South Dakota	754,844	1.09	786,399	857,175	796,954	868,680	801,939	874,114	801,845	874,011	800,462	872,504
Tennessee	5,689,283	2.01	6,230,852	12,524,013	6,502,017	13,069,054	6,780,670	13,629,147	7,073,125	14,216,981	7,380,634	14,835,074
Texas	20,851,820	1.33	24,648,888	32,783,021	26,585,801	35,359,115	28,634,896	38,084,412	30,865,134	41,050,628	33,317,744	44,312,600
Utah	2,233,169	1.11	2,595,013	2,880,464	2,783,040	3,089,174	2,990,094	3,319,004	3,225,680	3,580,505	3,485,367	3,868,757
Vermont	608,827	1.04	652,512	678,612	673,169	700,096	690,686	718,313	703,288	731,420	711,867	740,342
Virginia	7,078,515	1.6	8,010,245	12,816,392	8,466,864	13,546,982	8,917,395	14,267,832	9,364,304	14,982,886	9,825,019	15,720,030
Washington	5,894,121	1.3	6,541,963	8,504,552	6,950,610	9,035,793	7,432,136	9,661,777	7,996,400	10,395,320	8,624,801	11,212,241
West Virginia	1,808,344	1.17	1,829,141	2,140,095	1,822,758	2,132,627	1,801,112	2,107,301	1,766,435	2,066,729	1,719,959	2,012,352
Wisconsin	5,363,675	1.05	5,727,426	6,013,797	5,882,760	6,176,898	6,004,954	6,305,202	6,088,374	6,392,793	6,150,764	6,458,302
Wyoming	493,782	1.34	519,886	696,647	528,005	707,527	530,948	711,470	529,031	708,902	522,979	700,792
United States	281,421,906	1.38	308,935,581	426,331,102	322,365,787	444,864,786	335,804,546	463,410,273	349,439,199	482,226,095	363,584,435	501,746,520

Appendix G: External Chemical Analysis and Physical Characterization Data References

Alter, H. 1983. Municipal solid waste. New York, NY: Marcel Dekker.

Arola, R. A., R. C.Radcliffe, and J. B. Sturos. 1981. Characterizing chunkwood. In Chunkwood: production, characterization, and utilization. General Technical Report NC-145, St. Paul, MN: U.S. Department of Agriculture, Forest Service, North Central Forest Experiment Station.

Arola, R. A., and E. S. Miyata. 1981. Harvesting wood for energy. St. Paul, MN: U.S. Department of Agriculture Forest Service, Research Paper NC-200, North Central Forest Experiment Station.

Bridgeman, T. G., J. M. Jones, I. Shield, and P. T. Williams. 2008. Torrefaction of reed canary grass, wheat straw and willow to enhance solid fuel qualities and combustion properties. Fuel. 87:844–856.

California Energy Commission. March 2008. An assessment of biomass resources in California, 2007. Draft Report. Contract No. 500-01-016.

Chang, N. B., and E. Davila. 2008. Municipal solid waste characterizations and management strategies for the lower Rio Grande Valley, Texas. Waste Management. 28:776–794.

Clarke, M., and P. Guidotti. 1995. Waste incineration in the pulp and paper industry. Paper Technology. 36:26–30.

Dierenfeld, E. S., S. Atkinson, A. M. Craig, K. C. Walker, W. J. Streich, and M. Clauss, 2005. Mineral concentrations in serum/plasma and liver tissues of captive and free-ranging rhinoceros species. Zoo Biology. 24.

European Bioenergy Networks. March 2003. Biomass co-firing – An efficient way to reduce greenhouse gas emission. VTT Processes, Finland.

Evans, R. J., R. A. Knight, M. Onischak, and S. P. Babu. 1988. Development of biomass gasification to produce substitute fuels. Report PNL-6518. Richland, WA: Pacific Northwest Laboratory (PNL), p 14.

Fasina, O., T. Ranatunga, and B. Vaughan. 2007. Physical and chemical characteristics of biofuel feedstocks indigenous to southeastern United States. Paper No. 076247. Presented at the 2007 ASABE Annual International Meeting. Minneapolis, MN, June 17–20, 2007.

Garcia, R. A., and K. A. Rosentrater. 2008. Concentration of key elements in North American meat and bone meal. Biomass and Bioenergy 2008. 32:887–891.

Guar, S., and T. B. Reed. 1998.Thermal data for natural and synthetic fuels. New York, NY: Marcel Dekker, Inc.

Hanley, T. A., and J. D. McKendrick. November 1983. Seasonal changes in chemical composition and nutritive value of native forages in a spruce-hemlock forest, southeastern Alaska. Research Paper PNW-312. Portland, OR: U.S. Department of Agriculture, Forest Service, Pacific Northwest Forest and Range Experiment Station.

Khan, A. A., W. de Jong, P. J. Jansens, and H. Spliethoff. 2009. Biomass combustion in fluidized-bed boilers: Potential problems and remedies. Fuel Processing Technology. 90:21–50.

Kitani, O., and C. W. Hall. 1989. Biomass handbook. New York, NY: Grodon and Breach Science Publishers Ltd.

Krotscheck, A. W., and H. Sixta. February 2006. "Characterization of black liquor." in Recovery, Ch 9, Handbook of pulp. Hoboken, NJ: Wiley – VCH.

Kyari, M., A. Cunliffe, and P. T. Williams. 2005. Characterization of oils, gases, and char in relation to the pyroloysis of different brands of scrap automotive tires. Energy & Fuels, 19(3):1165–1173.

Lynd, L. R., C. E. Wyman, and T. U. Gerngross. 1999. Biocommodity engineering. Biotechnology Progress. 15:777–793.

McDaniel, J. May 2002. Biomass cogasification at Polk Power Station. Final Technical Report for Tampa Electric Company.

McNeil Technologies, Inc. 31 December 2003. Biomass resource assessment and utilization options for three counties in eastern Oregon. Report for Oregon Department of Energy.

Miles, T. R., T. R. Miles, Jr., L. L. Baxter, R. W. Byers, B. W. Jenkins, and L. L. Oden. 1996. Biomass bioenergy. 10:125–138.

Miller, B. G., S. V. Pisupati, D. Johnson, D. J. Clifford, M. W. Badger, R. W. Wasco, S. Falcone Miller, G. D. Mitchell, and D. Tillman. Enhanced biomass characterization: A foster wheeler energy corporation/ Penn State Initiative (accessed Dec 2008). http://www.brdisolutions.com/pdfs/bcota/abstracts/18/z177.pdf

Richard, T., N. Trautmann, M. Krasny, S. Frendeburg, and C. Stuart. January 2009. Substrate composition table. Ithaca, NY: Cornell University (accessed Jan 2009) http://compost.css.cornell.edu/calc/lignin.noframes.html

Thipse, S. S., C. Sheng, M. R. Booty, R. S. Magee, and J. W. Bozzelli. 2002. Chemical makeup and physical characterization of synthetic fuel and methods of heat content evaluation for studies on MWS incineration. Fuel. 81:211–217.

Thy, P., S. Grundvig, B. M. Jenkins, R. Shiraki, and C. E. Lesher. 2005. Analytical controlled losses of potassium from straw ashes. Energy fuels. 19 (6):2571–2574.

Tillman, D. A., and N. S. Harding. 2004. Fuels of opportunity: Characteristics and uses in combustion systems. Bridgewater, MA: Elsevier.

Tillman, D. A. 1991. The combustion of solid fuels and wastes. San Diego, CA: Academic Press, Inc.

Tsamba, A. J., W. Yang, W. Blasiak, and M. A. Wojtowicz. 2007. Cashew nut shells pyroloysis: individual gas evolution rates and yields. Energy Fuels. 21:2357–2362.

U.S. Department of Agriculture Soil Conservation Service. April 1992. Agricultural waste characteristics. Agriculture waste management field handbook. Ch 4, No. 210-AWMFH.

Valenzuela, M. B., C. W. Jones, and P. K. Agrawal. 2006. Batch aqueous-phase reforming of woody biomass. Energy & Fuels. 20(4):1744–1752.

Whitely, N., R. Ozao, R. Artiaga, Y. Cao, and W.-P. Pan. 2006. "Combustion." Pt I of Multi–utilization of chicken litter as biomass source. Energy Fuels. 20(6):2660–2665.

Appendix H: Definitions and Methods of Characterization Analysis

Various methods are used to determine biomass properties. The following list describes typical methods used for analyzing combustion feedstocks. Analyses may be conducted on an as-determined basis; i.e., samples were air-dried before analysis and the moisture losses were recorded, or reported on an as-received basis, meaning the samples are analyzed without prior drying.

Ash Content

The solid residue that remains after the biomass is utilized for energy production is measured by combusting the biomass in a weighed crucible inside of a laboratory furnace. When performed together with moisture, volatiles, and fixed carbon analyses, the total analysis is called "proximate" analysis.

Ash Melting Behavior

Ash melting behavior was not determined in the sources reviewed.

Bulk Density

Bulk density is the density of the loose fuel or ash. Here, "loose" means that the material has not been packed down, so the density measurement includes any air pockets that may form.

Chlorine Content

The chlorine content of biomass is often measured as part of the CHN analysis by including a chlorine analyzer for the product gas.

C, H, N Content

The carbon (C), hydrogen (H), and nitrogen (N) content of a biomass sample is typically measured by combusting the biomass in a test furnace and analyzing the product gas.

Energy Content/Calorific Value

Energy content is represented on as Btu/lb on a dry weight basis. This may be reported as a higher heating value (HHV) or a lower heating value (LHV), because not all laboratories specify which method is used. HHV measures the amount of energy liberated when fuel at 25 °C is combusted, cooled back to 25 °C, and all product water is condensed. LHV measures the amount of energy recovered when the combustion gas is only cooled to 150 °C, meaning the latent heat of water is not recovered. Energy content is generally reported with the proximate and/or ultimate analysis. In some cases, energy content may not be actually measured, but the calculated calorific value based on proximate and ultimate analysis may be reported.

Fixed Carbon

The combustible portion of the biomass that is not driven off as volatiles is measured by first driving off volatiles, then measuring ash content to determine the amount of fixed carbon remaining in the biomass.

Fluorine Content

Fluorine content was typically not determined in the sources reviewed.

Major Elements (Na, K, Ca, Mg, Si, P, Fe, Al, Ti)

The major elements present in biomass ash are generally determined by x-ray fluorescence (XRF). This technique can be performed using an electron-dispersive spectrometer (EDS) or a wavelength-dispersive spectrometer (WDS). The EERC's XRF analyzer uses WDS equipped with a rhodium x-ray tube and six analyzing crystals to determine the bulk chemistry of a sample. The sample is usually ground to a powder and pressed into a pellet or fused with a fluxing agent to produce a glass disc. Typically, it is assumed that all major elements are present as oxides in the ash when calculating ash composition. This may not be true if the ash contains significant carbonate, sulfate, or unoxidized material.

Minor Elements (Cd, Ti, Hg, Sb, As, Cr, Co, Cu, Mn, Ni, V, Pb, Sn, Zn)

These and other trace metals can be determined as part of an XRF analysis along with the major elements. However, most laboratories that use XRF for ash analysis (including the EERC) do not report the minor elements by default. As such, they are usually only reported when requested.

Moisture Content

The amount of water remaining in biomass is measured, typically by drying the biomass sample at around 100 °C for 2 hours, although exact methods may vary by fuel sample and laboratory.

Oxygen Content

The oxygen content of a biomass sample is typically determined by measuring the weight loss during CHN analysis. It is not actually possible to measure a combustion product for oxygen, but if the CHN content is known and the weight loss is known, then the weight of CHN can be subtracted from the weight loss to give the oxygen by difference.

Size Distribution

The distribution of particle sizes for a fuel or ash sample. May be measured by various techniques depending on the particle-size range and the capabilities of the analytical laboratory.

Sulfur Content

The sulfur content of biomass is often determined as part of the CHN analysis by measuring SO_2. When this is done in conjunction with oxygen analysis, the overall analysis is referred to as CHNOS or "ultimate" analysis.

Ultimate Analysis

The ultimate analysis includes the CHNOS results.

Volatiles

Elements or compounds found in biomass that become a gas under elevated temperatures or pressures are measured by heating the biomass (generally to 950 °C) under an inert atmosphere to drive off volatile components without combusting nonvolatile or "fixed" carbon.

REPORT DOCUMENTATION PAGE

Form Approved
OMB No. 0704-0188

1. REPORT DATE (DD-MM-YYYY)	2. REPORT TYPE	3. DATES COVERED (From - To)
24-02-2011	Final	

4. TITLE AND SUBTITLE
Progress in the Production of JP-8 Based Hydrogen and Advanced Tactical Fuels for Military Applications

5a. CONTRACT NUMBER

5b. GRANT NUMBER

5c. PROGRAM ELEMENT

6. AUTHOR(S)
Christopher J. Zygarlicke, Ted R. Aulich, Chad A. Wocken, Debra F. Pflughoeft-Hassett, Tera D. Buckley, John P. Hurley, Junhua Jiang, Benjamin G. Oster, Nikhil M. Patel, Anthony C. Snyder, Chang W. Sohn, and William T. Brown, III

5d. PROJECT NUMBER

5e. TASK NUMBER

5f. WORK UNIT NUMBER
137573

7. PERFORMING ORGANIZATION NAME(S) AND ADDRESS(ES)
U.S. Army Engineer Research and Development Center (ERDC)
Construction Engineering Research Laboratory (CERL)
PO Box 9005,
Champaign, IL 61826-9005

8. PERFORMING ORGANIZATION REPORT NUMBER
ERDC/CERL TR-11-2

9. SPONSORING / MONITORING AGENCY NAME(S) AND ADDRESS(ES)
Office of the Director, Defense, Research, and Engineering (ODDR&E)
1777 N. Kent, Suite 9030
Rosslyn, VA 22209

10. SPONSOR/MONITOR'S ACRONYM(S)
ASAALT

11. SPONSOR/MONITOR'S REPORT NUMBER(S)

12. DISTRIBUTION / AVAILABILITY STATEMENT
Approved for public release; distribution is unlimited.

13. SUPPLEMENTARY NOTES

14. ABSTRACT

Today's Army is heavily dependent on oil and its byproducts as the primary fuel for the force. Current predictions indicate that the decline of oil reserves will coincide with the timeline for implementing Army After Next (AAN) technologies, which are planned to make fossil fuel powered vehicles up to 75 percent more efficient. This work was undertaken to help achieve that objective by: (1) developing and optimizing the high-pressure water reforming (HPWR) concept for on-demand production of high-pressure Proton Exchange Membrane (PEM) fuel cell-quality hydrogen from JP-8 and other feedstocks; (2) developing advanced tactical fuels with JP-8 drop-in compatibility and superior hydrogen-reforming properties from domestic fossil or renewable feedstocks, and (3) advancing the development of fuel cell electric hybrid (FCEH) vehicles, and demonstrating those vehicles and hydrogen dispensing and refueling systems at military installations. This report provides the research analyses, findings, and results, and describes technology demonstrations.

15. SUBJECT TERMS
fuel cells, military vehicles, alternative energy

16. SECURITY CLASSIFICATION OF:			17. LIMITATION OF ABSTRACT	18. NUMBER OF PAGES	19a. NAME OF RESPONSIBLE PERSON
a. REPORT	b. ABSTRACT	c. THIS PAGE			19b. TELEPHONE NUMBER (include area code)
Unclassified	Unclassified	Unclassified	SAR	206	